



Plant Microbial Fuel Cell in Paddy Field: a power source for rural area

Emilius Sudirjo | 2020



Plant Microbial Fuel Cell in Paddy Field a power source for rural area

Emilius Sudirjo

2020

PROPOSITIONS

1. Co-production of electricity and food is possible by a tubular Plant-MFC in a paddy field. (This thesis)
2. The battery function of the Plant-MFC should be exploited since the electricity price cannot keep-up with developments on other renewable electricity sources. (This Thesis)
3. Demanding a sustainable lifestyle without providing assistance to people who do not know whether they can eat or not on the next day is killing them.
4. Comparing economic feasibility of things is futile as long as we keep creating new grand challenges over and over again.
5. Honesty rather than economic growth is the prime capital for human development.
6. Pursuing a PhD journey is like finding a route to hike a mountaintop.
7. Useless things do not exist as value comes with time, place and consciousness.

Propositions belonging to the thesis, entitle

“Plant Microbial Fuel Cell in Paddy Field: a power source for rural area”

Emilius Sudirjo

Wageningen, 12 February 2020

**Plant Microbial Fuel Cell in Paddy Field:
a power source for rural area**

Emilius Sudirjo

Thesis committee

Promotor

Prof. Dr C.J.N. Buisman
Professor of Biological Recovery and Re-Use Technology
Wageningen University & Research

Co-promotor

Dr D.P.B.T.B. Strik
Associate professor, Environmental Technology
Wageningen University & Research

Other members

Prof. Dr MHM Eppink, Wageningen University & Research
Dr D Pant, Flemish Institute for Technological Research (VITO), Mol, Belgium
Dr M Helder, Plant-e, B.V, Wageningen
Dr J Arends, Center for Microbial Ecology and Technology (CMET), Ghent University, Belgium

This research was conducted under the auspices of the Graduate School for Socio-Economic and Natural Sciences of the Environmental (SENSE)

Plant Microbial Fuel Cell in Paddy Field: a power source for rural area

Emilius Sudirjo

Thesis

Submitted in fulfilment of the requirements for the degree of doctor
at Wageningen University
by the authority of the Rector Magnificus,
Prof. Dr A.P.J. Mol,
in the presence of the
Thesis Committee appointed by the Academic Board
to be defended in public
on Wednesday 12 February 2020
at 01.30 p.m. in the Aula

Emilius Sudirjo

Plant Microbial Fuel Cell in Paddy Field: a power source for rural area, 222 pages

PhD thesis, Wageningen University, Wageningen, the Netherlands (2020)

With references, with summaries in English, Indonesia, and Balangin

ISBN: 978-94-6395-191-3

DOI: <https://doi.org/10.18174/505263>

ADIL KA'TALINO, BACURAMIN KA'SARUGA, BASENGAT KA'JUBATA

For my parents, wife and son

Table of Contents

Chapter 1	General introduction	9
Chapter 2	Marine sediment mixed with activated carbon allows electricity production and storage from internal and external sources: a new rechargeable bio battery exploiting bi-directional electron transfer properties	23
Chapter 3	Activated Carbon mixed with marine sediment suits as bioanode material for <i>Spartina anglica</i> Sediment/Plant Microbial Fuel Cells: plant growth, electricity generation and spatial microbial community diversity	55
Chapter 4	Performance and Long Distance Data Acquisition via LoRa Technology of a Tubular Plant Microbial Fuel Cell Located in a Paddy Field in West Kalimantan, Indonesia	95
Chapter 5	A Thin Layer of Activated Carbon Deposited on Polyurethane Cube Leads to New Conductive Bioanode for (Plant) Microbial Fuel Cell	135
Chapter 6	General Discussion	167
References		191
Summary/Ikhtisar/Isi Ringkas		209
Acknowledgments		215
Curriculum Vitae		217
List of Publications		219
SENSE Diploma		220

Chapter 2, 3, and 4 have been published as peer-reviewed scientific articles and Chapter 5 is under reviewed in a peer-reviewed journal. The text, figures and tables of the published and submitted articles have been adjusted to the PhD thesis format. References should be made to the original articles.

Chapter 1

General Introduction

1.1 Electricity in rural area is not equally distributed

Electricity is one of most efficient energy carriers [1,2] and has become an important driver for modern human lifestyle [3]. Electricity can be used directly with very high efficiency [2]. According to International Energy Agency (IEA), modern economies depend on reliable and affordable delivery of electricity [4]. Access to modern energy such as electricity is an important aspect of human development; there is a positive correlation between electricity consumption per capita (in kWh) and human development index (HDI) and also gross domestic product (GDP) from 120 countries [5].

Electricity can be generated both from fossil fuels (coal, oil, and gas) and renewable energy sources [6]. Renewable energy includes all energy sources that are continually replenished by nature and derived directly from the sun (e.g. thermal, photo-chemical, and photo-electric), indirectly from the sun (e.g. wind, hydropower, and photosynthetic energy stored in biomass), or from other natural phenomena (e.g. geothermal nuclear heat from earth core and tidal energy (moon)) [7]. Current world electricity generation is still dominated by fossil fuel sources (~70% of total generation) [6]. These conventional energy sources (based on oil, coal, and natural gas) have successfully driven modern economic progress [7]. However, the excessive fossil fuel consumption causes negative impact on the environment, increased health risk and global climate change [6–8]. A life cycle assessment on emissions has shown that CO₂ emission per generated power (kWh) is higher in the conventional systems of electricity generation (i.e. 975.3 g-CO₂/kWh for coal, 742.1 g-CO₂/kWh for Oil, and 607.6 g-CO₂/kWh for gas) compared to the one of renewable systems (i.e. 9.7-123.7 g-CO₂/kWh for Wind, 53.4-250 for solar PV, 35-178 g-CO₂/kWh for biomass, 13.6-202 for solar thermal, and 3.7-237 g-CO₂/kWh for hydro) [9]. Therefore, it is important to shift from conventional energy sources to low-carbon renewable electricity sources [10].

Global policies have shown a promising political will toward energy by the adoption of United Nations (UN) Sustainable Development Goals (SDGs) as part of 2030 Agenda to ensure access to affordable, sustainable and modern energy for all humans [11]. As an UN' member, Indonesia also takes action in such policy to reduce its dependency on fossil fuel energy sources. In its national energy plan, Indonesia aims to increase new and renewable energy in its energy mix from 5% in 2015 to >23% in 2025 and >31% in 2050 [12]. In the third quartile 2018, 12.32% electricity in Indonesia was generated from renewable energy sources [13].

It is almost impossible to imagine that nowadays people are living without electricity, especially in a city. For instance the effect to a city of a one day electricity cut off shows a high dependence on electricity; computer and lifts stop function; hospital sink to a care and maintenance level; and the

lights go out [3]. The world electrification is not equally distributed[11]. While people in developed countries are enjoying electricity for their modern life style, hundreds of millions of people in rural areas in developing countries do not have access to electricity. According to International Energy Agency, an estimated 1.1 billion people (14% of the global population) do not have access to electricity [11]. About 84% of those without electricity access live in rural areas and more than 95% of those living without electricity are in developing countries in sub-Saharan Africa and Asia (**Figure 1.1**).

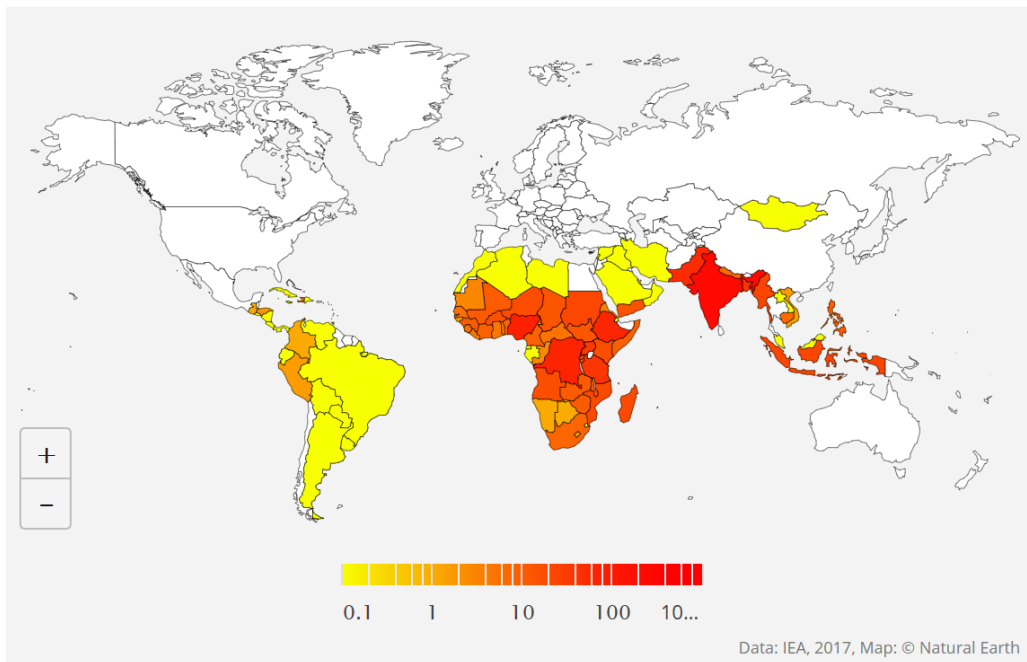


Figure 1.1 : Population without access to electricity, 2016. Logarithmic legend shows number of population (in millions); white colour means either all population have access to electricity or data were not reported (non-IEA member countries)

1.1.1 Electrification in Indonesia

As an archipelagic country of 17,508 islands (6,000 inhabited), electrification is a big challenge for Indonesia. In addition, according to a 2017 count, Indonesia population is 260,580,739 people, making it the world's fourth most populous nation after China, India and United States [14]. By 2018, medium voltage power distribution network (15-30 kV) and low voltage power distribution network (<6 kV) in Indonesia is 389,054.94 km and 953,560.46 km, respectively [15]. However, half of this distribution grid is located in Java Island. Despite national electrification ratio significantly increased (**Table 1.1**) from 80.51% in 2013 to 98.3% in 2018, its distribution (in provincial levels) is unequally

distributed ranging from 61.9 to 99.9%. From 66,921,705 electrified households in 2018, 2.43% of them have off-grid supplied electricity[15].

Table 1. 1: Indonesia electrification ratio from 2013 until 2018

TAHUN YEAR	JUMLAH RUMAH TANGGA NUMBER OF HOUSEHOLD	JUMLAH PELANGGAN RUMAH TANGGA ELECTRIFIED HOUSEHOLD	RASIO ELEKTRIFIKASI ELECTRIFICATION RATIO (%)
2013	64.204.615	51.688.927	80,51
2014	64.835.092	54.690.431	84,35
2015	65.669.197	57.983.048	88,30
2016	66.489.409	60.612.009	91,16
2017	67.228.573	64.105.549	95,35
2018	68.082.153	66.921.705	98,30

Source: Indonesia Electricity Statistics 2018 [15]

1.1.2 Typical electricity usage in rural areas of Indonesia

It is well-known that the lack of opportunity to access modern energy such as electricity is one of poverty aspects that needs to be tackled [5]. Access to electricity enable people to have economic opportunities for income generation, to save their time from time-consuming drudgery activities , and to have more enjoyable or educational activities [5]. In an area without electricity, people's activities are limited by the availability of day light, for instance a school cannot be started at early morning or late at night [16]. A study has shown that the first gained electricity for people in rural area is for lighting, communication (e.g. mobile phone) and a variety of educational delivery opportunities [17].

One of most obvious examples for electricity use is lighting. The need for light has been started long time ago in human history. The first record which shows humans were able to burn oil in lamps emerged more than 4500 years ago in Ur, an ancient city in southern Mesopotamia (modern day Iraq) [18]. Until today, many villagers in rural areas that do not have access to the electricity still burn oil/candles to get light [19]. It is also the case for people in Indonesia [20], even though the Indonesian government has stopped subsidy on kerosene since 2007 [21]. Based on my personal working experience since 2013 (as a civil servant at Mining and Energy Agency, Landak Regency, West Kalimantan Province, Indonesia), many people who live in rural area without access to the national electricity grid use the kerosene lamp for their light source. Some families who have a better financial condition use gasoline/diesel generator set to generate their own electricity. Such generator needs about 0.5-1.2 litre gasoline per hour for 0.85-2.2 KVA maximum power output [22,23].

Kerosene lamp only provides a poor quality of light between 1 and 6 lumens per square meter (lux), compared to typical western standard of 300 lux for tasks such reading [24,25]. One simple homemade kerosene lamp with a wick diameter of 4mm burns 5-8ml kerosene per hour and a non-pressurized kerosene lamp type (wick thickness/width of 2/22mm) burns 35-42 ml kerosene per hour [25]. About 7-9% of kerosene burned by this kind of wick lamps is converted into carbonaceous particulate matter that is nearly pure black carbon(BC)[19]. The largest amount of that particulates is PM_{2.5} which is well-known to have a negative impact on human health[26]. In addition, the use of kerosene lamps also has a risk of fire. Considering these negative effects, a replacement of kerosene lamps is desired, for instance with a small solar lighting kit [27,28].

1.1.3 Specific case on off-grid power in a remote area

An example case for electricity usage is given by a family who lives next to their paddy field in West Kalimantan, Indonesia (Sudirjo, 2019; unpublished). For their light source, this family utilizes a small solar lighting kit (*Table 1. 2*), which costs around Rp 500.000 (about 31 euro). In addition to this small solar lighting kit, a 50 Wp solar panel system, which consists of 12V50Ah NP-50-12 MF Battery; Intelligent PWM-20 Solar Charge Controller (*Figure 1. 2*) is used to supply electricity for portable LCD television and mobile phone charger (*Table 1. 2*).

Table 1. 2: Several home appliances in rural area and their energy demand

Home Appliances	Power Specifications	Reference
Lighting		
	5mm white LED	3.6 V; 20mA [29]
	Cree Xlamp XM-L2 High Power LEDs	2.85V; 700mA [30]
	Small solar Lighting Kit	4 Wp solar panel, 7.5V; 3000mAh Li-ion battery; 3 LED Light @5V, 200mA [31]
Mobile phone:		
	Nokia 110 Battery	capacity:3.7V; 800 mAh [32]
Smart Phone:		
	Asus Zenfone Selfie ZD551KL	3000 mAh Li-Polimer 3.7 V [33]
Television:		
	Portable LCD TV 9.5”TFT	12V; 2A [34]
	15.6 ELED TV 16 E1	Max 36W at 12V DC [35]
Digital satellite decoder:		
	Lombok Digital Satellite Receiver DV3 MMP-789	12V, 1A [36,37]

A). A farmer, Mr. Sipon, watched news on his portable LCD TV



B). On the roof there are several solar-PVs (circled in red): in small circle is a 4W solar DC lighting kit; in big circle is a-50 Wp solar panel for TV and Mobile phone charger and a-80Wp solar panel for LoRa system used in this research (see chapter 4). In front of the house: on the ground, there is newly harvested rice (still with its husk) is sun-dried before it goes to the rice mill; on the right corner, there is a satellite parabolic for television



Figure 1. 2: (A) A farmer and (B) his small house next to paddy field used for research in Chapter 4

1.2 (Plant) microbial fuel cell

1.2.1 Theory-performance-design-ideas on application

The first publication on phenomenon that the decompositions of organic compounds by micro-organism is accompanied by electrical energy generation was reported more than century ago [38]. Later on, this phenomenon was known as microbial fuel cell (MFC) [39]. Plant microbial fuel cell (Plant-MFC) is a further development from an MFC in which plants are integrated in the anode to provide continuous supply of organic compounds [40]. In this concept, carbon dioxide is fixed (via photosynthesis) and released as rhizodeposits (e.g root exudates) by the plants and are utilized by the microorganism that return the carbon dioxide into the atmosphere[40]. Plant-MFC is considered as a clean and renewable source of electricity ([40]. In principle, the Plant-MFC and the MFC operate on the same mechanism. A Plant-MFC consists of three major parts: anode, cathode and membrane or separator (*Figure 1. 3*).

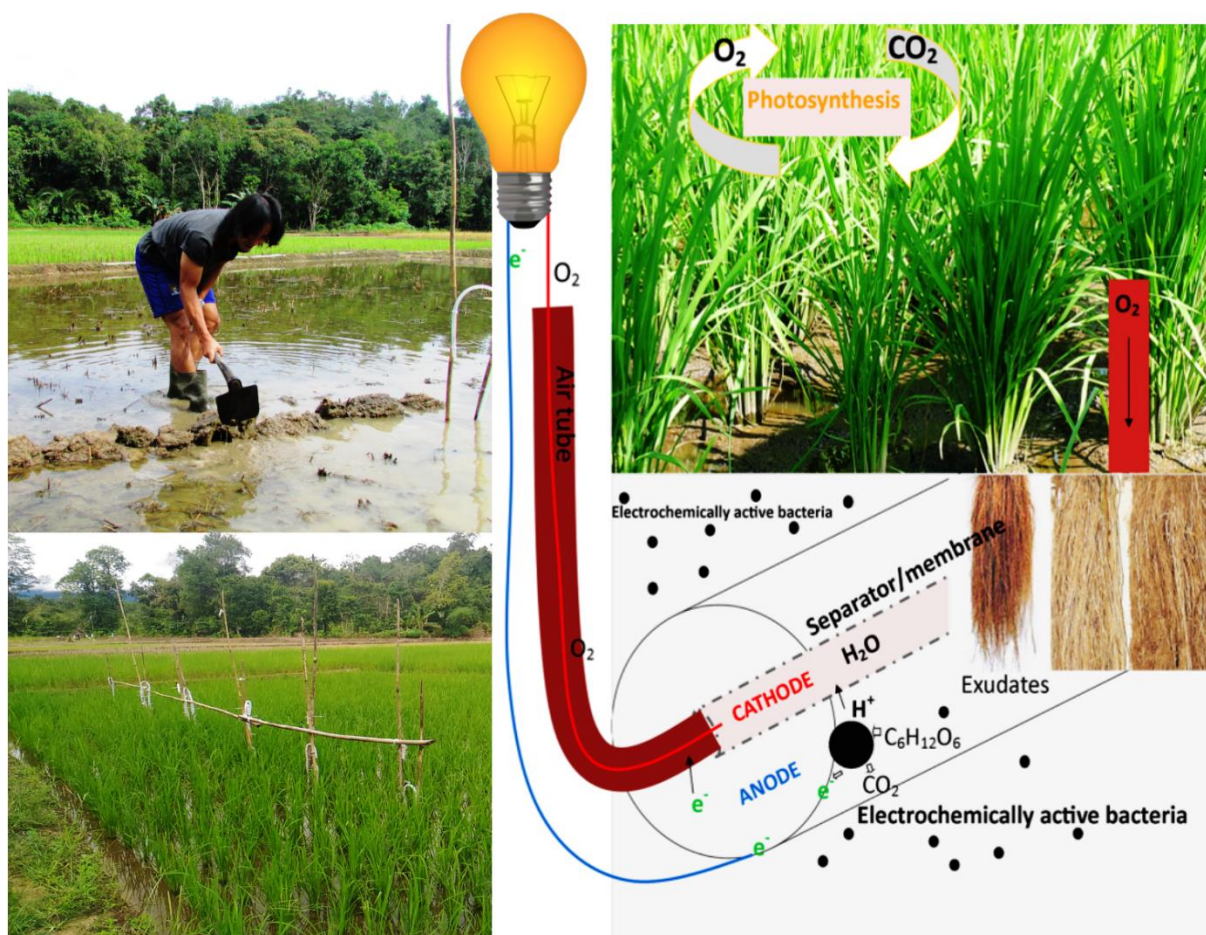


Figure 1. 3: An illustration of Plant-MFC in a rice paddy field, modified from Sudirjo et.al 2018 [41]

In the anode, electrochemically active bacteria (EAB) oxidize biodegradable substrates (ranging from pure compounds such as acetate and glucose to complex mixture of organic matters such as domestic waste, animal manure and wastewater) for their metabolism [42,43]. In Plant-MFC, a conductive anode material is installed as an electron acceptor for the released electrons [43]. These electrons then flow through an external load (such as an electronic device) to the cathode at which the final electron acceptor is reduced [43]. Simultaneously, to keep electro neutrality of the system ions move via the liquid medium (electrolyte) between the anode and the cathode [42], and electricity is generated from a Plant-MFC system.

Plant-MFC can be operated with or without a membrane. In the first development, especially in lab scale, Plant-MFC used membrane to separate between the anode and the cathode chamber [40,44,45]. However, a membrane is less preferred in a field application because of its cost [46]. As an alternative, membranes can be replaced with a non-conductive spacer as used in Chapter 3 [47] or not used at all by placing the anode and the cathode at a proper distance [48–50].

1.2.2 Energy potential from Plant-MFC

In the Plant-MFC system, the electricity production depends on the anode and the cathode potential differences as explained in the Equation (1.1) [51–53].

$$E_{OCP} = E_{OCP,cat} - E_{OCP,an} \quad (1.1)$$

E_{OCP} is the open cell potential in V, also known as theoretical potential. The $E_{OCP,cat}$ is the cathode potential at open cell potential in V and the $E_{OCP,an}$ is the anode potential at open cell potential in V.

In a Plant-MFC anode, oxidation may occur from different sources. Plant rhizodeposits include exudates (sugars, organic acids), secretions (polymeric carbohydrates and enzymes), lysates (dead plant cell materials) that are potentially available are oxidised by the EAB and other root-associated microbes to yield electrons [54]. In addition, also other soil redox processes also occur, like sulphide can be anaerobically oxidized to elemental sulphur (S^0) and SO_4^{2-} by phototrophic sulphur bacteria (*Chlorobium spp.*) [55]. In comparison, many type reductions also occurs in the cathode. In addition to the most common electron acceptor (oxygen), other electron acceptors are also present in the soil such as NO_3^- is reduced to N_2 , Mn^{4+} to Mn^{2+} , Fe^{3+} to Fe^{2+} , SO_4^{2-} to H_2S , S^{2+} or HS^- (depending upon pH) [56]. Some researchers used ferric cyanide ($K_3(FeCN)_6$) to increase their cathode potential [57–59]. However, for a sustainable Plant-MFC operation, an open-air cathode is preferred [43,47,60].

Due to complex processes that may occur in both the anode and the cathode, it is very difficult, or almost impossible, to determine the real theoretical cell potential (the anode or the cathode potential) from a Plant-MFC system. The most common approach to estimate the theoretical cell potential is using thermodynamics of the anode (*e.g.* acetate) and the cathode (*e.g.* oxygen) reaction[51]. In this approach, the anode and the cathode potential are calculated based on Gibbs free energy for a specific condition as extensively described by Logan [52]. The anodic oxidation reaction for acetate and the cathodic reduction reaction from oxygen to water are given as an example in **Table 1.3** [51].

Table 1.3 : Standard and actual potential of acetate oxidation and oxygen reduction

Reactions	E^0 (V vs Ag/AgCl)	E (Vvs Ag/AgCl)
Acetate oxidation		
$C_2H_3O_2^- + 4 H_2O \rightarrow 2 HCO_3^- + 9 H^+ + 8 e^-$	-0.018	-0.494
Oxygen to water		
$O_2 + 4 H^+ + 4 e^- \rightarrow 2 H_2O$	1.024	0.600

E^0 is standard potential under standard condition and the E is the actual potential (Acetate concentration 0.05M, $[H_2O] = 1M$; pH = 7; pO = 0.2 bar; T = 298K). Applying the same calculation concept as Equation 1.1, the theoretically cell potential for a Plant-MFC using acetate model substrate and oxygen as the final electron acceptor is 1.094 V.

In reality, internal resistance (R_{int}) causes the cell potential (Equation 1.2) from a Plant-MFC to be far below its theoretical value [51,53]. For instance during two week power generation Plant-MFC in a peat soil, the cell potential is ranging from 313 mV to 520 mV [60].

$$E_{cell} = E_{OCP} - i \cdot R_{int}, \quad (1.2)$$

E_{cell} is the measured cell potential in V, i is the current density in A/m^2 Plant Growth Area (PGA), and R_{int} is the internal resistance in $\Omega \cdot m^2$. There are several factors that cause internal resistance such as cathode over potential, anode over potential and potential losses due to ionic and transport losses, known as membrane potential [53]. Hence, the Equation (1.2) can be rewritten as Equation (1.3).

$$E_{cell} = E_{OCP} - \eta_{cath} - \eta_{an} - E_M, \quad (1.3)$$

η_{cath} is the cathode over potential in V, η_{an} is the anode over potential in V and the E_M is the membrane potential in V. Furthermore, the internal resistance can be differentiated into cathode resistance (R_{cath}), anode resistance (R_{an}) and membrane resistance (R_M) as described by Equation (1.4, 1.5, and 1.6).

$$R_{cath} = \frac{\eta_{cath}}{i} = \frac{E_{OCP,cath} - E_{cath}}{i}, \tag{1.4}$$

$$R_{an} = \frac{\eta_{an}}{i} = \frac{E_{an} - E_{OCP,an}}{i}, \tag{1.5}$$

$$R_M = \frac{E_M}{i} \tag{1.6}$$

E_{cath} is the measured cathode potential (V) and E_{an} is the measured anode potential (V). **Figure 1. 4** shows an illustration how the anode over potential, the cathode over potential and the membrane potential influence Plant-MFC cell potential.

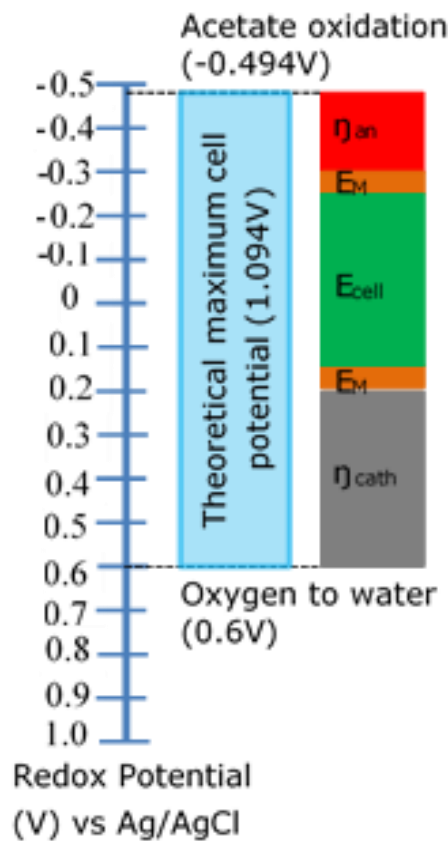


Figure 1. 4: An illustration of theoretical and actual cell potential of a Plant-MFC, modified from [61]. E_{cell} is measured cell potential in V, η_{cath} is the cathode over potential in V, η_{an} is the anode over potential in V and the E_M is the membrane potential in V

1.2.3 Improvement on Plant-MFC performances

Apart from substrate availability, several strategies have been done to improve Plant-MFC performance. For example, modifying plant growth medium[58], characterizing internal resistance [53], studying plant and microbe cooperation[48], developing and investigating electrode materials [53,62–64], and designing a new type reactor [44,60,64]. There are two common designs of Plant-MFC for a field application. The first one is a conventional design placing the anode in a lower anaerobic part (below the surface of the soil) and the cathode above the soil surface to obtain oxygen [48]. For a large scale application, this design is probably less practical because one needs to excavate the top layer of soil before anode installation. To avoid this excavation, Timmers proposed a second design, a tubular design of plant-MFC which could be installed with a horizontal drilling technique [64].

Plant-MFC is characterized as a low power system as they are currently relative small sized while power output are in order of 6 to 240 mW/m² plant growth area [48,65]. Therefore, we foresee that implementation of Plant-MFC should be based on this characteristic. Other prospective applications of Plant-MFC are described in an overview paper like: application can be combined with wastewater treatment, remediation of polluted sediments and surface water, greenhouse gas mitigation and bio sensing [54]. There are also devices available in the market that are powered by Plant-MFC technology such as Sprout ‘n Spark, Plant-e clock, and Living Light [66]. However, a large scale application of Plant-MFC is still not available yet.

In principle, Plant-MFC needs anaerobic (more reduce) conditions for their anode to generate electricity, and therefore wetlands are considered a suitable place to integrate this technology in a real life application [60]. It is not only because the enormous size of wetlands (around 10 million km² worldwide) but also the presence of alternative electron donor (*e.g.* sulphide, fossilized organic matters, biodegradable dissolved organic matters and dead biomass) is beneficial for Plant-MFC [60]. One of the largest types of wetland is paddy field [67]. With its current size in the world, paddy fields have a great potential to be integrated with plant-MFC technology.

1.3 Rice paddy production

For many people, rice is their staple food. In 2017, the average harvested area of rice paddy and rice paddy production in the world are about 167 million ha and 770 million tonnes, respectively [67]. As human population is growing, the need for rice paddy field and production to support basic human need for food is also growing (*Figure 1. 5*). Currently, more than 90% of world rice paddy had been produced in Asia, including Indonesia (*Figure 1. 6*).

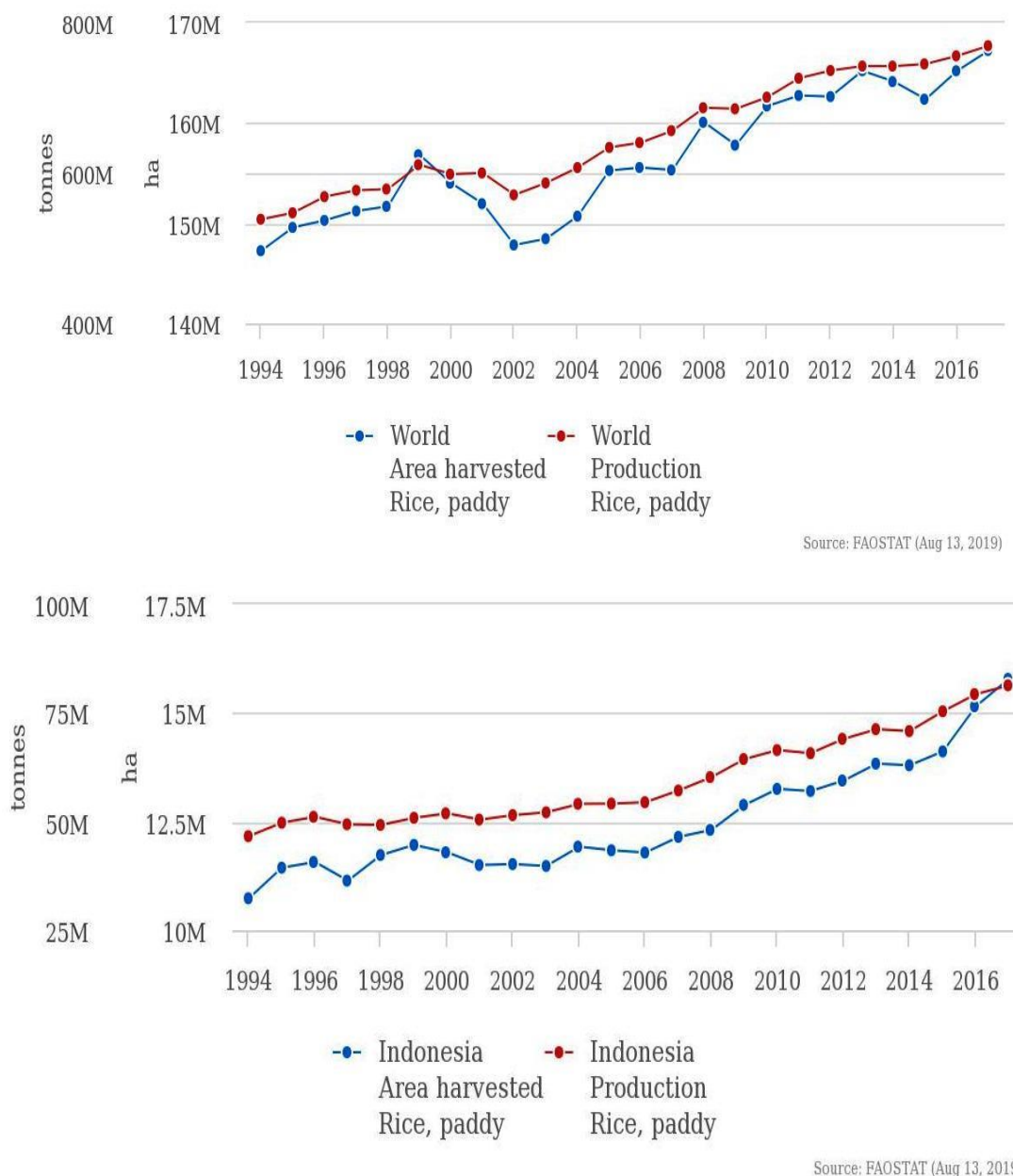


Figure 1. 5: Average production/yield quantities of rice paddy from 1994 until 2017 in World (above) and Indonesia (below)

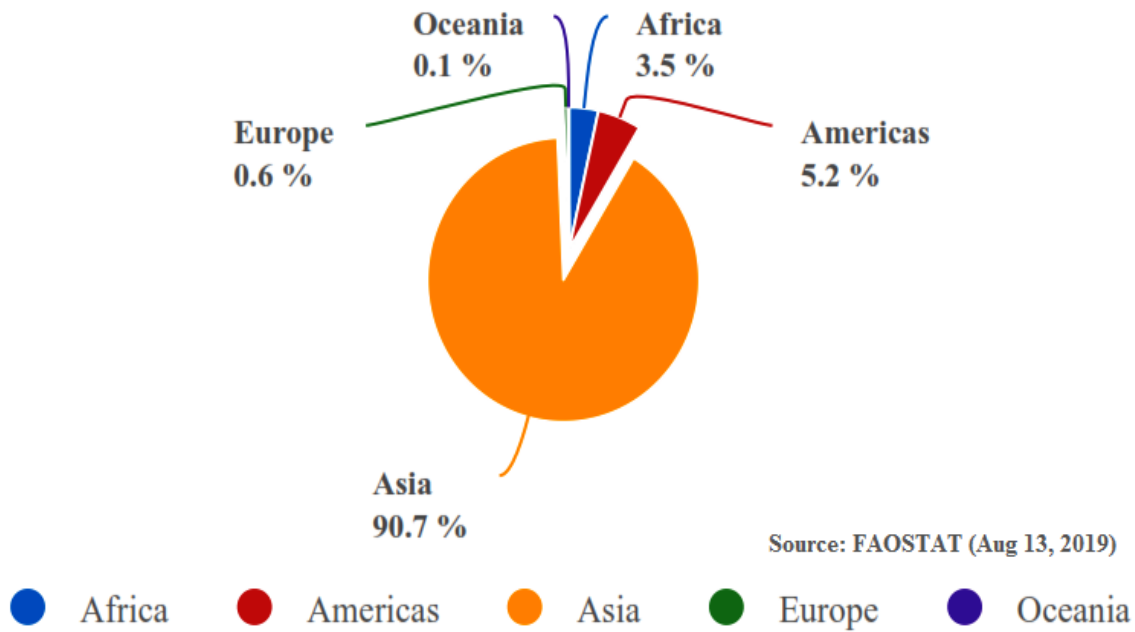


Figure 1. 6: Average production share of rice paddy by region from 1994 until 2017

Rice paddy is usually grown in a field that is flooded with water. The common practice for rice cultivation includes several activities such as: (a): preparation of land by ploughing; (b) seedling and transplanting of the rice paddy; (c) water management; (d) fertilization; (e) weeding, and (f) pest control. More detailed explanations about rice cultivation techniques are explained in Chapter 4.

1.4 Thesis objective

The objective of this thesis is to pre-assess the applicability of the Plant-MFC as a low power off-grid power source in a rural area for a theoretical Indonesian case. For this first, a technical design was made for a household in rural area of Indonesia based on the latest research developments. Next the applicability was assessed on technical, social, and environmental criteria as well as economics and some scenarios were suggested which could improve the real application. Values for a plant-MFC system to fulfil basic electricity needs were calculated.

1.5. Thesis outline

In this thesis, lab and field experimental results are presented. Chapter 2 and 3 of this thesis present the results from lab experiments. Chapter 5 combines results from lab and field experiment. And chapter 4 presents result from field experiment.

Chapter 2 of this thesis assesses the usage of sediment mixed with activated carbon (AC) for their applicability to generate and store electricity in a bio-electrochemical system (BES) or Microbial Fuel Cell (MFC) system. Here, charge and discharge properties of this mixture were studied.

In chapter 3, the previous studied electrodes in chapter 2 were tested in flat-plate Plant-MFCs with *Spartina anglica* for their performances in generating electricity and sustaining plant growth.

In chapter 4, a potential of rice paddy field to generate electricity was assessed by installing 3 tubular plant-MFCs and operating them for 4 crop seasons (from 28 October 2017 until 8 August 2019). This experiment was carried out in a rice paddy field in West Kalimantan, Indonesia.

In chapter 5, an alternative electrode was developed by a simple dipping method of AC powder onto polyurethane (PU) cubes. The PU/AC composites were tested both in lab and in paddy field.

Finally, in chapter 6, the applicability of Plant-MFC for off-grid power source in rural area is discussed. For this, technical, economic, social, and, environmental/safety/health criteria are briefly assessed. Finally, an outlook for plant-MFC development was given.

Chapter 2

Marine sediment mixed with activated carbon allows electricity production and storage from internal and external energy sources: a new rechargeable bio-battery with bi-directional electron transfer properties

Published as: Sudirjo, E.; Buisman, C.J.N.; Strik, D.P.B.T.B. Marine Sediment Mixed with Activated Carbon Allows Electricity Production and Storage from Internal and External Energy Sources: A New Rechargeable Bio-Battery with Bi-Directional Electron Transfer Properties. *Front. Microbiol.* 2019, 10, 934.

Abstract

Marine sediment has a great potential to generate electricity with a bio electrochemical system (BES) like the microbial fuel cell (MFC). In this study, we investigated the potential of marine sediment and activated carbon to generate and store electricity. Both internal and external energy supply was validated for storage behaviour. Four types of anode electrode compositions were investigated. Two types were mixtures of different volumes of activated carbon (AC) and Dutch Eastern Scheldt marine sediment (67% AC, 33% AC) and the others two were 100% AC or 100% marine sediment based. Each composition was duplicated. Operating these BES's under MFC mode with solely marine sediment as the anode electron donor resulted in the creation of a bio-battery. The recharge time of such bio-battery does depend on the fuel content and its usage. The results show that by usage of marine sediment and activated carbon (AC) electricity was generated and stored. The 100% AC and the 67% AC mixed with marine sediment electrode were over long term potentiostatic controlled at -100mV vs Ag/AgCl which resulted in a cathodic current and an applied voltage. After switching back to the MFC operation mode at 1000 ohm external load, the electrode turned into an anode and electricity was generated. This supports the hypothesis that external supply electrical energy was recovered via bi-directional electron transfer. With open cell voltage experiments these AC marine bioanodes showed internal supplied electric charge storage up to 100 mC at short self-charging times (10 and 60 seconds) and up to 2.4 C (3,666 C/m³ anode) at long charging time (1 hour). Using a hypothetical cell voltage of 0.2V, this value represents an internal electrical storage density of 0.3 mWh/kg AC marine anode. Furthermore, it was remarkable that the BES with 100% marine sediment based electrode also acted like a capacitor similar to the charge storage behaviors of the AC based bioanodes with a maximum volumetric storage of 1,373 C/m³ anode. These insights give opportunities to apply such BES systems as e.g. *ex-situ* bio-battery to store and use electricity for off-grid purpose in remote areas.

Keywords: Activated Carbon, Capacitance, Bio-Battery, Bio Anode, Marine Sediment, Charging, Discharging, Energy Storage

2.1 Introduction

Sediment microbial fuel cells (SMFC) are among the most studied bio electrochemical systems (BESs) which attracts attention from many researchers because of its ability to generate power and provide bioremediation [68]. In a SMFC the anode is for example placed into the anaerobic sediment and the cathode is placed on the upper position of the aerobic water layer [42,69,70]. In this paper, we will demonstrate the use of the SMFC for energy storage purposes.

Sediment contains not only organic matters [71] but also abundant electrochemically active bacteria (EAB) communities to generate electricity in the SMFC [42]. With these properties, the SMFC can be implemented as *in-situ* renewable electricity source [72]. The SMFC was tested for applications as an *in-situ* renewable power source for long term monitoring instruments like the oceanographic instrument, meteorological buoy, acoustic modem, telecommunication system, remote sensor, submersible ultrasonic receiver, turbidity meter, acoustic receiver or wireless temperature probe [70,73].

In theory, the microbial fuel cell (MFC) can continuously generate electricity as long as there is enough substrate to be utilised by EAB [52]. Apparently for the *in-situ* SMFC system, the substrate availability will not be a direct limiting factor to generate electricity at long terms because enormous amount of organic matter is present and supplied to the sediment [74–76].

The sediment organic matter is a primary energy source of the SMFC to produce power [70]. Marine or sea sediment is well known to be rich with organic carbon as a result of photosynthetic fixation of inorganic carbon by terrestrial and marine phytoplankton [76]. In coastal areas, these marine sediments can be inhabited by higher plants like *Spartina anglica*. The organic carbon in sediments can be measured as total organic carbon (TOC). In a low salt marsh estuarine intertidal sediment, which is dominated by *Spartina anglica* vegetation, the TOC at depth 0-0.2 m is about 2% [77]. This TOC gives a kind of maximum available fuel content of a SMFC.

There are two common methods to utilize MFC power for relatively high voltage applications, either using a DC-DC converter or using a capacitor [78]. A DC-DC converter allows us to continuously power low power consuming devices [79]. For example an SMFC was successfully powering a wireless telecommunication system by integrating a SMFC system and DC-DC converter [80]. A capacitor makes it also possible to intermittently powering high power consuming devices since electric charge is stored over time and released once needed [79].

In addition to substrate availability, also the electrode materials play an important factor for an MFC. The anode electrode is a structure which serves as an electron acceptor for the EAB. It is important to find an inexpensive and suitable material combining conductivity and high surface area with three dimensional structure [52,81,82]. Moreover, for integrating MFC technology with biomass production by planting plants, the anode material should be able to support plant's roots and be able to restore the electrical connectivity in the anode after disturbance [83].

Among possible anode materials, activated carbon (AC) granules seems to be a promising. Despite that (some) AC is apparent less conductive compare to graphite granule [84], its large surface area and porous structure [85] is suited for EAB growth. Several researches have shown that bacteria are able to grow on the AC and are forming biofilms [86–88]. This bio film has also shown a capability to store charge in the form of electrons in multi-heme c-type cytochromes [89,90]. In addition to its prospective to be a bioanode, AC has also a capacitive electron storage capability. Recent research on a single AC granule has shown that the AC can store electric charge [88]. This capacitive property is opening possibilities to store in-situ generated electricity within the MFC [91]. In addition, the system can be considered as a bio-battery.

A bio-battery is an energy storing system based on the redox reaction of organic compounds with the help of enzymes or bacteria. A bio-battery also has an anode, cathode, separator and electrolyte. In the anode, electrons and hydrogen ions are generated from oxidation reaction of sugar type organic compound, i.e. glucose. The hydrogen ions migrate to the cathode through a separator, and, together with electrons that pass through the outer circuit, they reduce oxygen into water [92].

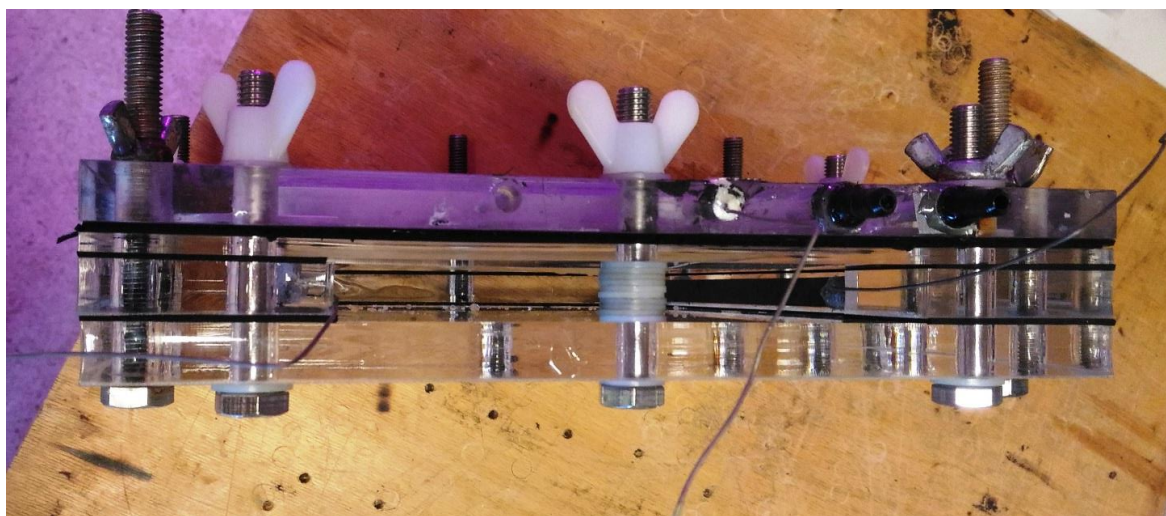
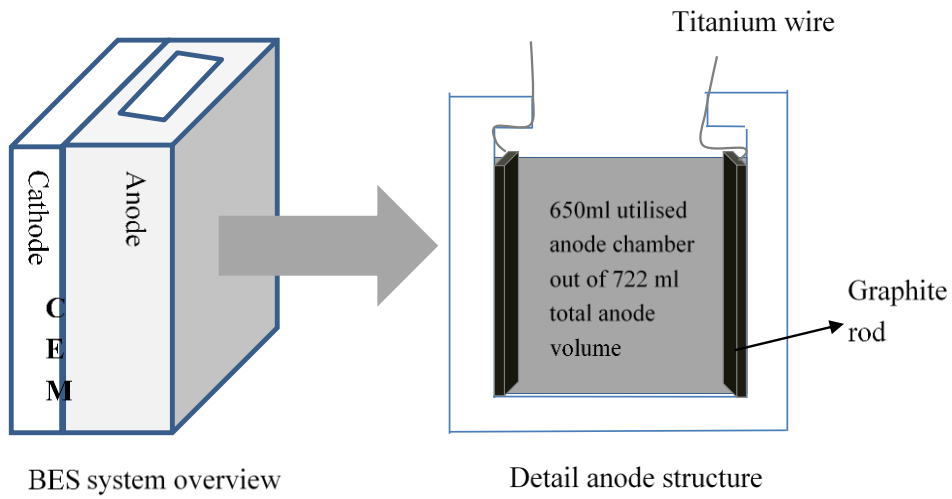
Considering the AC's properties mentioned above and the benefit of sediment it seems possible to integrate both of them in a MFC based bio-battery. Therefore, the objective of this study was to investigate the abilities of marine sediment and activated carbon to store and generate electricity in a bio-battery. This work allowed the development of a new kind of bio-battery with bi-directional electron transfer properties. Both external and internal supplied energy i.e. generated electricity could be stored at different time domains. To understand the behaviour of the bio-battery, several experiments were conducted to clarify: (i) the role of the sediment in providing fuel; (ii) the role of activated carbon in supporting bi-directional electron transport behaviour; and (iii) the role of sediment and activated carbon on in-situ charge storage behaviour.

2.2 Materials and Methods

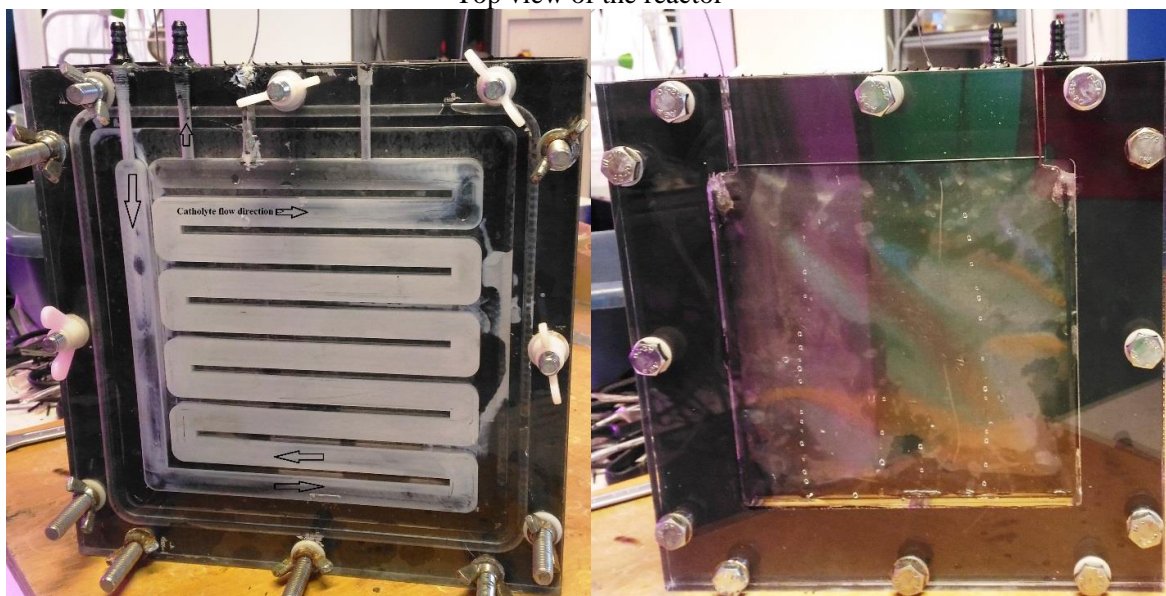
2.2.1 Experimental setup

Eight identical flat plate bio electrochemical system (BES) reactors made of acrylic glass were utilized for this experiment similar to Wetser, et al.2015 [65]. The vertically placed reactors had two compartments that either functioned as an anode or a cathode. Both compartments were separated with a cation exchange membrane (CEM) fumasep FKD-PK-75 PEEK-reinforces, 75 μ m. The anode compartment had a total volume of 722 ml (19cmx19cmx2cm) but only 650ml were filled with anode material. The anode compartment had an open space on the top (19cm x 2 cm). Two graphite rods (18cmx1cmx0.2cm) were used as current collectors. The current collectors were connected with titanium wire (1mm diameter) and glued in both sides of the anode chamber (**Figure 2. 1**). Stages of the BESs reactor preparation were presented in *Supplementary Figure S2. 4*.

In the cathode i.e. counter electrode compartment (22cmx22cmx1cm; with a winding channel for catholyte flow), graphite felt 22cmx22cm (3mm thickness, Grade WDF, National specialty product carbon and Graphite Felt, Taiwan) was used as an electrode. This electrode was woven with a titanium wire as a current collector. Nitrate-less, sulphate-less, ammonium bicarbonate-rich plant growth medium was utilized as catholyte [58]. The catholyte was aerated with ambient air using an aquarium pump and recirculated into the cathode chamber in a close cycle via a 1 liter bottle with a pump (Watson-Marlow 505S, Rotterdam, The Netherlands at 30 rpm). Total catholyte volume in the close cycle was maintained at 1 L. Both anode and cathode potential were measured and reported against 3M KCl Ag/AgCl reference electrode.



Top view of the reactor



Cathode side view with flow direction

Anode side view

Figure 2. 1: BES reactor schemes and pictures from different positions

This study utilized four different anode compositions which served as the electrode. The four anode compositions were two of mixing different volumes of AC (PK 1-3 Cabot Norit Nederlands BV, with apparent density of 290 g/L) and mixed with marine sediment (67% AC and 33% AC), 100% AC and 100% marine sediment (**Table 2.1**). The anode was further mixed with Nitrate-less, sulphate-less, ammonium-bicarbonate-rich plant growth medium [58] that was utilized as the anolyte (the exact composition is also given in the **Supplementary Table S2. 1**). Each composition was duplicated. The marine sediment (with density of 1.58 g/mL) was collected from tidal area of the Eastern Scheldt of the North Sea at Krabbendijke, Zeeland Province, The Netherlands (51.446710N, 4.093149E).

Table 2.1 : Anode compositions

BES	Volume Percentage		Composition (mL)		Composition (gr)	
	AC	Marine sediment	AC	Marine sediment	AC	Marine Sediment
1 & 2	100%	0%	650	0	188.5	0
3 & 4	0%	100%	0	650	0	1027
5 & 6	67%	33%	435.5	214.5	126.3	338.9
7 & 8	33%	67%	214.5	435.5	62.2	688.1

2.2.2 Operational of the reactors

All BES reactors were operated for 156 days. Within these 156 days two different experiments were conducted, which were the power generation experiment (day 1 - day72 and day 96 - day118) and the electricity storage experiment (day 72 – day 96 and day 118 – day 156). During the power generation experiment (MFC mode) two types of controls were alternately applied. First, an external load control in which the anode and the cathode were connected with 1000 ohm external load (day 1-day 5; day 14 – day 44; day 56-day 72; day 96-day 118). Secondly, a potentiostat control (day 5-day 14; day 44 – day 56) in which the anode potential was maintained at -100mV vs Ag/AgCl (Transients, Chrono Amperometry) with a potentiostat (Ivium Technologies, Eindhoven, The Netherlands). The anodes were controlled with a three electrode setup in which the anode was the working electrode, the cathode as the counter electrode and a reference electrode (Ag/AgCl type No: QM710X from QIS Oosterhout, The Netherlands) in the anode as the reference electrode. On day 105, 2 g/L of acetate in form of sodium acetate (NaAc) was added into each anode of the BESs and another 2 g/L NaAc was added to the anode of BES 1 and BES 2 on day 117 after sampling. The system was operated in the light and dark ratio of 14:10 hours within a climate chamber (Microclima 1750, Snijders Scientific, Tilburg, The Netherlands) at 20⁰ C and humidity of 70% similar to Wetser, et al 2015 [65].

During the electricity storage experiments, the reactors were only controlled with a potentiostat (Transients, mixed Mode). The experiment was executed by self-charging at open circuit and followed by discharging the BESs at 65mV anode potential. I.e. mode 1 (charging period) was set in open cell and mode 2 (discharge period) was set to a fixed potential (65mV). Each set of electricity storage experiments was performed for 40 times. Stored charge of the final 10 cycles was calculated as explained by [91], which is summarized as following Equation (2.1):

$$Q_s = Q_m - Q_{cont,d} \quad (2.1)$$

Where Q_s is the stored charge (C); Q_m is the measured charge (C) during discharge period which was logged with IviumSoft; and $Q_{cont,d}$ is the expected charge (C) at a steady-state current (A). The expected charge is a product of steady-state current (A) and time (t) during the discharge period. The steady-state current in this calculation was the average current of the last minute of each cycle.

Charge recovery and energy recovery was calculated within the first power generation experiment period from day 44 until 72. The charge recovery was calculated based on the Coulombs supplied current during the potentiostatic control (day 44 until day 55) versus Coulombs extracted during the external load control (day 56 until day 72) as given by Equation (2.2; 2.3 and 2.4).

$$Charge\ recovery = \frac{\sum Q_{discharging}}{\sum Q_{charging}} \quad (2.2)$$

$$Q_{charging} = I_{avg,charging} \times t_{charging} \quad (2.3)$$

Where $Q_{charging}$ is charge supplied during a potentiostatic control; $I_{avg,charging}$ is average current during potentiostatic control; and $t_{charging}$ is duration of the charging time. $Q_{charging}$ was calculated on a daily basis for day 44 until day 55 and the result was summarized as $\sum Q_{charging}$.

$$Q_{discharging} = I_{avg,discharging} \times t_{discharging} \quad (2.4)$$

Where $Q_{discharging}$ is charge extracted during the external control; $I_{avg,discharging}$ is average current during the external load control; and $t_{discharging}$ is duration of the discharging time. $Q_{discharging}$ was also calculated on a daily basis for day 56 until day 72 and the result was summarized as $\sum Q_{discharging}$.

The energy recovery (Equation 2.5) was a ratio between total output energy during the external load control (day 56 until day 72) and total input energy during the potentiostatic control (day 44 until day 55).

$$Energy\ recovery = \frac{E_{out}}{E_{in}} \quad (2.5)$$

Both output energy and input energy were calculated on a daily basis according to following Equations (2.6 and 2.7):

$$E_{input} = E_{applied} \times Q_{charging} \quad (2.6)$$

$$E_{out} = E_{cell} \times Q_{discharging} \quad (2.7)$$

Where E_{input} is input energy (J); E_{output} is output energy (J); $E_{applied}$ is applied cell potential during charging (-100mV) and E_{cell} is average obtained cell voltage during discharging at 1000 ohm.

2.2.3 Measurement and analysis

From day 21 until day 156, anode potentials, cathode potentials, membrane potentials and cell potentials were logged with a field point (National Instruments FP-2000; FP-AI-112) similar to Helder et al.2012 and Wetser et al.2015 [58,65]. Prior to mentioned period, the anode potentials, the cathode potentials and the cell potential were manually measured with a multimeter. Apart from data logger, during potentiostat control generated current was logged with IviumSoft of Ivium Technologies connected to a lab PC.

Every 1 or 2 weeks, liquid samples were taken from the anode and the cathode. Anolyte samples were taken using filtered syringe and catholyte samples were taken from cathode outlet before entering recirculating bottle. Samples were stored in -20°C for further analysis. Conductivity and pH were measured right after sample collections. Conductivity was measured using HQ440d multi pH/LDO/conductivity meter HACH and pH was measured using a PHM210 standard pH meter, MeterLab Radiometer analytical.

Acetate concentrations were determined by gas chromatography (Agilent 7890B, USA) as described earlier [93]. An HP-FFAP Column was used (25m x 0.32 mm x 0.50 μm). The detector (FID) and injection temperatures were 240 and 250 $^{\circ}\text{C}$, respectively. The oven temperature was 60 $^{\circ}\text{C}$ for 3 min, 21 $^{\circ}\text{C min}^{-1}$ up to 140 $^{\circ}\text{C}$, 8 $^{\circ}\text{C min}^{-1}$ up to 150 $^{\circ}\text{C}$ and constant for 1.5 min, 120 $^{\circ}\text{C min}^{-1}$ up to 200 $^{\circ}\text{C}$ and constant for 1.25 min, and finally 120 $^{\circ}\text{C min}^{-1}$ up to 240 $^{\circ}\text{C}$ and constant for 3.5 min. Helium was used as carrier gas at a flow of 1.25 mL min^{-1} for the first 3.5 min and 2 mL min^{-1} until the end of the run. 1 μL of sample was injected in the column. Acetate concentration result can be found in the *Supplementary Figure S2.3*.

2.3 Result and Discussion

2.3.1 Dutch Eastern Scheldt marine sediment is a suitable fuel to generate electricity with a bio-battery

The Eastern Scheldt marine was a suitable fuel to generate electricity with the BES. The designed system acted as a bio-battery. During the first 72 days operation of the two marine sediment BESs (BESs 3&4; i.e. without activated carbon), electricity was continuously generated during MFC operation mode (**Figure 2. 2A**). In this period, no additional substrate (acetate) was added. On average both BESs generated 0.1 ± 0.09 mA, which correlates with current density 26.3 mA/m^2 land use area (154 mA/m^3 anode volume) and a consequent power density of 2.63 mW/m^2 land (15.4 mW/m^3 anode volume). This result is lower than generated power with a graphite rod anode and intertidal sediment, which was 19.6 mW/m^2 projected land use [94]. A 50 mA/m^2 projected land use (20 mW/m^2) was reached with a 3D carbon cloth marine sediment anode while up to 100 mA/m^2 projected land use (55 mW/m^2) was reached with a carbon sponge marine sediment anode [95]. This result is also lower than a planted (*Spartina anglica*) marine sediment MFC which reached a 18 mW/m^2 (83 mA/m^2) plant growth area [96]. However, later on in the experiment the performance of these BESs were improved with a current density in range of 41 to 71 mA/m^2 possibly due to a more mature bioanode development (see **Supplementary Table S2. 2** for a complete performance set of all operated BESs).

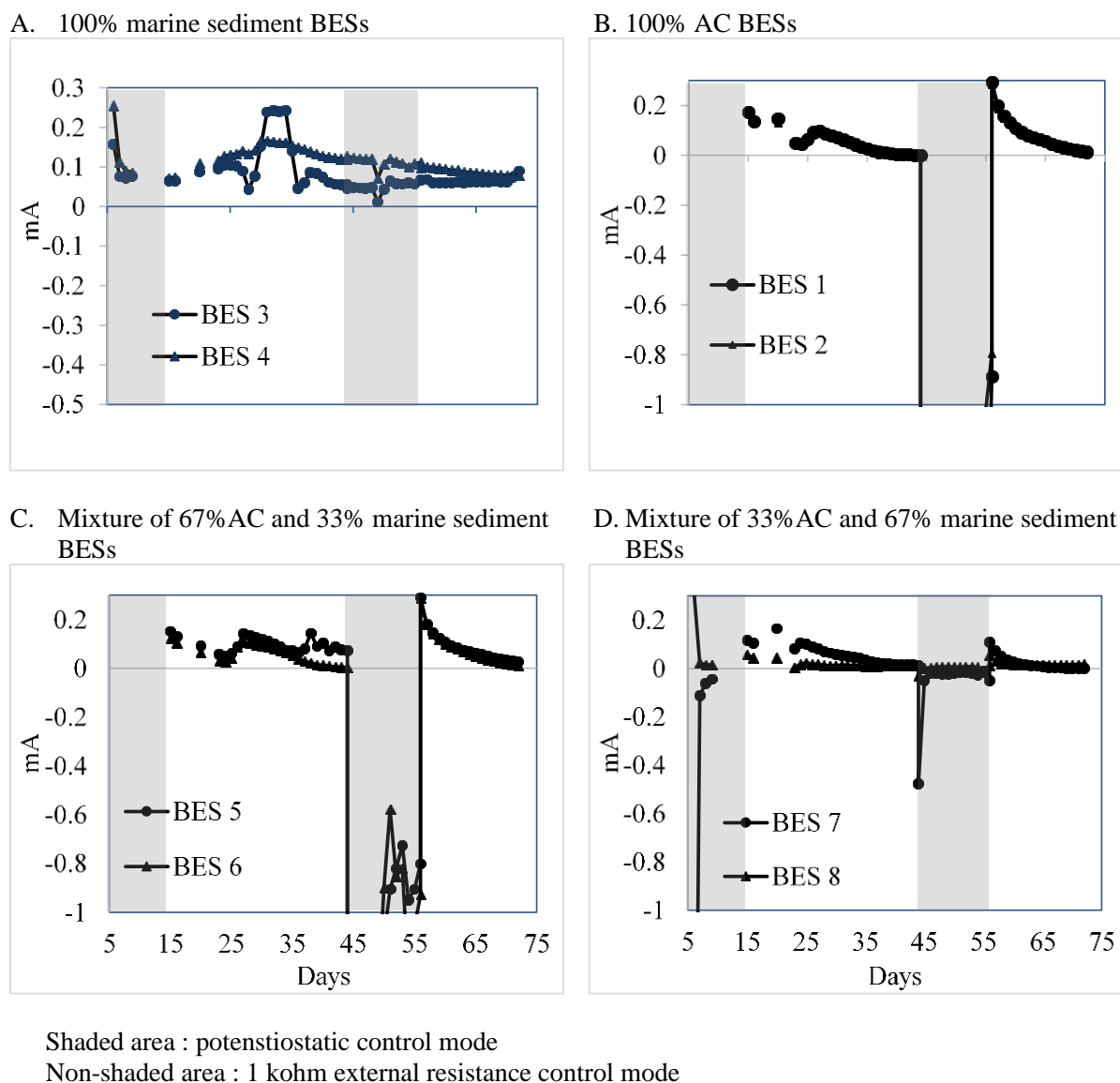


Figure 2. 2: Average daily current generation on different control modes for (A) 100% sediments BES 3&4, (B) 100% AC BES 1&2, (C) mixing 67% AC BES 5&6, (D) mixing 33% AC BES 7&8

In the studied 100% marine sediment BESs, just 2 small solid graphite sticks were used as both current collector and as anode electrode. These current collectors (0.00252 m^2 each) were vertically placed at both sides of the anode compartment with 18 cm distance (*Figure 2. 1*). The open space between the current collectors was filled with marine sediment. The electricity was generated within the bioanode while electrons were collected via the current collector. It is known that marine sediment can have apparent conductive properties which can also support transfer of generated electrons and/or ions from the bacteria in the sediment to the current collector [97,98]. Possibly that this phenomena was also apparent within this studied BES; however this was not further validated.

The recharging time of the bio-battery does depend on the fuel content and its usage. Assuming, a typical 2% TOC value as glucose as maximum available “fuel” to run an MFC filled with marine sediment, one can estimate the time after which the sediment has to be renewed. According to the TOC content and the extracted current of 0.1 mA in these studied BESs (26.3 mA/m² land use area or 154 mA/m³ anode volume), the MFC would run for 21 years assuming a low 10% Columbic efficiency. Of course also all used-material should hold this durability (*Supplementary Table S2. 3*). Long term experiments should be done to further clarify the durability of the bio-battery and clarify if all fuel is used over time. In case the current would be enhanced, the refill-time of the bio-battery would decrease significantly as show in (*Figure 2. 3*). By direct instalment of the MFC within the marine sediment, the MFC can warrant a prolonged electricity generation. Evenly plants like *Spartina anglica* can be integrated which will provide additional fuel via rhizodeposition and other loss of organic parts (e.g. via littering). Under natural conditions such planted marine sediment MFC located within a climate chamber has an estimated theoretical output between 0.14 and 0.34 W/m² depending on the plant growth [96].

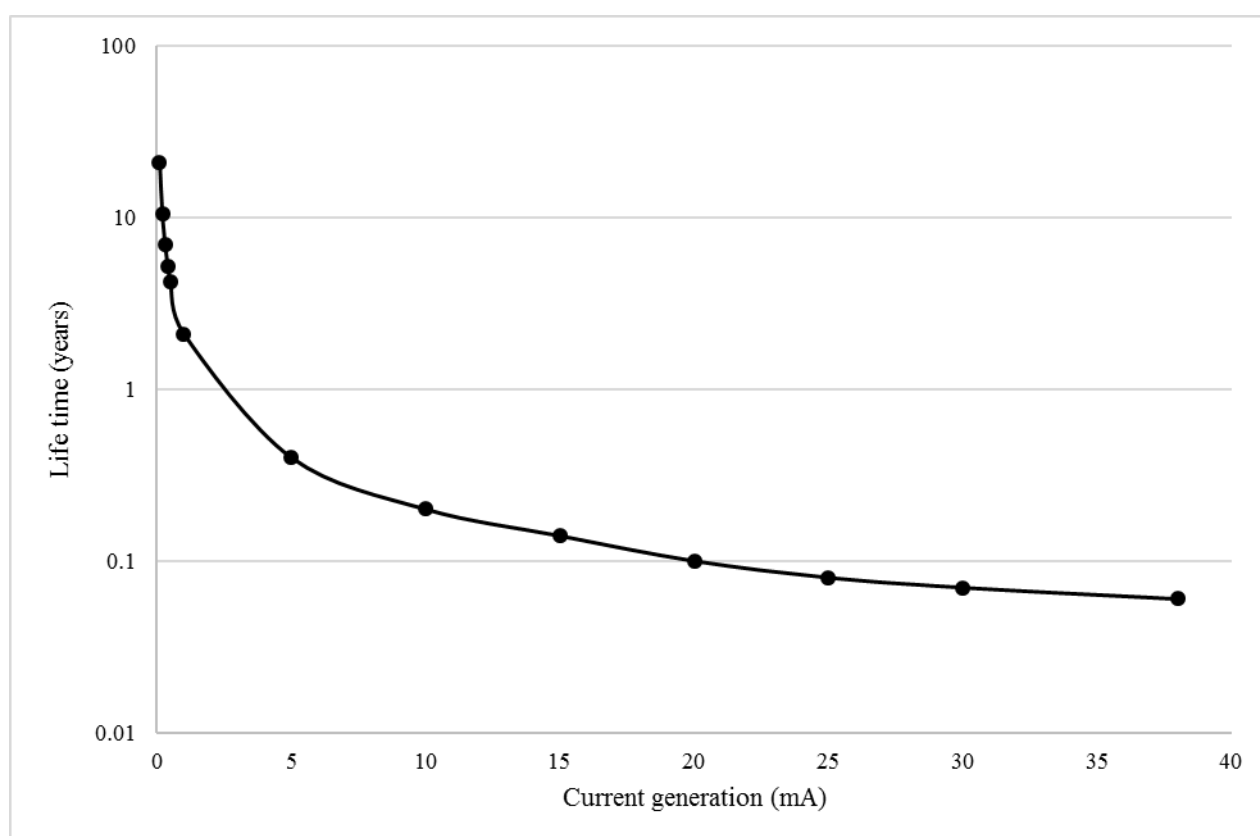


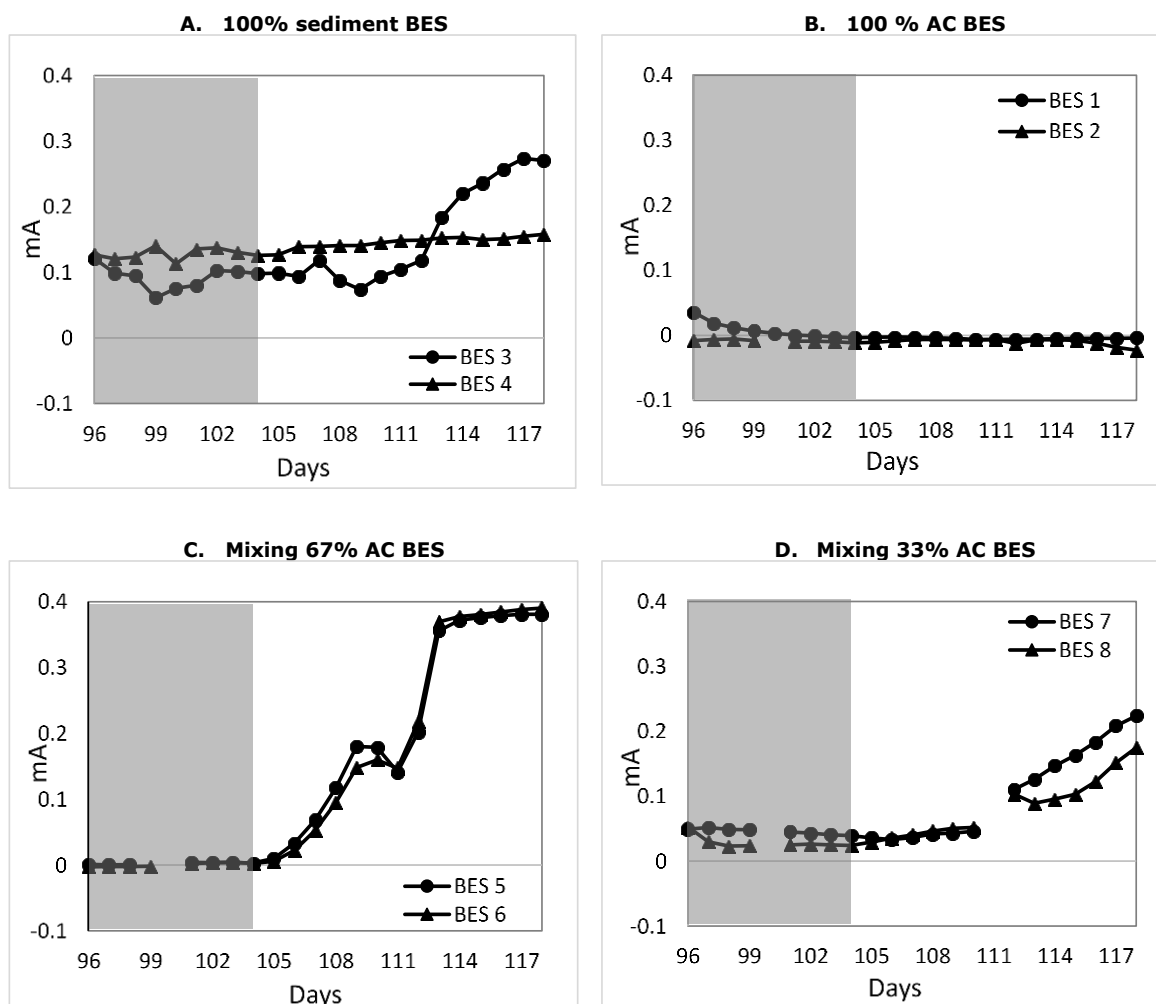
Figure 2. 3: Estimation of bio-battery lifetime based on current generation

2.3.2 Activated carbon granules have capacitive behaviour that allows external electricity storage in microbial medium electrolytes

Activated carbon based packed granular electrodes are suited as electrode material in both bioanodes as well as biocathodes [86,99,100]. Activated carbon is also used in super capacitors to store electricity [101]. However, to our best knowledge the role of these electrodes materials in saline microbial medium electrolytes is not investigated. The experimental result shows that the BESs with a 100% AC based anode (BES 1 & 2) is not able to generate electricity with just inoculum and no electron donor supply. This result can be clearly seen during long term operation with an external load (day 35 to 44) of BES 1 & 2 (**Figure 2. 2B**). Even after adding 2 g/L acetate on day 105, these BESs did not producing any current (**Figure 2. 4B**); possibly due to decay of the earlier supplied inoculum or absorption of nutrients on the AC may have limited the current generation. As such, these BESs acted as control experiments to validate the role of AC as electric charge storage material. During potentiostatic control (day 5 to 14 and day 44 to 55) the envisioned anode was actually acting as a cathode and electrical energy was added to the system at a controlled electrode potential of -100 mV (vs. Ag/AgCl). When the control mode was switched from potentiostatic control to external load (day 15 to 44 and day 56 to 72), BES 1 and 2 did generate a spontaneous anodic current starting at an electrode potential of 480 mV. In the later period, the current dropped harmonically towards zero until the electrode potential reached 14 mV. This phenomenon was evaluated as a kind of long-time charging (up to 11 days) and discharging (up to 29 days) behavior. The result shows that AC granules within anolyte medium are chargeable using externally supplied energy (i.e. electrical power) of which electricity was recovered later on. We assume that the inoculated electrochemically active bacteria did not play a crucial role during the charging and discharging while no electron donor was supplied. Still, microorganisms can do have capacitive properties which may affect the charge/discharge behavior [102]. The AC acted seemingly as a double layer chargeable capacitive electrode within a microbial growth medium electrolyte. This showed that bidirectional electron transfer was occurring within these systems. The nature of this electron transfer is in both directions (possible both bio- and electrochemically). The further mechanisms responsible for this need further clarification.

For BES 1 and 2 respectively, the charge recovery was 2.6% and 2.5% while the energy recovery was 0.29% and 0.26% resulting in an energy storage density of 22 kJ/m³ anode volume (0.02 Wh/kg used AC). This energy storage density is several order of magnitude lower than microbial rechargeable battery using acetate as the main energy carrier [103] or already optimized AC based super capacitors [101]. During discharge, an oxygen reducing cathode was used consisting of graphite felt. The same

electrode was used for a likely water oxidation reaction during the charging period. This graphite electrode was not specifically designed for both processes. The overall efficiencies are still low and need further investigation and optimisation, for instance on counter electrode and redox couple, to maximise the storage capacity.



Shaded area: before adding acetate; Non-shaded area: after adding acetate

Figure 2. 4: Effect of adding acetate on two weeks average daily performance at 1 kOhm

2.3.3 Combining marine sediment with activated carbon (AC) granules generates in-situ electricity and provides external supplied electricity storage in a bio electrochemical system (BES)

Bio electrochemical systems (BES 5, 6, 7 and 8) were also operated while combining marine sediment with activated carbon. After 156 days of operation, the marine sediment with AC BESs proved the

capability to generate electricity and storage of externally supplied electricity (**Figure 2. 2C & D & Figure 2. 4 C & D**). On the long term performance (until day 105) without adding additional substrates (acetate), the BESs current generation dependent on the sediment fraction. **Supplementary Table S2. 2** provides the average performance after long term MFC operation of the various BESs. Adding sufficient AC was beneficial to increase electricity generation. The highest current and power density were obtained with BES 5 & 6, which contained 67%AC and 33% sediment. The BES 7 & 8 with a lower AC content of 33% resulted in a reduced electricity generation with 50% at a range comparable with BES 1&2 which contained only sediment. Apparent sufficient AC must be added to create a benefit of the material; this finding is in line with earlier work that also showed that 67% of granular electrode material applied in soil MFCs was most beneficial [83]. The BESs were also temporarily poised at -100mV (similar to the BES with 100% activated carbon) to store external supplied electricity. A similar long charging/discharging phenomenon as compared to the 100% activated carbon (**Figure 2. 2 B**) was observed with 67%AC based BESs (**Figure 2. 2 C**) and 33%AC based BESs (**Figure 2. 2 D**) but was not shown with the 100% sediment anode BESs (**Figure 2. 2 A**). This result supports that activated carbon still had its capacitive chargeable behavior once mixed with marine sediment. The electricity could be stored for a long term period (10-20 days) while discharging took the same period. The observed phenomenon could possibly be exploited in-situ, within marine sediments mixed with activated carbon based BES, allowing e.g. (intermittently produced) electricity storage. Once the observed charge/discharge effect is combined with an electrorophic and electrogenic biofilm (operating at a sufficient low voltage range)[104]; additional current could be also stored in microbial metabolites like CO or even acetate [103].

For a better understanding, the explanation of storage capacity phenomena will be further discussed for the period between day 44 and day 72. During the potentiostatic control (day 44 - 55), anode voltage was kept at -100mV because theoretically a more positive anode potential will help bacteria to gain more energy per electron transfer than a lower one [105]. As can be seen, during potentiostatic control only the 100% sediment BESs were able to generate electricity (see **Figure 2. 2 A**). While for the other BESs which did not generate current, their anode was receiving and storing electrons driven by the potentiostat (**Supplementary Figure S2. 1 & Supplementary Figure S2. 2**). From **Figure 2. 2**, one can see the more AC carbon fraction in the anode, the more negative i.e. cathodic current generation was observed. On day 56 when the control mode was switched to external load (MFC mode), stored electrons were released.

Current generation for 100% AC based BESs (1&2) increased from about -1.7 mA to 0.28 mA and for 67% AC based BESs(5 & 6) increased from about -1 mA to 0.29 mA while for 33% AC based BESs(7 &8) increased from -0.05mA to 0.1 mA and from 0.01mA to 0.05mA, respectively. This supports that the storing capacity has a positive correlation with the amount of AC in the anode. After 16 days operation with external load (1000 ohm), on day 72 the current of all AC BESs decreased towards 0 mA, reaching a complete discharge. Similar phenomena were also observed during day 15 to day 45.

Furthermore, acetate addition to the all sediment containing BESs enhanced current generation except for 100% AC based BESs (*Figure 2. 4*, day 105). The sole AC BESs was producing zero current before and after acetate addition. For the sediment containing BESs, this enhancement indicates a substrate limitation (concentration or availability) in which the electrochemically active bacteria in the anode cannot utilise more complex remaining substrates from the sea sediment because of different microbial metabolism [106]. Added acetate is possibly utilized by the EAB which enhances their growth resulted in increasing current generation. Result of this research also indicated that 67%AC based BESs perform better compared to other BESs in this research. However, it remains unclear why the duplicate of only sea-sediment BES behaved differently upon the acetate addition.

2.3.4 Internal generated electricity storage is feasible in AC granules mixed with marine sediment BES

Capacitive bioanode electrodes can store internally generated electrons (obtained from the supplied fuel) within the double layer and/or capacitive biofilm of the bioelectrode [91]. The experiments, as explained before in a long term operation, showed that externally supplied electrical energy can apparently be stored in AC granules mixed with sea-sediment BESs. Considering this capability, further experiments were conducted to understand effect of AC granules marine sediment mixture on electricity storage from the internal source (i.e. the sediment itself). Experiments were conducted within two periods. The first period was before adding acetate (between day 72 and day 96) and the second one was after adding acetate (between day 118 and day 156). In these sets of experiments, internal charging was executed by setting the BESs at open cell voltage condition. Discharging was performed at constant controlled anode potential (65mV vs Ag/AgCl). Various charging times (CT) and discharging times (DT) were applied to identify feasible conditions for internal electricity supply and storage. The overall results did show that internal charging is feasible; although the phenomenon was depending on the type of electrode and composition of sediment and AC as further discussed.

Figure 2. 5 shows a typical response of storage behavior. Here the first cycle had an OCV of 4 hours before the experiment was started and a DT of 120 sec, which was followed by 39 charge & discharge cycles of respectively 60 and 60 seconds. During discharge the average maximum current of the 40 cycle was 9 mA while the average stable current was 6mA. During OCV the anode potential dropped repetitively with 10 mV. Based on 40 cycles experiment, the average stored charge on last 10 cycle was determined at 19.3 mC. In some experiments (as shown in **Figure 2. 5**), the first cycle had a higher current than the consequent repetitive cycles; this was in-line with a longer OCV time used for the first cycles. An observation linked to this was the apparently higher drop of anode potential. The anode potential during OCV drops over time. Theoretically, the EAB will generate electrons which polarise the electrode to more reduced conditions by reducing redox compounds and/or by direct electrode reduction and consequent accumulation of electric charge in the double layer of the bioelectrode. Also possible pH/salt gradients which negatively affect the anode potential may start to disappear [53]. After connecting the electrical circuit, the electrons will be released during discharging process. During the first cycle phenomena, the OCV is providing more time to create reducing conditions and allow a higher current. After repetitive applied OCV, more stable conditions arise which allow a stable discharge phenomenon.

Various experiments show successful and unsuccessful charging behaviors. **Table 2. 2** provides the overview of all conducted experiments with all key properties (**Table 2. 2 : A.** Highest current; **B.** Stable current; **C.** Anode potential drop; & **D.** Stored charge). In the first phase experiment, BES 8 (e.g. exp. 1c; 33% AC - 67%sediment) was the first marine AC based bioanode which showed a self-charging and storage capability. The stored charge from the applied CT of 180 seconds was 2.3 mC (exp.1c). All other BESs with AC within the bioanodes (BES 1, 2, 5, 6, & 7) were not able to discharge current (see all red in **Table 2. 2 A & B**). Instead, the BESs were externally charged by the potentiostat at 65mV. This was shown by the negative (or zero) current both at the beginning of discharge period (average highest current on the last 10 cycles) and at the last period of discharge (average stable current on last 10 cycles). Thus unsuccessful self-charging in the first experiment could be caused by the low current generation as can be seen from day 72 when the first period was started, which was only 0.02mA, from the anode of 67% and 33% AC BESs (**Figure 2. 2 C & D**). Such possible relatively short self-charging period (10-180 second), could be insufficient to (fully) charge a high capacitive AC anode [101].

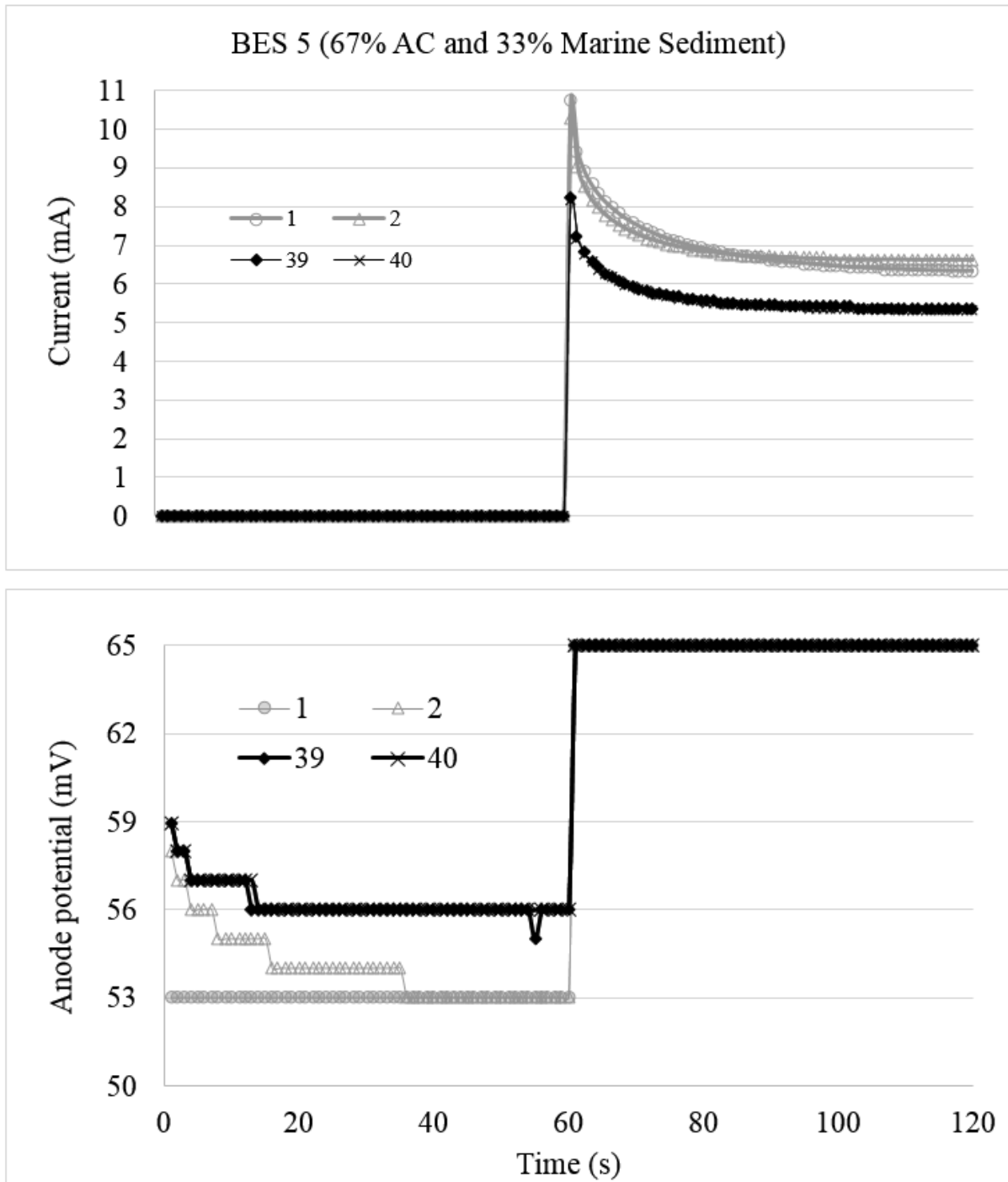


Figure 2. 5: First cycle phenomena at CT 60 sec and DT 60 sec on day 142. The first two cycles and the last two cycles of experimental results were shown

Table 2. 2: Internal generated electricity storage experiment

Exp no.	CT	DT (sec)	Cycles	Exp Day	A. Highest current as average from the final 10 cycles (mA)*								B. Stable current as average from the final 10 cycles(mA)*							
					BES 1	BES 2	BES 3	BES 4	BES 5	BES 6	BES 7	BES 8	BES 1	BES 2	BES 3	BES 4	BES 5	BES 6	BES 7	BES 8
1a	60	3780	40	75	-0.4	-0.5	0.1	0.1	-0.2	-0.3	0	0	-0.4	-0.5	0.1	0.1	-0.2	-0.3	0	0.03
1b	60	3780	40	78	-1.0	-1.1	0.9	1.1	-0.7	0.6	0	0.1	-0.7	-0.6	0.1	0.1	-0.2	0.2	0	0.02
1c	180	3780	40	83	-2.3	-1.1	1.8	2.2	-1.2	-1.4	0	0.1	-1.8	-0.6	0.1	0.1	-0.4	-0.6	0	0.03
1d	10	3780	40	90	-3.1	-1.2	0.3	0.3	-0.6	-1.3	0	0	-2.5	-0.7	0.1	0.1	-0.2	-0.6	0	0.02
2a	10	3780	40	127	n.a	n.a	2.3	1.3	8.0	7.5	1.5	0.9	n.a	n.a	0.7	0.4	5.8	5.8	0.9	0.6
2b	60	3780	40	133	n.a	n.a	5.9	3.4	4.2	3.9	1.7	1.4	n.a	n.a	0.7	0.4	2.6	2.4	0.0	0.6
2c	10	180	40	138	-6.3	-8.4	3.5	1.8	39	27	9.2	1.9	-6.3	-7.2	1.0	0.5	28	23	6.3	1.2
2d	60	180	40	138	-3.3	-9.5	9.0	4.4	39	42	6	2.4	-7.3	-5.4	1.0	0.5	22	38	3.1	1.0
2e	60	180	40	141	-0.6	-3.3	7.7	3.4	7.3	4.5	2.0	1.7	-0.4	-2.5	0.9	0.4	4.6	3.4	1.0	0.7
2f	3600	3600	10	141	2.3	0.0	18.0	22.1	9.2	3.9	6.2	11	1.8	0.2	1.0	0.4	3.7	2.6	1.0	0.6
2g	60	60	40	142	1.7	0.6	9.6	4.3	8.4	3.7	4.5	2.9	1.6	0.4	1.2	0.5	5.4	2.8	2.3	1.3
2h	10	10	40	142	1.1	0.7	4.2	1.8	7.7	3.5	4.0	2.6	1.8	0.5	1.4	0.6	5.8	2.9	2.7	1.7
2i	3600	1080	15	142	1.3	0.3	17.2	n.a	n.a	0.9	n.a	8.0	1.3	0.1	0.8	n.a	n.a	0.5	n.a	0.4
2j	3600	3600	15	142	n.a	n.a	n.a	22.7	4.9	n.a	5.8	n.a	n.a	n.a	n.a	0.4	2.0	n.a	1.0	n.a
					C. Anode potential drop at open circuit from the discharge voltage from the final 10 cycles (mV)**								D. Average stored charge from the finals 10 cycle (mC)***							
1a	60	3780	40	75	-1	-1	221	125	-1	-2	-1	2	n.c	n.c	1	0.9	n.c	n.c	n.c	0.8
1b	60	3780	40	78	-1	-2	126	68	1	17	0	1	n.c	n.c	5	4.7	n.c	n.c	n.c	0.5
1c	180	3780	40	83	-2	-1	188	99	-2	-7	0	1	n.c	n.c	13	14	n.c	n.c	n.c	2.3
1d	10	3780	40	90	-3	-1	131	88	-4	-16	-1	1	n.c	n.c	0.6	0.9	n.c	n.c	n.c	-0.1
2a	10	3780	40	127	n.a	n.a	251	156	39	73	18	27	n.a	n.a	8.2	3.9	151	348	7.3	13
2b	60	3780	40	133	n.a	n.a	273	186	13	62	21	42	n.a	n.a	34	21	112	68	45	35
2c	10	180	40	138	-18	-38	576	531	171	177	486	509	19.0	-97	7.1	4.2	117	36	33	6.8
2d	60	180	40	138	-8	-21	539	488	130	152	229	396	-26	-152	34	19	275	129	39	23
2e	60	180	40	141	-1	-4	315	206	9	8	18	44	-1.3	-6.7	30	14	23	14	13	15
2f	3600	3600	10	141	0	-3	483	443	16	11	59	240	483	-119	893	545	238	657	1531	1600
2g	60	60	40	142	1	0	502	470	12	7	75	303	57	0.05	35	15	19	7.7	16	15
2h	10	10	40	142	1	0	446	357	11	7	43	89	5.2	0.3	5.4	2.4	3.8	1.1	2.5	1.8
2i	3600	1080	15	142	2	0	492	n.a	n.a	7	n.a	191	4085	4.7	785	n.a	n.a	616	n.a	1406
2j	3600	3600	15	142	n.a	n.a	n.a	442	12	n.a	64	n.a	n.a	n.a	n.a	539	119	n.a	1389	n.a

DT = Discharging Time; CT = Self Charging Time ; n.a = not available ; n.c = not calculated

First phase (non shaded): Before adding acetate; Second phase (shaded): After adding acetate; * a positive current means that charge was recovered; a negative current shows that charge was supplied and not recovered; ** a negative value means that anode potential

increased, while the positive values means that the anode potential decreased; *** a positive value means that self-charging from the anode worked while a negative value means that no charge was recovered due to negative or zero current.

BES 1 & 2= 100 % Activated Carbon (AC)

BES 3 & 4 = 100 % Marine Sediment (MS)

BES 5 & 6 = 67 % AC & 33% MS

BES 7 & 8 = 33% AC & 67% MS

Internal charging with AC marine bioanode was feasible with well performing bioanodes. With the insight of the first internal charging experiment, we executed second round of experiments after acetate addition; allowing further bioanode development and availability of more electrons for self-charging. These experiments were started after the BESs showed current. The AC mixed with sea-sediment BESs (0.17 – 0.35 mA) and also non-mixed sea-sediment BESs (0.16-0.27 mA) were generating the highest current (*Figure 2. 4*).

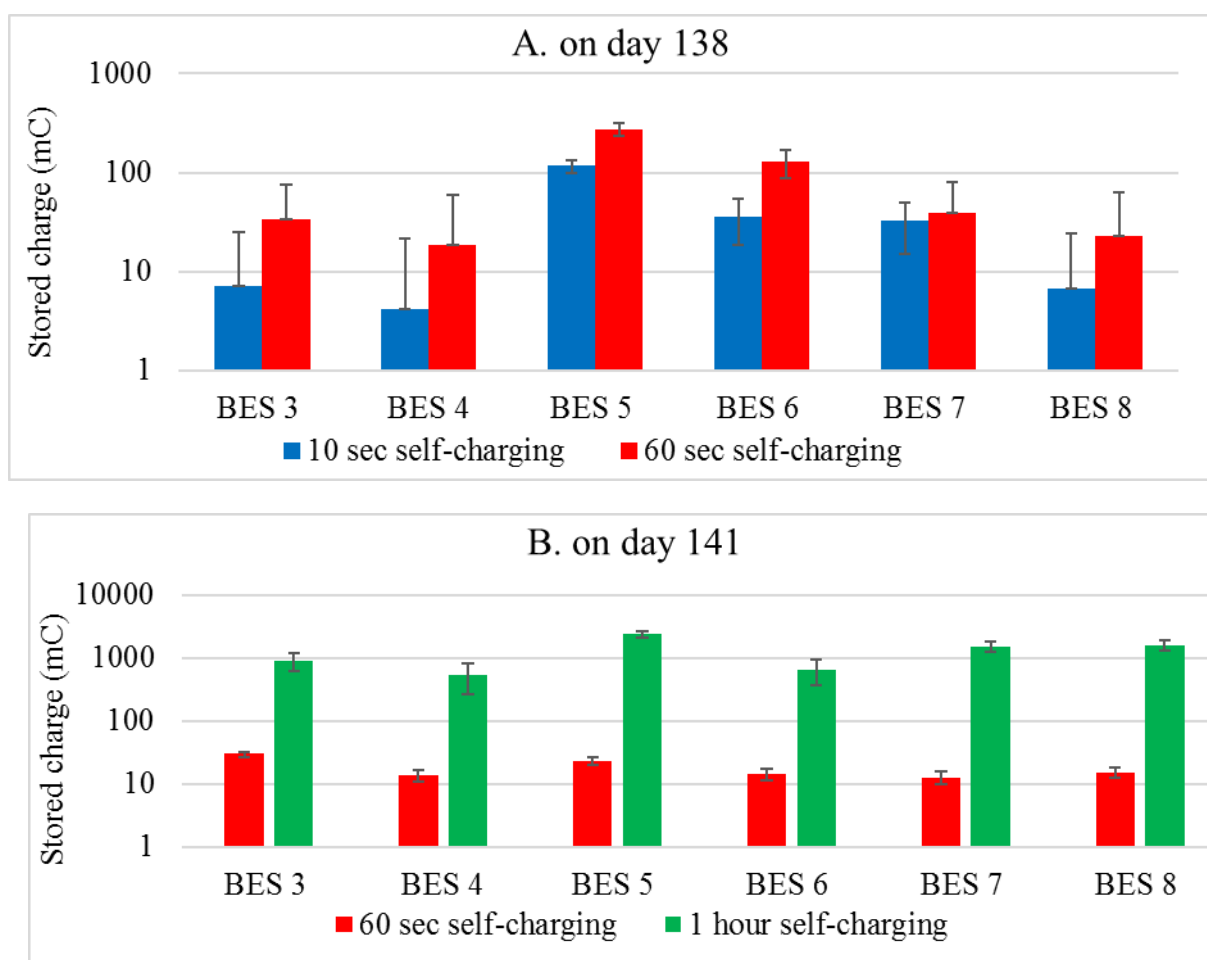
After the addition of acetate and start-up of the bioanodes, the second period of self-charging experiments was conducted. Self-charging and storage was evidently shown with 33% and 67% AC bioanodes as well as the 100% marine BESs. The charge storage capacities were all positive for these electrodes as shown by the available data of the average stored charge in shaded area from *Table 2. 2 D* (experiments 2a until 2j). For the 100% AC bioanode (BES 1&2), self-charge and storage was most evidently observed at the end of the experiments on day 142 (e.g. exp. 2i) which was probably related due to the later start-up. During the OCV period of self-charging, the anode potential will typically drop because of EABs activity and charging of the double layer. The speed of anode potential drop is influenced by the capacitive properties of the anode material [91]. The more capacitive the anode, the slower the anode potential drop will be as more charge can be stored at a specific energy level (i.e. potential). Therefore, for a non-capacitive electrode, the anode potential drop will faster approach the average i.e. stable open cell anode potential. This theory was in line with the presented experimental results in *Table 2. 2C* for e.g. day 142. The anode potential drop was for the same CT time, the highest with 100% sediment BESs (3&4) and dropped with increasing AC content from 33% AC BESs (7&8), 67% AC BESs (5&6) to 100% AC BESs (1&2).

The successful self-charging and storage experiments support that chemical energy from the marine sediment and/or acetate was utilized with the EAB and used for self-charging of capacitive activated carbon bioanode during open circuit. This result is in line with single granule AC bioanode performance which showed electricity storage [88]. In this experiment we also found out that the

sediment BESs were also able to store electricity (see e.g. **Table 2. 2**. Exp.2h). Evidently, this kind of self-charge and storage capability behaviour could not be due to activated carbon since this material was absent. This could indicate other storage mechanisms in the sediment. One possible mechanism is that in the marine sediment easily accessible redox compounds exist which can take-up released electrons during self-charging time and release them during discharging time. For instance during the self-charging, the released electrons from EAB can reduce NAD^+ into NADH [107]. When discharged at high anodic potential (65mV), NADH can be oxidised back to NAD^+ and release electrons. Another possible mechanism is the existence of sulphate reducing bacteria (SRB) and sulphide oxidising bacteria (SOB). SRB are able to reduce sulphate into sulphide or elemental sulphur and later on the SOB can oxidise sulphide and elemental sulphur back to sulphate [108,109]. Both species are naturally present in marine sediment and known to be able to have syntrophic growth during oxygen limitation [110]. Sulphide oxidation was also proven to generate electricity in both a mixed culture [111] and a pure culture [112] MFC system with the electrode as an electron acceptor. Therefore, the metabolism of the SRB and SOB could play a role in delivering and taking up electrons while storing them via intracellular storage compounds. Naturally present humic substances in the marine sediment, such as humic acid and fluvic acid, could also involve in the charge storage [113]. The humic substances could serve as electron shuttles in the marine sediment BES. Microorganism could transfer the electrons to the humic substances, then the reduces humic substances can rapidly reduce iron (III) oxides [98]. The self-charge and storage capability could also be quinone based compounds [114]. The anode potential drop was much higher with pure marine sediment bioanodes (more than 300mV) than the AC based electrode. This phenomenon shows the absence of activated carbon double layer capacitance as can be seen from experiment 2h on **Table 2. 2C**. We can expect that during the applied OCV the anode condition change. Earlier work on the electrochemical characterisation of comparable BESs (Plant-MFCs) explained that anode and membrane resistance decrease during current interruption [53]. As such, a lower internal resistance due to an OCV would lead to a temporarily higher current as observed with the self-charging experiment. To what extent the enhanced current was due to internal resistance changes and/or a potential sediment capacitive or other biological storage mechanisms was not assessed.

During the second phase of self-charging experiments, the effect of self-charging time was investigated by conducting electricity storage experiment on three different self-charging times (10 sec; 60 sec and 1 hour). The experiment was conducted on day 138, day 141 and day 142. On day 138, 10 sec and 60 sec self-charging times with same discharging time (180 sec) were performed. On day 141, 60 sec and 1 hour self-charging time with 180 sec and 1 hour discharging times, respectively,

were carried out. Finally, on day 142, 10 sec, 60 sec and 1 hour self-charging times were executed with 10 sec, 60 sec and 3 hours discharging time, respectively. In the self-charging experiments, stored electric charges must be generated by the bio anode of BES. We noticed that storage properties were not constant over time although the same CT and DT were applied (e.g. **Table 2. 2D** exp 2d & 2e). Here the comparison of the results of the self-charging effect on stored charge was presented on the basis of each day of the experiment (**Figure 2. 6**). BES 1 and 2 were excluded from discussion because they were not fully started up yet. The BES 1 and BES 2 started to generate current on day 141 right after the long charging-discharging period (**Table 2. 2B**, experiment 2f). This current generation was considered due to a long charging effect from external sources as described earlier in the section 3.2.



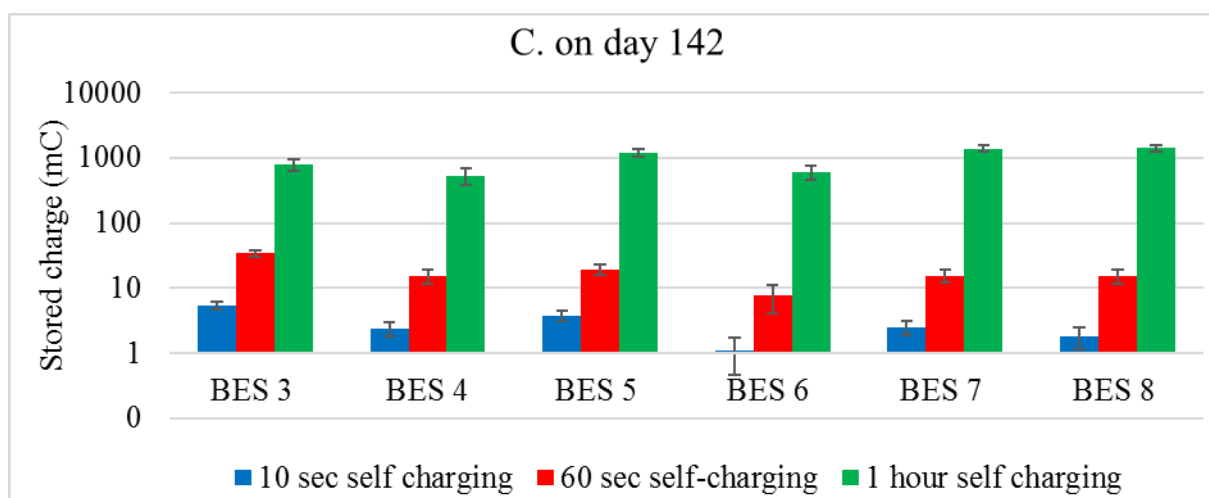


Figure 2. 6: The effect of charging time on stored charge (mC)

A long self-charging time up to 1 hour enhances charge storage. Based on results on **Figure 2. 6** one can see that for each BES the self-charging time has a positive correlation with stored charge. Stored charge increased when self-charging time was prolonged. Changing self-charging time from 10 sec to 60 sec (**Figure 2. 6 A & C**) did increase stored charge between 1.2 and 9 times. Increasing the self-charging time with 60 times (from 60 sec to 1 hour; **Figure 2. 6 B & C**) increased stored charge between 22 and 40 times for the marine BESs 3 and 4, and 45 to 120 times for the AC marine bioanodes of BESs 5, 6, 7, and 8. The increase of stored charge for the AC bioanode did increase with several orders of magnitude which illustrates that even more charge could be stored. The self-charging bioanode had a maximum measured storage capacity of 2,383 mC (**Table 2. 2**, exp 2f. BES 5) which corresponds to a volumetric storage of 3,666 C/m³ anode which enables electrons release at an anode energy level of 65 mV vs Ag/AgCl. If we take a hypothetical cell voltage of 0.2V, this would represent an electrical energy density of 0.3 mWh per kg mixed anode which is about 33,000 times lower than a super capacitor which can store up to 10 Wh per kg [115]. Furthermore, it is remarkable that the marine sediment BES acts like a capacitor similar to the charge storage behaviors as AC based bioanodes with a maximum volumetric storage of 1,373 C/m³ anode at a charge recovery of 57%. Taking the same hypothetical cell voltage of 0.2 V, this charge storage represents a potential capacitive battery energy property of 0.05 mWh per kg marine sediment.

At a short self-charging time, a higher percentage of AC enhanced stored charge. Based on an overview graph of all results (can be downloaded from provided link at the supplementary data) on the final 10 cycles on all electricity storage experiment, it can be seen that the number of measured charge was from the highest to the lowest as follows: 67% AC anode, 33% AC anode and 100%

sediment (0% AC) anode. On the other hand, the effect of anode composition on stored charge is influenced by self-charging time. At short self-charging time (10 sec & 60 sec) the effect of anode composition on stored charge is following the pattern of measured charge (**Figure 2. 7A**). However at longer self-charging time (1 hour) stored charge on different anode compositions are relatively the same (**Figure 2. 7B**).

Figure 2. 7 explains the influence of the anode composition on the stored charge. It shows the average stored charge from the duplicated BESs, namely 67% AC (BES 5 & BES 6), 33% AC (BES 7 & BES 8), and 100% Sediment (BES 3 & BES 4). The storage properties of different anode compositions in **Figure 2. 7** should be compared according to the experimental day because the current output of each BES varied from one day to another day. . Therefore, a comparison between self-charging time at 10s and 60 should not be evaluated from day 127 and day 133 but from day 138. Remarkable is that at shorter time more AC presences (67%) is enhancing the storage capability. On the other hand, at longer self-charging time the 100% marine sediment anode is seemingly able to store a similar amount of electric charge as much as in 67% and 33% AC anodes.

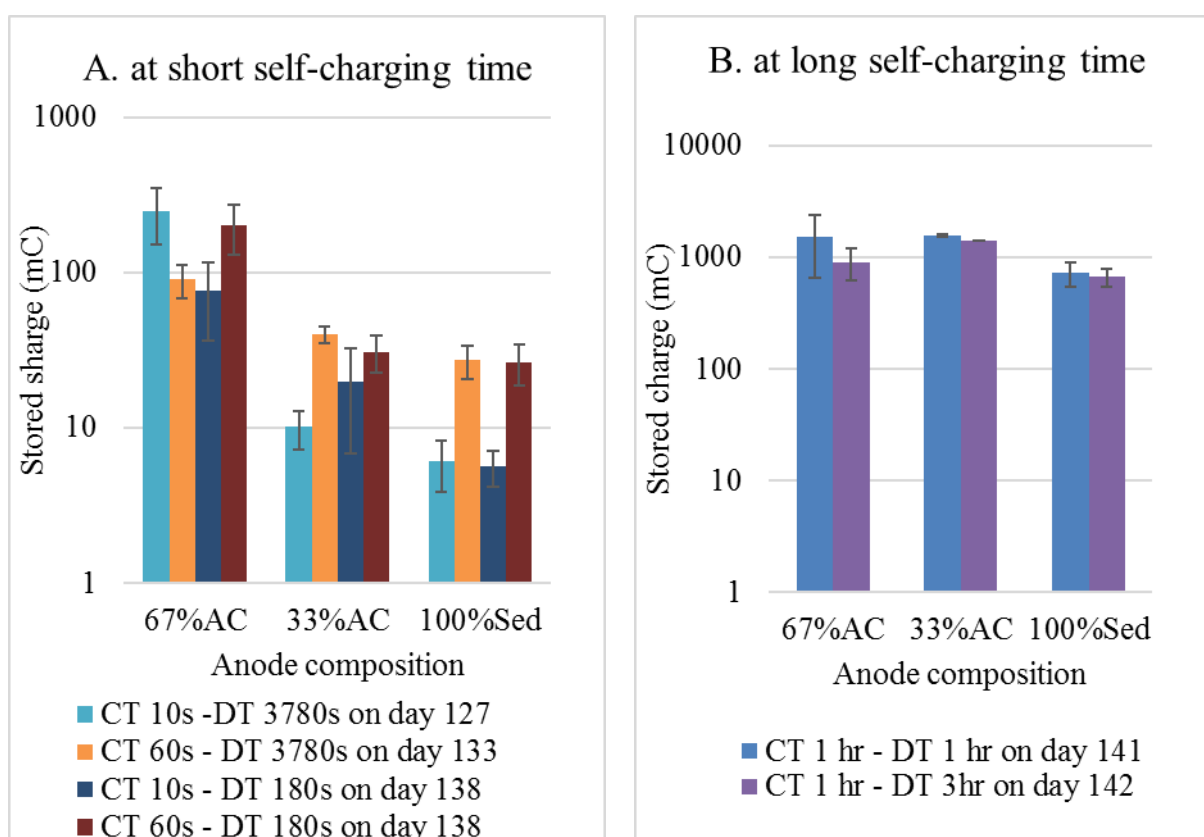


Figure 2. 7: Effect of anode composition on stored charge at different charging and discharging

2.4 Conclusion & Outlook

The study showed that marine sediment and activated carbon were able to store and generate electricity which is of possible use in rechargeable bio-batteries. The Dutch marine sediment was a suitable fuel to generate electricity. Installing this system within real outdoor sediments could warrant a long life-time due to the continuous supply of fuel. The used activated carbon granules showed within a microbial medium electrolyte a capacitive behavior which allowed external electricity storage. Combining marine sediment with activated carbon granules allowed both electricity generation from the supplied sediment and provided external supplied energy storage. The energy recovery of the bio-battery was rather low but can be optimised by an improved counter electrode. It was also shown that internal charging (during OCV) of bioanodes is feasible with mixed activated carbon and marine sediment. Evenly the marine sediment itself showed a similar storage behavior although the mechanisms responsible for this are to be further revealed. Charging time up to 1 hours enhanced charge storage up $1,373 \text{ C/m}^3$ with a charge recovery of 57% and an apparent capacitive battery energy property of 0.05 mWh per kg marine sediment.

2.5 Acknowledgements

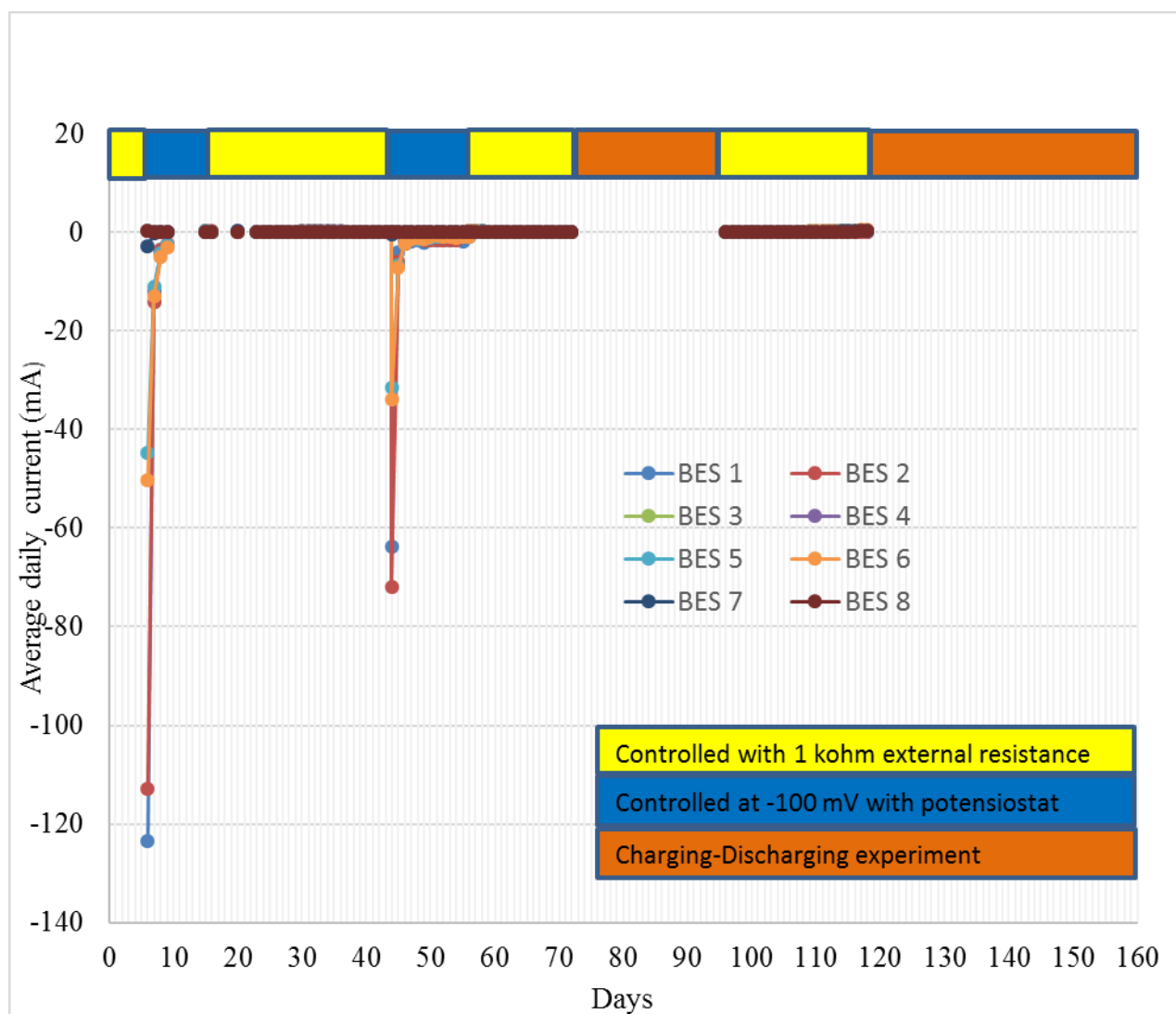
This research was financially funded by Government of Landak Regency, West Kalimantan Province, Republic of Indonesia under MoU with Wageningen University & Research No 6160030150.

2.6 Supplementary Materials Chapter 2

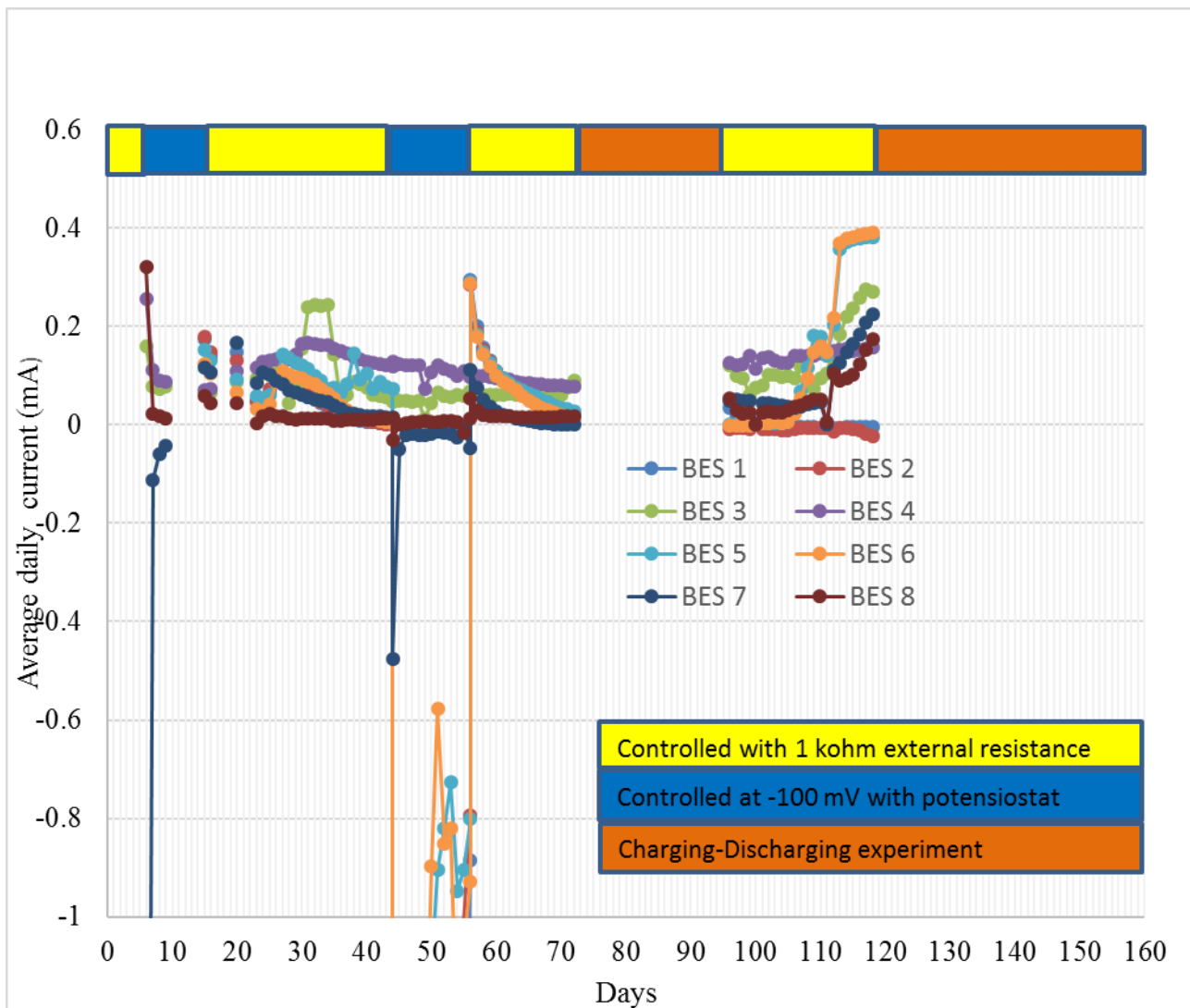
2.6.1 Supplementary Data

Raw iviumstat data from charging and discharging experiment and its overview graph can be downloaded from <https://easy.dans.knaw.nl/ui/home> via this DOI link: <https://doi.org/10.17026/dans-xed-8qkv>

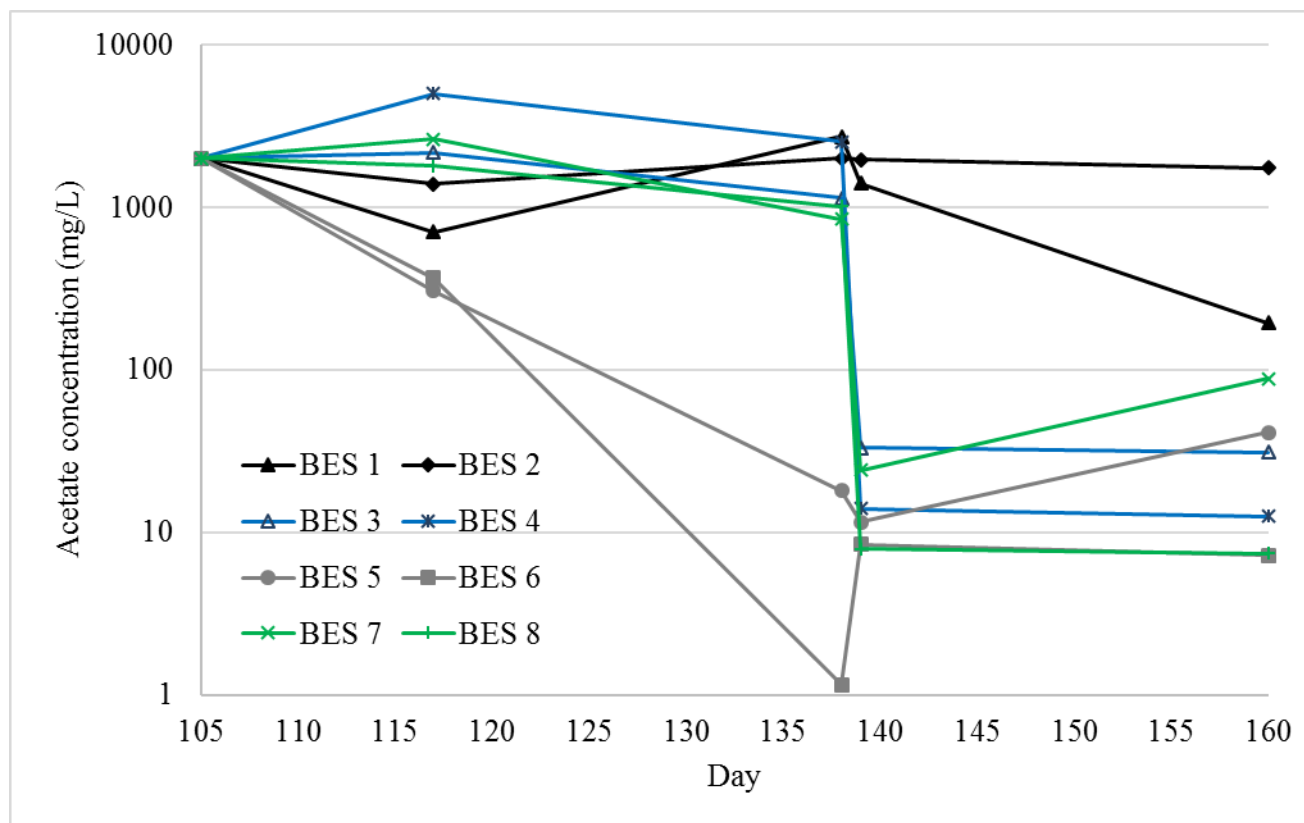
2.6.2 Supplementary Figures



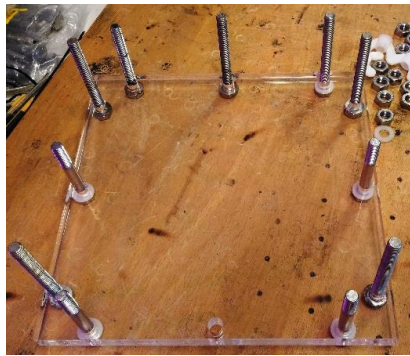
Supplementary Figure S2. 1: Average daily performance of all bio electrochemical systems (BESs) for the entire research period. Figure 2 and Figure 4 in the article are scale-modified from this original figure



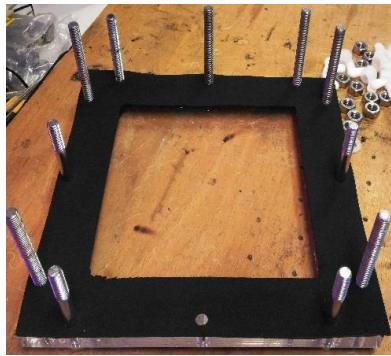
Supplementary Figure S2. 2: Average daily performance of all bio electrochemical systems (BESs) for the entire research period. In this figure to show a clear result on positive current from all BESs, the y-axis is cut between -1 mA and 0.6 mA



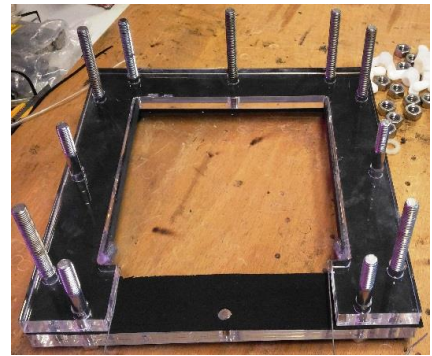
Supplementary Figure S2. 3: Acetate concentration in the anolyte of the BESs. At day 150, all BESs were injected with 2 g/L NaAc. After sampling on day 117, additional 2 g/L NaAc was added into BES 1 and BES 2



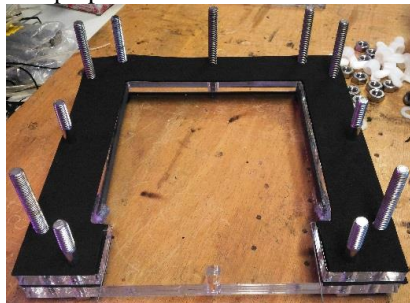
a. Solid end plate with bolts was prepared



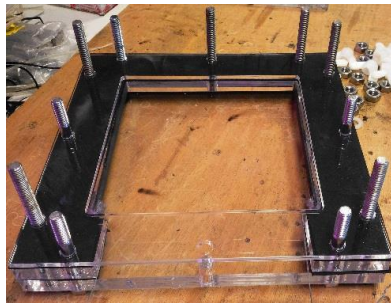
b. Black gasket was placed



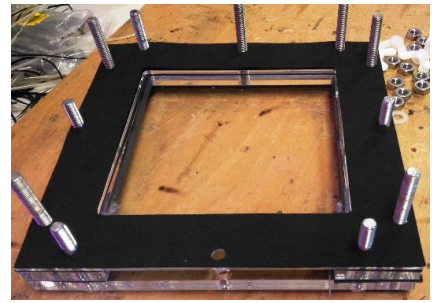
c. Anode plate was placed



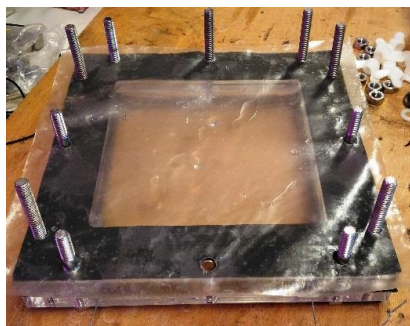
d. Black gasket was placed again



e. A support plate was placed



f. Another gasket was placed again



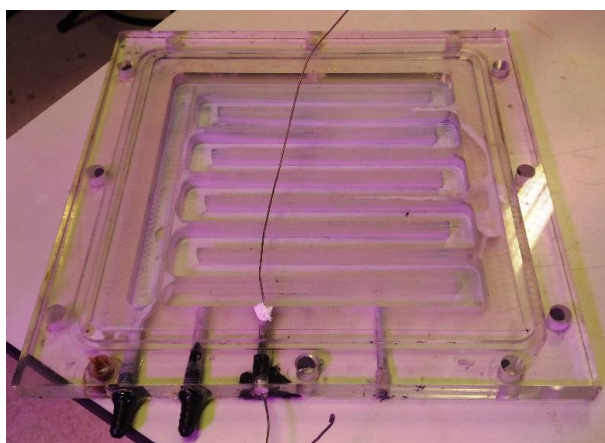
g. CEM was placed



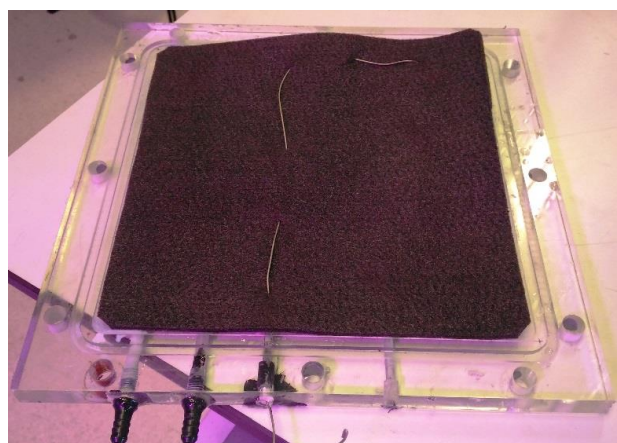
h. Gasket was placed again



i. Finally, cathode plate was placed and reactor was tightened up with the nuts



j. Cathode plate with winding channel



k. Graphite felt was woven with a current collector (Ti wire)

Supplementary Figure S2. 4: Stages of the BESs reactor preparation

2.6.3 Supplementary Tables

Supplementary Table S2. 1: Modified Hoagland Medium (Nitrate-less, sulphate-less, ammonium-bicarbonate-rich plant growth medium) composition used in this study

Compounds	Concentration (mg/L)
Macronutrients	
NH ₄ HCO ₃	553.43
CaCl ₂	222
NH ₄ H ₂ PO ₄	115.08
MgSO ₄ .7H ₂ O	123.24
KCl	223.68
NaCl	5000
C ₁₄ H ₁₈ N ₃ O ₁₀ Fe	10
Na ₂ SiO ₃ .9H ₂ O	142.10
Micronutrients (Arno-E)	
KCl	0.466
H ₃ BO ₃	0.193
MnSO ₄ .H ₂ O	0.042
ZnSO ₄ .7H ₂ O	0.072
CuSO ₄ .5H ₂ O	0.016
H ₂ MoO ₄ (85% MoO ₃)	0.01
NaFeDTPA (10% Fe)	1.498

Supplementary Table S2. 2: Average performance of the BESs reactors at the MFC mode from day 117 to 118 before the second charging and discharging experiment was performed

Properties	BES 1	BES 2	BES 3	BES 4	BES 5	BES 6	BES 7	BES 8
Anode Potential (mV)	95.91	104.93	-403.28	-303.29	-426.38	-438.56	-11.45	-269.42
Cell Potential (mV)	-4.40	-20.01	273.08	156.06	381.02	389.17	213.59	159.22
Current (mA)	0.00	-0.02	0.27	0.16	0.38	0.39	0.21	0.16
Current densities (mA/m ²)	-1.16	-5.27	71.86	41.07	100.27	102.41	56.21	41.90
Current densities (mA/m ³)	-6.76	-30.79	420.12	240.09	586.18	598.72	328.60	244.96
Power (mW)	n.a.	n.a.	0.07	0.02	0.15	0.15	0.05	0.03
Power densities (mW/m ²)	n.a.	n.a.	19.62	6.41	38.20	39.86	12.01	6.67
Power densities (mW/m ³)	0.03	0.62	114.73	37.47	223.35	233.00	70.19	39.00

Supplementary Table S2. 3: Calculation for bio-battery life time using TOC value of marine sediment. Figure 2.3 in the article was made based on this calculation

TOC sea sediment is between 0.5-2%	
Sediment weight in 100% sediment BES (3&4) system	1027 g
TOC weight in our BES 3& 4 (use 2% TOC for calculation)	20.54 g
TOC available based on 10% Coulombic efficiency	2.054 g
molar mass C	12 g/mol
mol C	1.71167 mol
number of C	1.03E+24 atom
number of electron *	4.12E+24 atom
*Based on acetate or glucose anodic oxidation reaction, 1 C generates 4 electrons [61]	
measured electron flow (current)	0.1 mA
Q (C)=I(A).t(s) at 1 second	0.0001 C
Charge on 1 electron = 1.6×10^{-19} Coulomb	
actual electron flow	6.24E+14 e/s
Time to finish the sediment fuel	6.60E+08 s (20.9 years)
Based on the above calculation, a simulation with other currents (up to 38mA which is the highest stable current as average from the final 10 cycles in this research) was made as following:	
Current (mA)	Year
0.2	10.5
0.3	7
0.4	5.2
0.5	4.2
1	2.1
5	0.4
10	0.2
15	0.14
20	0.1
25	0.08
30	0.07
38	0.06

TOC= Total Organic Carbon; C=Carbon

Chapter 3

Activated Carbon Mixed with Marine Sediment is Suitable as Bioanode Material for *Spartina Anglica* Sediment/Plant Microbial Fuel Cell: Plant Growth, Electricity Generation, and Spatial Microbial Community Diversity

Published as: Sudirjo, E.; Buisman, C.J.N.; Strik, D.P.B.T.B. Activated Carbon Mixed with Marine Sediment is Suitable as Bioanode Material for *Spartina anglica* Sediment/Plant Microbial Fuel Cell: Plant Growth, Electricity Generation, and Spatial Microbial Community Diversity. *Water* **2019**, *11*, 1810.

Abstract

Wetlands cover a significant part of the world's land surface area. Wetlands are permanently or temporarily inundated with water and rich in nutrients. Therefore, wetlands equipped with Plant-Microbial Fuel Cells (Plant-MFC) can provide a new source of electricity by converting organic matter with the help of electrochemically active bacteria. In addition, sediments provide a source of electron donors to generate electricity from available (organic) matters. Eight lab-wetlands systems in the shape of flat-plate Plant-MFC were constructed. Here, four wetland compositions with activated carbon and/or marine sediment functioning as anodes were investigated for their suitability as a bioanode in a Plant-MFC system. Results show that *Spartina anglica* grew in all of the plant-MFCs, although the growth was less fertile in the 100% activated carbon (AC100) Plant-MFC. Based on long-term performance (2 weeks) under 1000 ohm external load, the 33% activated carbon (AC33) Plant-MFC outperformed the other Plant-MFCs in terms of current density (16.1 mA/m² plant growth area) and power density (1.04 mW/m² plant growth area). Results also show a high diversity of microbial communities dominated by *Proteobacteria* with 42.5%–69.7% relative abundance. Principal Coordinates Analysis shows clear different bacterial communities between 100% marine sediment (MS100) Plant-MFC and AC33 Plant-MFC. This result indicates that the bacterial communities were affected by the anode composition. In addition, small worms (Annelida phylum) were found to live around the plant roots within the anode of the wetland with MS100. These findings show that the mixture of activated carbon and marine sediment are suitable material for bioanodes and could be useful for the application of Plant-MFC in a real wetland. Moreover, the usage of activated carbon could provide an additional function like wetland remediation or restoration, and even coastal protection.

Keywords: Marine Sediment; Activated Carbon; Constructed Wetlands; Sediment-MFC; Plant-MFC; Bioanode; Microbial Community

3.1 Introduction

Wetlands has been known as one of the world's most important type of ecosystems, which play a critical role in climate change, biodiversity, hydrology, and human health [116]. For instance, wetlands provide a range of ecosystem services including fresh water; nutrient cycling; food and fiber production; carbon fixation and storage; flood mitigation and water storage; water treatment and purification; and habitats for biodiversity. About 5-10% of the world's land surface is covered by wetlands [117]. A recent study reported that the global wetland area is between 15 and 16 million km², in which about 8.9-9.5% is coastal wetlands [118]. Unfortunately, despite of their critical role wetlands are facing a serious problem of losses caused by human activities [116]. This loss was comparable to previous study reporting that between 1970 and 2008, natural wetland declined globally by about 30% [119].

Sediment pollution by human activities is a major problem for wetland ecosystems [120]. By nature, wetland sediments are able to remedy themselves from pollutants, such as petroleum hydrocarbon pollutants, due to presence of diverse microbial communities [121]. However, in some cases such as to control hydrophobic organic compounds (HOCs), an *in-situ* amendment by human interference is applied for sediment remediation by e.g. addition of activated carbon (AC), which is most widely used for *in-situ* sediment sequestration and immobilization [122]. The capability of AC adsorbs organic compounds is controlled either by physical interaction or by chemical interaction between AC surface area and adsorbents. The adsorption rate is influenced by molecular size of the organic compounds and distribution of the AC pores [123,124]. The activated carbon materials have three types of pores: micropores (<2nm), mesopores (2-50nm), and macropores (>50nm). The surface area of AC is determined by the presence and distribution of these pores [125]. *In-situ* sediment treatment using activated carbon (AC) has been demonstrated in full-scale projects, up to 100 ha of application area. *In-situ* treatment of sediment HOCs using sorptive AC-bearing materials has progressed from an innovative sediment remediation approach to a proven reliable technology [122].

Sediments are also new sources to generate electricity with a so called sediment microbial fuel cell [72]. Hereby the anode of the fuel cell is driven by oxidation of sediment sulfide (a side-product of microbial oxidation of sedimentary organic matters) and oxidation of sedimentary organic carbon converted by electrochemically active microorganisms. The *in-situ* AC amendment in sediment could be coupled with sediment microbial fuel cell installation for concurrent production of renewable energy and bioremediation of pollutants such as heavy metals and HOC's. Various sediments both in marine and fresh water environments are suited to generating electricity [68]. Even living plants could

be included in such systems, providing additional services as known for the so-called Plant-Microbial Fuel Cells (Plant-MFC).

Actually wetlands inhabited with the Plant-MFC can provide a new (additional) source of bioelectricity and have a potential to reduce eutrophication and promote plant growth [126,127]. The Plant-MFC is envisioned as a sustainable *in-situ* bioelectricity source which can avoid competition between food and energy production [40], *e.g.* Plant-MFC could be combined with rice paddy production [48,50,63,128]. Plant-MFC converts solar energy into bioelectricity via plant rhizodeposits and electrochemically active bacteria (EAB) [40,57]. Several studies have been conducted to increase Plant-MFC performance such as investigating optimum anode position under soil [63], modifying plant growth medium [58], characterizing internal resistance [53], comparing power output from different sediment types [96], designing new reactors [44,60,64], studying plant and microbe cooperation [48] and developing and investigating various electrode materials [57,62–64]. The highest 2 weeks average power density of 240 mW/m² plant growth area was achieved in a plant-MFC when integrated with oxygen reducing biocathode [65]. For a large scale application, plant-MFC is potentially integrated in wetland by which various functions could be combined including electricity generation, sediment remediation, plant growth support and as protection of coastal areas [46,96].

Plant-MFCs were embedded with vascular plants, macrophytes and bryophytes as well as their combination with sediments, natural and constructed wetlands. From a recent review paper, at least 40 plant species have been utilized in the Plant-MFC system [54]. Among those species, *Spartina anglica* is one of the most model species [57,58,60,65,129,130]. *S. anglica* is known as an invasive species that has sustained more than a century of evolution. It can tolerate a wide range of environmental conditions and grows on a variety of substrates, including clays, fine silts, organic mud, sands and shingle. As a result, *S. anglica* can occupy the seaward edge of salt marshes [131,132]. There are several economic and societal effects of *S. anglica*. It has a potential for coastal protection because it can absorb wave energy. It has also been planted for estuary reclamation [131]. In an upper tidal zone wetland, *S. anglica* grows as a pioneer plant [133]. *S. anglica* is also used as a green manure in China in which 50 kg of *S. anglica* biomass are approximately equivalent to 0.5 kg of urea [133].

In a long term real application, one of the challenges for Plant-MFC technology is simultaneously harvesting maximum power, remaining plant vitality, and preventing electrode material from deteriorating over time [134]. Research has shown that the long term power output of a *S. anglica* plant-MFC was fluctuating while the plant was growing [130]. Several anode materials have been

used in the Plant-MFCs to produce electricity. Among them were graphite granule and tezontle (a volcanic slag) [135], graphite felt/mat [40,44,48,60,62,65], graphite granules/grains [57,136,137], carbon fiber [138], nano-catalyzed graphite disc, rolled steel mesh with graphite fiber [139], and stainless steel mesh with biochar [140].

Although many studies about the anode materials for a Plant-MFC have been conducted, to our best knowledge, there is no study yet using activated carbon (AC) in the Plant-MFCs while studying the effect of marine sediment. It is well known that the activated carbon is a suitable bioanode material for microbial fuel cells fed with acetate [88,141]. Recent work (Chapter 2) also showed that a mixture of AC and marine sediment is able to store and generate electricity [142]. Activated carbon was chosen in our study because it has a potential to be integrated with soil/wetland amendments; it is a suitable bioanode material that can be mixed with sea-sediment; and it has the ability to support plant growth [41]. Such AC can be produced from an agricultural byproduct like rice husks, rice bran, sugarcane bagasse, walnut shells, and olive stones [143,144] and can also be utilized for soil amendment to increase agricultural production without negatively affect the soil bacteria community [145,146]. Therefore, the main objective of this study was to investigate the suitability of a mixture of activated carbon and marine sediment as a bioanode in a plant-MFC system with *Spartina anglica*. Here it was studied how different mixtures of the activated carbon (AC) and the marine sediment (MS) as an anode material affected the plant vitality, electricity generation and spatial microbial community. Overall, the results provide insights that the Plant-MFC anode, consisting of activated carbon and marine sediments, has a potential to be tested in a demo-scale wetlands to generate electricity and providing additional functions like wetland remediation or restoration, and eventually coastal protection [147–149].

3.2 Materials and Methods

3.2.1 Experimental setup

Lab constructed wetlands were prepared by planting *Spartina anglica* in the anode chamber of eight successfully operated flat-plate reactors from the bioelectrochemical system (BES) experiment in Chapter 2 [142]. Since the plants were transplanted, in this study the reactors were re-named as Plant-MFC instead of BES using the same numbering as the earlier study. The reactors consisted of two compartments in which one functioned as an anode and another as a cathode. A cation exchange membrane (fumasep FGD-PK-75 PEEK-reinforced, 75 μ m, Fumatech, Bietenheim-Bissingen, Germany) separated the anode and the cathode compartment. In the anode, two graphite rods (18 x 1

x 0.2 cm) connected with titanium wire were glued in both side of the anode, functioning as current collector. A complete description and preparation steps how to build the reactors were presented in Chapter 2 [142].

Four different anode compositions were used to fill the anode compartments (650ml). Plant-MFC 1 and Plant-MFC 2, this duplicate was named as AC100, were filled with 100% activated carbon (AC); Plant-MFC 3 and Plant-MFC 4, this duplicate was named as MS100, were only filled with marine sediment; Plant-MFC 5 and Plant-MFC 6, this duplicate was named as AC67, were filled with a mixture of 67 % AC and 33% marine sediment; and Plant-MFC 7 and Plant-MFC 8, this duplicate was named as AC33, were filled with a mixture of 33% AC and 67% marine sediment. The utilized AC is granular activated carbon PK 1-3(Cabot Norit Netherlands BV, with apparent density of 290 g/L, Amersfoort, The Netherlands).

In the cathode compartment (22cmx22cmx1cm; with a winding channel for catholyte flow), graphite felt was used as an electrode. This graphite felt (22cmx22cm; 3mm thickness, Grade WDF, National specialty product carbon and Graphite Felt, Morgan Advance Materials(Taiwan)Co., LTD., Kaohsiung, Taiwan) was woven with a titanium wire as a current collector. From day 1-105, a nitrate-less, sulfate-less, ammonium-rich plant growth medium was utilized as catholyte. Then from day 105 until the end of the experiment, the plant growth medium catholyte was replaced with demi water. In both cases, the catholyte was aerated with ambient air using an aquarium pump and recirculated into the cathode chamber in a close cycle via a 1 liter bottle with a pump (Watson-Marlow 505S, Rotterdam, The Netherlands at 30 rpm). Total catholyte volume in the close cycle was maintained at 1L[142].

Common cordgrass (*Spartina anglica*), together with the marine sediment, was collected from a tidal area wetland at Krabbendijke, The Netherlands (51.446710N, 4.093149E). Prior to being integrated into the reactors, the grasses were kept outside at ambient temperature for one month in a container with marine sediment from their original habitat. The grasses were kept in a waterlogged condition by adding tap water to the container. Young stems with a length of 10 - 15 cm were selected from the container for the experiment. These stems were carefully pulled out from their clumps to avoid root damage. All remaining soil/marine sediment was gently cleaned with flowing tap water.

The plant stems were transplanted in the anode chamber of the reactor by burying their root from an open space on the top side of the anode known as plant growth area or PGA (19 x 2 cm). The roots were buried in a depth between 2 and 3 cm. The number of planted stems varied between 6 and 12 stems per reactor (*Supplementary Table S3. 1*).

The plant growth was maintained with a nitrate-less, sulfate-less, ammonium-rich plant growth medium [58,142] which was continuously pumped into the anode chamber by using a MINIPULS 3 GILSON pump at 4 $\mu\text{l/s}$ flowrate. This plant growth medium also kept the anode of plant-MFCs in a waterlogged condition. On day 150 until 160, the pump was stopped to dry the anodes.

3.2.2 Operations

All Plant-MFCs were operated in the dark and light ratio of 10:14 h within a climate chamber (Microclima 1750, Snijders Scientific, Tilburg, Netherlands) at 25⁰C and humidity of 70%. All potentials were measured and reported against 3M KCl Ag/AgCl reference electrode (QIS, Oosterhout, Netherlands). The photosynthetically active radiation (PAR) light intensity was measured with a light meter (LI-250A; Li-Cor Quantum Q44722 sensor, Li-Cor ®Biosciences, Lincoln, NE, USA) at 12 different positions in the middle height of the climate chamber. The average PAR was 470.4 \pm 12.14 $\mu\text{mol s}^{-1} \text{m}^{-2}$. Two control modes were alternately applied; a potentiostat control mode (day 1-101 and day 176-190) was used to control the anode potential at -100mV vs Ag/AgCl (Transients, Chronoamperometry; Ivium Technologies BV, Eindhoven, The Netherlands); an external load control mode (day 102 -175) was applied by connecting a 1000 Ohm external load between the anode and the cathode. During the potentiostat control mode, the anode potential was controlled with a three electrode setup in which the anode was the working electrode, the cathode as the counter electrode and a reference electrode (Ag/AgCl type No: QM710X QIS, ProSense BV, Oosterhout, The Netherlands) in the anode as the reference electrode. A picture of a full-grown Plant-MFC 3 (MS100) is shown in *Figure 3. 1*.

On day 28, a polarization test was conducted to evaluate the power output from all Plant-MFCs. The polarization was performed with a potentiostat by changing the anode potential of the plant-MFC every 10 minutes using the three electrodes setup in which the anode was a working electrode. Prior to the polarization, the plant-MFCs were operated at an open cell condition for 1 hour to determine the minimum anode potential for each plant-MFC. Based on the anode potential at the open cell condition, the anode potentials sequences for polarizations were decided as following: -100mV, -80mV, -60mV, -40mV, -20mV, 0mV, +20mV, 0mV, -20mV, -40mV, -60mV, -80mV, -100mV (for AC100, AC67, and AC33) and -320mV, -270mV, -220mV, -170mV, -120mV, -70mV, -20mV, 30mV, -20mV, -70mV, -120mV, -170mV, -220mV, -270mV, -320mV (for MS100). Current generation was logged every second with the Iviumsoft. The average current generation from every last minute of the anode potential was used to calculate the power output. For the calculation of the power output, 200 mV hypothetical oxygen reduction cathode potential was used since this value

was easily reached by an oxygen reducing biocathodes applied in a Plant-MFC[65]. The current density and power density were normalized to plant growth area (PGA) and to the anode volume.



Figure 3. 1: Full-grown *Spartina anglica* in plant-MFC 3 (MS100); (A) inside the climate chamber and (B) at the end of the experiment

3.2.3 Measurement and Analysis

Data were logged every minute according to the control mode. During the potentiostat control mode, generated current was logged with the IviumSoft of Ivium Technologies connected to a lab personal computer and during the external load control mode, the anode potentials, the cathode potentials, the membrane potentials and the cell potentials were logged with a field point (National Instruments FP-2000; FP-AI-112, National Instrument Netherlands BV, Woerden, The Netherlands) similar to previous study[142].

3.2.3.1 pH, Conductivity and Acetate analysis

Catholyte and anolyte samples were taken continually from the reactor. Catholyte samples were taken from the cathode outlet prior entering the catholyte circulation bottle. The anolyte samples were taken using a syringe via a soil moisture sampler (10 RHIZON MOM 5 cm female luer; article no. 19.21.22F from Rhizosphere Research Product, Wageningen, The Netherlands) whose end tip was placed in the middle of the anode chamber. The pH and conductivity were directly measured after sampling by using a HACH HQ440d multi pH/LDO/conductivity meter (Hach Company, Loveland Colorado, CO, USA). Samples for acetate analysis were kept in a fridge at -20°C to be measured later using gas chromatography as describe earlier in Chapter 2 [93,142].

3.2.3.2 Plant growth monitoring

Plant growth was monitored by counting the number of the living stems and summarizing the height of living stems. The stems' height was measured from the top-end-plate of the anode to the leaf tip of each stem. The accumulative stem height for every Plant-MFC was calculated by summing up all living stem height in the reactor. These data were continually sampled until the end of the experiment.

At the end of the experiment (day 190), all biomass (both above and belowground biomass) were harvested from all reactors. The roots were rinsed in a flowing tap water to remove soil and activated carbon. Dried biomass was determined after drying at room temperature for 3 months until constant weight was reached. Biomass yield (kg/m^2) was calculated and normalized per plant growth area (PGA) which was 0.0038 m^2 per Plant-MFC.

3.2.3.3 DNA analysis

At the end of the experiment (day 190), about 3 ml biomass samples from anode components (mixture of marine sediment, AC and plant roots) were taken for DNA analysis. Samples were taken from the MS100 (Plant-MFC 3 and Plant-MFC 4) and the AC33 (Plant-MFC 7 and Plant-MFC 8). For every reactor, five biomass samples were collected. Biomass samples were taken from five different locations in the anode as marked on **Figure 3. 2**. These five sample locations were clustered in two zones: upper zone (until 5cm below the anode surface) and lower zone (from 5 to 20 cm below the anode surface). The upper zone (UZ) sample points were (A) UZ-AN (anode) and (C) UZ-CC (current collector). The lower zone sample points were (B) LZ-RO (roots), (D) LZ-AN (anode), and (E) LZ-CC (current collector). In the MS100 plant-MFC, the anode biomass samples (UZ-AN and LZ-AN) contained marine sediment; the current collector biomass samples (UZ-CC and LZ-CC) contained marine sediment that were attached on the current collector. While, in the AC33 plant-MFC, the anode biomass samples (UZ-AN and LZ-AN) contained AC and marine sediment; the current collector biomass samples (UZ-CC and LZ-CC) contained AC and marine sediment that were

attached on the current collector. In total, 20 samples were collected. The samples were stored immediately in -80°C freezer after collection before the DNA sequencing was performed.

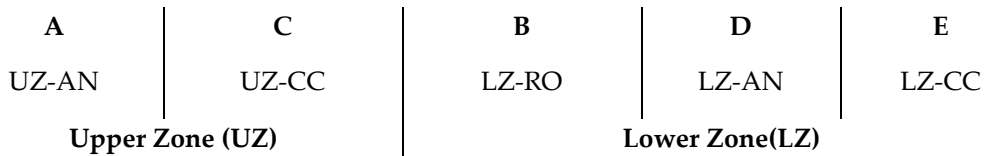
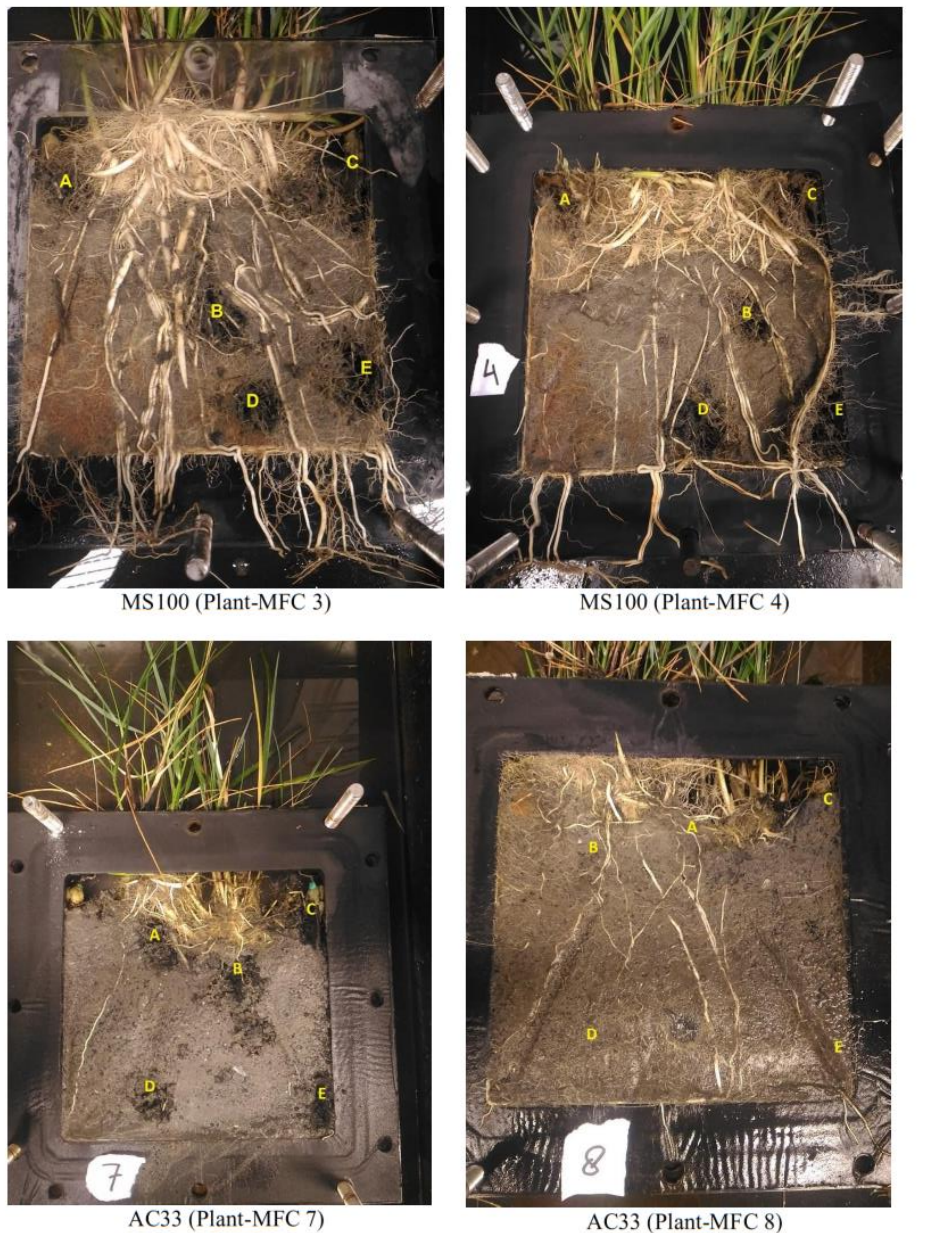


Figure 3. 2: DNA analysis sampling points

Steps of sequencing was performed similar to de Smit et al work [150]. DNA was extracted from the samples using the PowerSoil[®] DNA isolation kit according to their manual instruction manual with some modifications [SI Method S1]. The extracted DNA was quantified using Qubit[®] and diluted to 5 ng/μl as the final template DNA concentration for PCRs. The V3-V4 regions of 16s rDNA from the isolated DNA (template DNA) was amplified using the primer sets provided by Takahashi et al which allowing simultaneous amplification of bacterial and archaean 16s rDNA. The illumina library generation methods were subsequently used to generate DNA sequence data [151].

After acquiring rDNA sequence data a statistical analysis allowed operational taxonomic unit (OTU) picking, using the SILVA version 128 16S reference database and uclust [152,153]. The Ribosomal Database Project (RDP) classifier (version 2.2) [154] was trained with the same SILVA reference database and subsequently used to classify the OTUs. Taxonomic analysis was performed using QIIME software version 1.9.1[155]. This bioinformatics process was performed on 21 August 2018. From the acquired data, a heat map such as shown in the supplementary (**Supplementary Table S3. 2; Supplementary Table S3. 3; Supplementary Table S3. 4**) was made using Microsoft Excel 2016.

Beta diversity analysis was performed to measure the extent of similarity/dissimilarity between microbial populations comprising samples and sample groups by calculating different distance matrices. Based on the unweighted UniFrac beta diversity, a Principal Coordinates Analysis (PCoA) with a 3D ordination was plotted through QIIME using Emperor Software from the beta diversity data to compare group of samples based on the phylogenetic or count-based distance metrics [156]. From the PCoA, one can see the similarity and dissimilarity among the group of samples. Objects that are ordinated closer together have smaller dissimilarity values than those ordinated further apart.

3.2.4 Calculations

The plant-MFC current density was plotted as a daily average as shown in **Supplementary Figure S3. 1**. During potentiostat control mode, the daily average current was directly calculated from the generated current that was logged every minute with the Iviumsoft. During the external load control mode, prior to calculate the daily average current, the generated current (I_{gen}), in ampere (A), was calculated with Equation (3.1).

$$I_{\text{gen}} = V_{\text{cell}} / R \quad (3.1)$$

V_{cell} is cell potential (V) and R is the applied external load (ohm)

Power output (P), in Watt (W), was calculated depending on the control mode. Equation (3.2) was used to calculate the power output during the potentiostat control mode and Equation (3.3) was used to calculate the power output during the external load control mode.

$$P = V_{\text{hyp}} \cdot I_{\text{pot}} \quad (3.2)$$

V_{hyp} is 0.2 volt hypothetical cell potential and I_{pot} is current output measured and logged with the potentiostat.

$$P = I_{\text{gen}}^2 \cdot R \quad (3.3)$$

I_{gen} is generated current (A) as calculated from Equation (3.1) and R is applied external load (ohm).

Both current density and power density were normalized to the plant growth area (PGA) and to the anode volume.

3.3 Results and Discussion

3.3.1 Mixture of Activated Carbon (AC) and Marine Sediment Effect on Plant Growth

Plants were growing in all reactors for 190 days after transplantation regardless of their control mode, even at negative current. This growth was proven by the increase in the number of living stems (**Figure 3. 3**) and in the accumulative stems height (**Figure 3. 4**). The number of living stems increased to between two and eight times from their initial size (**Figure 3. 3**). The accumulative stems height varied between 2 and 10 m at the end of experiment (**Figure 3. 4**). The plant ability to grow in such anode environment proves that the mixture of activated carbon and marine sediment are suitable materials for a Plant-MFC. For a visual comparison, **Supplementary Figure S3. 2** and **Supplementary Figure S3. 3** show plants condition at the moment they were planted and at the end of the experiment. The similar plant species was able to grow up to 703 days in the graphite felt anode of a flat-plate plant-MFC [44]. In other studies with the same plants species and a similar type of reactor, the plant vitality was reported to increase from nine stems in the beginning to 25 stems (2.8 times) after 56 days and further increases to more than 30 stems (3.3 times) after 140 days [65].

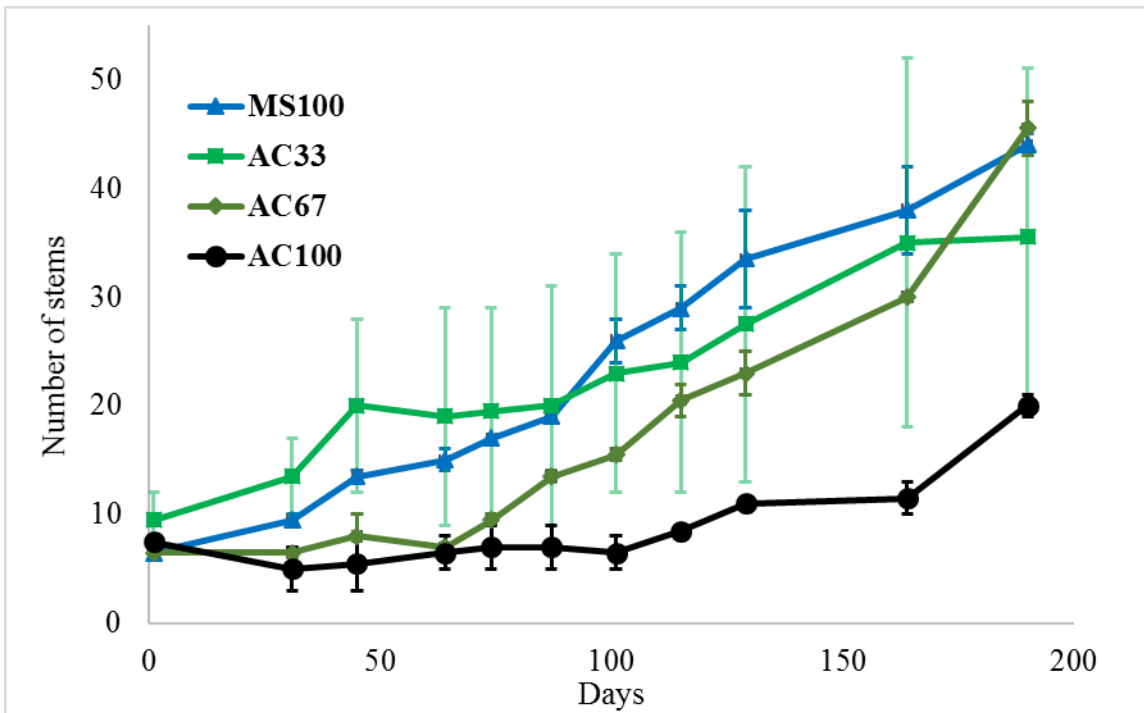


Figure 3. 3: Average number of living stems on different Plant- MFC reactors

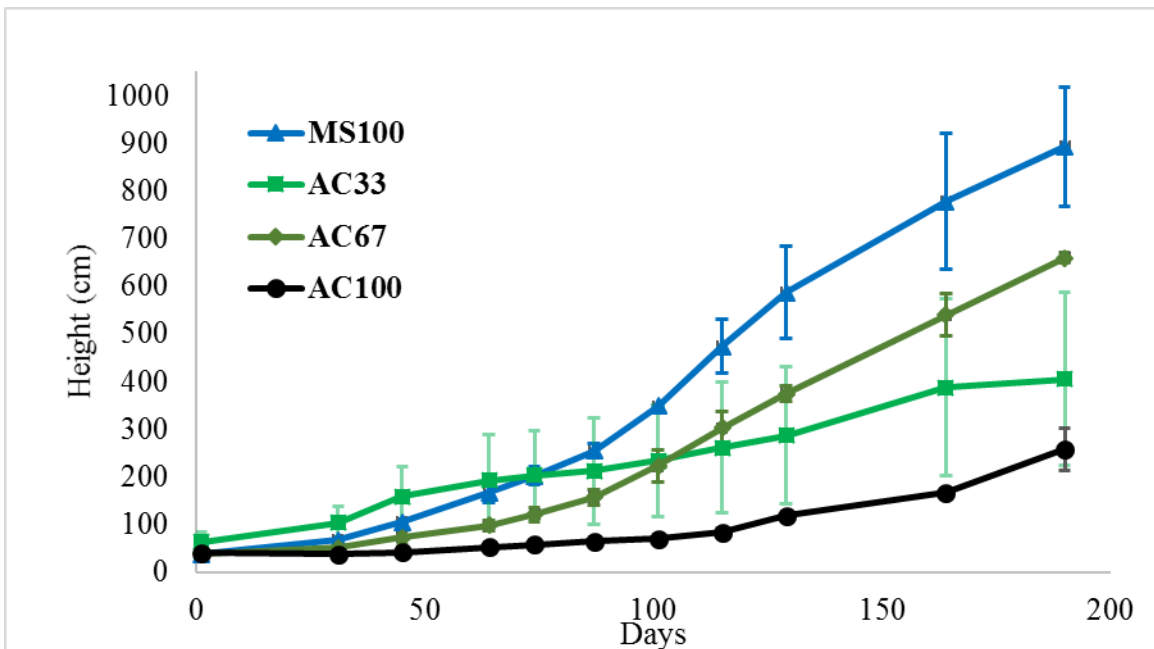


Figure 3. 4: Accumulative total stems height on different Plant-MFC reactors

Duplicate analysis shows that the AC100 Plant-MFC has less plant growth in term of the number of living stems (**Figure 3. 3**) and the total stem height (**Figure 3. 4**) compared to the other anode compositions. Evidently, more replicates are needed to provide statistical supported evidence that can lead to strong conclusions. Nevertheless, the actual measured reduced plant growth could be due to nutrient limitation for plants and/or bacteria in the reactor because of adsorption capability from activated carbon [144]. Other studies have proven that activated carbon is able to adsorb various compounds such as acetate, ammonium, phosphate, nitrate, sulphate, and metal ions [157–164]. In this study, the nutrient supply was mainly from plant growth medium and leftover acetate (**Supplementary Table S3. 5**) from a previous experiment. Conductivity and pH remained in the same order of magnitude in both the anolyte and catholyte (**Supplementary Table S3. 5**). This suggests that still some salts/nutrients are available; though whether specific nutrients were becoming limiting could not be revealed. We can speculate there may be mechanisms that *Spartina* plants in the long term can desorb nutrients by changing rhizosphere conditions as known for e.g. phosphate leaching plants [165,166]. The number of stems in the other anode compositions (MS100, AC 33 and AC67) were growing well. It is difficult to elaborate on which anode composition is possibly performing better based on these two parameters because the error bars from those three anode compositions were overlapping (**Figure 3. 3** and **Figure 3. 4**). Further research with more compositions and replicates is recommended to determine the best composition of mixing between marine sediment and activated carbon. However, the measured data shows that mixing marine sediment with activated carbon had a higher plant vitality than sole use of activated carbon. The use of marine sediment may have been beneficial because it has plenty of organic matters including nutrients [76] that can be utilized by plants for their growth and by the electrochemically active bacteria to generate electricity as shown in Chapter 2 [142].

Plant growth can also be assessed through biomass production. In this research, it is remarkably that the less growth AC100 Plant-MFCs dry biomass yields (**Supplementary Table S3. 6**) are still comparable to literature reporting a yield of *S. anglica* under natural condition between 0.48-1.85 kg/m² for above ground dry biomass and 0.78-3.11 kg/m² for below ground dry biomass [57]. The other Plant-MFCs are, as expected, producing more biomass compared to AC100 Plant-MFC. Both the above and the lower ground dry biomass from AC33 and AC67 Plant-MFCs were also within the range of natural yield of *S. anglica* and slightly higher than natural condition (**Supplementary Table S3. 6**). The dry biomass yield for MS100 Plant-MFC was higher than that in the natural condition. The biomass production from Plant-MFC could still be increased because the earlier research with *S. anglica* using graphite grain as anode media was able to harvest 6 kg/m² above ground dry biomass

and 15 kg/m² below ground dry biomass [57]. These biomass yield differences might be explained as growth conditions (e.g. temperature and light intensity) are different in the natural and laboratory-experimental conditions. In addition to the plant growth, we also observed that small-red segmented worms, with diameter between 1 and 3 mm and length between 5 and 8 cm, were able to live/survive in the anode part of the MS100 plant-MFC (**Figure 3. 5**). These worms, based on their physical appearances possibly from Annelida phylum [167], are natural decomposers which maintain soil fertility by altering soil compositions through decomposing and transforming organic matter [168]. The latter provides support that the bioanode does support (some) biodiversity.



Figure 3. 5: Worms in the anode plant-MFC 3 (MS100) surviving during 190 day operation

3.3.2 Mixture of Marine Sediment and Activated Carbon Generating Electricity in Plant-MFCs

Results show that all plant-MFCs generated power when operated at 1000 ohm external load as shown in **Figure 3. 6**. The AC33 plant-MFC seems to be best suited for generating electricity. The average duplicate AC33 plant-MFC generated higher current density in a long-term operation compared to the other plant-MFCs. On average, the MS100 Plant-MFC delivered less current in comparison with the other Plant-MFCs. This Plant-MFC continuously generated positive current regardless of their applied control mode. When all anode chambers were dry, in a period between day 150 and 160, the current output was zero for all of plant-MFCs. Unlike the MS100 plant-MFCs, the current output of the AC100 plant-MFC reached up to 42.6 mA/m² at the first time the external load was operated. Then, the current output decreased gradually reaching zero. A similar phenomenon was also showed by the AC67 plant-MFC. The high current phenomenon at the beginning of the external load operation, as shown by AC100 and AC67 Plant-MFC, was caused by the capacitive behaviour of the activated carbon anode as described earlier in Chapter 2 [142]. At that time, the envisioned anode was actually acting as a cathode and electrical charges were added to the system. Later on, when the control mode was switched to the external load, the stored electrical charges were released as an anodic current which harmonically went towards zero [142].

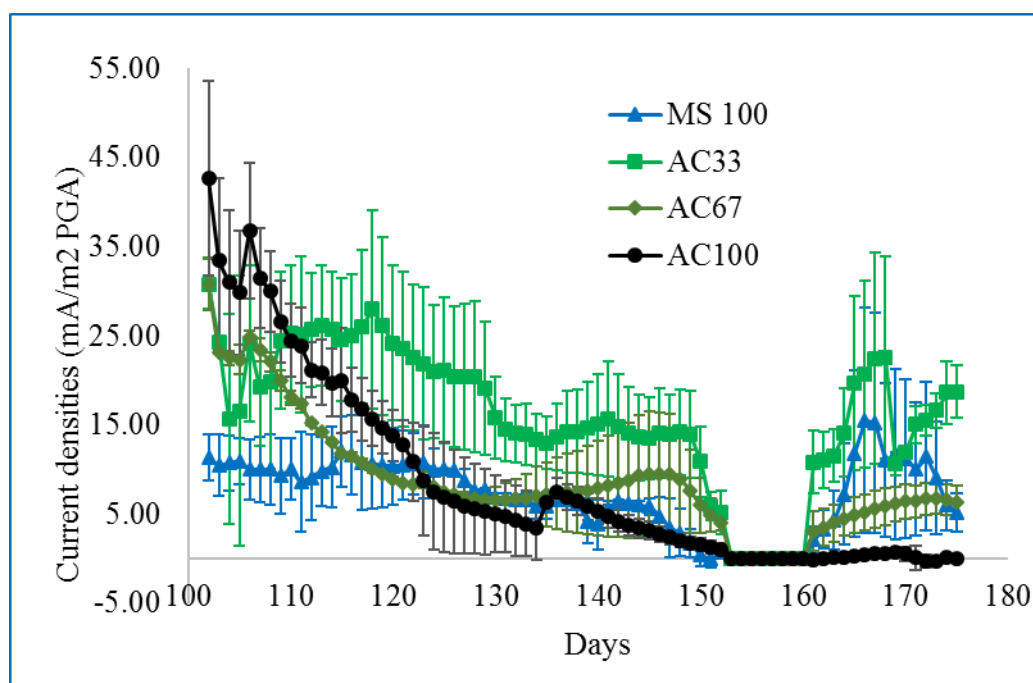


Figure 3. 6: Average current output (mA/m² plant growth area (PGA)) of Plant-MFC with variation bars. The current output reached zero when anodes were dried

During the potentiostatic controls, only MS100 and AC33 Plant-MFCs generated electricity (*Supplementary Figure S3. 1*). Instead of generating power, the other Plant-MFCs (AC67 and AC100) had a negative current production, indicating a capacitive behavior effect. At this moment, electric charges were stored in the anode. This capacitive behavior had been studied earlier in activated carbon-based bioanodes in a bioelectrochemical system [88,91,142]. The capacitive behaviour was not observed in the MS100 plant-MFCs and less obvious in the AC33 plant-MFC. It was not clear why the AC100 duplicate behaved differently during the first potentiostatic control. However, both AC100 duplicates showed a similar trend, generating a negative current, on the second potentiostatic control.

After the plant growth medium pump had been stopped, all plant-MFCs anode became dry (day 150-160) because of the evaporation process and uptake by plant roots. As a result, all plant-MFCs delivered no current. There are some possible explanations on this situation. First, dry anodes become more aerobic because oxygen would easily penetrate through pores of the activated carbon particles and the marine sediment. As a result the anaerobic EAB activity will more likely be outcompeted by aerobic bacteria in substrate utilization and thus hinder the yield of EAB in the anode [169]. Second, even though the anaerobic oxidation was still occurring in some parts of the anode, the generated electrons will soon utilize the available oxygen in the anode side as their acceptor. This fact gives a useful insight that when a wetland becomes dry, it may lose its function as a “home” for important anaerobic processes. However, in a temporary dry wetland, e.g. in an intertidal wetland, the oxygen diffusion into sediment can accelerate the aerobic degradation of some high molecular weight compounds into a low molecular weight compounds which later on can be utilized by the EAB under anaerobic condition to generate electricity [169]. Therefore, a plant-MFC installed in a salt marsh, which influenced by tidal advection, generated more than 10 times more power than the same plant-MFC in a peat soil [96]. The fact that all plant-MFCs delivered zero current at a dry condition might also be useful for wetland mitigation. For instance, one could design and install a less required power sensor powered by a plant-MFC. This bio sensor could be coupled with an internet of things (IoT) application [170] to monitor a wetland condition, *i.e.* water level.

On day 160, the plant growth medium was pumped back. The current generation of all plant-MFCs were recovered except for the AC100 plant-MFC. The AC100 plant-MFC was hardly recovered and generated almost zero current until end of the external load control mode. Therefore, the average and maximum current and power densities of this last 2 weeks (day 160-175) operation under the external load mode after recovering from the dry period was preferable to compare the result of this study with other studies (*Table 3. 1*).

Table 3. 1: Average and maximum current and power densities of several Plant-MFC systems

Reactor type/ <i>Plant species</i>	Anode / Current collector	Cathode	Current density (mA/m ² PGA)		Power density (mW/m ² PGA)		Method	Ref
			Av.	Max	Av.	Max		
Flat plate <i>Spartina anglica</i>	Marine sediment/ small graphite rod (MS100)	Graphite felt, air cathode	9.01	15.49	0.37	0.91	A	This study
			(2 weeks)	45*	(2 weeks)	8*		
			-	(0.3A/m3)*	-	(46 mW/m ³)*	D	
Flat plate <i>Spartina anglica</i>	33%AC+67% marine sediment/ small graphite rod (AC33)	Graphite felt, air cathode	16.01	22.53	1.04	1.93	A	This study
			(2 weeks)	819*	(2 weeks)	148*		
			-	(4.8A/m3)*	-	(863 mW/m ³)*	D	
Flat plate <i>Spartina anglica</i>	67%AC+33% marine sediment/ small graphite rod (AC67)	Graphite felt, air cathode	5.46	8.42	0.12	0.27	A	This study
			(2 weeks)	12,496*	(2 weeks)	2,249*		
			-	(73 A/m3)*	-	(13150mW/m ³)*	D	
Flat plate <i>Spartina anglica</i>	AC/ small graphite rod (AC100)	Graphite felt, air cathode	0.2	1.58	0.00	0.00	A	This study
			(2 weeks)	19,752*	(2 weeks)	3,555*		
			-	11.5 A/m3*	-	(20786 mW/m ³)*	D	
Flat-plate <i>Spartina anglica</i>	Graphite felt/ gold wire	Graphite felt, Ferric cyanide cathode	74-384	469	47-155	211	A	[58]
			(4 weeks)		(4 weeks)			
Cylindrical <i>Spartina anglica</i>	Graphite grain/Graphite rod	Graphite felt/gold wire, Potassium ferric cyanide	-	-	21	-	A	[57]
					(8weeks)			
			-	-	-	222	C	
Flat plate with two cathode compartment <i>Spartina anglica</i>	Graphite felt/golden wire	Graphite felt/golden wire, oxygen reducing biocathode	-	-	-	679	C	[65]
			-	-	240	-	B	
					(2 weeks)			
Polyacrylic plastic cylinder <i>Ipomoea aquatica</i>	Granular activated carbon/ stainless steel mesh	Granular activated carbon/ stainless steel mesh, air cathode	-	0.66 A/m3	-	274 mW/m3	C	[171]
Organic glass pipe <i>Phragmites australis</i>	Activated granular carbon/ stainless steel mesh	Activated granular carbon, air cathode	-	0.49A/m3	-	4.5(200 mW/m3)	C	[172]
Polycarbonate plastic cylinder <i>Ipomoea aquatica</i>	Thick granular activated carbon/ titanium wire	Stainless steel mesh, air cathode	-	-	-	12.42	C	[173]
Glass cylinder <i>Spartina anglica</i>	Graphite granules/golden wire	Graphite felt, air cathode	-	-	-	79	C	[130]
Modular <i>Sedum species</i>	Carbon felt	AC/graphite rood, air cathode	-	5	-	114.6 (μW/m ²)	C	[174]
Perspex tubes Rice(<i>Oryza sativa</i>)	Graphite granule/vermiculite /carbon rod	Graphite felt interwoven carbon rod, air cathode	-	580	-	72	D	[136]
Circular graphite felt electrode in a rice paddy field Rice (<i>Oryza sativa</i>)	Graphite felt connected via epoxy encapsulated wires	Graphite felt with platinum catalyst connected via epoxy encapsulated wires, air cathode	-	-	-	140	D	[50]

Method of operation: A: Continuous operation at 1000 ohm; B: 2 week continuous operation at 600mV cell voltage controlled with potentiostat; C: Polarization curve with external resistance; D: Potentiostat polarization; PGA = Plant growth area. Hyphens mean data are not calculated/not available. *These maximum power outputs were done at day 28 during the potentiostatic control mode (Supplementary Figure S3.7). The high current and power density could be influenced by capacitive properties of the anode material that was charged and discharged using external power. This power could be utilize with care to e.g. harvest a peak power to charge external capacitors or provide a power peak to start-up small electronic devices. These high current and power outputs are not to be considered as actual performance of the sediment/plant microbial fuel cell since they do not represent a long-term performance and are the results of the potentiostatic operation.

In this study, insights on the possible link between plant roots and current/power generation were also observed. Based on the below ground biomass yield and pictures of the roots at the end of the experiment (**Supplementary Table S3. 6** and **Supplementary Figure S3. 4**), the root densities from the highest to the lowest were in the MS100, AC67, AC33, and AC100 Plant-MFC. There was a small difference between root density in the MS100 and the AC67 Plant-MFCs. Results show a correlation ($R^2=0.6$) between the current density and the root density of the Plant-MFC (**Supplementary Figure S3. 5**). The average current density of AC33 Plant-MFC was 1.04, higher than those of AC67 (0.12 mA/m²) and MS100 (0.37 mA/m²). The plant roots are able to transport oxygen into the anode [169,175,176]. The oxygen concentration at the *S. anglica* root surface could reach up to 85 $\mu\text{mol L}^{-1}$ and the radial oxygen loss across the root surface ranged from 250 to 300 nmol m⁻²s⁻¹[175]. The increase of oxygen concentration in the anode will promote the oxidation reaction, which theoretically increase the anode potential. Thus it will negatively affect the current and power generation [53,176]. Therefore, the anode should be placed in a proper distance to avoid or reduce the negative effect of oxygen loss from the roots [169].

It is challenging to compare the result of one study with other studies because of the variation in the system (i.e electrode materials, plant growth, sediment use, reactor size, operation condition, control method, etc). Comparing the maximal power output is less preferred because it does not really show the capability of such system to deliver continuous power for a long period. Here, we compare our result with the average power generation for a minimum period of 2 week performance. In **Table 3. 1**, we provide a comparison with other studies which have some similarities with our study. These studies show lower than average current density of 74-384 mA/m² (power density of 47-155 mW/m²) using similar type of flat-plate reactor and plant species on a graphite felt anode [58]. Another plant-MFC with graphite grains anode was able to generate average power output of 22 mW/m² for eight weeks [57]. However, both studies utilized ferric cyanide as catholyte instead of water.

Based on this comparison, it seems that mixing marine sediment with activated carbon influences the power output of a plant-MFC system; however, another explanation for this could be plant difference in biomass growth (**Figure 3. 3** and **Figure 3. 4**). More plants may produce more rhizodeposits. It is also not evident that the highest amount of used marine sediment was leading to the highest current density since the AC33 plant-MFC performed better compared than the others plant-MFCs. Based on two weeks performance, the AC33 plant-MFC generated current on average 16.01 mA/m² PGA (22.53 mA/m² PGA max). This result was comparable with sediment-MFC from previous study, which used mixture of 50% granular carbon (1-5mm) with sand as an anode material fed with 20mM sodium acetate as electron donor. After 3 week of incubation, the sediment-MFC reached an average

current density of 25 ± 7.74 mA/m² with a maximum of 37.9 mA/m² [83]. It should be noted that without the presence of plants and solely fed with sodium acetate, the mixture of 33% granular carbon with sand sediment-MFC only generated maximum of 5mA/m² of current density after 2 week operation [83]. The cathode performance of the studied systems may have affected the MS100 but did not likely limit the bioanode of the other Plant-MFCs. The recorded anode and cathode potentials from day 160 onwards shows that the cathode potential was not likely to limit the current generation (**Supplementary Figure S3.6**). Some Plant-MFCs (MS100 and AC33) fluctuated on current and anode/cathode potential. Since this did not happen in both duplicates, it could not be attributed to the type of electrode materials used. Other parameters that may cause this phenomenon need to be further investigated while several Plant-MFC reports show dynamic behaviour [130]. The cathode potentials of the AC33 and the AC67 were in between +100 and +300 mV except in the end of one of the AC33. The cathodes of AC100 varied between +60 and +100 mV. All these cathode potentials are higher or comparable to the cathode potentials reported for an abiotic oxygen reduction process within a similar flat-plate Plant-MFC reported by Wetser [65]. The measured anode potential in all systems (except the MS100) were mostly rather high (> 0.070 V) compared to other Plant-MFC studies with *Glyceria maxima* plants showing a significant anode resistance[53]. This supports that the cathodes of our studies were not limited for the oxygen reduction using the produced electrons at the anode. For the MS100, the anode and cathode potentials were fluctuating providing possible limitations on the cathode as well as on the anode during the experiment. Further studies with more replicates and more variations on AC, different electrode materials and marine sediment percentages are needed to draw conclusions on using such electrode materials long term. Even so, the electric conductivity of the marine sediments itself and the activated carbon bed and their mixtures should be investigated while both materials have shown to have an electric conductivity which is relevant in microbial fuel cells [97,177]

3.3.3 Diverse Microbial Communities

Spatially diverse microbial communities were observed in this study. Based on alpha rarefaction plots, the observed_otus (70000 sequences per sample) for MS100 Plant-MFC 3, MS100 Plant-MFC 4, AC33 Plant-MFC 7 and AC33 Plant-MFC 8 were 6308, 7077, 8173 and 9177, respectively. The Principal Coordinates Analysis (PCoA) shows that the MS100 Plant-MFC and the AC33 plant-MFC communities are distinctly separated between each other even though they come from the same marine sediment inocula (**Figure 3. 7**). In addition, there is a clear difference between upper zone and lower zone microbial communities, especially in the MS100 plant-MFC. This result indicates that the bacterial communities are influenced by the anode composition/material.

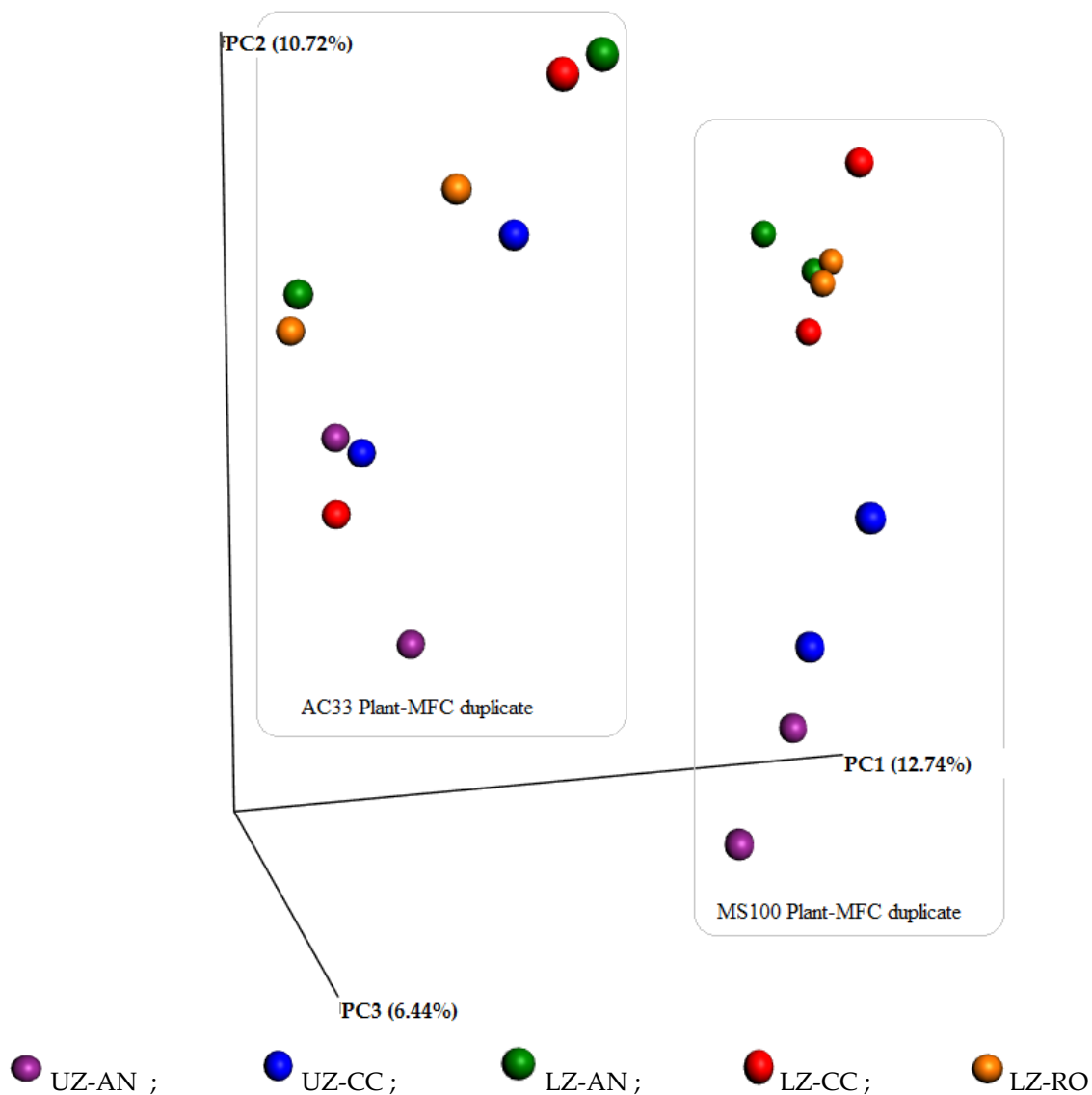


Figure 3. 7 : Unweighted UniFrac Principal Coordinates Analysis (PCoA) of plant-MFC microbial communities

Technical duplicate Plant-MFC microbial analysis results from all the MS100 and AC33 plant-MFCs shows that the archaea do not play an important role in the plant-MFC electricity generation process since they were not abundantly available (0.39% - 1.93%). Bacteria were found with a high relative abundance in the Plant-MFCs system of 85.2 to 97.7%. A total of 63 phyla were observed in this study with a relative abundance of minimum 1%. **Figure 3. 8** shows four most dominant phyla that accounted for 64-81% of the total population. They were, from the most to the least dominant, *Proteobacteria*, *Bacteroidetes*, *Chloroflexi* and *Verrucomicrobia*. Looking deep into the *Proteobacteria* phylum diversity, it was dominated by *Gamma proteobacteria* (20.2-50.2%), *Delta proteobacteria* (26.2-44.5%), *Beta proteobacteria* (3.4-27.8%), *Alpha proteobacteria* (11.7-21.6%),

and *Epsilon proteobacteria* (2.2-11.6%). More detailed relative abundance of classes within a phylum from the four most abundance phyla is presented in **Supplementary Figure S3. 8**, **Supplementary Table S3. 2**, **Supplementary Table S3. 3**, and **Supplementary Table S3. 4**. This result is similar with previous study in *Glyceria maxima* Plant-MFC anode rhizosphere bacterial community which found that *Proteobacteria* were the most abundant phylum [137]. The dominance of *Proteobacteria* is also consistent with root-associated microbial communities in other rhizosphere sediment of salt marshes [178–180].

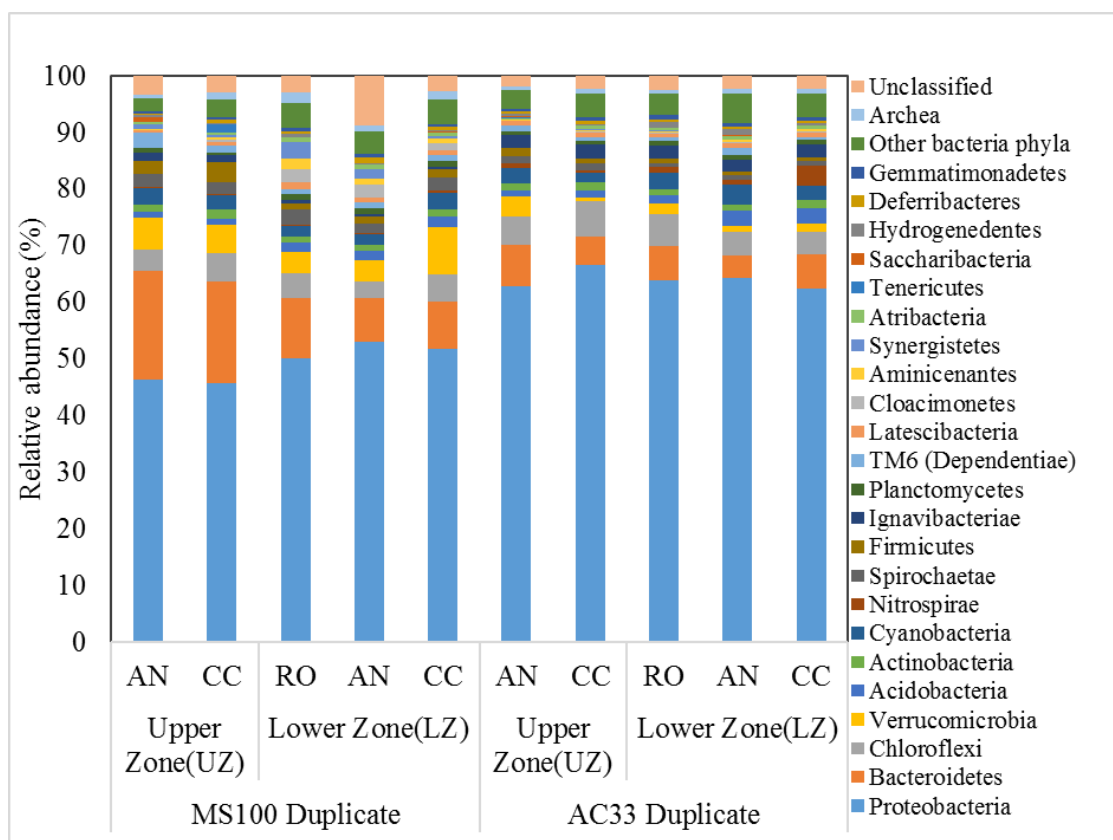


Figure 3. 8: Bacterial and Archaea phyla

The dominance of *Proteobacteria* in such lab-wetland system are well known and most of them are responsible for sulphur cycle in the sediment. Sulphate reduction is the dominant respiration of the anaerobic marine sediment in the salt marshes vegetation [178]. Sulphate-reducing bacteria (SRB) play an important role in the marine carbon and sulphur cycle [181]. For instance, one family from *Deltaproteobacteria*, *Desulfobulbaceae* is known as “cable bacteria”. These bacteria are globally found in the marine sediment and able to transport electrons over a long distance by coupling sulphide oxidation and oxygen reduction [182,183]. At least more than 220 species of 60 genera of SRB have been described. They spread within the bacteria (*Firmicutes*, *Proteobacteria*, *Nitrospira*, and *Thermodesulfobacteria*) and the archaea (*Euryarchaeota* and *Crenarchaeota*)[184]. In the near-

surface sediment (20cm), *Desulfobacteraceae* (*Desulfosarcina*, *Desulfobacterium* and *Desulfococcus*) were reported as the dominant sulfate reducing bacteria followed by *Desulfobulbaceae* family [181]. Meanwhile, in the salt marshes sediment colonized by *Spartina alterniflora* plant species, *Chromatiales* and *Thiotrichales* are dominant sulfur oxidizing bacteria in the upper 5 cm sediment. *Epsilonproteobacteria*-related sulfur-oxidizer tended to increase on *Spartina* roots compared to surrounding sediment. *Desulfobacteraceae* and *Desulfobulbaceae* were also the dominant sulfate-reducing bacteria [185].

3.4 Conclusions and Outlook

The study shows that mixed of marine sediment and activated carbon in a wetland plant-MFC bioanode can generate electricity and is suitable for plants growth. The *Spartina anglica* growth rate was different which may be caused by the mixing extent of the materials. On average, the 33AC plant-MFC generated higher current and power density compared to other plant-MFCs. A spatial diverse microbial community was observed in both MS100 and AC33 Plant-MFC with *Proteobacteria* as the most abundant phyla. It looks that the microbial communities were affected by the anode composition and also by the spatial position. Overall, the results provide new insights that show the potential to test *Spartina anglica* demo-scale wetlands to generate electricity. The advantage of AC over other electrode materials is the provision of additional functions like electricity storage or sediment remediation.

3.5 Associated Content

All data generated or analyzed during this study are included in this published article (and its Supporting Information files). Microbiota data (raw 16s rDNA amplicon sequences) is submitted to the EBI database (<https://www.ebi.ac.uk/ena>) under accession number PRJEB33916. Raw experimental data is available in the DANS-EASY database (<https://doi.org/10.17026/dans-253-tk8w>).

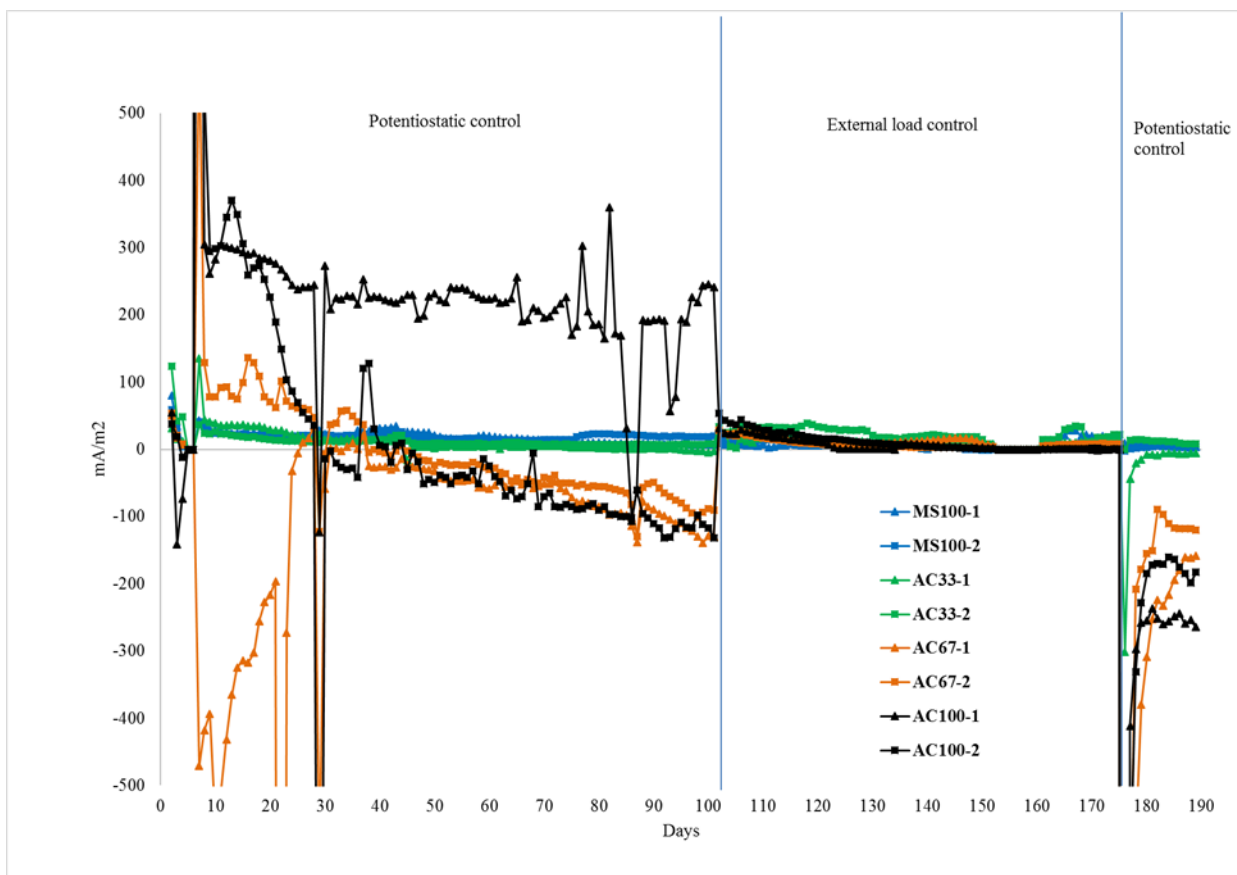
3.6 Acknowledgment

This research was funded by Government of Landak Regency, West Kalimantan Province, Republic of Indonesia under an MoU with Wageningen University & Research, No 6160030150. The authors thank to Andrea Aldas Vargas, Carlos Contreras Davila, Kasper de Leeuw, Pieter Gremmen and Rieks de Rienk for their help on the DNA extraction.

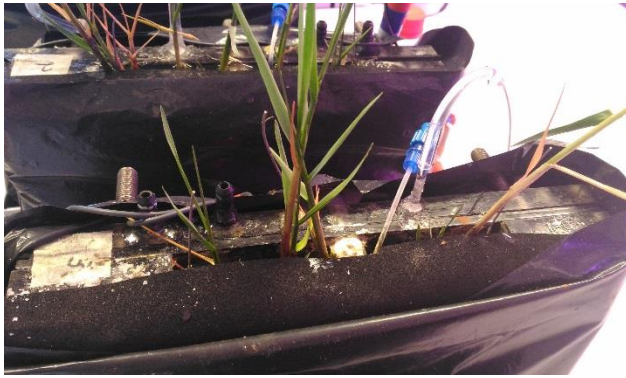
3.7 Supplementary Materials Chapter 3

The following supplementary materials are available online at <http://www.mdpi.com/2073-4441/11/9/1810/s1>

3.7.1 Supplementary Figures



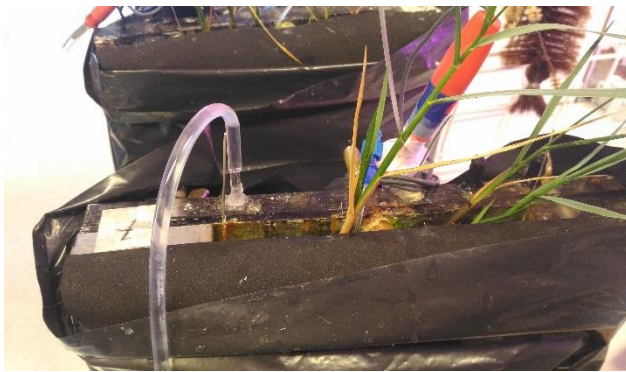
Supplementary Figure S3. 1: Plant-MFC performance on two different control modes



MS100 (Plant-MFC 3)



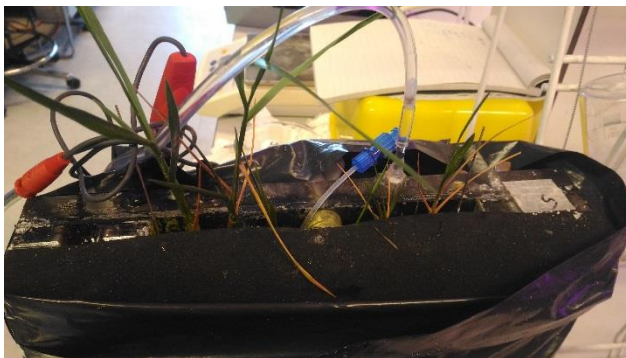
MS100 (Plant-MFC 4)



AC33 (Plant-MFC 7)



AC33 (Plant-MFC 8)



AC67 (Plant-MFC 5)



AC67 (Plant-MFC 6)

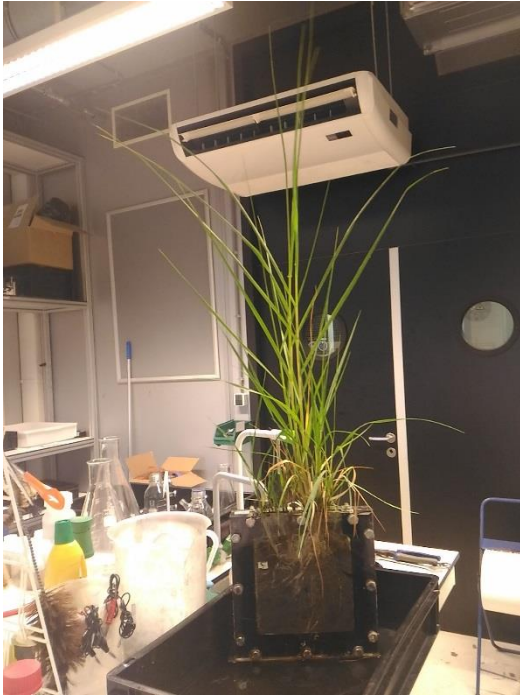


AC100 (Plant-MFC1)



AC100 (Plant-MFC2)

Supplementary Figure S3. 2: Plant condition at the beginning of the experiment (during transplantation)



MS100 (Plant-MFC 3)



MS100 (Plant-MFC 4)



AC33 (Plant-MFC 7)



AC33 (Plant-MFC 8)

Supplementary Figure S3.3, cont'



AC67 (Plant-MFC 5)



AC67 (Plant-MFC 6)



AC100 (Plant-MFC1)



AC100 (Plant-MFC2)

Supplementary Figure S3. 3: Plant conditions at the end of the experiment. Showing roots penetration; stem and leaf conditions



MS100 (Plant-MFC 3)



MS100 (Plant-MFC 4)



AC33 (Plant-MFC 7)

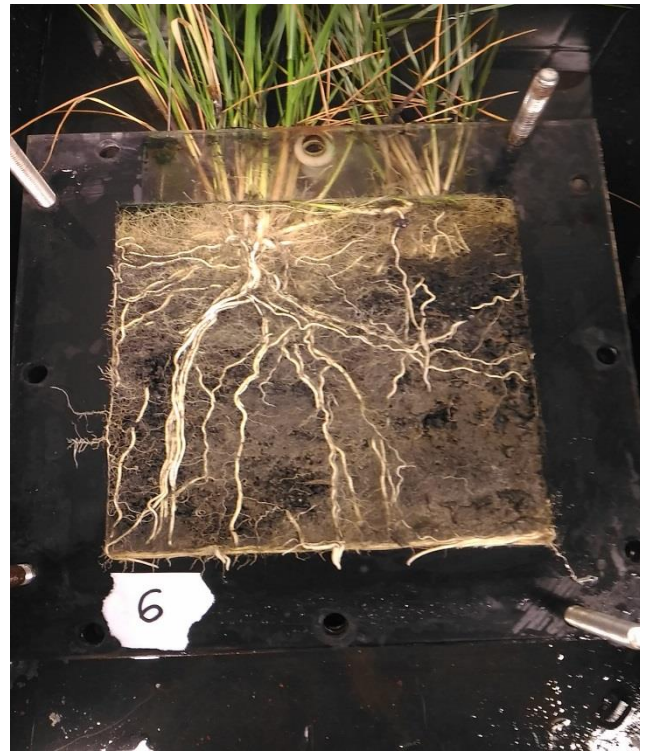


AC33 (Plant-MFC 8)

Supplementary Figure S3.4, cont'



AC67 (Plant-MFC 5)



AC67 (Plant-MFC 6)

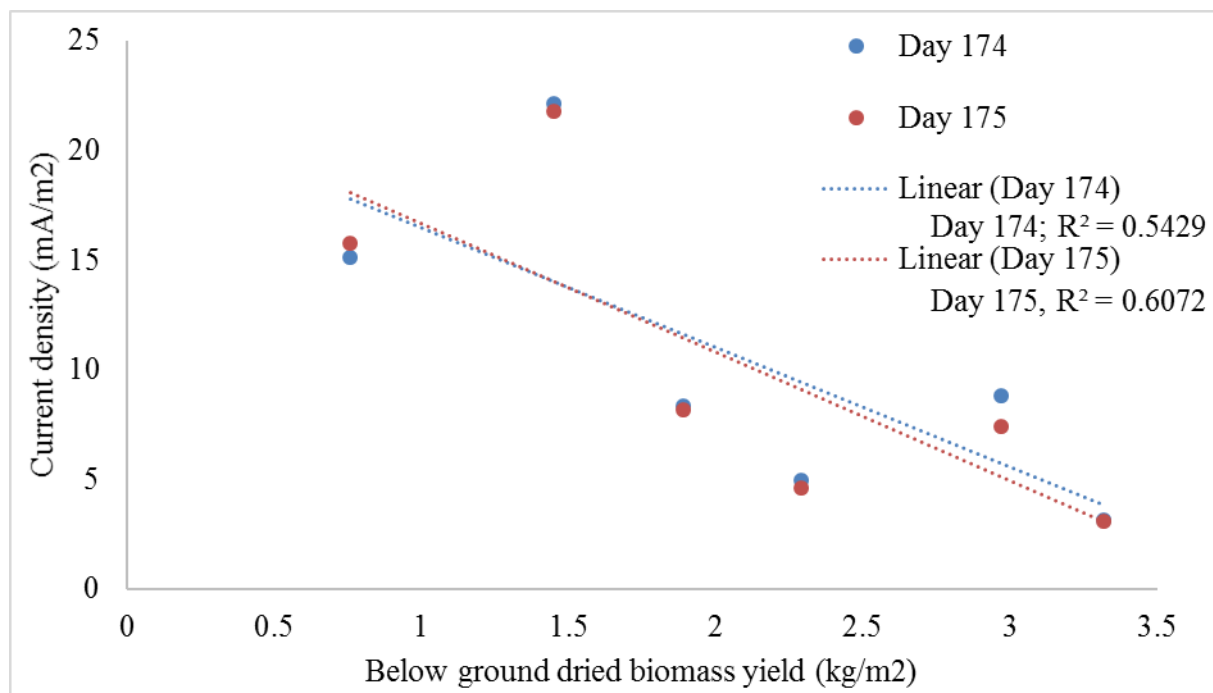


AC100 (Plant-MFC1)

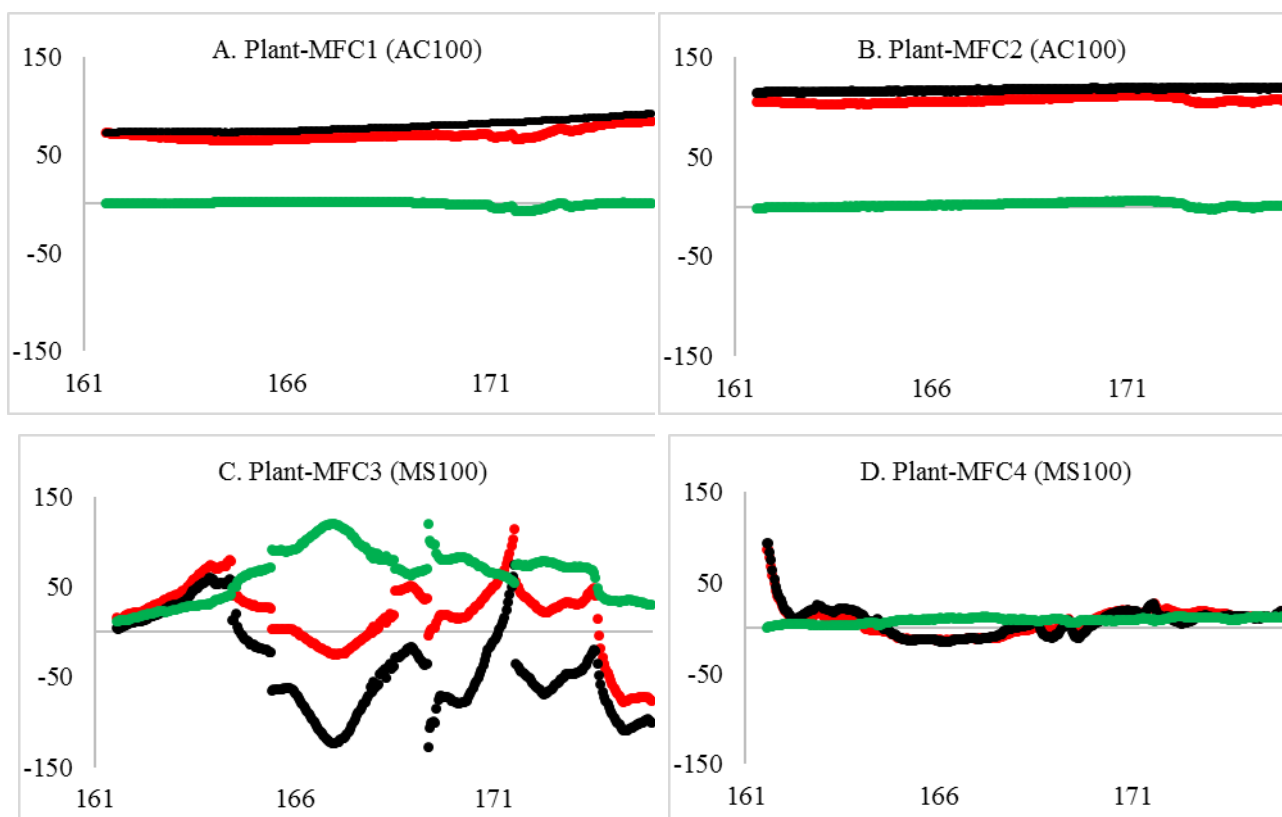


AC100 (Plant-MFC2)

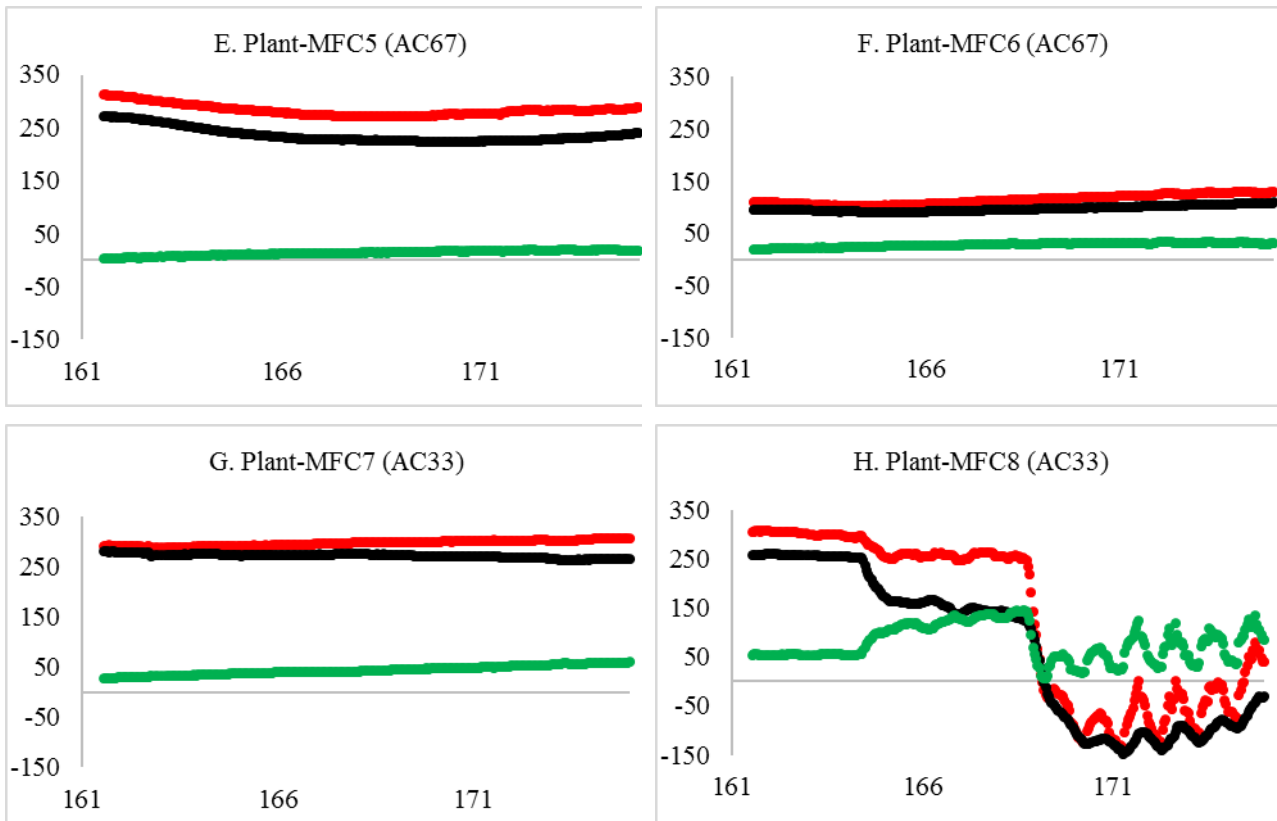
Supplementary Figure S3. 4: Root conditions at the end of the experiment



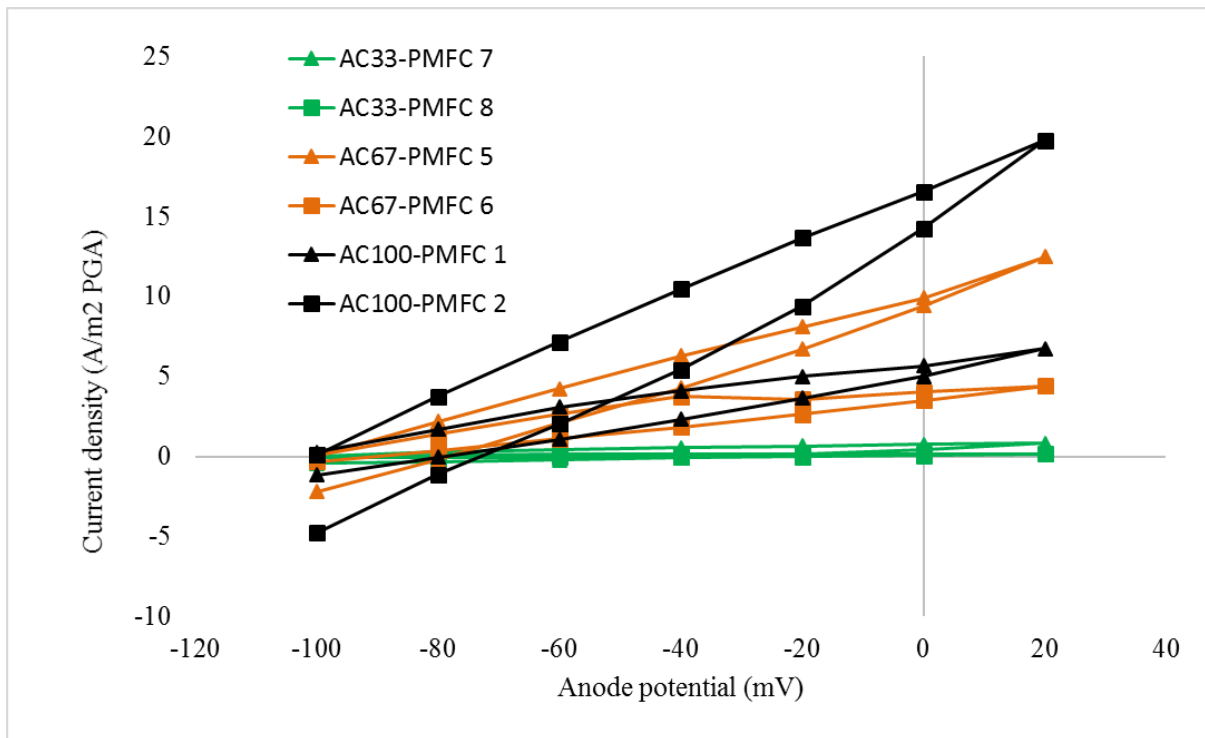
Supplementary Figure S3. 5: Correlation between root density and current density. Below ground dried biomass was calculated from harvested roots in the end of the experiments (day 190)



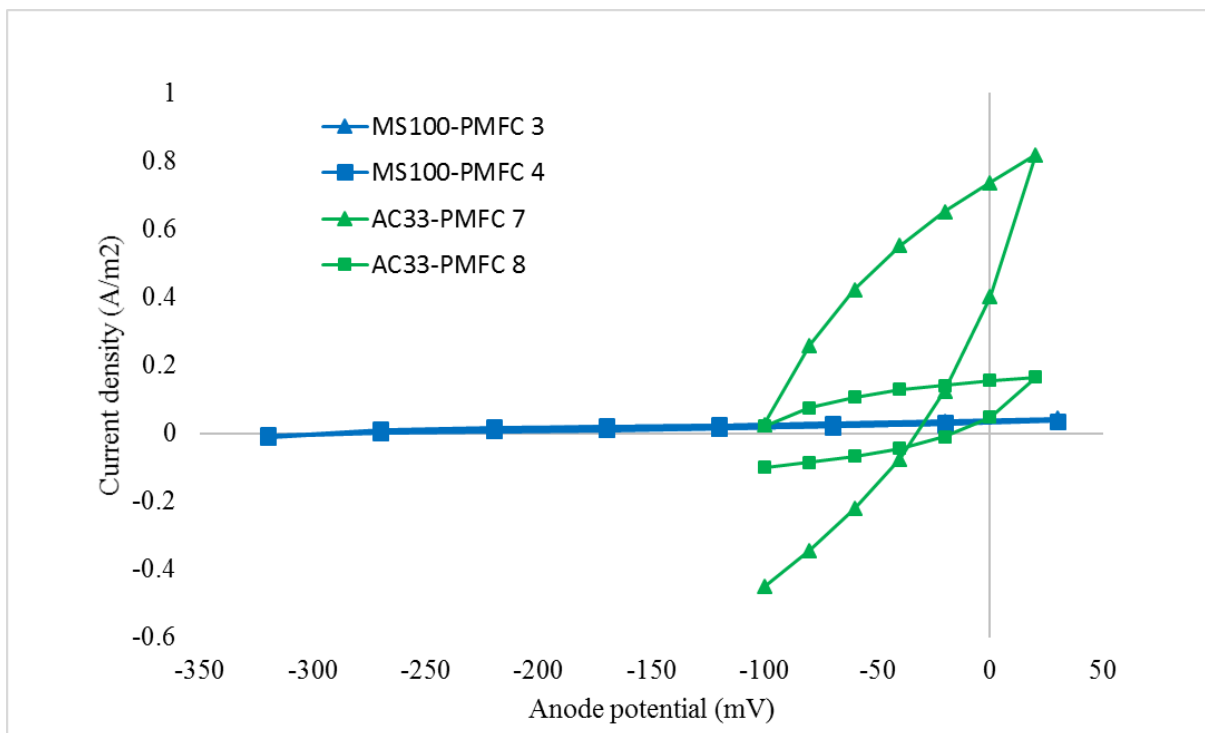
Supplementary Figure S3.6, cont'



Supplementary Figure S3. 6: Anode potential (black), Cathode Potential (red) and Cell potential (Green) of plant-MFCs between day 161 and 175. The vertical axes are the potential (mV) and the horizontal axes are the day

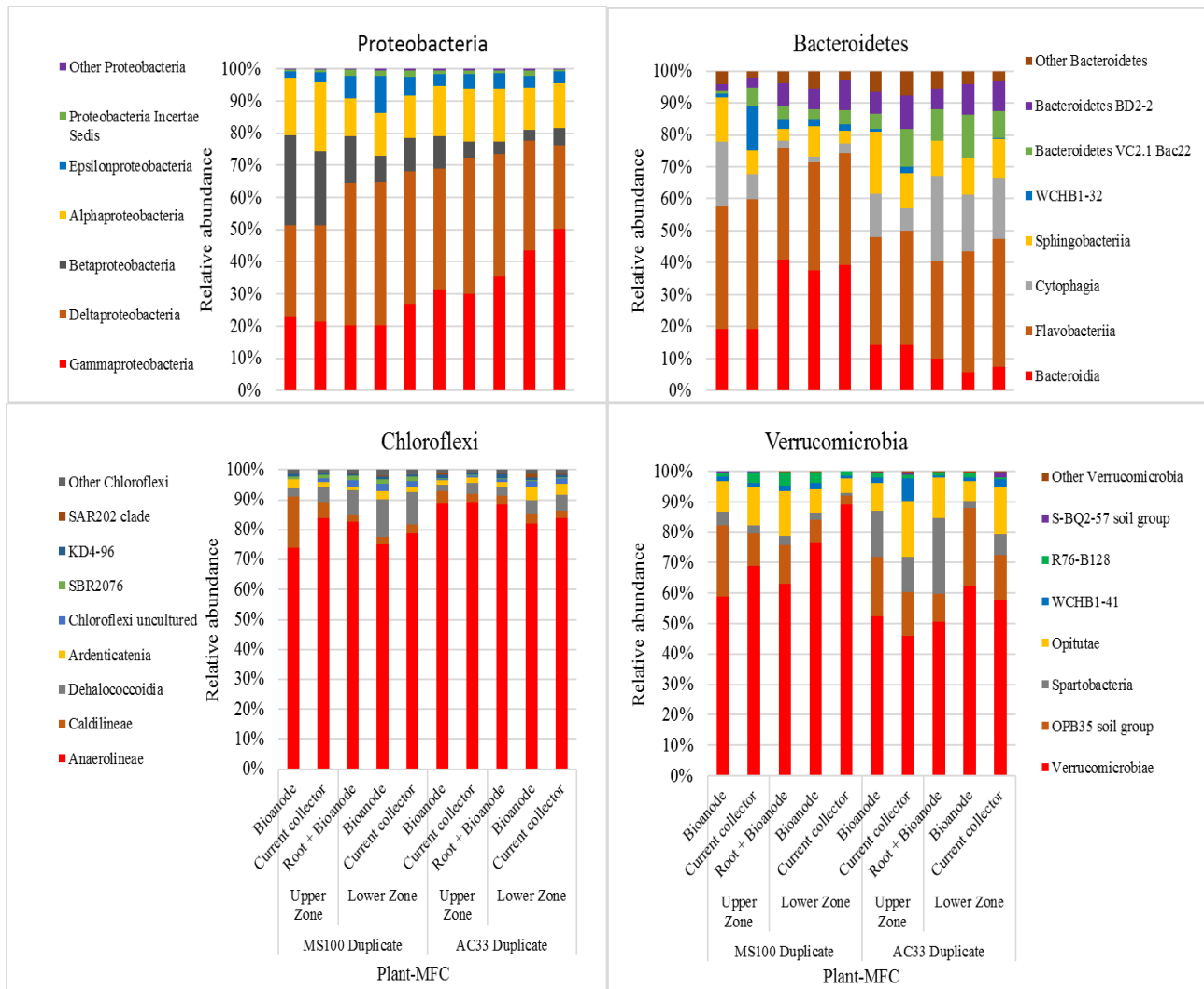


(a)



(b)

Supplementary Figure S3. 7: Polarization curve on day 28. (a) All Plant-MFCs, excluding MS100 Plant-MFCs. (b) Zoom in for MS100 and AC33 Plant-MFCs



Supplementary Figure S3. 8: Relative abundance of classes within a phylum from 4 most abundance phyla

3.7.2 Supplementary Tables

Supplementary Table S3. 1: Initial planted plants compositions

Systems	Wet mass of the stems (gr)	Number of planted stems
Plant-MFC 1 (AC100)	37.8	7
Plant-MFC 2 (AC100)	35.7	8
Plant-MFC 3 (MS100)	35.1	6
Plant-MFC 4 (MS100)	33.4	7
Plant-MFC 5 (AC67)	31.7	7
Plant-MFC 6 (AC67)	37.2	6
Plant-MFC 7 (AC33)	36.8	7
Plant-MFC 8 (AC33)	32.4	12

Supplementary Table S3. 2: Most abundant bacteria at order level with at least 5% relative abundance. Heat map abundance colors: red >5%; orange 2 to 5%; white <2%

CLASS ORDER	Average relative abundant (\pm standard error)									
	MS100 Duplicate					AC33 Duplicate				
	Upper Zone		Lower Zone			Upper Zone		Lower Zone		
	Bioanode (Sediment)	Current collector	Root+ Bioanode	Bioanode	Current collector	Bioanode (Sediment)	Current collector	Root+ Bioanode	Bioanode	Current collector
Deltaproteobacteria Desulfobacterales	6.95 ± 2.66	8.85 ± 0.75	10.76 ± 2.29	16.26 ± 0.63	15.1 ± 1.1	13.15 ± 0.58	14.4 ± 1.16	15.06 ± 1.47	16.85 ± 8.25	10.86 ± 6.29
Gammaproteobacteria Chromatiales	1.8 ± 0.46	2.41 ± 0.08	4.59 ± 1.25	6.04 ± 1.17	7.77 ± 2.54	6.5 ± 0.15	6.98 ± 1.78	7.29 ± 0.89	5.26 ± 0.12	8.46 ± 2.61
Flavobacteriia Flavobacteriales	8.15 ± 4.79	7.59 ± 3.43	6.95 ± 0.34	2.52 ± 0.47	2.95 ± 0.29	2.42 ± 0.53	1.78 ± 0.12	1.87 ± 0.2	1.35 ± 0.22	2.56 ± 1.02
Betaproteobacteria Hydrogenophilales	9.47 ± 0.15	4.99 ± 0.19	3.87 ± 0.17	1.12 ± 0.96	1.52 ± 1.38	1.87 ± 0.72	1.15 ± 0.52	0.66 ± 0.42	0.26 ± 0.04	0.66 ± 0.6
Verrucomicrobiae Verrucomicrobiales	3.35 ± 0.38	3.98 ± 3.1	1.27 ± 0.77	3 ± 0.56	7.42 ± 0.83	1.72 ± 0.7	0.31 ± 0.02	0.99 ± 0.66	0.77 ± 0.63	0.82 ± 0.24
Epsilonproteobacteria Campylobacteriales	1.03 ± 0.19	1.47 ± 0.18	2.9 ± 0.67	6.13 ± 1.64	3.06 ± 1.32	2.24 ± 0.19	2.98 ± 0.04	2.96 ± 0.72	2.25 ± 0.75	2.22 ± 0.65
Deltaproteobacteria Desulfuromonadales	2.85 ± 1.09	1.44 ± 0.24	1.6 ± 0.38	2.58 ± 1.32	1.49 ± 0.41	7.52 ± 5.46	10.29 ± 4.38	5.91 ± 0.75	0.4 ± 0	0.58 ± 0.1
Gammaproteobacteria Gammaproteobacteria Incertae Sedis	0.99 ± 0.15	1.27 ± 0.34	1.14 ± 0.4	1.64 ± 1	1.39 ± 0.06	3.07 ± 1.17	5.24 ± 1.5	6.45 ± 0.31	6.76 ± 1.59	6.51 ± 1.47
Anaerolineae Anaerolineales	2.76 ± 0.08	4.18 ± 0.22	3.76 ± 0.56	2.07 ± 0.97	3.72 ± 0.21	4.34 ± 0.72	5.56 ± 0.29	4.95 ± 0.3	3.51 ± 1.59	3.29 ± 0.04

Supplementary Table S3. 3: Most abundant bacteria at family level with at least 5% relative abundance. Heat map abundance colors: red >5%; orange 2 to 5%; white <2%

Order Family	Average relative abundant (\pm standard error)									
	MS100 Duplicate					AC33 Duplicate				
	Upper Zone		Lower Zone			Upper Zone		Lower Zone		
	Bioanode (Sediment)	Current collector	Root + Bioanode	Bioanode	Current collector	Bioanode (Sediment)	Current collector	Root + Bioanode	Bioanode	Current collector
Desulfobacterales; Desulfobacteraceae	4.56 ± 1.67	6.22 ± 0.16	13.41 ± 2.24	13.79 ± 0.94	12.24 ± 0.26	7.64 ± 0.78	10.11 ± 1.01	9.11 ± 0.14	8.25 ± 1.39	6.31 ± 2.65
Chromatiales; Ectothiorhodospiraceae	1.37 ± 0.23	1.7 ± 0.1	4.84 ± 1.48	5.05 ± 1.08	6.39 ± 2.15	6.11 ± 0.35	6.2 ± 1.65	6.67 ± 0.85	4.25 ± 0.09	7.79 ± 3.06
Anaerolineales; Anaerolineaceae	2.76 ± 0.08	4.18 ± 0.22	3.69 ± 0.56	2.07 ± 0.97	3.72 ± 0.21	4.34 ± 0.72	5.56 ± 0.29	4.95 ± 0.3	3.51 ± 1.59	3.29 ± 0.04
Hydrogenophilales; Hydrogenophilaceae	9.47 ± 0.15	4.99 ± 0.19	2.38 ± 0.17	1.12 ± 0.96	1.52 ± 1.38	1.87 ± 0.72	1.15 ± 0.52	0.66 ± 0.42	0.26 ± 0.04	0.66 ± 0.6
Flavobacteriales; Flavobacteriaceae	7.66 ± 4.64	7.3 ± 3.36	2.9 ± 0.34	2.41 ± 0.5	2.69 ± 0.26	1.55 ± 0.4	1.25 ± 0.03	1.02 ± 0.28	1.27 ± 0.23	1.59 ± 0.29
Campylobacterales; Helicobacteraceae	1 ± 0.19	1.43 ± 0.2	3.33 ± 0.6	5.86 ± 1.68	2.93 ± 1.2	2.16 ± 0.15	2.87 ± 0.04	2.95 ± 0.72	2.24 ± 0.75	2.19 ± 0.68
Verrucomicrobiales; Verrucomicrobiaceae	3.27 ± 0.39	3.96 ± 3.1	2.37 ± 0.74	2.93 ± 0.57	7.34 ± 0.82	1.69 ± 0.7	0.27 ± 0.01	0.94 ± 0.65	0.72 ± 0.65	0.77 ± 0.24
Desulfobacterales; Desulfobulbaceae	2.39 ± 0.99	2.63 ± 0.58	2.31 ± 0.06	2.46 ± 0.31	2.83 ± 0.83	5.5 ± 0.2	4.28 ± 0.14	5.94 ± 1.33	8.59 ± 6.86	4.54 ± 3.64
Gammaproteobacteria Incertae Sedis; Unknown Family	0.99 ± 0.15	1.27 ± 0.34	1.08 ± 0.4	1.64 ± 1	1.39 ± 0.06	3.07 ± 1.17	5.24 ± 1.5	6.45 ± 0.31	6.76 ± 1.59	6.51 ± 1.47
Desulfuromonadales; Desulfuromonadaceae	0.62 ± 0.1	0.4 ± 0.18	0.37 ± 0.06	0.52 ± 0.03	0.55 ± 0.18	6.57 ± 4.92	9.78 ± 4.4	5.5 ± 0.84	0.07 ± 0.01	0.31 ± 0.21

Supplementary Table S3. 4: Most abundant bacteria at genera level with at least 3% relative abundance. Heat map abundance colors: red >3%; orange 1-3%; white <1%

Order Family Genus	Average relative abundant (\pm standard error)									
	MS100 Duplicate					AC33 Duplicate				
	Upper Zone		Lower Zone			Upper Zone		Lower Zone		
	Bioanode (Sediment)	Current collector	Root + Bioanode	Bioanode	Current collector	Bioanode (Sediment)	Current collector	Root + Bioanode	Bioanode	Current collector
Burkholderiales; Alcaligenaceae; Castellaniella	1.47 ± 0.8	2.17 ± 0.25	5.62 ± 0.04	6.48 ± 0.74	4.95 ± 0.05	3.28 ± 0.51	2.88 ± 0.18	3.75 ± 0.19	2.99 ± 0.53	3.97 ± 0.77
Hydrogenophilales; Hydrogenophilaceae; uncultured	2.25 ± 0.17	3.25 ± 0.25	2.98 ± 0.53	1.55 ± 0.74	2.88 ± 0.27	3.63 ± 0.52	4.17 ± 0.2	4.11 ± 0.25	2.89 ± 1.23	2.95 ± 0.05
Propionibacteriales; Propionibacteriaceae; Brooklawnia	0.77 ± 0	0.66 ± 0.1	3.67 ± 1.7	2.56 ± 1.02	2.12 ± 0.11	5.06 ± 0.74	3.62 ± 1.61	4.55 ± 0.16	1.97 ± 0.34	2.53 ± 3.67
Xanthomonadales; Xanthomonadaceae; Thermomonas	3.23 ± 0.49	2.82 ± 0.05	2.91 ± 0.23	8.64 ± 5.78	2.74 ± 0.25	1.92 ± 0.06	2.66 ± 0.39	2.37 ± 0.56	2.16 ± 0.24	2.41 ± 0.06
SAR324 clade; Uncultured δ proteobacterium; uncultured delta proteobacterium	0.12 ± 0.02	0.15 ± 0.08	1.31 ± 0.85	3.1 ± 2.64	0.72 ± 0.66	0.71 ± 0.28	0.08 ± 0.04	0.03 ± 0	0.05 ± 0.02	0.04 ± 0.11
uncultured bacterium (ML635J-21); uncultured bacterium; uncultured bacterium	3.02 ± 2.49	0.47 ± 0.36	0.12 ± 0.08	0.05 ± 0.05	0.06 ± 0.04	0.11 ± 0.01	0.42 ± 0.1	0.82 ± 0.46	0.41 ± 0.19	0.1 ± 0.21
Phycisphaerales; Phycisphaeraceae; Z195MB87	0.42 ± 0.1	1.44 ± 0.3	0.66 ± 0.11	0.74 ± 0.36	1.15 ± 0.47	2.92 ± 0.59	1.56 ± 0.44	3.8 ± 1.75	6.81 ± 6.03	3.3 ± 2.42
Rickettsiales; Rickettsiaceae; uncultured	0.37 ± 0.12	0.59 ± 0.07	0.29 ± 0.19	0.45 ± 0.3	0.65 ± 0.15	1.98 ± 0.82	2.68 ± 1.21	4.04 ± 0.13	4.14 ± 0.13	3.61 ± 1.64
Cytophagales; Cyclobacteriaceae; Indibacter	0.39 ± 0.08	0.28 ± 0.18	0.24 ± 0.05	0.33 ± 0.07	0.44 ± 0.16	6.36 ± 4.95	2.64 ± 4.32	5.34 ± 0.85	0.02 ± 0.01	0.15 ± 0.06
Subsection ICyanobacteria; Family I; Synechococcus	0.75 ± 0.09	0.78 ± 0.24	0.37 ± 0.15	0.3 ± 0.18	0.53 ± 0.32	1.42 ± 0.68	1.16 ± 0.33	1.16 ± 0.4	3.18 ± 1.42	1.95 ± 0.47

Supplementary Table S3. 5: Acetate concentration, pH and ionic conductivity from anolyte and catholyte of Plant- MFCs

Days	AC100- PMFC 1	AC100- PMFC 2	MS100- PMFC 3	MS100- PMFC 4	AC67- PMFC 5	AC67- PMFC 6	AC33- PMFC 7	AC33- PMFC 8
Acetate concentration in the anolyte (mg/l)								
1	195	1752	31	13	41	7	89	7
22	6	9	17	5	5	6	8	7
31	0	0	0	0	0	0	0	0
37	0	0	0	0	0	0	0	0
45	0	0	0	0	0	0	0	0
77	n.a	n.a	n.a	n.a	n.a	n.a	n.a	n.a
105	n.a	n.a	n.a	n.a	n.a	n.a	n.a	n.a
190	n.a	n.a	n.a	n.a	n.a	n.a	n.a	n.a
Anolyte pH								
1	8.94	9.38	9.14	9.17	9.15	8.77	8.98	9.12
22	6.72	6.76	7.72	7.95	7.56	7.06	7.29	7.95
31	6.22	6.72	7.22	7.73	7.15	6.77	7.4	7.51
37	6.45	7.23	7.38	7.73	7.18	6.99	7.27	7.46
45	7.19	6.99	7.32	7.37	7.08	7.02	7.04	7.46
77	7.2	7.23	6.79	6.69	6.6	6.85	6.77	6.92
105	n.a	n.a	n.a	n.a	n.a	n.a	n.a	n.a
190	7.28	7.41	6.71	6.24	7.07	6.63	6.75	7.05
Anolyte ionic conductivity (S/m)								
1	0.783	0.77	0.966	1.084	0.676	0.941	0.905	0.764
22	0.829	0.767	0.927	0.932	0.841	0.938	0.932	0.824
31	0.929	0.758	0.964	0.953	0.933	0.879	0.9	0.851
37	0.862	0.751	0.984	0.931	0.926	0.899	0.903	0.892
45	0.903	0.769	1.017	0.941	0.98	0.904	0.987	0.926
77	1.044	0.722	1.248	0.945	1.004	0.954	0.978	0.997
105	n.a	n.a	n.a	n.a	n.a	n.a	n.a	n.a
190	0.441	0.447	0.379	0.298	0.342	0.591	0.404	0.341
Catholyte pH								
1	9.19	8.55	8.78	8.81	8.98	9.22	9.02	9.09
22	8.16	8.36	6.12	5.4	7.98	8.2	5.68	5.71
31	7.72	8.26	6.54	6.83	7.65	8.28	6.21	6.6
37	n.a	n.a	n.a	n.a	n.a	n.a	n.a	n.a
45	7.99	8.25	5.37	7.55	7.7	8.41	6.63	7.14
77	7.59	7.79	7.05	7.47	7.69	8.36	7.1	7.55
105	6.5	6.22	6.23	6.68	7.03	7.72	6.46	6.85
190	n.a	n.a	n.a	n.a	n.a	n.a	n.a	n.a
Catholyte ionic conductivity (S/m)								
1	0.764	0.388	0.558	0.616	0.284	0.532	0.55	0.476
22	0.703	0.413	0.558	0.589	0.745	0.574	0.649	0.499
31	0.744	0.433	0.591	0.519	0.638	0.569	0.665	0.541
37	n.a	n.a	n.a	n.a	n.a	n.a	n.a	n.a
45	0.803	0.45	0.845	0.576	0.686	0.659	0.75	0.57
77	0.745	0.376	0.722	0.508	0.678	0.569	0.689	0.663
105	0.887	0.571	0.926	0.655	0.774	0.689	0.86	0.718
190	n.a	n.a	n.a	n.a	n.a	n.a	n.a	n.a

n.a = not analysed

Supplementary Table S3. 6: Dried biomass yield after 190 days

Reactors	Above ground biomass Yield (Kg/m ² PGA)	Below ground biomass yield (Kg/m ² PGA)
MS100 (Plant-MFC 3)	2.74	2.97
MS100 (Plant-MFC4)	2.29	3.32
AC33 (Plant-MFC7)	0.45	0.76
AC33 (Plant-MFC8)	0.82	1.45
AC67 (Plant-MFC 5)	1.71	2.29
AC67 (Plant-MFC 6)	1.47	1.89
AC 100 (Plant-MFC 1)	0.63	0.79
AC100 (Plant- MFC 2)	0.47	0.87

3.7.3 Supplementary Methods

Supplementary Methods S3. 1: DNA extraction protocol modification

A. DNA extraction: Power soil® DNA Isolation Kit

Original procedure Instruction manual version 07272016 PowerSoil® DNA Isolation Kit can be downloaded from <https://mobio.com/media/wysiwyg/pdfs/protocols/12888.pdf>

The procedure is the same mentioned in the manual on pages 10-11.

Some modifications have been done and they are described by steps.

3 – After this step put samples in heat block at 55 degrees Celsius for 15 min.

6 – Tubes were centrifuged per 1 minutes instead of 30 seconds

14 – Solution C4 was added twice (600 uL first time and 500 ul second time) and vortexed twice as well.

15 – Spin filter was loaded with 650 uL instead of 675 uL to leave space on the tube for centrifugation.

20 – 30 uL of solution C6 were added instead of 100 uL. This was done because we didn't know what could be the DNA concentration and we didn't want to dilute the DNA.

23 – Put in heatblock for 15 min 55degrees Celsius just before spinning C6 down.

B. DNA quantification – Qubit

No modifications to the protocol were made. Qubit® dsDNA HS Assay Kits protocol can be downloaded from:

https://assets.thermofisher.com/TFS-Assets/LSG/manuals/Qubit_dsDNA_HS_Assay_UG.pdf

C. DNA concentration - Speed Vac

Original protocol on Concentrator 5301 Eppendorf can be downloaded from https://sydney.edu.au/medicine/bosch/facilities/molecular-biology/5301_900_017_11_0906_en.pdf

Evaporation with heating was used (page 21 – section 3)

The temperature used was 45C and the time was between 5-10 minutes.

Chapter 4

Performance and Long Distance Data Acquisition via LoRa Technology of a Tubular Plant Microbial Fuel Cell Located in a Paddy Field in West Kalimantan, Indonesia

Published as: Sudirjo, E.; de Jager, P.; Buisman, C.J.N; Strik, D.P.B.T.B. Performance and Long Distance Data Acquisition via LoRa Technology of a Tubular Plant Microbial Fuel Cell Located in a Paddy Field in West Kalimantan, Indonesia. *Sensors* **2019**, *19*, 4647.

Abstract

Plant Microbial Fuel Cell (Plant-MFC) has been studied both in the lab and in a field. So far, the field studies were limited to a more conventional Plant-MFC design, which submerges the anode in the soil and places the cathode above the soil surface. However, for a large scale application tubular Plant-MFC is considered more practical since it needs no top soil excavation. In this study, 1 meter length tubular design Plant-MFC was installed in triplicates in a paddy field in West Kalimantan, Indonesia. The Plant-MFC reactors were operated for 4 growing seasons. The rice paddy was grown in a standard cultivation process without any additional treatment due to the reactor installation. An online data acquisition using LoRa technology was developed to investigate the performance of the tubular Plant-MFC over the final whole rice paddy growing season. Overall, the four crop seasons, the Plant-MFC installation did not show a complete detrimental negative effect on rice paddy growth. Based on continuous data analysis during the fourth crop season, a continuous electricity generation was achieved during a wet period in the crop season. Electricity generation dynamics were observed before, during and after the wet periods that were explained by paddy field management. A maximum daily average density from the triplicate Plant-MFCs reached 9.6 mW/m^2 plant growth area. In one crop season, $9.5 - 15 \text{ Wh/m}^2$ electricity can be continuously generated at an average of $0.4 \pm 0.1 \text{ mW}$ per meter tube. The Plant-MFC also shows a potential to be used as a bio sensor, e.g. rain event indicator, during a dry period between the crop seasons.

Keywords: Tubular, Plant, Microbial Fuel Cell, Electricity, Rice, Paddy Fields, LoRa, Bioelectrochemical system

4.1 Introduction

Plant microbial fuel cells (Plant-MFC) has drawn the attention of many researchers since its first proof of principle performance using Reed mannagrass (*Glyceria maxima*)[40]. In principle the Plant-MFC is based on the microbial fuel cell (MFC) in which electrochemically active bacteria (EAB) generate electrons from substrates (i.e. glucose or acetate) in the anode; the generated electrons are transferred to the anode electrode and flow via an external load to the cathode side. In the cathode, these electron react with final electron acceptor (i.e. oxygen) and protons [52]. The electricity production depends on the anode and the cathode potential differences, in which the cell potential is the cathode potential minus the anode potential[51–53]. The common approach to estimate the theoretical cell potential is using thermodynamics of the anode (e.g acetate) and the cathode (e.g oxygen) reaction calculated based on Gibbs free energy at a specific condition [51,52]. For instance, the acetate oxidation ($C_2H_3O_2^- + 4 H_2O \rightarrow 2 HCO_3^- + 9 H^+ + 8 e^-$) and oxygen reduction ($O_2 + 4 H^+ + 4 e^- \rightarrow 2 H_2O$) potential at a specific condition (acetate concentration 0.05M, $[H_2O] = 1M$; pH = 7; pO = 0.2 bar; T = 298K) against Ag/AgCl reference electrode are -0.494 V and 0.6 V, respectively[51]. Therefore, a theoretical MFC cell potential using acetate model substrate and oxygen as the final electron acceptor is 1.094V. In addition, the Plant-MFC has growing plants which provide substrates in form of rhizodeposits that warrant electron donor availability for electrochemically active bacteria (EAB) to generate electricity[40].

The Plant-MFC has been studied both in the lab [40,45,57,60,62,65,96,130,136,138,186–189] as well in field studies [48–50,63,128,190]. So far, the field studies were using a conventional design of plant-MFC which put the anode in a lower anaerobic part (below the surface of the soil) and the cathode above the soil surface to obtain oxygen[48]. For a large scale application, this design is less practical because one needs to excavate the top layer of soil before anode installation. To avoid this excavation, Timmers proposed a new tubular design of Plant-MFC which could be installed using a horizontal drilling technique[64]. Plant-MFC's can potentially be applied in wet agricultural lands because it does not tend to disturb the surface that can in this case still be used for food production. Once implemented in for example a rice paddy, a challenge is the (re-)use of the Plant-MFC over consequent rice cultivation cycles. Rice paddies are typically manually and/or mechanically managed via various activities: (a): preparation of land by ploughing; (b) seedling and transplanting of the rice paddy; (c) water management; (d) fertilization; (e) weeding, and (f) pest control. This rice paddy management should not destruct the Plant-MFC so it can be used many years. Also the rice plant growth can potentially negatively affect the Plant-MFC performance by e.g. root growth into the cathode electrode which would provide rhizodeposits at the wrong electrode. Another potential

negative effect is the excretion of oxygen at the anode, causing inhibition due to cathodic reduction reactions at the anode[187]. Earlier tubular plant-MFC's were evaluated during long-term lab-based peat soil wetlands tests reaching a two week average power generation of 21mWm^{-2} plant growth area(PGA)[60].

Wetlands are considered the suitable place to integrate Plant-MFC's technology in a real life application because a Plant-MFC requires anaerobic conditions for their anode (to minimise competing oxygen reduction processes) and allow plants growth to supply rhizodeposits and other potential organic substrates to generate electricity (like organic plant matter remains after plants harvesting or leaf littering) [46]. The total amount of paddy fields represent one of largest types of wetlands. In 2017, the average harvested area of paddy fields and the rice paddy production in world are about 167million ha and 770 million tonnes of rice, respectively [67]. As human population is growing, the need for paddy field and production to support basic human need for food is also growing. More than 90% of world rice paddy has been produced in Asia[67]. With its current size in the world, paddy fields have a great potential to be integrated with plant-MFC technology. Plant-MFC also has potential to reduce methane emission from paddy field; a well-known potent greenhouse-gas[136,140].

Even though there were several studies about Plant-MFC's in a field, to our best knowledge there is no study performed yet on the performance of tubular Plant-MFC's in a paddy field. The objective of this study was to investigate the performance of tubular plant-MFC in a tropical paddy field, providing data analysis over a whole rice paddy growing cycle. Electricity generation, rice growth and microbial community were studied. An online data acquisition method using a long range (LoRa) technology was developed since local manual measurements on electricity generation could not be done at sufficient intervals [191–193]. The paddy field area had no connection to the electricity grid and there were no long-range transmissions network available. Therefore, a local LoRa network was set-up. The end devices using 2 Volt input (2xAA alkaline battery) were connected to the Plant-MFC to measure voltages and temperature. A LoRa gateway was installed and locally powered by a solar power system. This gateway provided the communication with the data acquisition devices via LoRa connection and sent the collected data to a LoRa network server through an IP connection (3G internet)[191]. The set-up and performance of this long distance data acquisition and transfer from West Kalimantan, Indonesia to Wageningen, The Netherlands, is also discussed.

4.2 Materials and Methods

4.2.1 Paddy field

An existing paddy field in West Kalimantan, Indonesia (0.919215N, 109.468182E; elevation 100m above sea level) was used for the experiment. This paddy field was cultivated using a common agricultural practice in that area. The rice paddy (*Oriza sativa* L. var Inpari 30 Ciherang Sub 1) was transplanted twice per year which are in May and November (**Table 4. 1**). The rice paddy growth phase are shown in **Figure 4. 1**. Prior to transplantation, the rice paddy seeds were grown in a nursery site for 20-30 days. Afterward, the rice paddy were manually transplanted by farmers in the soil in lines with a distance between 15cm and 25 cm. During the seedling period, soil was prepared by ploughing it with a hand tractor. The ploughing was preceded by flowing water into the paddy field (about 7 days) to make the soil softer. The ploughing was done per plot and in line with water flow direction from both up- and downstream. The water was kept flowing between 5-10cm above the ground in the paddy field until ripening period. The soil was dried in the last 2-3 weeks before harvest.

Table 4. 1: Research phase on four different crop seasons

Crop season	Transplantation (date)	Harvesting (date)	Applied load Plant-MFC (ohm)	Electricity Measurement
I	6 November 2017	10 February 2018	470	Multimeter
II	16 May 2018	6 August 2018	470	Multimeter
II	8 November 2018	13 February 2019	470	Multimeter
IV	13 May 2019	7 August 2019	1000	LORA

Rice paddy maintenance includes of several activities such as fertilization, pest control, weeding, and water management. The fertilization was applied twice for one crop season. The first fertilization was about 7 days before transplantation day (TD) after the ploughing and the second fertilization was 7 days after TD. In the first fertilization, three kinds of fertilizer were applied together, which are Urea (PT.Pupuk Sriwidjaja, Palembang, Indonesia), NPK Phonska (PT.Petrokimia Gresik, Gresik, Indonesia) and Petroganik (PT. Pupuk Indonesia (PERSERO) Group, Cikampek, Indonesia). In the second fertilization, only urea and NPK Phonska were applied in the paddy field. The application of fertilizer followed the dosage stated on the package. During the fertilization, water inlet and outlet

was closed for 2-3 days so that the fertilizers dissolved and seeped into the soil. After that the water was slowly put back into the paddy field with a small flow.

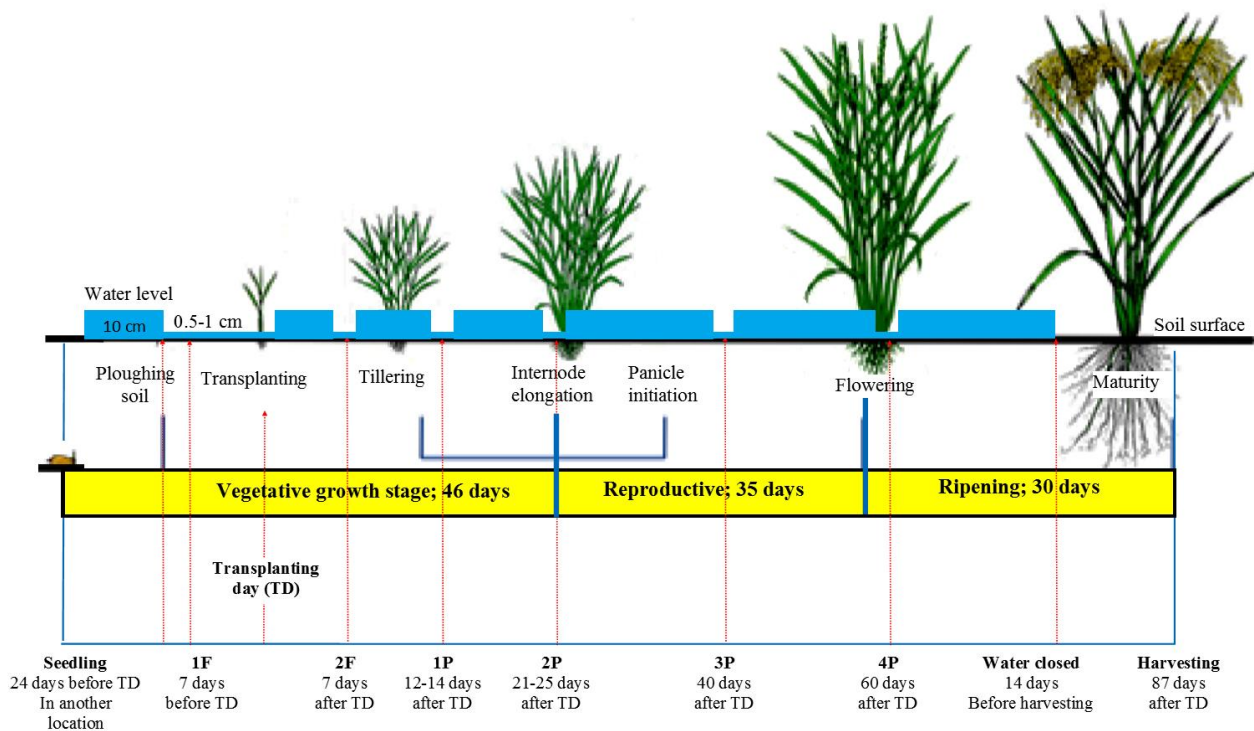


Figure 4. 1: Growth phase of rice paddy with water, fertilizer and pesticide management. Adapted from [31] under CC BY NC SA3.0 license. F = Fertilization; P= Pest control with insecticides.

The pest control was done by using molluscicides and insecticides. The molluscicides (Keong Tox, PT.Santani Sejahtera, Indonesia) was applied 1 day before the first fertilization to control snail, *Pomacea spp*, (known as keong mas in Indonesian). The insecticides were distributed by spraying mixture of Mipcindo 50WP (PT. Inti Everspring Indonesia, Mangunreja-Serang, Indonesia) and Imidacloprid 96TC (PT.Catur Agro Dinamika, Pamulang Tangerang Selatan, Indonesia). The mixing ratio between Mipcindo and Imidacloprid was 3:1 (tablespoon) for 25 liter water. The insecticides spraying was done three times during the crop season which were 12-14 days after TD, 21-25 days after TD and 40 days after TD. In addition, if walang sangit (*Leptocorisa oratorius*) and wereng (a general term to call the plant-liquid sucking insect from *Hemiptera* order) were still seen a lot, another insecticides spraying was done (at 60 days after TD) with a mixing ratio 3:2.

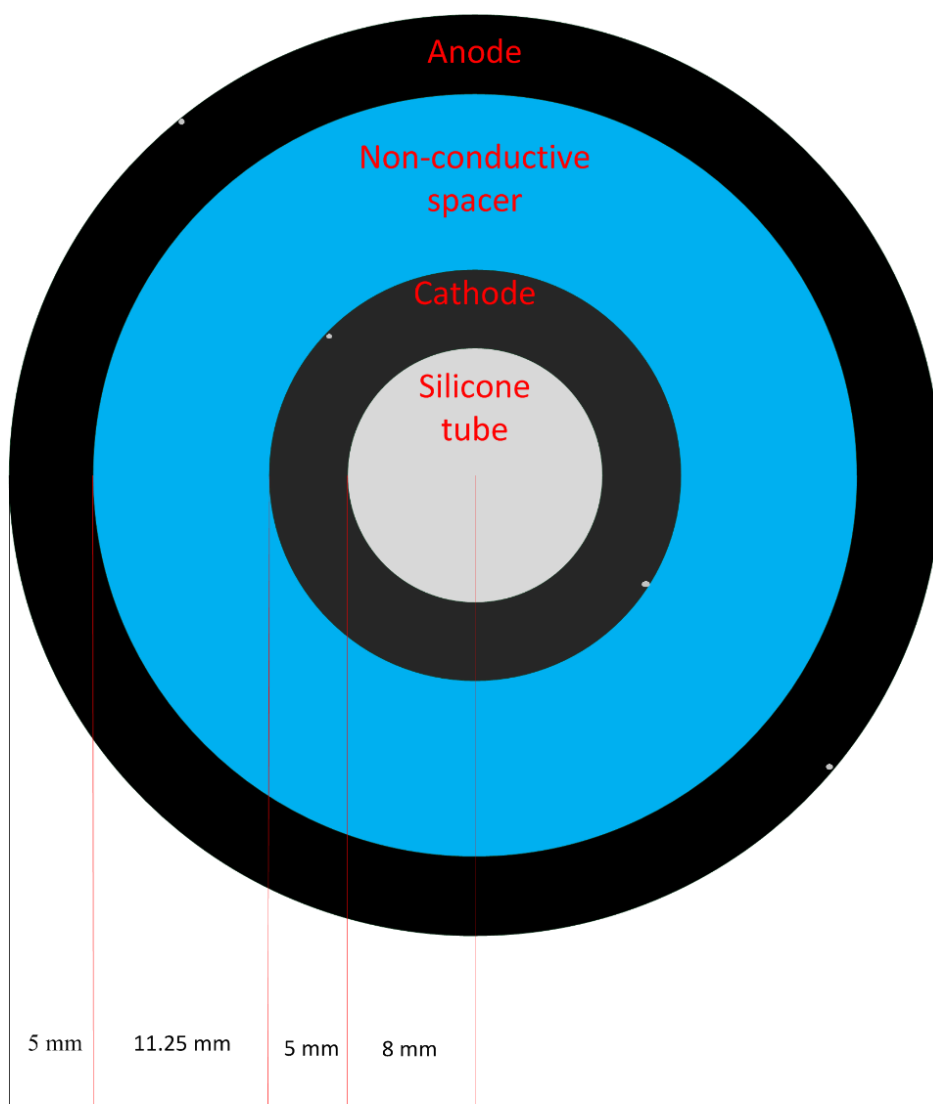
Water management plays an important role in rice paddy cultivation. Before applying the molluscicides water was reduced to about 0.5-1cm above the ground. This water level was kept until the first fertilization and the transplantation day. Three day after the TD water level was slowly

increased to the normal level. The same mechanism was done during the second fertilization. Apart from these period, the water level was kept on the normal level (5-10 cm above the soil) following the rice paddy growth phase. The continuous flooding also functions to reduce weeds. In the studied paddy field, weeds growth was hampered because the fields were well ploughed. Therefore, weeding was only manually extracted if they were spotted. The water flow was stopped 2-3 weeks before harvest day.

The Inpari 30 Ciherang Sub 1 paddy is well-known as a flood-tolerant variety. It can tolerate submergence of up to 14 days [194]. According to Indonesian Center for Rice Research, Indonesian Agency for Agricultural Research and Development, Ministry of Agriculture Republic of Indonesia (*Balai Besar Penelitian Tanaman Padi, Badan Penelitian dan Pengembangan Pertanian, Kementerian Pertanian Republik Indonesia*), this variety has an average productivity of 7.2 ton/ha and the harvest time is 111 day after seedling[195].

4.2.2 Electricity Generation

On October 28th, 2017, three tubular plant microbial fuel cells (tubular plant-MFCs) were installed in the paddy field (**Figure 4. 2**). The plant-MFC reactors were installed in lines next to each other from west to east (**Supplementary Figure S4.1**). Distance between reactors was 30cm. The tubular plant-MFC was manufactured by Plant-e (Wageningen, The Netherlands) according to similar design used by Wetser, et al [60]. As base transparent silicon tube (VMQ silicone, 12/16 mm inner/outer diameter; rubbermagazijn.nl, Zoetermeer, The Netherlands) was used to supply oxygen. Consequently the cathode felt, the spacer and finally the anode felt was wrapped around this tube. Both the anode and the cathode were made of carbon felt (KFA-5mm thickness, SGL Carbon GmbH, Bonn, Germany). The electrode length of each tubular plant-MFC was 1 meter and the width for the anode and the cathode was 19cm and 10 cm, respectively. Spacer was made from non-conductive materials to prevent short circuiting, but is otherwise completely permeable (air filter cloth DA/290, DACT Filter- & Milieutechniek, Kerkrade, The Netherlands). Titanium wire (grade 2, 0.5mm; Titaniumshop BV, Kampen, The Netherlands) was used as current collector both in the anode and the cathode side. The current collector was tied and wrapped around the cathode and the anode as shown in the **Figure 4. 2**.



Plant-MFC Diameter = 58.5 mm

Figure 4. 2: Plant-MFC tubular reactor before installation (above) and its schematic cross-section view (below). Two grey dots on the outer side of the anode and the cathode represent titanium wire current collector.

The tubular plant-MFCs were installed manually by hoeing the top soil of the paddy field prior to the transplantation. The tubular plant-MFCs were placed about 10-15 cm below the soil (*Figure 4. 3*). Both ends of the silicone tubes were bended down with the open hole facing ground to avoid rain water going into the tube that can affect air i.e. oxygen supply to the cathode.



Figure 4. 3: Installed tubular Plant-MFC installation (see shaded area) just before covering the tube with paddy field soil

4.2.3 Measurements and Analysis

Plant-MFC reactor performances were evaluated based on anode potential, cathode potential and cell potential, in combination with different applied external loads. In the first three crop seasons, data were irregularly measured with a digital multimeter (Fluke, Fluke Europe B.V., Eindhoven, The Netherlands). All potentials were measured and reported against a 3M KCl Ag/AgCl reference electrode (QIS, Oosterhout, Netherlands). The anode reference electrode was fixed on the anode surface with a cable tie and the cathode reference electrode was inserted in the tube between the cathode and spacer. In the fourth crop season, data (the anode potential, the cathode potential, the cell potential and temperature) were automatically logged using LoRa technology (AE Sensors B.V, Dordrecht, The Netherlands). The temperatures were measure 50cm above the ground using the temperature sensor integrated in the same LoRa data acquisition technology.

Rainfall data were obtain from the two nearest weather station, which are Mempawah Climatology Station (0.07500N, 109.19000E ; 2m above sea level) about 100km at South- South West of research

area and Paloh Climatology Station (1.74000N, 109.30000E ;15m above sea level) about 100 KM at North-North West of the research area.

Soil samples were collected (on 30 June 2018) from 6 different locations for microbial community analysis (**Figure 4. 4**). Samples were grouped into 3: Group I (Samples A and C) was soil that attached on the anode from mid plant-MFC; Group II (samples B and D) was soil that attached on the anode from end of the plant-MFC; and Group III (samples E and F) was from soil with 2 m distance from plant-MFC 1 and 2. After collection, samples were kept in a 30ml-tube container and keep in 4⁰C fridge. The next day samples were transported for 48hours with a cool-ice box for DNA extraction to Genetika Lab, Jakarta (PT. Genetika Science Indonesia), a partner company from 1st BASE Axil Scientific Pte Ltd, Singapore.

Sequencing steps were performed by 1st BASE[196] as following: the universal primers that targeted the V3V4 regions were used for amplification. The quantity and quality of the PCR product that targeted the V3V4 regions were measured using Tapestation 4200, picogreen and nanodrop. All the samples passed the QC measurement and proceed straight for a library preparation. The libraries were prepared using Illumina 16s metagenomics library prep kit and their quality and quantity were determine using Agilent Tapestation 4200, Picogreen and qPCR. These libraries were then pooled according to the protocol recommended by the Illumina and proceed straight to sequencing using MiSeq platform at 2x301PE format by 1st BASE Axil Scientific Pte Ltd, Singapore.

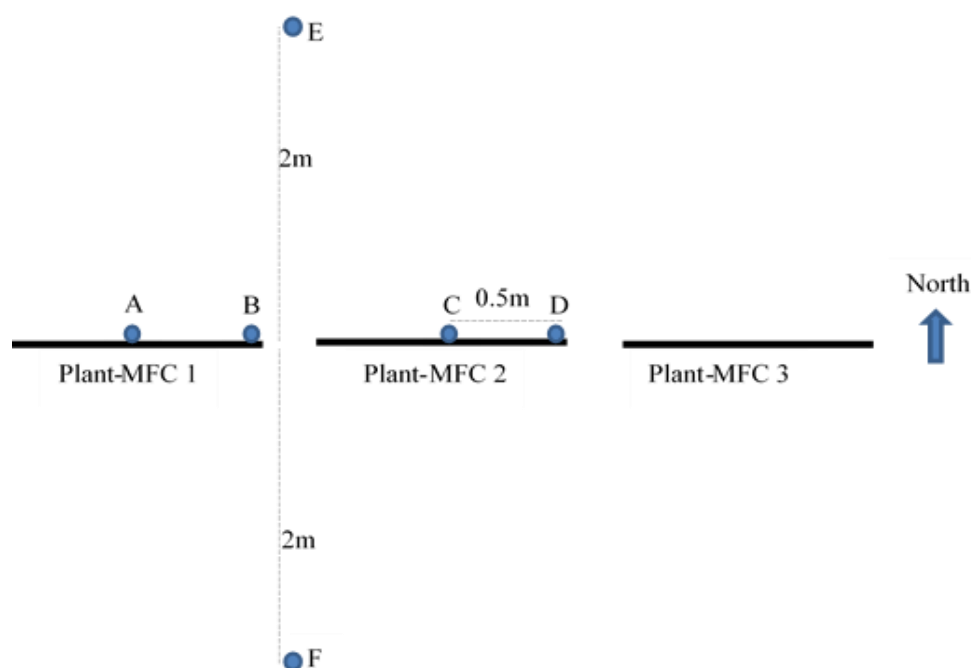


Figure 4. 4: Soil samples collection points (A, B, C, D, E, and F).

During the harvest time from the third and the fourth crop season, aboveground biomass was collected from 12 different locations. Three locations (above plant-MFC) were a 1-square-meter area above each plant-MFC reactors and another six location (1 metre from plant-MFC) were a 1-square-metre area both to the north and to the south from each reactor (*Supplementary Figure S4.2*). In the fourth crop season, the biomass was only collected from the north part of the plant-MFC reactors. Biomass was cut about 5 cm from the ground. After collection, wet biomass was weighted using a manual 10-kg counterweights scale with a precision of 100gr.

4.2.4 Long Distance data acquisition

Eight wireless voltage meters (AE sensors, Dordrecht, the Netherlands) were installed as data acquisition on 14 February 2019 between crop season 3 and 4. Each sensor has three inputs; one common ground and two completely differential inputs. For each installed tube, a reference sensor (3M KCl Ag/AgCl reference electrode, QIS, Oosterhout, Netherlands) was installed which was connected to the common ground. Both the anode and cathode were measured completely differential against the reference input. Each voltage meter is built into a watertight junction box and is powered by two AA batteries, the projected operating time at Borneo conditions with four measurements per hour is at least one year. The voltage meters have a Laird RM186-SM module (LoRa/BLE 868MHz LoRa EU) implemented and can be approached by Bluetooth through the Laird Toolkit app to check it's status and connectivity (*Figure 4. 5*). Through the same module, data can be sent through the LoRaWAN network (Long Range Wide Area Network). Since the voltage sensors, including the Laird module, were manufactured in the Netherlands, they used the EU LoRaWAN protocol which cannot be used out of the EU. Moreover, there was no LoRaWAN network enrolled yet at the research site. We therefore also installed a Gateway (Laird RG186 LoRa Gateway, Laird Connectivity) on site that was connected through the locally installed WiFi network dongle (ZTE MIFI Router, InternationalSIM, Terborg, The Netherlands) (*Figure 4. 5*). This Wifi network was finally made possible through the available 3G mobile phone network (IM3 Ooredoo, PT. Indosat Tbk, Jakarta, Indonesia). Due to the lack of available electricity on site, the whole system is powered by a locally installed battery system (100Wp solar panel, 100 AH 12 V Rechargeable Sealed Lead Acid Battery; PWM20 Solar Charge Controller) on solar panels. Data is temporary stored by the sensors and sent in CSV-format on a daily basis to pre-defined email addresses of the involved researchers in the Netherlands. This data logging equipment was co-designed and/or manufactured with support by Plant-e B.V (Wageningen, The Netherlands) & AE Sensors B.V (Dordrecht, The Netherlands).

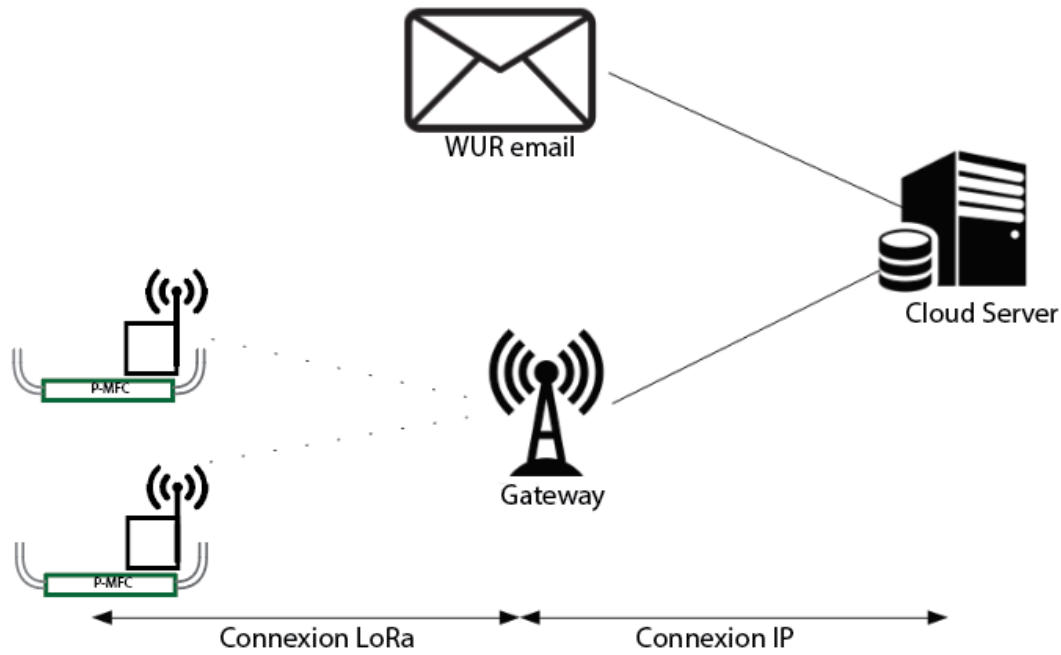


Figure 4. 5: Online data acquisition system

4.2.5 Calculation

Current generation was calculated according to Equation 4.1.

$$I = \frac{V}{R}, \quad (4.1)$$

I is current production in Ampere (A), V is cell potential in Volt (V) and R is applied load in Ohm (Ω).

Power generation was calculated according to Equation 4.2 or Equation 4.3.

$$P = V \times I, \quad (4.2)$$

$$P = I^2 \times R, \quad (4.3)$$

P is power output in Watt (W), V is cell potential in Volt (V), I is current production in Ampere (A) and R is applied load in Ohm (Ω).

Current density (A/m²) and Power density (W/m²) were obtained by dividing the current production and the power output with plant growth area (PGA). The PGA was 0.0585 m². Energy density (Wh/m²) was obtained by multiplying the power density with the time (h) it was generated.

Internal resistance (R_{int}) is calculated according to equation 4.4 [53].

$$R_{int} = \frac{E_{OCP} - E_{cell}}{i}, \quad (4.4)$$

E_{OCP} is the open cell potential in V, E_{cell} is the measured cell potential in V, i is the current density in A/m² and R_{int} is the internal resistance in $\Omega.m^2$.

Internal resistance is the accumulation of resistances in the Plant-MFC system due to anode overpotential (η_{an}), cathode over potential (η_{cath}) and membrane potential (E_m)[53]. Cathode internal resistance (R_{cath}) and anode internal resistance (R_{an}) are calculated according to equation 4.5 and equation 4.6, respectively.

$$R_{cath} = \frac{\eta_{cath}}{i} = \frac{E_{OCP,cath} - E_{cath}}{i}, \quad (4.5)$$

$$R_{an} = \frac{\eta_{an}}{i} = \frac{E_{an} - E_{OCP,an}}{i}, \quad (4.6)$$

$E_{OCP,cath}$ is the cathode potential at open cell potential (V), $E_{OCP, an}$ is the anode potential at open cell potential(V), E_{cath} is the measured cathode potential (V) and E_{an} is the measured anode potential (V). The internal resistance is reported normalized to the PGA.

In this study, the theoretical cathodic reduction reaction potential of oxygen to water (-0.494V vs Ag/AgCl) is considered as the cathode potential at open cell condition ($E_{OCP,cath}$). The theoretical anodic oxidation reaction of acetate (0.6V vs Ag/AgCl) is used as the anode potential at open condition ($E_{OCP, an}$). Thus, the open cell potential is 1.094V vs Ag/AgCl [51,52].

The maximum power generation was evaluated by a polarization technique. Polarization was conducted on 29 November 2017. First, plant-MFC was operated at an open cell condition (external load was disconnected) for 10 minutes. After that the external load was reconnected and changed every 10 minutes from high to low in order. The external loads used for the polarization were 1000 ohm, 470 ohm, 220 ohm, 100 ohm, and 10 ohm. Cell potential generated from the plant-MFCs for every operated external load were measured with a multimeter after 10 minutes operation. From these cell potential, current generation and power generation were calculated according to equation 4.1 and 4.2 and normalized to PGA. Note that this is not an indicator for the actual long term performance of the Plant-MFC since this method does allow to take capacitive current into account.

4.3 Results

4.3.1 Rice paddy maintenance, growth and production above Plant-MFC application

The tested Plant-MFCs did generate electricity and the paddy field maintenance was for this field study not strongly influenced. The rice paddy owner took care not to destruct a buried tube during land preparation and other maintenance activities. Rice plants did grow and produced rice during the experiments (*Supplementary Figure S4.2*). In all four crop seasons, no negative effect was observed in the rice paddy growth due to the tubular plant-MFC installation (*Supplementary Figure S4.3*). Conversely, the aboveground biomass production was on average between 27% and 35% higher above the tubular plant-MFC installation compared to one meter away from that location (*Table 4. 2*). Although one cannot claim that this increase was due to the plant-MFC installation as there is variation in biomass production possible due to e.g. so called border effect [197]. This result is still important to prove that the co-installation of the Plant-MFC in a paddy field is suitable both for food and electricity generation. At moment of submission of this paper, the Plant-MFCs are still installed and no signs of impairment on the technology were revealed (data not shown). Further continuation could show the durability of the Plant-MFC and provide information on required maintenance. No maintenance was required in the first two years.

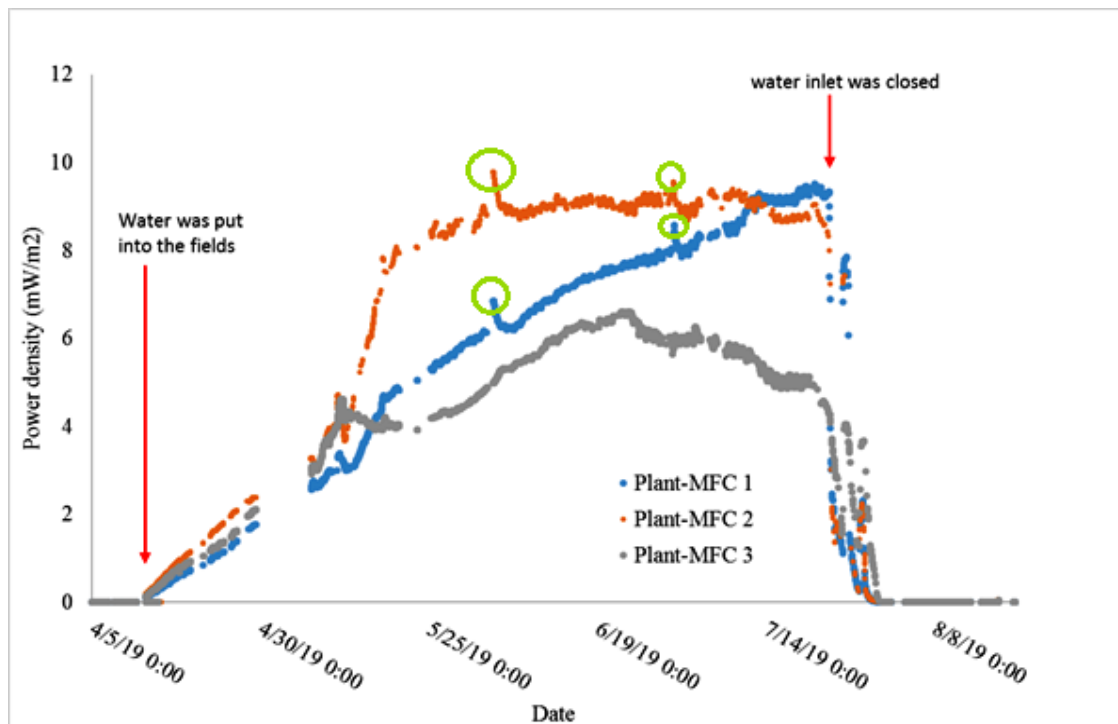
Table 4. 2: Average aboveground wet biomass (Kg/m²)

	3rd Crop season	4th crop season
Above Plant-MFC	3±0.5	4.6±0.7
One meter from Plant-MFC	2.3±0.5	3.4±0.8

4.3.2 Continuous power production during the rice growing season

During the rice growing season, a continuous electricity production was achieved (*Figure 4. 6A & B* and *Supplementary Figure S4.4*). A proper analysis was obtained from the fourth crop season in which data were automatically logged using LoRa technology. Maximum daily average power density of the triplicate experiment reached 9.6 mW/m² PGA (*Figure 4. 6A*). Plant-MFC 2 was able to continuously generate a power density of 8.5 mW/m² PGA for 60 days on the fourth growth season (*Figure 4. 6A*). Based on 72 days current generation in the fourth crop season during waterlogged conditions, 9.5 - 15Wh/m² PGA energy density (at an average of 0.4±0.1 mW per meter tube) was achieved.

A. Power density



B. Anode and Cathode Potential

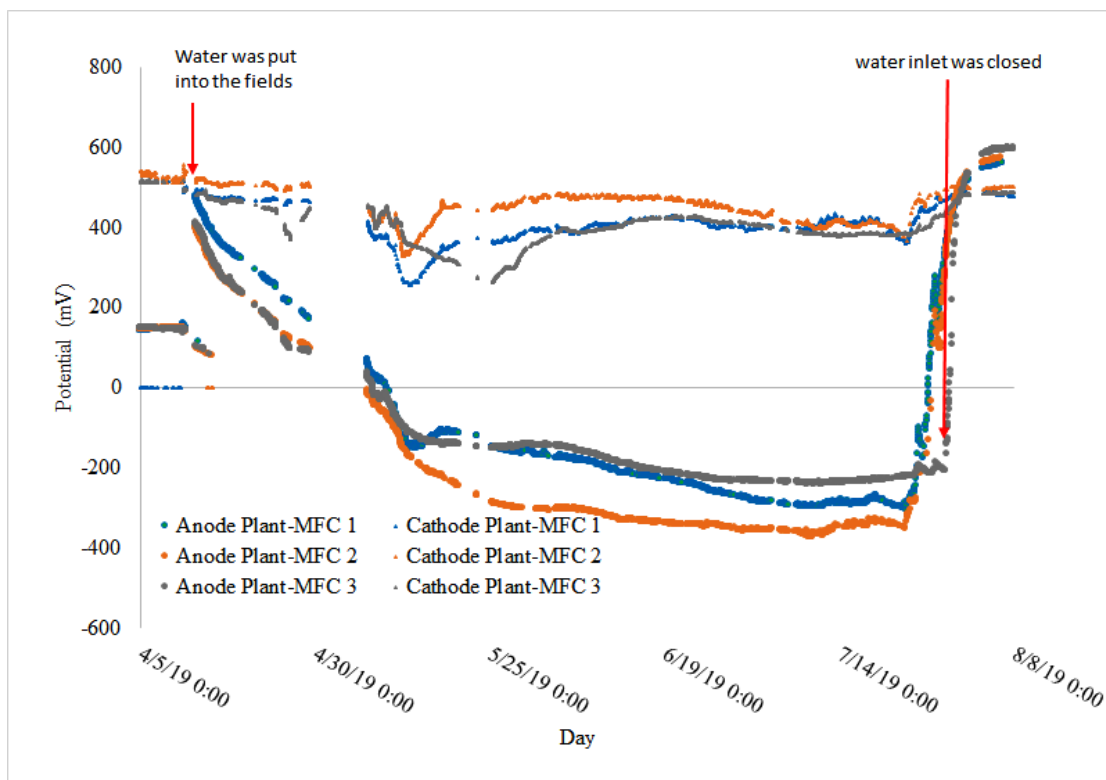


Figure 4. 6: Tubular plant-MFCs performances during fourth crop season: (A) Power density, and (B) Anode and Cathode Potential

Maximum of 44 mW/m² PGA power density was achieved using polarization curve; this maximum power density must be carefully evaluated because it may be influenced by a capacitive current as explained in Chapter 3 [45] (*Supplementary Figure S4.5*). This result was in the same order with other Plant-MFC power density in the paddy field (*Table 4. 3*). There were several peaks in power density (shown in green circles; best visible at Plant-MFC 1 and 2) as shown in *Figure 4. 6A*. Such peaks may have different origins that may be related to the management of the rice paddy as a response to supply of fertilizer or potentially pesticides. They could have an effect on the electrochemically active bacteria in the paddy field. There is no direct evidence to support this last hypothesis, though it is known that pesticides on wetland have effects on rice field microflora [198]. In addition, it could be that the degradation of Isoprocab/Mipcin (from Mipcindo 50) and Imidacloprid (both chemicals have an aromatic structure like in hexachlorobenzene) might provide an additional substrate for the EAB to generate electricity as have been shown that pesticide hexachlorobenzene degradation is enhanced in a soil MFC while generating electricity [199]. Also, it is known that addition of compost can affect current generation in Plant-MFC as well as that specific nutrients could include additional electron donor for electricity generation like in the case for urea obtained from urine [200–202].

Table 4. 3: Performances from selected Plant-MFC system using rice of tubular designs

Plant-MFC types, Anode and Cathode materials	Plant species	Maximum power density (mW/m ² PGA)	Reference
Paddy field Anode: Graphite felt below the soil surface Graphite felt above the soil surface, air cathode	Rice (<i>Oryza sativa</i>)	6	[48]
Lab, Container Plant-MFC Anode: graphite mat and graphite rod Cathode: graphite granule, graphite rod, 100mM K ₃ Fe(CN) ₆	Rice (<i>Oryza sativa</i>)	30	[62]
Paddy field Anode: Graphite felt Cathode: Graphite felt modified with platinum catalyst, air cathode	Rice (<i>Oryza sativa</i>)	14	[63]
Paddy field Anode: graphite felt Cathode: graphite felt modified with platinum catalyst, air cathode	Rice (<i>Oryza sativa</i>)	19	[49]
Paddy field Anode: Graphite felt Cathode: Graphite felt with platinum catalyst modified with polystyrene-foam bars to maintain buoyancy	Rice (<i>Oryza sativa</i>)	80	[128]
Lab-Perspex tubes Anode: graphite granule, vermiculite, carbon rod. Cathode: graphite felt interwoven carbon felt, air cathode	Rice (<i>Oryza sativa</i>)	72	[136]

Rice paddy-field MFC Anode: Circular graphite felt Cathode: Graphite felt with platinum catalyst, air cathode	Rice (<i>Oryza sativa</i>)	140	[50]
PVC Pot Plant-MFC Anode: graphite felt interwoven with copper wire, soil from paddy field Cathode: graphite felt interwoven with copper wire, air cathode	Rice (<i>Oryza sativa</i>)	4.5	[203]
Lab-tubular Plant-MFC from PVC with membrane Anode: graphite felt, graphite granule, golden wire Cathode: thick graphite felt, golden wire current collector, $5\text{mol.m}^{-3} \text{K}_3\text{Fe}(\text{CN})_6$	Reed mannagrass (<i>Glyceria maxima</i>)	18 12*	[64]
Tubular Plant-MFC with membrane and silicone gas diffusion layer in a lab constructed wetland. Anode: graphite felt and graphite stick Cathode: graphite felt with golden wire current collector, air cathode	<i>Phragmites australis</i> <i>Spartine anglica</i>	22 ^a 82 ^a	[60]
Tubular Plant-MFC without membrane with silicone tube air way in paddy field. Anode: graphite felt and titanium wire current collector Cathode: graphite felt and titanium wire current collector, air cathode	Rice (<i>Oryza sativa</i>)	44 9.6 ^a 8.5 ^b	This study

*Average power density; ^a maximum daily average power generation; ^b average continuous power generation for 60 days

In the fourth crop season, before the paddy field was irrigated the anode potentials were almost similar to the cathode potential which were around 500mV (**Figure 4. 6 B**). At this point, anode over potential was higher than cathode over potential. Thus, the anode resistance was higher than the cathode resistance (**Figure 4. 7**). There were several points that the anode potential went down to around 300-100mV. These phenomena will be discussed further in section 3.4. When the paddy fields were watered, the anode potentials gradually decreased up to -369mV while the cathode potential remained stable around 400mV (**Figure 4. 6B**). This means that the cathode over potential was relatively stable and the anode over potential decreased. However, when the irrigation was stopped the anode potential increased rapidly and became higher than the cathode potential (**Figure 4. 6 B** and **Figure 4. 7**). This indicated a rapid increase in the anode over potential over the cathode over potential. Based on this, one can conclude that the cathode is not the limiting factor in this Plant-MFC as can be seen from **Figure 4. 7**. In addition, the weak peaks in the anode and the cathode potential profile in **Figure 4. 7** may be related to diurnal (day and night) effect as described in other studies [65]. However we did not specifically study this effect on this article.

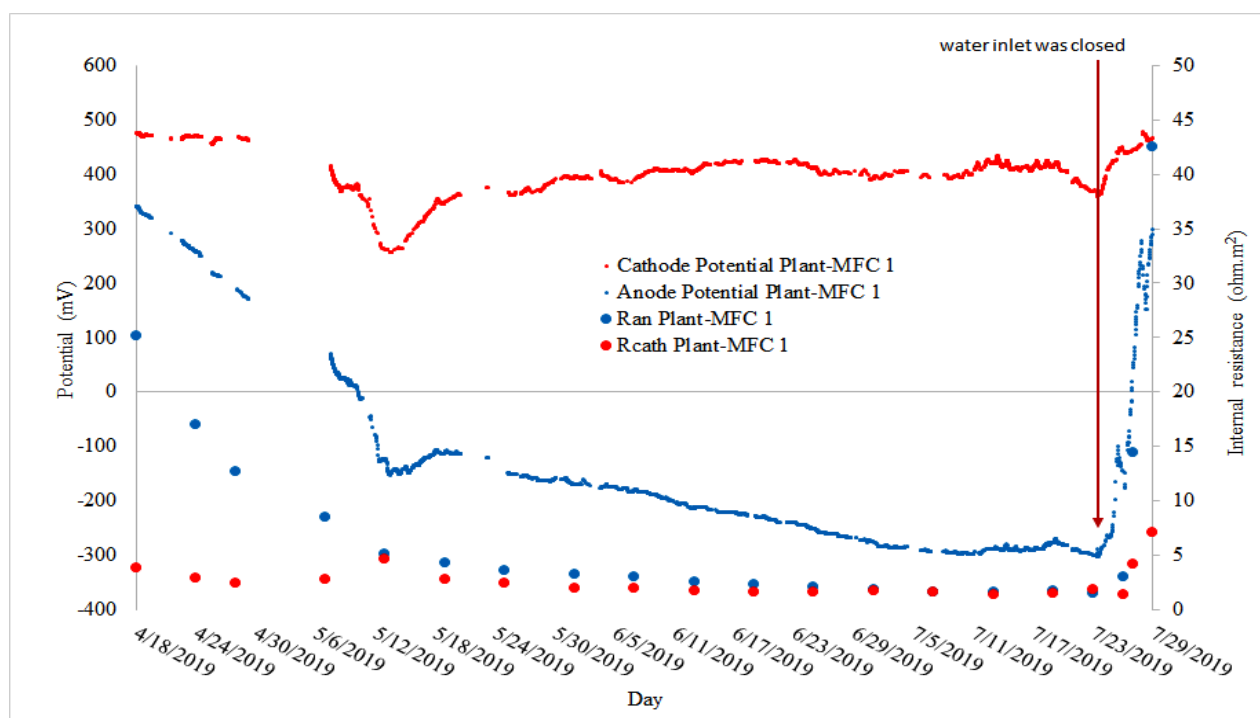


Figure 4. 7: Anode and cathode internal resistance on Plant-MFC 1 during the fourth crop season

4.3.3 Microbial community in the paddy field

Microbial analysis shows that bacteria dominated the archaea in the paddy field soil. Total relative abundance of archaea was only $1.5 \pm 0.8\%$ (**Figure 4. 8**). In the phyla level, Acidobacteria were the predominant bacteria followed by Proteobacteria, Planctomycetes and Verrucomicrobia. The bacterial communities in the paddy field were diverse (**Supplementary Table S4.1**). At least more than 520 genera were identified. Proteobacteria are mainly from classes Betaproteobacteria, Deltaproteobacteria and Alphaproteobacteria.

In general, the microbial communities from soil attached on the anode and the soil 2m apart from the anode are relatively similar (**Figure 4. 8**). However, there is an exception for *Proteobacteria* which were less enriched on the soil attached on the anode of Plant-MFC. This difference is related to *Comamonadaceae* family (order: *Burkholderiales*, Class: *Betaproteobacteria*). In the class level, Betaproteobacteria relative abundance was slightly higher in the soil far from the plant-MFC ($18.5 \pm 1\%$) than in the soil attached on the anode Plant-MFC ($10.5 \pm 4\%$). In the order level *Burkholderiales* were more abundance in the soil far from reactor (9-16%) and less abundance in the soil attached to the anode (0.8-4.7%). This was from *Comamonadaceae* family which found to be

more abundance in the soil far from Plant-MFC ($12\pm 4\%$) than in the soil attached on the anode of Plant-MFC ($1.7\pm 1.3\%$). However, the genera level of this family are cannot be identified.

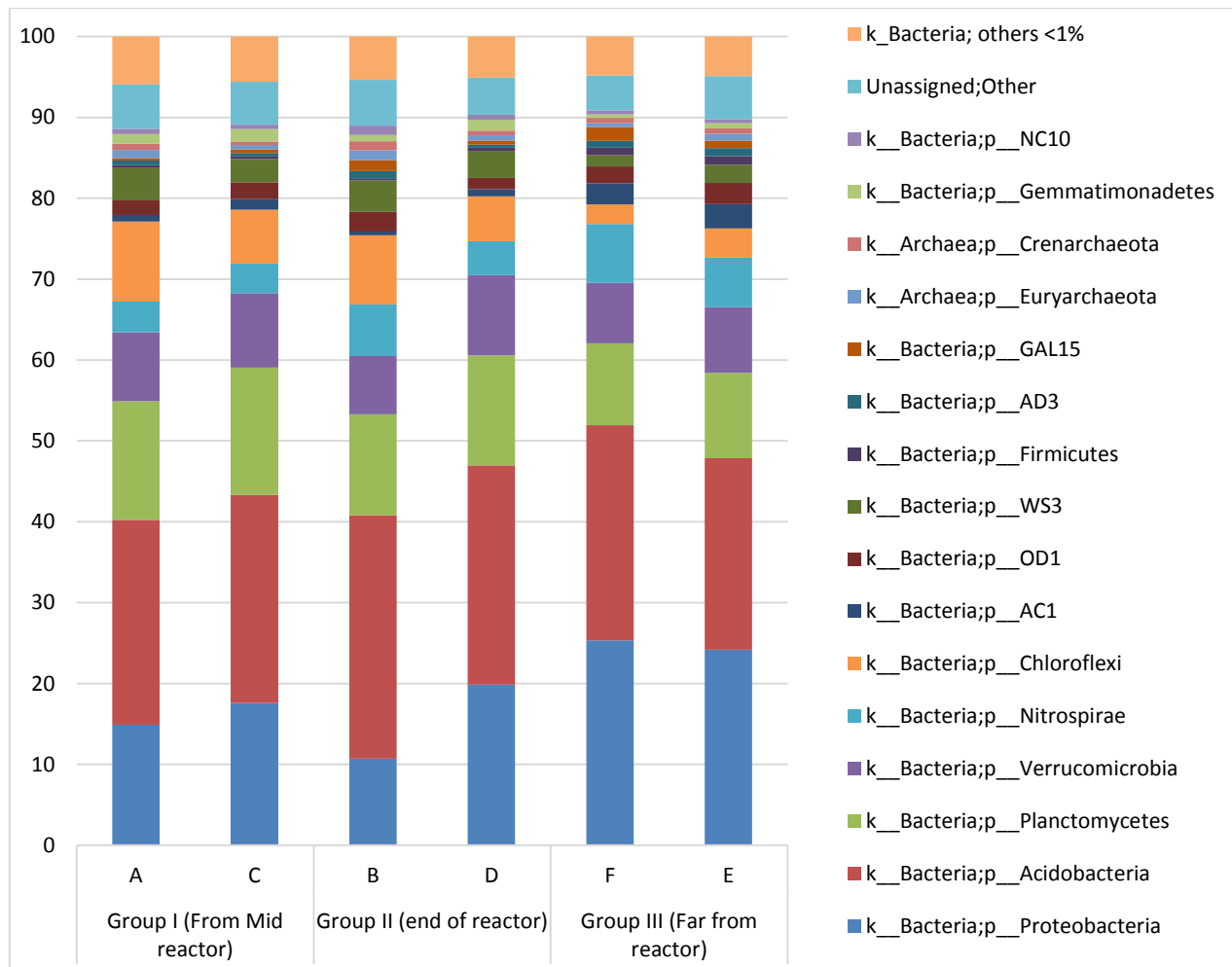


Figure 4. 8: Microbial communities in the paddy field soil with relative abundance $>1\%$. Y-axis shows relative abundance in % and X-axis (A, B, C, D, E and F) indicates the soil sample locations as described in Figure 4.4

Result also shows that Deltaproteobacteria are presence in all soil samples with relative abundance of $2.7\pm 0.2\%$. These bacteria were enriched on the anode of Plant-MFC using rice plants [186]. Some species within Deltaproteobacteria class that known to generate electricity are Geobacter, Deferrisoma, and Desulfobulbus [186].

4.3.4 Plant-MFC can indicate a rain event as biosensor

In between the crop seasons, the test paddy field was left in a dry condition. At these moment there was a non-continuous electricity production. During dry conditions the anode potential quickly increased to equal the cathode potential. However, there were several points in this period that the

anode potential went down and cell potential peaks were observed (**Figure 4. 9**). As the Plant-MFC likes anaerobic water logged conditions for the anode to generate electricity, these peaks suggested that the paddy field was inundated by water. Since the irrigation water was stopped to enter the area, the only possible reason of this inundation was rain. Since there is no rain data from the research site, rain data from two nearest climatology stations were utilized to predict the rain event in the research site.

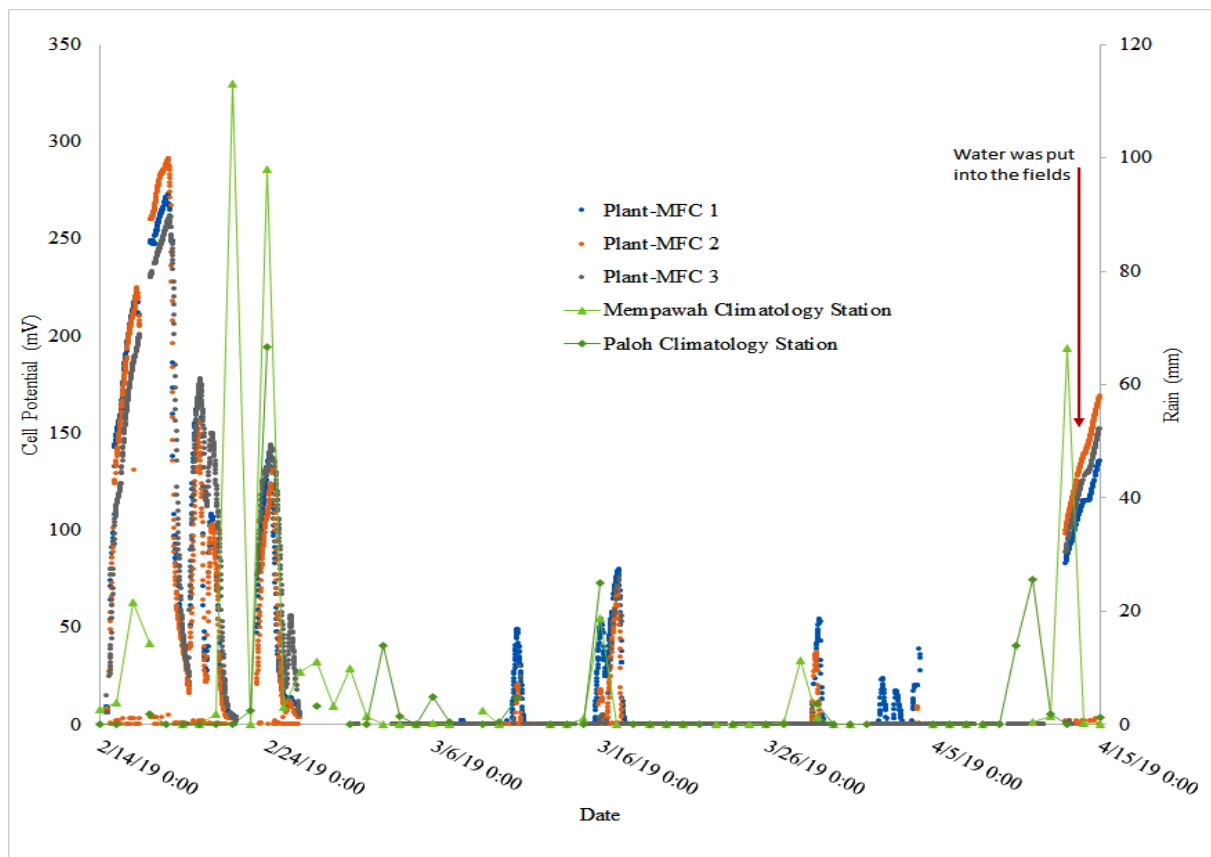


Figure 4. 9: Cell potential peak (possibly) due to rain events. The rain events were obtained from the two nearest climatology stations.

Plotting the rain data (**Supplementary Table S4.2**) and the cell potential peak on the same graph as shown in **Figure 4. 9**, one can see that there is some correlations between rain and the cell potential peaks. This result suggests that there is a possibility to utilize Plant-MFC as a bio indicator (such as rain event or wetland drying indicator). In **Figure 4. 9**, there are some rain events (around 27 February 2019 to 6 March 2019) occurred without accompanied by cell potential peaks. In addition, there are some peaks occurring (around 30 March 2019 to 5 April 2019) when there are no rain. In both cases, they happened on low rainfall (<20mm). The first case indicates that the rain state did not reach the research site. Moreover, the second case might indicate there is local rain in the research site. It should be noted that there is a mountain close by the research site. *Bawang* mountain (*Bawang* means Onion

in Indonesia Language) is situated about 8 km to the west side of the research site. Bawang mountain is stretching for 15 km from (0.856579, 109.465752) to (0.960704, 109.360416). The local climate of the research site is also influenced by the present of this mountain, for instance the orographic rainfall [204]. Therefore, an actual rain data from the Plant-MFC installation location are needed to further clarify this correlation. In this study, although it is known that temperature does affect current generation in the lab, temperature is not likely to influence the plant-MFC performances since temperature in the research site was rather constant during the day and night [205] (*Supplementary Figure S4.6*).

4.3.5 Data acquisition via low range network integrated with 3G network enable long distance auto data collection

Right after installation, the performance of the data acquisition was tested by comparing the anode potential, the cathode potential and the cell potential measured manually with a multimeter and result delivered from the LoRa data logger. This step is important for data validation. During this research, there were 4 times data transfer disconnections. However, the connection was automatically reconnected again after 2-3 days and only one time there was a need to restart the LoRa gateway. This problem was most likely happened because of the 3G network in the research site was not stable due to weather conditions. Since this research site is located in an area without electricity grid, it is important to maintain the electricity supply for the system. In addition, enough credit on the mobile phone network was also a key to send the data to the 3G network. Based on this experience, LoRa technology is reliable to be utilized for automatic online long distance data acquisition.

4.4 Conclusions

Based on this study, we can conclude that installing a plant- MFC in a paddy field is possible and is generating electricity for over several crop cycles. Tubular plant-MFC can generate electricity continuously during the crop season as long as the rice paddy was flooded. In one crop season, 9.5-15 Wh/m² PGA electricity energy can be generated continuously. In between the crop seasons, Plant-MFC may be utilized as a rain event indicator. This opens an opportunity to utilize Plant-MFC technology as a biosensor. An automatic long distance data transfer is possible via LoRa technology.

4.5 Associated Content

Microbiota data (raw 16s rDNA amplicon sequences) is submitted to the EBI database (<https://www.ebi.ac.uk/ena>) under accession number PRJEB34787.

4.6 Acknowledgments

This research was funded by Government of Landak Regency, West Kalimantan Province, Republic of Indonesia under an MoU with Wageningen University & Research, No 6160030150. Authors thank to Sipon and Yakobus Samunti who allowed this research carried out in their paddy field and provided data about standard method for their paddy field cultivation; to Hans van der Marel for his support with LoRa sensor design.

4.7 Supplementary Materials Chapter 4

The following are available online at <https://www.mdpi.com/1424-8220/19/21/4647/s1>

4.7.1 Supplementary Figures

Figure S4.1. Plant-MFC installation in the paddy field. Tubular Plant-MFCs were installed prior to paddy transplantation

S4.1. A. Soil was manually hoed about 10-15 cm deep



S4.1.B. Tubular Plant-MFCs were installed in the soil by David Strik (left) and Emilius Sudirjo (right). Both silicones tube end were supported with bamboo sticks



S4.1.C. Plant-MFC after installation. From left to right: Plant-MFC1, Plant-MFC2, Plant-MFC3, and two other Plant-MFC that is not related to this study



Figure S4.2. Aboveground biomass collection during the third crop season (on 13 February 2019)

S4.2.A. Harvesting aboveground biomass at one square meter area (marked with bamboo sticks) on top of Plant-MFC1



S4.2. B. Plant-MFCs reactor (under soil marked with bamboo sticks) after biomass collection



S4.2. C. Nine 1-square meter plots for aboveground biomass collection

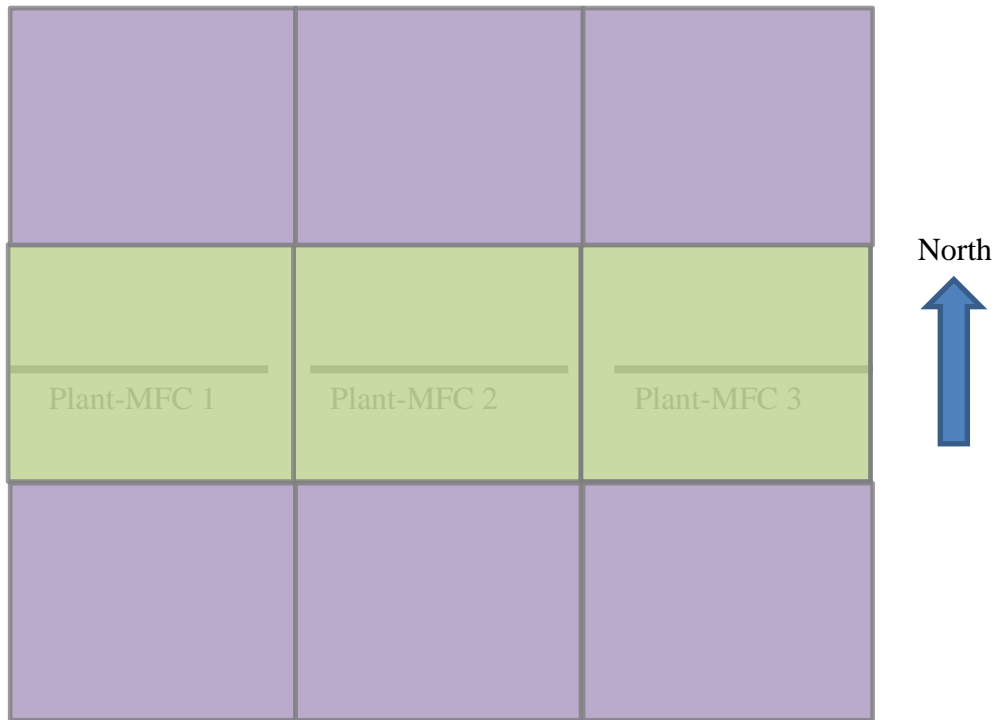


Figure S4.3. Rice paddy visual observation from different stage of growth

Figure S4.3. A 29 November 2017



Figure S4.3. B 30 June 2018



Figure S4.3. C 17 July 2018



Figure S4.3.D 13 February 2019 (Plant-MFC1)



Figure S4.3.E 13 February 2019 (Plant-MFC2)



Figure S4.3.F 13 February 2019 (Plant-MFC31)



Figure S4.3.G 5 August 2019 (Under the small roof is LoRa sensor)



Figure S4.4. Plant-MFC performance manually measured with a multimeter before LoRa data acquisition installation

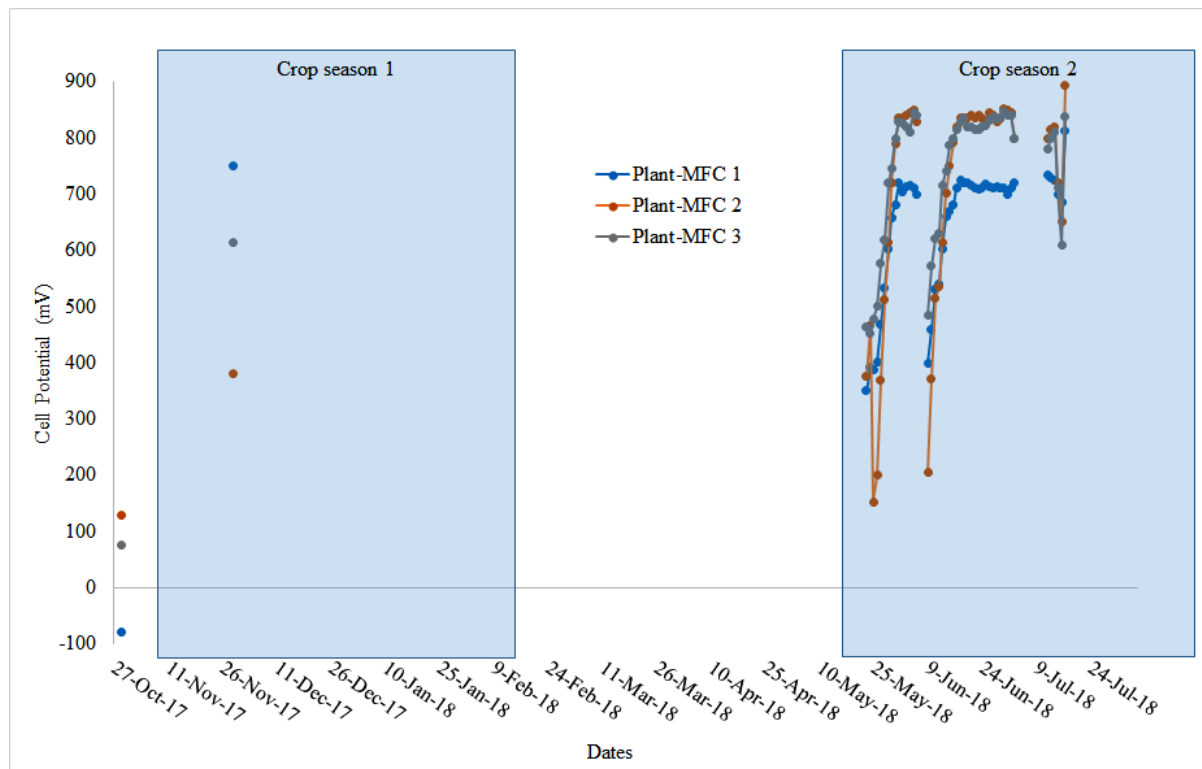


Figure S4.5. Polarization curve on 29 November 2017. Current density, cell potential and power density

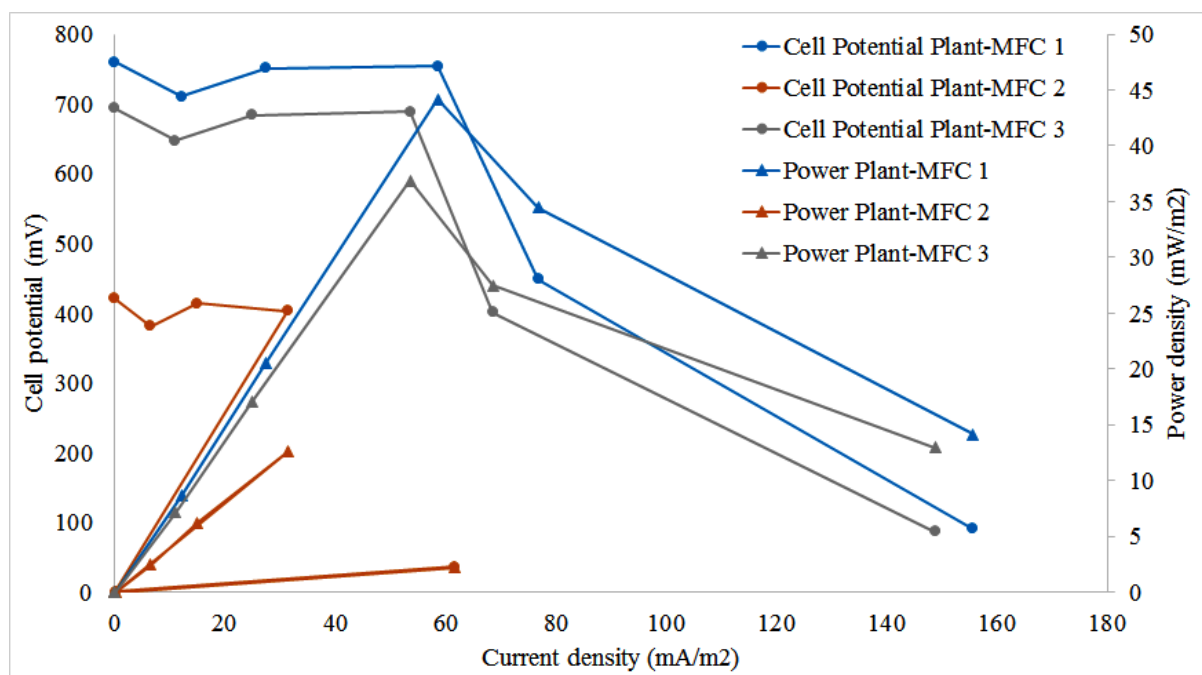
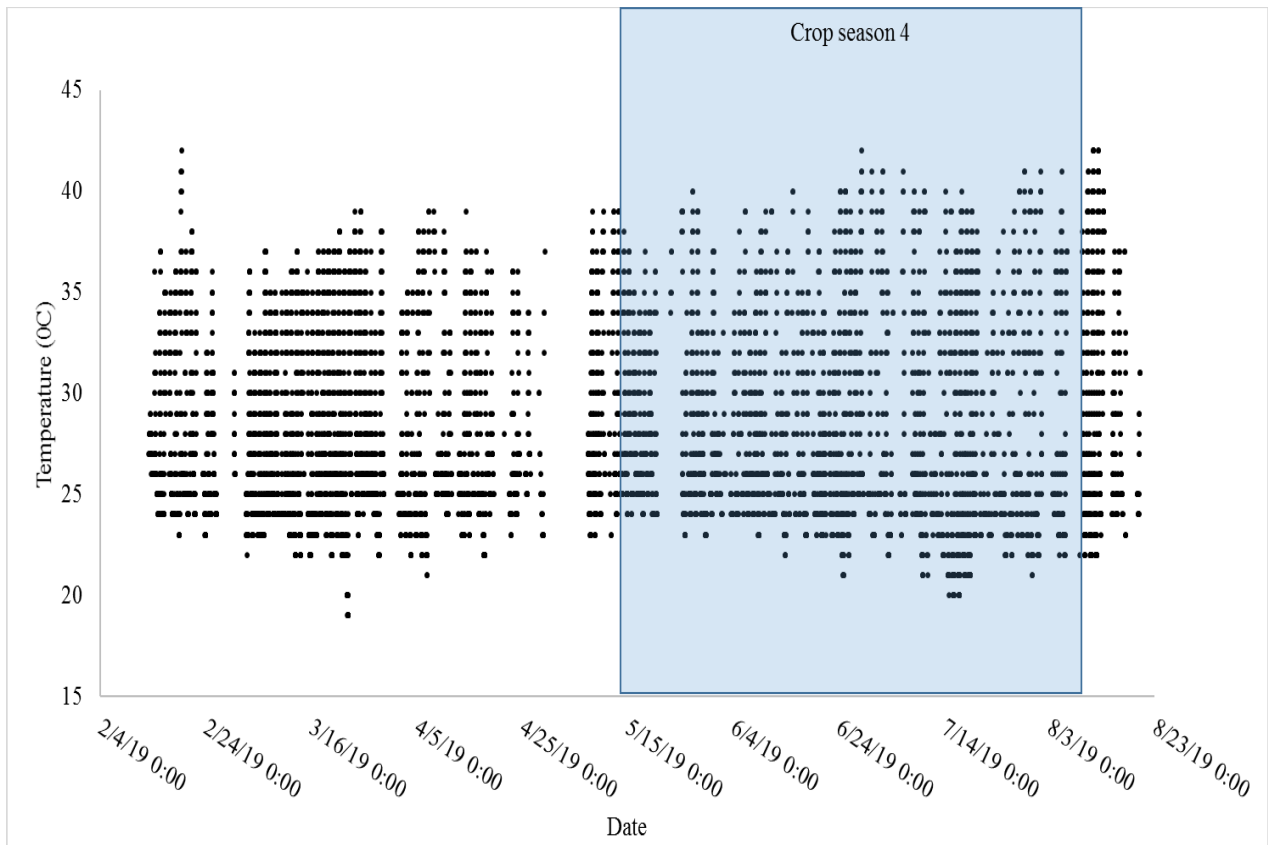


Figure S4.6. Temperature in fluctuation during the fourth crop season



4.7.2 Supplementary Tables

Table S4.1. Microbial Relative abundance (%) for classes, orders, families and genera

Table S1.A Classes

Kingdom	Phyla	Classes	Group I (From Mid reactor)		Group II (end of reactor)		Group III (Far from reactor)	
			A	C	B	D	F	E
k_Bacteria	p__Proteobacteria	c__Betaproteobacteria	9.75	11.67	6.38	14.03	19.35	17.60
k_Bacteria	p__Acidobacteria	c__Solibacteres	7.15	7.37	8.63	8.32	9.41	7.65
k_Bacteria	p__Nitrospirae	c__Nitrospira	3.78	3.66	6.39	4.19	7.26	6.11
k_Bacteria	p__Acidobacteria	c__Acidobacteria-6	4.45	7.26	5.93	6.31	7.97	5.89
k_Bacteria	p__Planctomycetes	c__Planctomycetia	5.27	6.04	5.28	4.30	4.73	3.78
k_Bacteria	p__Verrucomicrobia	c__[Methylacidiphilae]	3.81	3.90	3.74	4.09	3.79	3.64
k_Bacteria	p__Acidobacteria	c__Acidobacteriia	5.29	4.23	5.43	4.64	3.31	3.63
k_Bacteria	p__Planctomycetes	c__Phycisphaerae	7.08	6.89	4.42	6.48	2.75	3.34
k_Bacteria	p__Proteobacteria	c__Alphaproteobacteria	1.76	2.52	1.61	2.12	2.86	3.32
k_Bacteria	p__AC1	c__HDBW-WB69	0.75	1.21	0.41	0.84	2.55	2.92
k_Bacteria	p__Planctomycetes	c__BD7-11	1.44	1.89	2.07	1.97	1.99	2.84
k_Bacteria	p__Verrucomicrobia	c__[Pedosphaerae]	3.89	4.06	2.74	4.64	2.20	2.74
k_Bacteria	p__Proteobacteria	c__Deltaproteobacteria	2.54	2.54	2.41	2.86	2.69	2.47
k_Bacteria	p__Acidobacteria	c__BPC102	3.06	2.21	3.19	2.85	1.70	2.26
k_Bacteria	p__WS3	c__PRR-12	4.10	2.90	3.89	3.35	1.40	2.25
k_Bacteria	p__Acidobacteria	c__DA052	3.03	2.41	3.81	2.42	2.05	1.99
k_Bacteria	p__OD1	c__ZB2	1.46	1.72	2.02	1.03	0.94	1.53
k_Bacteria	p__Verrucomicrobia	c__[Spartobacteria]	0.61	0.81	0.60	0.73	1.27	1.45
k_Bacteria	p__Chloroflexi	c__Ellin6529	3.75	2.55	1.13	2.39	0.77	1.25
k_Bacteria	p__Chloroflexi	c__Anaerolineae	3.01	2.13	3.12	1.75	0.55	1.02
k_Bacteria	p__Firmicutes	c__Clostridia	0.22	0.18	0.15	0.35	0.69	1.01
k_Bacteria	p__AD3	c__ABS-6	0.57	0.42	0.96	0.37	0.81	1.00
k_Bacteria	p__GAL15	c__unknown	0.31	0.45	1.35	0.51	1.70	0.92
k_Bacteria	p__Chloroflexi	c__Ktedonobacteria	2.60	1.51	3.49	0.84	0.21	0.79
k_Bacteria	p__Gemmatimonadetes	c__Gemm-1	1.03	1.32	0.64	1.16	0.41	0.60
k_Bacteria	p__NC10	c__12-24	0.66	0.55	1.14	0.64	0.51	0.49
		Others classes <1%	18.65	17.59	19.07	16.82	16.11	17.52
		TOTAL	100	100	100	100	100	100

Table S4.1. B Orders

Kingdom	Phyla	Classes	Orders	Group I (From Mid reactor)		Group II (end of reactor)		Group III (Far from reactor)	
				A	C	B	D	F	E
k_Bacteria	p__Proteobacteria	c__Betaproteobacteria	o__Burkholderiales	1.687	1.197	0.828	4.738	16.184	8.949
k_Bacteria	p__Acidobacteria	c__Solibacteres	o__Solibacterales	6.923	7.027	8.420	7.878	9.210	7.426
k_Bacteria	p__Nitrospirae	c__Nitrospira	o__Nitrospirales	3.783	3.658	6.389	4.186	7.264	6.114
k_Bacteria	p__Acidobacteria	c__Acidobacteria-6	o__iii1-15	3.959	6.498	5.551	5.826	7.913	5.779
k_Bacteria	p__Proteobacteria	c__Betaproteobacteria	o__Neisseriales	2.544	5.136	1.846	2.090	0.209	3.749
k_Bacteria	p__Acidobacteria	c__Acidobacteriia	o__Acidobacteriales	5.287	4.225	5.428	4.637	3.308	3.627
k_Bacteria	p__Verrucomicrobia	c__[Methylacidiphilae]	o__S-BQ2-57	3.806	3.893	3.715	4.081	3.742	3.553
k_Bacteria	p__AC1	c__HDBW-WB69	o__unknown	0.752	1.210	0.412	0.838	2.552	2.924
k_Bacteria	p__Planctomycetes	c__BD7-11	o__unknown	1.440	1.895	2.069	1.968	1.994	2.835
k_Bacteria	p__Verrucomicrobia	c__[Pedosphaerae]	o__[Pedosphaerales]	3.891	4.062	2.740	4.637	2.203	2.741
k_Bacteria	p__Proteobacteria	c__Betaproteobacteria	o__Rhodocyclales	2.896	2.944	1.755	3.055	0.815	2.678
k_Bacteria	p__Planctomycetes	c__Planctomycetia	o__Gemmatales	3.756	4.285	4.152	3.249	3.431	2.608
k_Bacteria	p__Planctomycetes	c__Phycisphaerae	o__WD2101	5.201	5.020	3.408	4.857	2.128	2.439
k_Bacteria	p__WS3	c__PRR-12	o__Sediment-1	4.077	2.886	3.878	3.342	1.399	2.251
k_Bacteria	p__Acidobacteria	c__BPC102	o__MVS-40	3.012	2.157	3.084	2.745	1.571	2.135
k_Bacteria	p__Proteobacteria	c__Alphaproteobacteria	o__Rhodospirillales	0.767	1.348	0.881	1.103	1.260	2.038
k_Bacteria	p__Acidobacteria	c__DA052	o__Ellin6513	3.029	2.413	3.810	2.424	2.048	1.988
k_Bacteria	p__OD1	c__ZB2	o__unknown	1.456	1.722	2.020	1.030	0.943	1.531
k_Bacteria	p__Verrucomicrobia	c__[Spartobacteria]	o__[Chthoniobacterales]	0.608	0.809	0.603	0.734	1.265	1.451
k_Bacteria	p__Chloroflexi	c__Ellin6529	o__unknown	3.746	2.545	1.126	2.389	0.772	1.254
k_Bacteria	p__Proteobacteria	c__Deltaproteobacteria	o__Myxococcales	1.481	1.480	1.096	1.353	0.734	1.108
k_Bacteria	p__AD3	c__ABS-6	o__unknown	0.566	0.419	0.957	0.368	0.815	1.000
k_Bacteria	p__GAL15	c__unknown	o__unknown	0.307	0.454	1.347	0.510	1.699	0.919
k_Bacteria	p__Chloroflexi	c__Anaerolineae	o__A31	2.466	1.461	2.676	1.281	0.477	0.828
k_Bacteria	p__Proteobacteria	c__Betaproteobacteria	o__Methylophilales	0.865	0.095	0.115	1.784	1.421	0.792
k_Bacteria	p__Gemmatimonadetes	c__Gemm-1	o__unknown	1.028	1.323	0.643	1.159	0.407	0.595
k_Bacteria	p__Chloroflexi	c__Ktedonobacteria	o__Thermogemmatisporales	1.815	0.888	2.885	0.494	0.107	0.518
k_Bacteria	p__Planctomycetes	c__Phycisphaerae	o__CPla-3	1.199	1.009	0.320	0.821	0.172	0.382
			Other orders <1%	27.655	27.939	27.848	26.423	23.957	25.785
			TOTAL	100	100	100	100	100	100

Table S4.1.C Families

Kingdom	Phyla	Classes	Orders	Families	Group I (From Mid reactor)		Group II (end of reactor)		Group III (Far from reactor)	
					A	C	B	D	F	E
k_Bacteria	p_Proteobacteria	c_Betaproteobacteria	o_Burkholderiales	f_Comamonadaceae	1.3	0.6	0.4	4.5	15.9	8.6
k_Bacteria	p_Acidobacteria	c_Acidobacteria-6	o_iii1-15	f_	3.6	5.9	5.3	5.3	7.6	5.4
Unassigned	Other	Other	Other	Other	5.4	5.3	5.7	4.5	4.3	5.3
k_Bacteria	p_Acidobacteria	c_Solibacteres	o_Solibacterales	f_	2.6	2.9	3.8	3.7	4.9	3.8
k_Bacteria	p_Proteobacteria	c_Betaproteobacteria	o_Neisseriales	f_Neisseriaceae	2.5	5.1	1.8	2.1	0.2	3.7
k_Bacteria	p_Acidobacteria	c_Acidobacteriia	o_Acidobacteriales	f_Koribacteraceae	5.2	4.2	5.4	4.5	3.3	3.6
k_Bacteria	p_Verrucomicrobia	c_[Methylacidiphilae]	o_S-BQ2-57	f_	3.8	3.9	3.7	4.1	3.7	3.6
k_Bacteria	p_Nitrospirae	c_Nitrospira	o_Nitrospirales	f_0319-6A21	1.9	1.9	3.4	1.9	4.0	3.1
k_Bacteria	p_AC1	c_HDBW-WB69	o_	f_	0.8	1.2	0.4	0.8	2.6	2.9
k_Bacteria	p_Planctomycetes	c_BD7-11	o_	f_	1.4	1.9	2.1	2.0	2.0	2.8
k_Bacteria	p_Proteobacteria	c_Betaproteobacteria	o_Rhodocyclales	f_Rhodocyclaceae	2.9	2.9	1.8	3.1	0.8	2.7
k_Bacteria	p_Planctomycetes	c_Phycisphaerae	o_WD2101	f_	5.2	5.0	3.4	4.9	2.1	2.4
k_Bacteria	p_Acidobacteria	c_Solibacteres	o_Solibacterales	f_Solibacteraceae	3.4	3.1	3.3	3.0	2.3	2.2
k_Bacteria	p_Acidobacteria	c_BPC102	o_MVS-40	f_	3.0	2.2	3.1	2.7	1.6	2.1
k_Bacteria	p_Planctomycetes	c_Planctomycetia	o_Gemmatales	f_Gemmataceae	2.8	3.4	3.1	2.7	3.1	2.1
k_Bacteria	p_Proteobacteria	c_Alphaproteobacteria	o_Rhodospirillales	f_Rhodospirillaceae	0.7	1.3	0.9	1.1	1.3	2.0
k_Bacteria	p_Acidobacteria	c_DA052	o_Ellin6513	f_	3.0	2.4	3.8	2.4	2.0	2.0
k_Bacteria	p_WS3	c_PRR-12	o_Sediment-1	f_PRR-10	3.1	2.1	3.0	2.5	1.1	1.7
				f_[Thermodesulfovi						
k_Bacteria	p_Nitrospirae	c_Nitrospira	o_Nitrospirales	brionaceae]	1.0	0.9	1.5	1.4	1.5	1.6
k_Bacteria	p_OD1	c_ZB2	o_	f_	1.5	1.7	2.0	1.0	0.9	1.5
				f_[Chthoniobacterac						
k_Bacteria	p_Verrucomicrobia	c_[Spartobacteria]	o_[Chthoniobacterales]	eae]	0.6	0.8	0.6	0.7	1.3	1.5
k_Bacteria	p_Chloroflexi	c_Ellin6529	o_	f_	3.7	2.5	1.1	2.4	0.8	1.3
k_Bacteria	p_Verrucomicrobia	c_[Pedosphaerae]	o_[Pedosphaerales]	f_	1.2	1.2	0.9	1.8	0.8	1.2
k_Bacteria	p_AD3	c_ABS-6	o_	f_	0.6	0.4	1.0	0.4	0.8	1.0
k_Bacteria	p_Verrucomicrobia	c_[Pedosphaerae]	o_[Pedosphaerales]	f_auto67_4W	1.3	1.5	0.6	1.7	0.7	0.9
k_Bacteria	p_GAL15	c_	o_	f_	0.3	0.5	1.3	0.5	1.7	0.9
k_Bacteria	p_Acidobacteria	c_Solibacteres	o_Solibacterales	f_PAUC26f	0.5	0.5	0.9	0.6	1.5	0.9
k_Bacteria	p_Nitrospirae	c_Nitrospira	o_Nitrospirales	f_Nitrospiraceae	0.3	0.5	0.8	0.3	1.1	0.9
k_Bacteria	p_Chloroflexi	c_Anaerolineae	o_A31	f_	2.4	1.4	2.7	1.2	0.5	0.8
k_Bacteria	p_Proteobacteria	c_Betaproteobacteria	o_Methylophilales	f_Methylophilaceae	0.8	0.0	0.1	1.7	1.4	0.7
k_Bacteria	p_Gemmatimonadetes	c_Gemm-1	o_	f_	1.0	1.3	0.6	1.2	0.4	0.6
k_Bacteria	p_Verrucomicrobia	c_[Pedosphaerae]	o_[Pedosphaerales]	f_Ellin515	1.2	1.2	1.0	1.0	0.7	0.6

k_Bacteria	p_Chloroflexi	c_Ktedonobacteria	o_Thermogemmatissporales	f_Thermogemmatisporaceae	1.8	0.9	2.9	0.5	0.1	0.5
k_Bacteria	p_Planctomycetes	c_Planctomycetia	o_Gemmatales	f_Isosphaeraceae	1.0	0.9	1.0	0.6	0.3	0.5
k_Bacteria	p_Proteobacteria	c_Betaproteobacteria	o_MND1	f__	0.8	0.9	0.7	1.0	0.3	0.5
k_Bacteria	p_Planctomycetes	c_Phycisphaerae	o_CPla-3	f__	1.2	1.0	0.3	0.8	0.2	0.4
Other Families <1%					26.0	26.5	25.4	25.3	22.2	23.6
TOTAL					100	100	100	100	100	100

Table S4.1. D Genera

Kingdom	Phyla	Classes	Orders	Families	Genera	Group I (From Mid reactor)		Group II (end of reactor)		Group III (Far from reactor)	
						A	C	B	D	F	E
k_Bacteria	p_Acidobacteria	c_Acidobacteria-6	o_iii1-15	f__	g_unknown	3.60	5.87	5.35	5.29	7.61	5.44
k_Bacteria	p_Proteobacteria	c_Betaproteobacteria	o_Burkholderiales	f_Comamonadaceae	g_unknown	1.00	0.37	0.34	0.93	1.75	4.06
k_Bacteria	p_Acidobacteria	c_Solibacteres	o_Solibacterales	f__	g_unknown	2.59	2.89	3.76	3.68	4.92	3.81
k_Bacteria	p_Verrucomicrobia	c_[Methylacidiphilae]	o_S-BQ2-57	f__	g_unknown	3.81	3.89	3.72	4.08	3.74	3.55
k_Bacteria	p_Nitrospirae	c_Nitrospira	o_Nitrospirales	f_0319-6A21	g_unknown	1.86	1.88	3.38	1.93	3.98	3.13
k_Bacteria	p_AC1	c_HDBW-WB69	o__	f__	g_unknown	0.75	1.21	0.41	0.84	2.55	2.92
k_Bacteria	p_Planctomycetes	c_BD7-11	o__	f__	g_unknown	1.44	1.89	2.07	1.97	1.99	2.84
k_Bacteria	p_Proteobacteria	c_Betaproteobacteria	o_Burkholderiales	f_Comamonadaceae	g_Hydrogenophaga	0.21	0.11	0.03	3.00	8	2.80
k_Bacteria	p_Acidobacteria	c_Acidobacteriia	o_Acidobacteriales	f_Koribacteraceae	g_unknown	4.54	3.49	4.61	3.61	2.47	2.64
k_Bacteria	p_Planctomycetes	c_Phycisphaerae	o_WD2101	f__	g_unknown	5.20	5.02	3.41	4.86	2.13	2.44
k_Bacteria	p_Acidobacteria	c_Solibacteres	o_Solibacterales	f_Solibacteraceae	Solibacter	3.35	3.06	3.26	2.98	2.32	2.22
k_Bacteria	p_Acidobacteria	c_BPC102	o_MVS-40	f__	g_unknown	3.01	2.16	3.08	2.75	1.57	2.13
k_Bacteria	p_Proteobacteria	c_Alphaproteobacteri	o_Rhodospirillales	f_Rhodospirillaceae	g_unknown	0.71	1.30	0.86	1.04	1.16	2.01
k_Bacteria	p_Acidobacteria	c_DA052	o_Ellin6513	f__	g_unknown	3.03	2.41	3.81	2.42	2.05	1.99
k_Bacteria	p_Proteobacteria	c_Betaproteobacteria	o_Neisseriales	f_Neisseriaceae	g_Vogesella	0.75	1.03	0.60	0.38	0.10	1.91
k_Bacteria	p_Planctomycetes	c_Planctomycetia	o_Gemmatales	f_Gemmataceae	g_unknown	2.47	2.84	3.04	2.42	2.96	1.87
k_Bacteria	p_WS3	c_PRR-12	o_Sediment-1	f_PRR-10	g_unknown	3.11	2.10	3.02	2.50	1.10	1.70
k_Bacteria	p_Proteobacteria	c_Betaproteobacteria	o_Neisseriales	f_Neisseriaceae	Other	1.63	3.77	1.13	1.57	0.11	1.55
k_Bacteria	p_OD1	c_ZB2	o__	f__	g_unknown	1.46	1.72	2.02	1.03	0.94	1.53

k_Bacteria	p_Chloroflexi	c_Ellin6529	o__	f__	g_unknown	3.75	2.55	1.13	2.39	0.77	1.25
k_Bacteria	p_Proteobacteria	c_Betaproteobacteria	o_Rhodocyclales	f_Rhodocyclaceae	g_unknown	2.30	2.45	1.52	2.43	0.40	1.22
k_Bacteria	p_Verrucomicrobia	c_[Pedosphaerae]	o_[Pedosphaerales]	f__	g_unknown	1.24	1.21	0.94	1.83	0.79	1.16
k_Bacteria	p_AD3	c_ABS-6	o__	f__	g_unknown	0.57	0.42	0.96	0.37	0.81	1.00
k_Bacteria	p_Verrucomicrobia	c_[Pedosphaerae]	o_[Pedosphaerales]	f__auto67_4W	g_unknown	1.29	1.50	0.63	1.70	0.69	0.93
k_Bacteria	p_GAL15	c__	o__	f__	g_unknown	0.31	0.45	1.35	0.51	1.70	0.92
k_Bacteria	p_Acidobacteria	c_Solibacteres	o_Solibacterales	f_PAUC26f	g__	0.46	0.47	0.94	0.65	1.49	0.85
k_Bacteria	p_Chloroflexi	c_Anaerolineae	o_A31	f__	g_unknown	2.42	1.44	2.66	1.24	0.47	0.81
k_Bacteria	p_Proteobacteria	c_Betaproteobacteria	o_Methylophilales	f_Methylophilaceae	g__	0.80	0.05	0.10	1.69	1.38	0.74
k_Bacteria	p_Gemmatimonadetes	c_Gemm-1	o__	f__	g_unknown	1.03	1.32	0.64	1.16	0.41	0.60
k_Bacteria	p_Verrucomicrobia	c_[Pedosphaerae]	o_[Pedosphaerales]	f_Ellin515	g__	1.24	1.22	1.05	1.02	0.66	0.58
k_Bacteria	p_Chloroflexi	c_Ktedonobacteria	o_Thermogemmatisporales	f_Thermogemmatisporaceae	g__	1.81	0.89	2.88	0.49	0.11	0.52
k_Bacteria	p_Planctomycetes	c_Planctomycetia	o_Gemmatales	f_Isosphaeraceae	g__	0.97	0.89	1.01	0.56	0.31	0.49
k_Bacteria	p_Planctomycetes	c_Phycisphaerae	o_CPla-3	f__	g_unknown	1.20	1.01	0.32	0.82	0.17	0.38
Unassigned	Other	Other	Other	Other	Unassigned_Other	5.44	5.31	5.69	4.55	4.28	5.30
					Other genera <1%	30.6	31.8	30.2	31.3	29.7	32.7
					TOTAL	100	100	100	100	100	100

Table S4.2. Rainfall data vs peak at Plant-MFC during dry period between crop season 3 & 4

Date	Mempawah climatology station			Paloh climatology station			Rain possibility in the research site
	Rain (mm)	Wind direction	rain states	Rain (mm)	Wind Direction	Rain states	
14-Feb-19	2.80	NE	moderate rain	0	C	no rain	High possibility
15-Feb-19	4.00	C	moderate rain	0.1	C	drizzle	Low possibility
16-Feb-19	21.50	NE	heavy rain	8888	na	data not available	High possibility
17-Feb-19	14.30	C	heavy rain	1.8	C	drizzle	Low possibility
18-Feb-19	8888	C	data not available	0	C	no rain	unknown
19-Feb-19	0.00	E	no rain	0	C	no rain	unknown
20-Feb-19	0.00	NE	no rain	0	C	no rain	unknown
21-Feb-19	1.80	C	drizzle	0	C	no rain	unknown
22-Feb-19	113.00	E	storm	0	N	no rain	High possibility
23-Feb-19	0.00	NE	no rain	2.5	C	moderate rain	Low possibility
24-Feb-19	98.10	NE	storm	66.7	C	storm	High possibility
25-Feb-19	3.10	C	moderate rain	8888	na	data not available	Low possibility
26-Feb-19	9.30	E	moderate rain	8888	na	data not available	Low possibility
27-Feb-19	11.2	NE	heavy rain	3.4	C	moderate rain	High possibility
28-Feb-19	3.3	NE	moderate rain	8888	C	data not available	High possibility
1-Mar-19	10	C	heavy rain	0	C	no rain	Low possibility
2-Mar-19	1.5	W	drizzle	0	C	no rain	unknown
3-Mar-19	0	C	no rain	14	C	heavy rain	unknown
4-Mar-19	0	C	no rain	1.5	C	drizzle	unknown
5-Mar-19	0	C	no rain	0	C	no rain	unknown
6-Mar-19	0.2	C	drizzle	4.9	C	moderate rain	unknown

7-Mar-19	0	E	no rain	0.4	C	drizzle	unknown
8-Mar-19	na	W	data not available	8888	na	data not available	unknown
9-Mar-19	2.50	C	moderate rain	0	C	no rain	Low possibility
10-Mar-19	0.00	W	no rain	0.5	N	drizzle	unknown
11-Mar-19	na	C	data not available	4.7	C	moderate rain	unknown
12-Mar-19	na	na	data not available	8888	C	data not available	unknown
13-Mar-19	0	W	no rain	0	C	no rain	unknown
14-Mar-19	0	C	no rain	0	C	no rain	unknown
15-Mar-19	1	NE	drizzle	0	C	no rain	unknown
16-Mar-19	18.8	C	heavy rain	25.1	C	heavy rain	High possibility
17-Mar-19	0	NE	no rain	8888	C	data not available	unknown
18-Mar-19	8888	na	data not available	0	C	no rain	unknown
19-Mar-19	0	C	no rain	0	C	no rain	unknown
20-Mar-19	0	W	no rain	0	C	no rain	unknown
21-Mar-19	0	SW	no rain	0	C	no rain	unknown
22-Mar-19	8888	na	data not available	0	C	no rain	unknown
23-Mar-19	0	W	no rain	8888	na	data not available	unknown
24-Mar-19	0	W	no rain	0	C	no rain	unknown
25-Mar-19	0	SW	no rain	8888	N	data not available	unknown
26-Mar-19	0	NE	no rain	0	C	no rain	unknown
27-Mar-19	0.4	W	drizzle	0	C	no rain	High possibility
28-Mar-19	11.4	SW	heavy rain	8888	na	data not available	High possibility
29-Mar-19	1.3	SW	drizzle	3.8	C	moderate rain	High possibility
30-Mar-19	0	SW	no rain	0	C	no rain	unknown

31-Mar-19	0	W	no rain	0	C	no rain	unknown
1-Apr-19	8888	W	data not available	0	C	no rain	unknown
2-Apr-19	8888	na	data not available	8888	C	data not available	unknown
3-Apr-19	8888	na	data not available	8888	na	data not available	unknown
4-Apr-19	8888	na	data not available	8888	na	data not available	unknown
5-Apr-19	0	C	no rain	0	C	no rain	unknown
6-Apr-19	0	W	no rain	0	C	no rain	unknown
7-Apr-19	0	C	no rain	0	N	no rain	unknown
8-Apr-19	0	W	no rain	0	C	no rain	unknown
9-Apr-19	8888	na	data not available	0	C	no rain	unknown
10-Apr-19	8888	na	data not available	13.9	C	heavy rain	High possibility
11-Apr-19	0.4	C	drizzle	25.7	E	heavy rain	High possibility
12-Apr-19	1.5	SW	drizzle	1.8	C	drizzle	unknown
13-Apr-19	66.4	C	storm	0.1	C	drizzle	unknown
14-Apr-19	0.2	E	drizzle	8888	na	data not available	unknown
15-Apr-19	0	SW	no rain	1.3	N	drizzle	unknown

0mm = no rain; 0-2.5 mm= drizzle; 2,5-10 = moderate rain; 10-50 = heavy rain; >50= storm; 8888 = data not available; na = not available;

C = calm (0 m/s)

Rain possibility in the research site was predicted based on the rain state and the wind direction from the climatology stations.

Chapter 5

A Thin Layer of Activated Carbon Deposited on Polyurethane Cube Leads to New Conductive Bioanode for (Plant) Microbial Fuel Cell

This chapter is under reviewed in energies-665601: Sudirjo, E.; Constantino Diaz, P.Y; Cociancich, M; Lisman, R; Snik, C; Buisman, C.J.N.; Strik, D.P.B.T.B.

Abstract

Large-scale implementation of (plant) microbial fuel cells is greatly limited by high electrode costs. In this work, we study the potential of exploiting electrochemically active self-assembled biofilms in fabricating three-dimensional bioelectrodes for (plant) microbial fuel cells with minimum use of electrode materials. Three-dimensional robust bioanodes were successfully developed with inexpensive polyurethane foams (PU) and activated carbon (AC). The PU/AC electrode bases were fabricated via a water-based sorption of AC particles on the surface of the PU cubes. The electrical current was enhanced by growth of bacteria on the PU/AC bioanode while sole current collectors produced minor current. Growth and electrochemical activity of the biofilm were shown with SEM imaging and DNA sequencing of the microbial community. Electric conductivity of the PU/AC electrode enhance over time during bioanode development. The maximum current and power density of an acetate fed MFC reached $3\text{mA}/\text{m}^2$ projected surface area of anode compartment and $22\text{mW}/\text{m}^3$ anode compartment. The field test of the Plant-MFC reached a maximum performance of $0.9\text{ mW}/\text{m}^2$ plant growth area at a current density of $5.6\text{ mA}/\text{m}^2$ PGA. A paddy field test showed that the PU/AC electrode was suitable as an anode material in combination with a graphite felt cathode. Finally, this study offers insights on the role of electrochemically active biofilms as natural enhancers of the conductivity of electrodes and as transformers of inert low-cost electrode materials into living electron acceptors.

Keywords: Polyurethane, Microbial Fuel Cell, Activated Carbon, Bioanode, Conductive biofilms

5.1 Introduction

In a bioelectrochemical system (BES) application such as (Plant) Microbial Fuel Cell, electrode is a crucial part because of its function to accept released electrons from electrochemically active bacteria in the anode and to transfer the electrons to the final electron acceptor in the cathode [51,52]. Especially in plant microbial fuel cell with its relative low current density, large amounts of electrodes are required. One of the most utilized electrodes is graphite felt [40,48–50,58,60,63–65,96,126,130,130,136,137]. So far, in the best two weeks performance of a plant microbial fuel cell (Plant-MFC) utilizing graphite felt both for the anode and the cathode, 240 mW/m² of power output was achieved [65]. Although graphite felt has shown itself to be a good electrode, its price (around € 62/m²) has become an inhibiting factor in real applications [46]. For instance, the electrode cost (with graphite felt) for a tubular Plant-MFC are between 30 and 78% of the total cost [46]. Therefore, it is necessary to find an alternative cheaper electrode ideally without compromising on the performance.

An innovative alternative to reduce the electrode cost is using microorganism to fabricate bioelectrodes [65,206]. These bioelectrodes consist of the biocatalyst of electrochemically active bacteria which grow in a biofilm that by itself can be highly conductive and as electrode itself [207]. Long term performance microbial colonization on the electrode surface structure resulted in a high current density [82,208]. Several studies show, for instance Xie et al [82], a conductive and macroporous three-dimensional scaffold is the most suitable material for such a bio electrode. In this sense, a wide variety of materials has been studied as three-dimensional bioanodes, which focus both on attaining high performing bioelectrodes and on a practically implementable bioanodes as well as cost reduction [209]. However, the cost reduction is still a challenge for the electrode production because the preparation techniques for some of the three-dimensional bioanodes are often fabricated with advanced materials and fabrication methods such as electropolymerization of pyrrole and carbonized sponges coated with polyaniline [208,210,211].

Desirable features to design a scalable bioanode are cost-effectiveness, high power output, good biocompatibility to support microbial growth and can be scaled-up[208]. Based on these features, this study considers reticulated polyurethane (PU) foam as the core three-dimensional structure using activated carbon (AC) as the coating material as a practical bioanode. On one hand, PU foam facilitates the open structure to support internal and external biofilm growth, bacterial accessibility and efficient transport of substrates[212,213]. On the other hand, AC confers a high surface area, hydrophilicity and conductivity to the surface of the PU foams[212,214,215]. Research (Chapter 2

and Chapter 3) showed that AC is a suitable material for bioanode growth [45,88,142]. Foremost, both materials PU and AC have a lower cost (<€1 per kg) than most common electrode materials, such as graphite felt, graphene cloth, graphite foam and carbon nanotubes foam[216,217].

The use of PU foams fabricated with conductive materials as electrode materials has been successfully described before [208,212,218]. However, these electrodes were fabricated using additional high-energy input processes (*e.g.* carbonisation of the PU [212]), expensive material (*e.g.* carbon nano tubes [213,219]), and complex method (*e.g.* sonication and polymerization of polypyrrole [220]). To reduce materials investment cost we investigated to exploit the electrochemically active and conductive biofilm as much as possible while using PU as carrier materials and a just thin/minimum layer of conductive activated carbon materials. Therefore, the objective of this study was to validate if the polyurethane foams coated with the activated carbon can perform as platform bioanodes for harvesting electric current in microbial fuel cells (MFCs). Hence, the role of the biofilm, the role of the bioanolyte and more importantly the performance and limitations of the PU/AC bioanodes were investigated. Furthermore, the field test result of PU/AC electrode in a paddy field is also presented.

5.2 Material and Methods

5.2.1 Preparation of PU/AC composites

Composites consisted of reticulated PU cubic foams (Recticel, Ltd, Belgium) coated with milled AC (Norit PK 1-3, Norit Nederland BV, The Netherlands). All PU foams had dimensions of 1.5 cm x 1.5 cm x 1.5 cm, a density of 30.4 kg m⁻³ and a porosity of 20 pores per inch (PPI) which is approximately equal to a pore diameter of 13 μm. The AC bulk density is 240-400 kg/m³[221]. First, the granular AC was milled into fine particles with a miller machine (SM2000, Retsch GmbH, Germany). The particle size distribution of the activated carbon ($D_{10} = 2.9 \pm 1.25 \mu\text{m}$, $D_{50} = 4.5 \pm 1.13 \mu\text{m}$, $D_{90} = 8.6 \pm 1.01 \mu\text{m}$) was measured with Laser Diffraction Technique (LA-960 HORIBA Scientific, HORIBA Instrument, INC, Irvine, USA). PU foams were washed with demineralized water and dried at 105°C overnight. Then, a coating solution was prepared by mixing 4 gL⁻¹ of AC with 400 mL of demineralized water in a beaker of 600 mL under magnetic stirring. The stirring speed and water temperature were controlled at 500 to 600 rpm and 30 °C, respectively. After that, PU foams were coated in batches of four sponges by dipping them into the coating solution for one hour at constant stirring and 30 °C temperature in a climatized room. Foams were carefully dropped in sequence and

kept in the middle of the vortex. Afterwards, the PU/AC composites were gently rinsed with demineralized water and dried at 105 °C overnight. Loads of activated carbon attached to the PU foams were calculated via gravimetric mass balances as given in Equation (5.1).

$$W_{AC} = \frac{W_f - W_i}{W_f} \times 100 \quad (5.1)$$

where W_{AC} was the % of AC attached to foams, W_f was the final weight after treatment and W_i was the initial weight of plain foams [218].

5.2.2 MFCs setup

The experimental setup consisted of six flat-plate MFCs similar to earlier work[222]. Each MFC had two single flow channels (one for the cathode and one for the anode) separated by a cation exchange membrane (Fumasep FKD-PK-75, Fumatech, Braunschweig, Germany). Each channel had a projected surface area of 22 cm² and a volume of 33 mL. The 33 mL anode volume was filled with or without three-dimensional electrode material as described in **Table 5. 1**. The cathode consisted of a flat graphite-Al₂O₃ blasted plate (Müller & Rössner GmbH & Co., Troisdorf, Germany) and four graphite felt layers with a thickness of 3 mm (FMI Composites Ltd., Galashiels, Scotland) inside the channel to increase the surface area. The anode integrated the anode material and two titanium current collectors with a length of 11 cm (No. 299, D=1 mm, Ti-gr1) separated by a distance of 5.5 cm (**Figure 5. 1**). Of the six reactors (**Table 5. 1**), in three of them, the anode material was eleven cube foams with one coating of activated carbon (PU/AC composites). One of the MFCs with PU/AC composites (PU/AC Inoculum) was used to grow the bioanodes and use the anolyte as inoculum for the other two (PU/AC I and PU/AC II). One MFC had as anode material a graphite felt (KFA-5mm, SGL Carbon GmbH, Bonn, Germany) layer to confirm that the used medium and inoculum in all MFCs were not limiting the development of bioanodes. The last two MFCs (Ti-CC I and Ti-CC II) deprived of anodes and used only Ti wire as current collectors that possibly act as anode.

Table 5. 1: MFC reactors name with their anode materials and functions

Reactors name	Anode materials	Function
PU/AC I	PU/AC composites	Studied reactor. Operated for 28 days
PU/AC II	PU/AC composites	Studied reactor. Operated for 28 days
PU/AC Inoculum	PU/AC composites	Inoculate reactor. Operated for 70 days
Graphite felt	Graphite felt	Control. Operated for 73 days
Ti-CC I	Only current collector (Ti Wire)	Blank reactor. Operated for 83 days
Ti-CC II	Only current collector (Ti Wire)	Blank reactor. Operated for 83 days

Note: PU/AC I and II were started after 42 days operation of the PU/AC Inoculum. PU/AC Inoculum result are not shown.

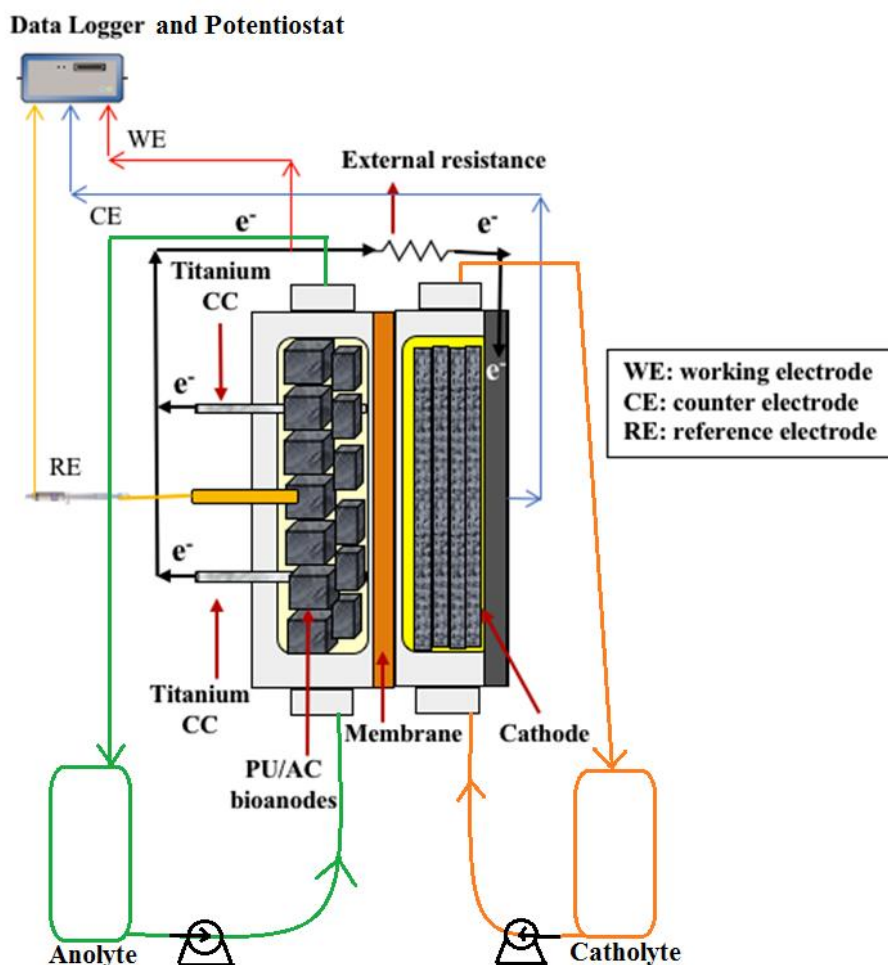


Figure 5. 1: Schematic illustration of the experimental set-up (MFC reactor). The number of PU/AC composites in the anode is 11 cubes

5.2.3 MFCs operation

MFCs were operated under recirculation and anaerobic conditions within an acclimatized room at 30°C. The flow rates were 3.5 mLs⁻¹ for the anolytes and 3.3 mLs⁻¹ for the catholytes. The anolytes had 0.020 M sodium acetate, 10 gL⁻¹ sodium 2-bromoethane sulfonate and macro and micronutrients as described earlier (*Supplementary Table S5.1* and *Supplementary Table S5.2*) [206]. Anolyte compartments were equipped with Ag/AgCl, 3M KCl reference electrodes (QIS, Oosterhout, The Netherlands). In the catholytes, 0.05 M potassium ferricyanide was chemically reduced in 0.05 M phosphate buffer at pH 7. On day one, both catholytes and anolytes were flushed with N₂ gas (purity >99.9%) for one hour to remove oxygen. This was done to prevent oxygen diffusion from the cathode to the anode which may hamper the development of the bioanode [58]. Then, anolytes were inoculated with 11% v/v of mixed culture bacteria grown on acetate from previous experiments[65,88]. Acetate

(2 g/L sodium acetate) was further regularly (about every 2-4 days) injected into the anolyte to prevent substrate depletion. MFCs were operated with an external resistance of 50 k Ω . The pH of anolytes was manually controlled at 7 (± 0.5) with anaerobic NaOH and HCl solutions to provide favourable conditions for electrochemically active bacteria[40]. Catholytes were replenished with fresh catholytes after cell voltages had decreased more than 150 mV. Anolytes were protected from light as much as possible with aluminium foil to prevent photosynthetic microorganisms from growing. Additionally, the actual current collectors were replaced by clean titanium wires after successful development of bioanodes.

5.2.4 Measurements

5.2.4.1 Electrochemical measurements

For all MFCs, anode and cathode potential were measured versus the reference electrodes placed in the anode chamber. Potentials were collected every 600 seconds via Fieldpoint modules (National Instruments, USA) connected to a computer with Labview Software (Labview 2013, National Instruments, USA). All the electrochemical experiments were carried out with a potentiostat (Iviumstat, Ivium Technologies, The Netherlands). To know the maximum performance of the bioanodes polarization curves were performed in-situ with a three-electrode setup from a potential of -500 mV to 50 mV, in steps of 50 mV every 600 seconds[52]. In this setup, anodes were the working electrodes while the cathodes were the counter electrodes. The reference electrodes were located in the anode chamber. The cells were set to open cell for 30 minutes before the polarization curves. The average current measured for each anode potential in the last 60 seconds is shown in the results.

Furthermore, to support understanding in electron-transfer in-situ and ex-situ cyclic voltammetries (CVs) were done under anaerobic conditions as in previous MFC research [223,224]. The in-situ CVs were done with a three-electrode setup (anodes were the working electrodes) from a potential of 50 mV to -400 mV and increased back to 50 mV at a scan rate of 1 mV/s [225]. Three cycles were performed considering the last cycle as the result. The in-situ measurements were performed in MFCs after the start-up phase ($t=3$ days), the replacement of current collectors (on days 20) and the replacement of old anolytes for fresh ones ($t=25$ days). These fresh-anolytes were free of inoculum and acetate and were flushed for one hour with pure N₂. In addition, the ex-situ CVs were performed in the replaced anolytes with a three-electrode setup using an Ag/AgCl, 3 M KCl reference electrode and two titanium wires integrating a graphite felt-layer of 1.5 x 2 cm as the counter and working electrodes (*Supplementary Figure S5.1*). The counter and working electrodes were placed in the anolyte under continuous N₂ flushing; the electrodes were just in contact with the anolyte. The set

range for ex-situ CVs was from 50 mV to -400 mV at a scan rate of 5 mVs⁻¹. Both scan rates, 1 mV/s and 5 mVs⁻¹, were not destructive for the biofilm according to the literature[52,226].

Moreover, ohmic resistances of bioanodes were measured in-situ over time and ex-situ at the end of experiments via electrochemical impedance spectrometry (EIS) (*Supplementary Figure S 5.2*). All EIS were carried out with a two-electrode setup at an applied cell voltage of 0V, an amplitude of 0.01V and 26 frequencies in the range of 10⁻⁴ to 10⁶ Hz [52,227]. The reported ohmic resistances were obtained as described earlier [40]. Particularly for the ex-situ measurements, a device with gold-plated electrodes was constructed for measuring the PU/AC bioanodes (*Figure 5. 2*). The electrodes had a gold layer thickness of 3 nm (Haveman Edelmetaal, Voorburg, Netherlands). A single PU-cube (dimensions as earlier mentioned with 1.5 by 1.5 by 1.5 cm) was fixed between the electrodes to measure resistance; the distance between the electrodes was fixed at 1.2 cm and the cube pressed with about 20% volume reduction. The measurements were under saturated conditions with acetate-free anolyte previously flushed with N₂ for one hour. To achieve saturated conditions 1.5 mL of anolyte media were injected with a syringe in the centre of the sponge and from the bottom towards the top. Between measurements, the device and electrodes were cleaned with tissues and pure ethanol. Uncoated PU foams were measured with the same technique to assess the influence of the biofilm on the conductivity of the composites. Particularly, in *Figure 5. 8*, PU/AC/BIO I has one less measurement than PU/AC/BIO II because one sample from PU/AC/BIO I went to microbial analysis.

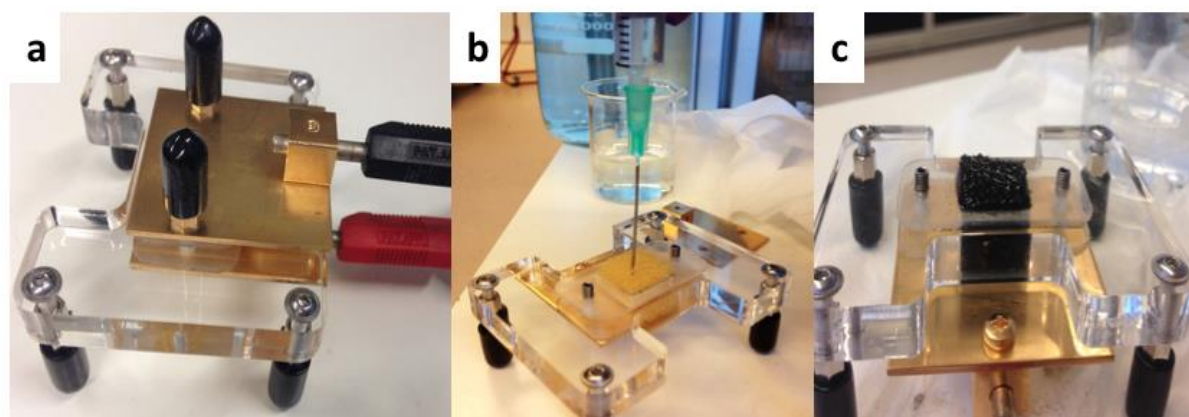


Figure 5. 2: (a) Ex-situ conductivity device with two electrodes. (b) Overview of anolyte media injection to achieve saturated conditions. (c) Visual example of saturated conditions for ex-situ EIS measurement

5.2.4.2 Physicochemical and reactants measurements

The pH was manually measured with a pH meter (Meter Lab PHM210, Radiometer Analytical, France) while the conductivity of anolytes was measured with a multi-parameter meter (HQ440D,

HACH, USA). Acetate, bicarbonate, ferricyanide and ferrocyanide concentrations were measured to evaluate the performance of the bioanodes [52,228]. Acetate concentrations were measured in a gas chromatographer (7890B GC Systems, Agilent Technologies, USA) as described in previous research[206]. Bicarbonate concentration in anolytes was measured directly in a total organic carbon analyser (TOC-LCPH E200, Shimadzu, Japan). Ferricyanide and ferrocyanide concentrations were determined as described by Skyllas-Kazacos, et.al [229] via spectrophotometry at 260 nm and 420 nm (Infinite M200PRO, TECAN, Switzerland) with a cell of 10 mm (100-QS, Hellma Analytics, Germany) (*Supplementary Figure S5.3*).

5.2.4.3 Microscopic and microbial analysis

At the end of experiments, MFCs were disassembled and bioanodes were put in a solution of 2.5 % glutaraldehyde in phosphate buffer 0.1 M for scanning electrons microscopy (SEM)[230]. Subsequently, samples were rinsed 3 times in 0.1 M phosphate buffer pH=7.2 and were post-fixed using 1% osmium tetroxide for 1 hour. The samples were dehydrated in a graded ethanol solutions in water – 30%, 50%, 70%, 80%, 90%, 96%, 2 x 100% (for 10 min each). Then, samples were critical point dried (CPD) with carbon dioxide in a Leica EM CPD300 (Leica Microsystems GmbH, Wetzlar, Germany). Afterwards, samples were mounted on SEM stubs by carbon adhesive tabs (EMS, Washington, USA) and subsequently coated with 12nm Tungsten (Leica, MED 020, Germany). Samples were analysed at 2 KV, 6 pA, in a field emission scanning electron microscope (Magellan 400, FEI Company, Eindhoven, The Netherlands).

Samples (anolyte and electrode) for microbial analysis were taken on day 28 (from PU/AC I) and day 70 (from PU/AC Inoculum). The samples were immediately stored in an -80⁰C freezer after collection until the DNA sequencing was conducted. Sequencing steps were performed similar to the work of de Smit [150] and Chapter 3 [45].

5.2.5 Calculations

The Coulombic efficiency (CE) was calculated from Equation (5.2):

$$CE = \frac{I_{measured}}{I_{available}} \times 100 \quad (5.2)$$

where $I_{measured}$ is the current being produced and $I_{available}$ is the maximum current theoretically possible given the consumed acetate[52,231].

The total Ohmic resistance of the bioanode electrodes was calculated based on earlier research [232] and in-situ Ohmic resistance measurements over time (Table S5.3). Therefore, as in a circuit in series, the total resistance ($R_{\text{Ohmic-bioanode}}$) was the sum of the ohmic resistances involved ($R_{\text{Ohmic-bioanode}}=R_S + R_{\text{BIO}} + R_{\text{CR}} + R_{\text{PU/AC}}$). Thus, the studied resistances were the anolyte resistance (R_S), the biofilm resistance (R_{BIO}), the contact resistance between PU/AC electrodes and titanium current collectors (R_{CR}) and the resistance of electrodes without biofilm ($R_{\text{PU/AC}}$). Moreover, it was assumed that the R_{CR} was equal to 1Ω as earlier indicated by [233] and that the R_S was the inverse of the anolyte conductivity multiplied by the distance between current collectors. For the $R_{\text{PU/AC}}$, it was the initial ohmic resistance that was deducted from the measured in-situ R_{Ohmic} bioanode before inoculation of anolytes. The R_{BIO} was supposed zero at start and later on deducted from the difference between $R_{\text{PU/AC}}$ and subsequent ohmic resistances after inoculation.

5.2.6 Field test

The similar PU/AC electrode was tested in a paddy field in West Kalimantan, Indonesia. Two tubular plant microbial fuel cell (Plant-MFC) similar to previously used in paddy field experiment but with a length of 50cm were prepared (Chapter 4). A 10 litre bucket filled with 5 litre water and 100 gram of activated carbon was used to prepare this electrode at 30°C . Then the PU sheet (Medium Filter Foam $50 \times 50 \times 2$ cm, Vijver Techniek (VT), Enschede, The Netherlands) was submerged in the bucket and mixed for 20minute with a mixer (Heidolph Type RZR1, Heidolph Instruments GmbH&CO.KG, Schwabach, Germany). In the first tubular Plant-MFCs (**Figure 5. 3**), both anode and cathode utilised the PU/AC electrode. While in the other one, the PU/AC was only utilised as anode while the cathode still used graphite felt. Both tubular Plant-MFCs were installed as described in Chapter 4 and operated at 1000 ohm external load [47]. Anode potential and cathode potential were measure against Ag/AgCl reference electrode and the potential data were logged with voltage sensor connected to a LoRa network as earlier described in Chapter 4 [47]. Current density and power density was normalized to plant growth area ($\text{PGA}=0.02925 \text{ m}^2$) as described in Chapter 4 [47].



Figure 5. 3: Materials and completely constructed tubular Plant-MFC with PU/AC electrode

5.3 Result and Discussion

5.3.1 A rough surface of activated carbon was created on the carbon-polyurethane by a simple water-based dipping method

In this study, a simple electrode made of activated carbon deposited on the surface of reticulated polyurethane cube was successfully developed (*Figure 5. 4*). Results show that on average 3.3 mg/PU cube ($\sim 1 \text{ kg m}^{-3}$) of AC appears to be adsorbed on the surface of the polyurethane cube. The activated carbon was stuck on the polyurethane surface due to the water absorption capacity of the PU foams (earlier described by [234,235]), the high adsorption capacity of the AC particles [236] at the provided 30 °C temperature and mixing. The same procedure at room temperature resulted into less adsorption and was therefore not investigated. There is a clear difference between the uncoated and coated PU cube (*Figure 5. 4 d* and *e*). In SEM images one can see that the AC-coating created a surface no longer clean and flat but a rough surface with deposits forming crevices of different micro-sizes. Dry weight measurements confirmed that 3.3 mg per cubes of AC was deposited. Based on the total surface area available and considering an even distribution the AC layer was estimated to be on average between 2.5 and 4 micrometres (typical specific surface area of 20 PPI polyurethane is $984 \text{ m}^2/\text{m}^3$ [237]). Furthermore, the remaining macro-porosity of the reticulated PU cube (*Figure 5. 4 f*) could potentially help to achieve internal and external bacterial colonization as well as long-term performance as demonstrated by Huysman and Xie [218,238]. In this sense, it could prevent clogging which has been a technical challenge for three-dimensional bioanodes with pores smaller than $10 \mu\text{m}$ after six months of operation in MFCs [239].

Result shows that activated carbon coating on the PU cube's surface improved the PU conductivity, which is indicated by the decrease on the ohmic resistivity (*Figure 5. 5*). A double coating (PU/AC/AC) with the same method on the previously coated PU/AC is not necessary because it hardly improved the conductivity (*Figure 5. 5*). This might be due to the limited adsorption capacity of AC on the PU's surface.

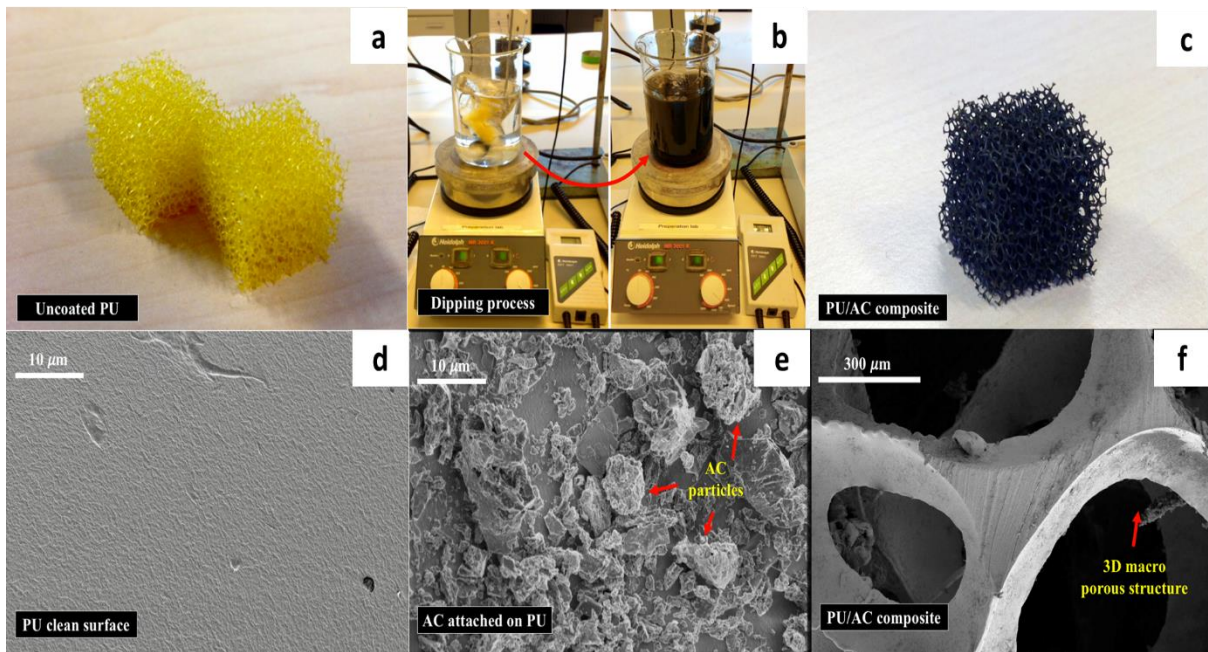


Figure 5. 4: (a) Uncoated clean polyurethane cube (1.5 x 1.5 x 1.5 cm); (b) Water-based process to coat the PU foam with activated carbon(AC); (c) PU/AC composites after coating; (d) SEM image of the uncoated PU foam's surface; (e) SEM Image of the PU/AC composite's surface; (f) SEM image of the PU/AC composite's macroscale structure

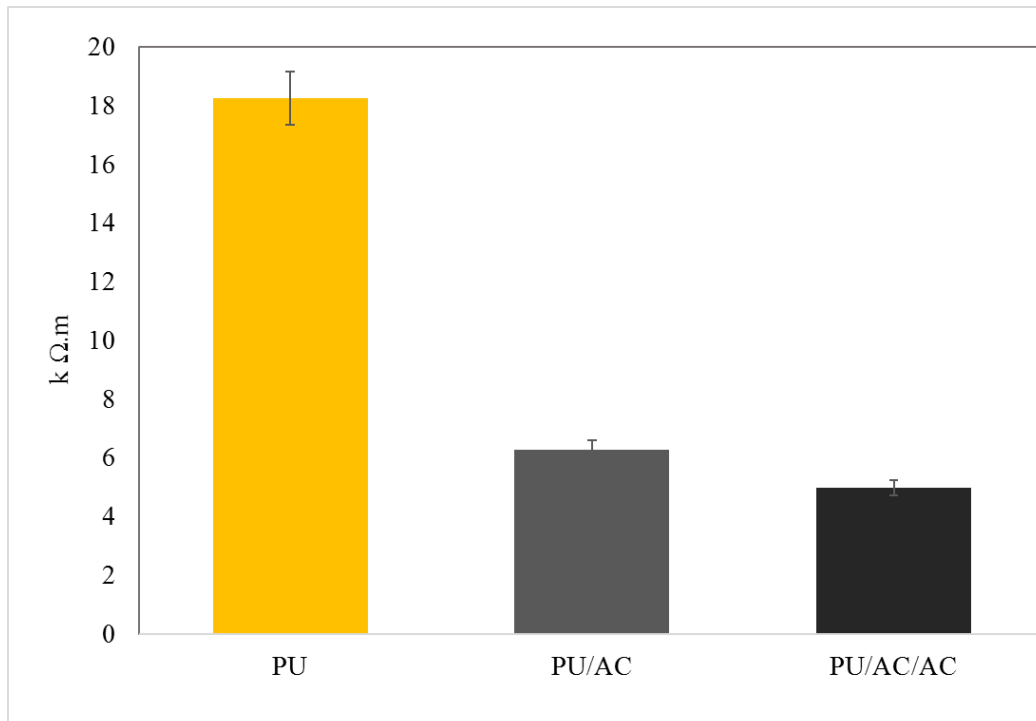


Figure 5. 5: Ex-situ measurement of ohmic resistivity. (PU) polyurethane cube before coated with Activated Carbon; (PU/AC) polyurethane cube after coated with activated carbon; (PU/AC/AC) polyurethane cube double coated with activated carbon. For comparison, the ohmic resistivity of the graphite felt is according the specifications (exact methode not provided) $<1 \Omega \cdot m$ (SGL Carbon)

5.3.2 PU/AC works as bioanode and likely electrochemically active bacteria grown on the PU/AC improve its conductivity

Newly developed PU/AC electrode acts as electron acceptor in an MFC anode. The PU/AC electrode accepted electrons that were liberated by the EAB and transported them via external load to the graphite felt cathode, thus electricity was generated. *Figure 5. 6* shows that the PU/AC MFCs delivered electricity when used as anode while the blanks (only current collector/Ti wire) delivered no significant electricity. Both reactors, PU/AC I and PU/AC II, produced electricity in the same order with a maximum power density of 22 mWm^{-3} and 10.4 mWm^{-3} respectively. When the current collectors were removed (dashed red line) and replaced with a new one, the PU/AC MFCs delivered no current anymore. This could be explained by a disturbance of a connection of the current collector (CC) to the PU/AC. Possibly there were also EAB grown in the biofilm that improved connectivity of the current collector to the PU/AC. Another explanation would be that the removed current collector contained the primary EAB; however, since the Blank experiments (only current collectors) showed no significant electricity generation the role of the current collector as electrode can be neglected. *Figure 5. 7a* supports that the biofilm was enabling the development of PU/AC electron acceptor because a SEM image of the surface of a CC showed no bacterial attachment. The poor biofilm attachment to the CCs demonstrated their unsuitability as anode material possibly due to their reduced biocompatibility and micro and macro-porous features[82]. With this proof-of-principle of a PU/AC bioelectrode the current and power density reached 3 mA/m^2 projected surface area of anode compartment and 22 mW/m^3 anode compartment, respectively. Columbic efficiency was low. The PU/AC I and PU/AC II only reached 0.07% and 0.02%, respectively. This low columbic efficiency could be caused by competing processes in the anode such as syntropic acetate oxidizing microbes that convert acetate into CO_2 and H_2 , which were flushed out via the anolyte bottle. Though improvement will be needed to reach more significant current densities reached for bioanode in order of 25 kA/m^3 [240].

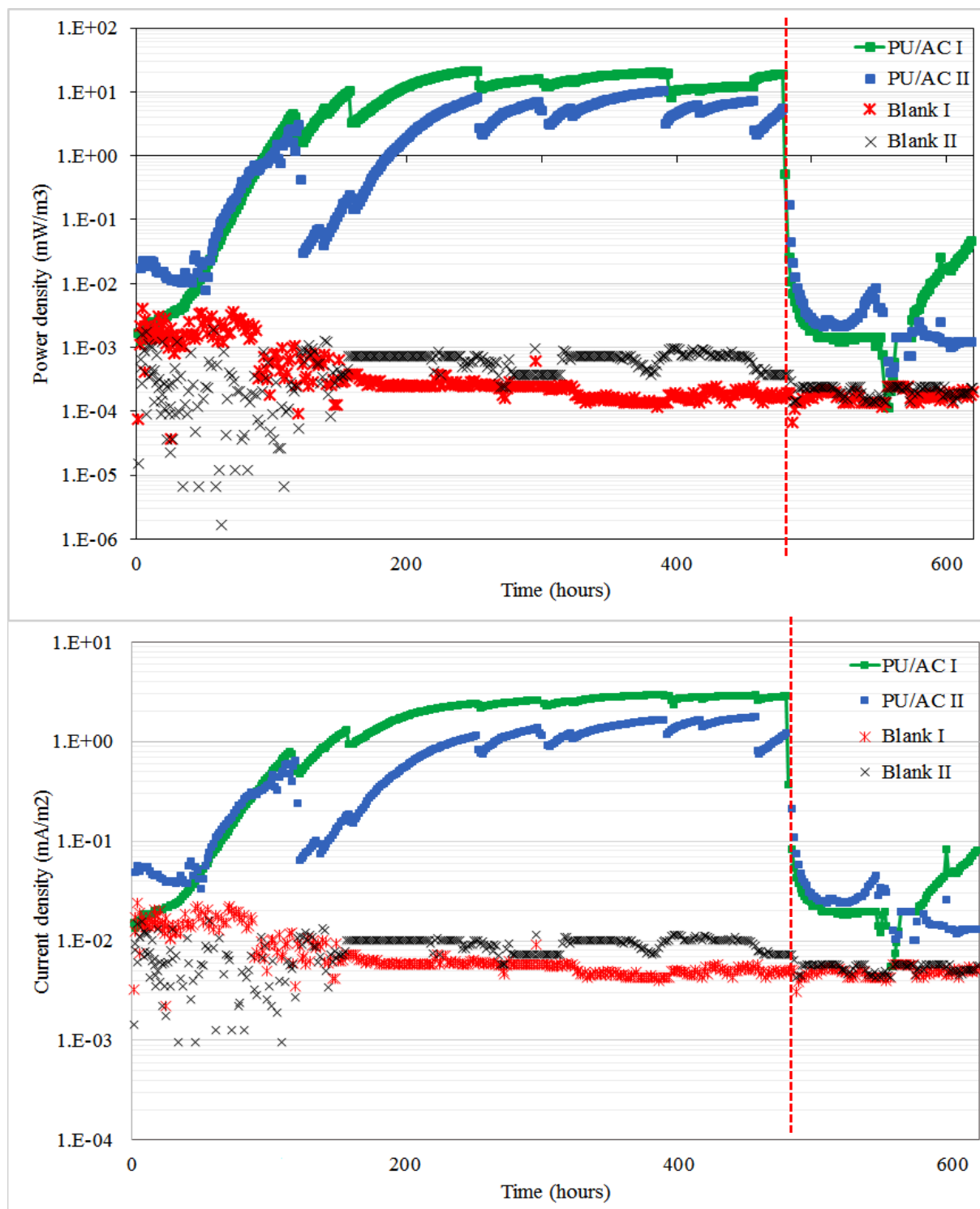


Figure 5. 6 : PU/AC electrode is able to deliver electricity in an MFC. (a) Power densities obtained in PU/AC bioanodes and blanks; the anode compartment volume was used for normalization. (b) Current densities obtained overtime and cathode and anode potentials; the projected surface area of anode compartment was used for normalization. The dashed (red) lines indicate the replacement of current collectors on day 20

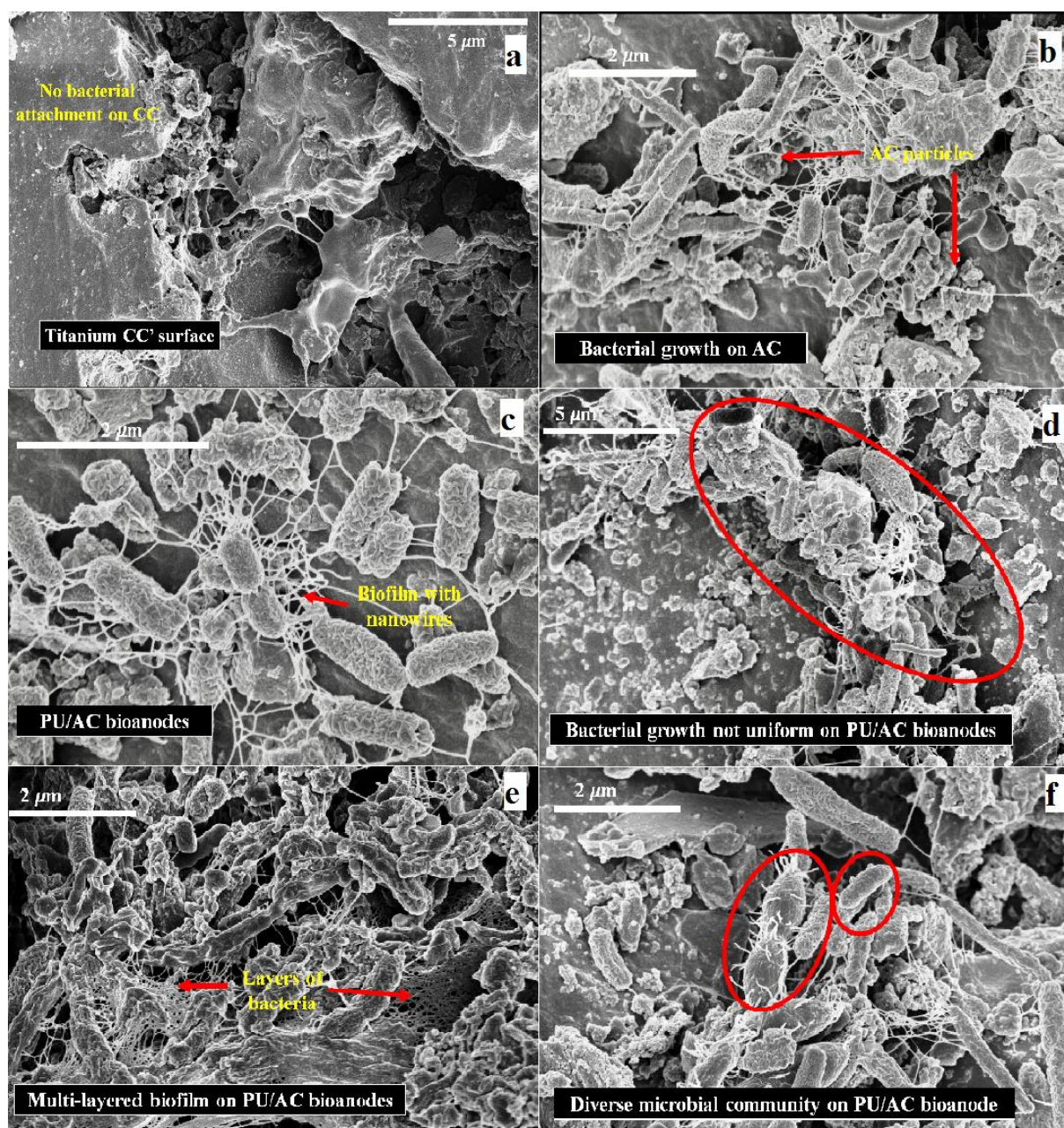


Figure 5. 7: Electrochemically active bacteria. (a) Surface of the Titanium current collector after deconstruction of MFCs. (b) Biofilm development on PU/AC composite showing strong interaction between microbial nanowires and AC particles. (c) PU/AC composite with a self-assembled biofilm, showing nanowires (pili) development. (d) Biofilm growth was not uniformly developed on PU/AC composites. (e) Multi-layered biofilm formation and solid deposits after 70 days of operation in the reactor which anolyte was used as inoculum. (f) Diverse microbial community on the PU/AC bioanode

Electrochemically active bacteria (EAB) seemingly did grow on the PU/AC electrode. The SEM images (**Figure 5. 7**) indicate that PU/AC foams were colonized by microbial communities spread onto the surface and forming wire structures. These observed structures could be the remains of

extracellular polymeric substances part of biofilms[226] and/or (nano) wires connections also called conductive pili[42] which acts as long-distance electron transport carriers. The biofilm was transforming the inert PU/AC composites into living electron acceptor terminals. The growth of the biofilm suggested that the mechanism of electron transport was through these wires (**Figure 5. 7 (c)** shows a spider-web kind of wires and (f) shows short wires of microbes connecting to the electrode). Though, these wires could (e.g. partly) also be exocellular polymer substances (EPS) of which biofilms are made of. However, direct electron transfer or indirect through mediators have been described for MFCs [241,242]. It is not possible to define the exact mechanism of electron transfer for a mixed culture with the current state of knowledge[242].

Results also show that the EAB also increase the PU/AC conductivity. In the end of the experiment, ex-situ ohmic resistivity was measured. Clean PU, Clean PU/AC (not used in experiment) and PU/AC with biofilms (from MFC 1 and 2) were measured with a gold-plated device as describe in the material and method. **Figure 5. 8** clearly shows that PU/AC electrodes with biofilm have lower (~4 times) ohmic resistivity compared to the clean PU/AC. This ohmic resistivity is still ~400 time higher than one of graphite felt (insert picture in **Figure 5. 8**).

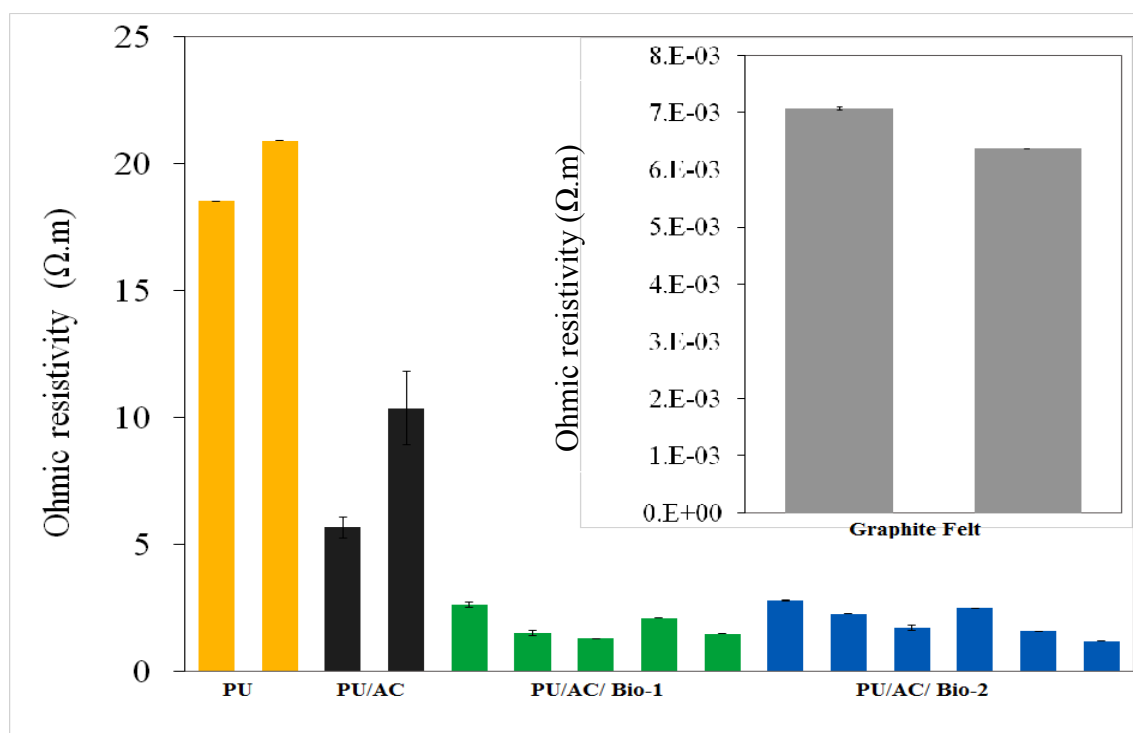


Figure 5. 8: Ex-situ Ohmic resistivity measured in the end of the experiment. Insert is the measured ohmic resistivity (Ω.m) of graphite felt. The same colour bars are replicates. PU/AC/BIO I has one less measurement than PU/AC/BIO II because one sample from PU/AC/BIO I went to microbial analysis

The conductivity of the biofilm developed on the PU/AC composites was on average $\sim 1.5 \text{ mS cm}^{-1}$ (**Table 5. 2**). Therefore, the increment of the conductivity of the PU/AC composites suggested that biofilms can modify the surface of the electrodes which is of interest for MFCs development. For instance, this bio-conductivity may be of great importance for the minimum use of electrode material. In this sense, biofilms can be carefully developed for an optimal design of electrodes in which the biofilm enriches the conductivity[243]. This finding is consistent with other studies that have also indicated the bio-conductivity of biofilms. **Table 5. 2** shows that electrochemically active biofilms (EABFs) are conductive while different types of biofilm are less conductive or natural insulators[207,243,244]. Since the conductivity and current density of this PU/AC study is lower than other bioanodes there is likely room for improvement. A longer term operation or fed-batch adding of AC materials may enhance the performance due to more biofilm development or encapsulation of conductive AC properties. This potential improvement is supported by earlier work to enhance performance of bioanodes for microbial electro synthesis which showed that adding carbon nanotubes during operation did improve performance[245]. Furthermore, research on conductive biofilms has shown that the conductivity of a biofilm varies between microorganisms[207] and that higher conductivity is achieved in biofilms with nanowires structures in both biofilms with mixed and pure cultures[244]. Therefore, the observed nanowire structures (**Figure 5. 7**) may have contributed to the bio-conductivity in the PU/AC/BIO.

Table 5. 2: Biofilm conductivities reported in the literature

Biofilm description	Microorganism	Conductivity	Anode material	Measurement	Reference
EABF- anodic	Mixed culture	$\sim 2.4 \text{ mS cm}^{-1}$	Two-gold electrode	In situ two-electrodes	[246]
EABF- anodic	Mixed culture (<i>Geobacter</i> spp.was 52%)	$250 \mu\text{S cm}^{-1}$	Two-gold electrode	In situ two-electrodes	[207]
EABF- anodic	Mixed culture	$6.1 \mu\text{S cm}^{-1}$	Two-gold electrodes	In situ two-electrodes	[247]
EABF- anodic	Mixed culture	$125 \mu\text{S cm}^{-1}$	Gold electrode	In situ two-electrodes	[243]
Methanogenic anodic biofilm	Mixed culture	$\sim 33.7 \mu\text{S cm}^{-1}$	Gold electrode	In situ two-electrodes	[243]
Fermentative anodic biofilm	Mixed culture	$\sim 0.5 \mu\text{S cm}^{-1}$	Gold electrode	In situ two-electrodes	[243]
EABF- anodic	<i>Geobacter sulfurreducens</i>	$\sim 5 \text{ mS cm}^{-1}$	Gold electrode	In-situ two-probe, four-probe and, conformal mapping	[244]
EABF- anodic	Mixed culture	$\sim 679 \mu\text{S cm}^{-1}$	Two-gold electrodes	In situ two-electrodes	[248]
EABF- anodic	Mixed culture	$\sim 285 \mu\text{S cm}^{-1}$	Gold electrode	In situ two-electrodes	[248]
EABF- anodic	Mixed culture	$\sim 1.5 \text{ mS cm}^{-1}$ *	PU/AC composites	Ex-situ two-electrodes	This study

*See Supplementary Table S5.4 for calculations.

For the bioanolyte, its role was shown with cyclic voltammeteries (**Figure 5. 9**). The ex-situ CVs done in the anolytes removed from MFCs gave interesting findings (**Figure 5. 9 a and b**). One can see that in all anolytes indistinctly of the anode material a redox peak was observed around -200 mV. Therefore, it is evident that the bacteria were producing exogenous mediators[223,241,249] as no peaks were observed in the fresh abiotic anolyte (**Figure 5. 9**). The presence of exogenous mediators suggested that bacteria capable of electron transport through redox mediators were present in the bioanolyte.

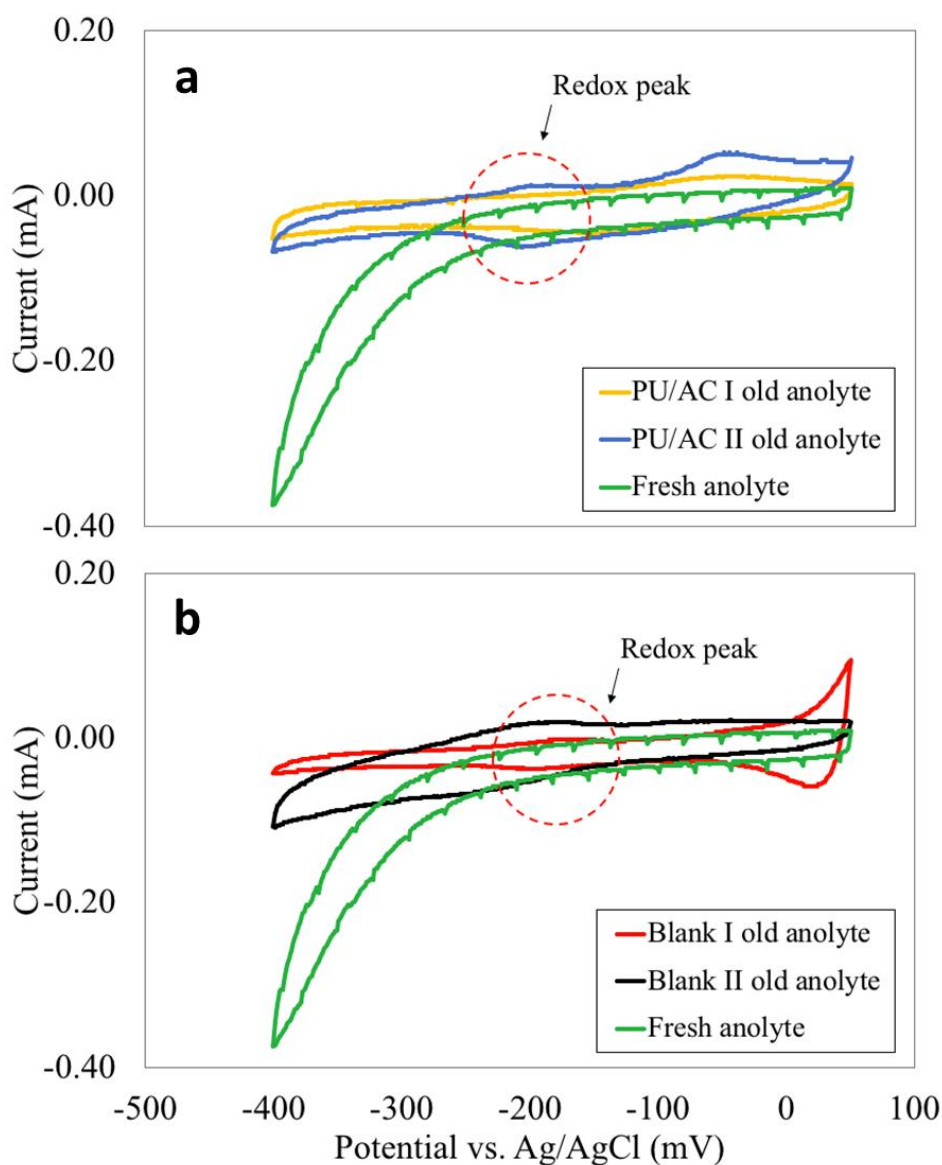


Figure 5. 9 : (a) Ex-situ CVs in old and fresh anolyte from PU/AC I and PU/AC II. (b) Ex-situ CVs in old and fresh anolyte from Blank I and Blank II

5.3.5 Diverse Microbial community both in the bioanode and bioanolyte predominantly by Proteobacteria

The microbial analysis shows that there is no apparent different between microbial communities in the anolyte and on the PU/AC electrode (sponges). *Figure 5. 10* shows the microbial community relative abundance (>1%) in samples. The microbial communities were predominantly by *Proteobacteria* phyla, followed by *Bacteroidetes*, *Synergistetes*, *Firmicutes* and *Spirochaetae*, respectively (*Figure 5. 10*). The electricity is possibly generated by some genera within *Proteobacteria* phyla that are known to electrochemically active such as *Geobacter*, *Deferrisoma*, and *Desulfobulbus* [186]. Additionally, *Supplementary Table S5.5A-E* shows all the microorganisms that were relatively abundant ($\geq 1\%$) from phyla to genus level.

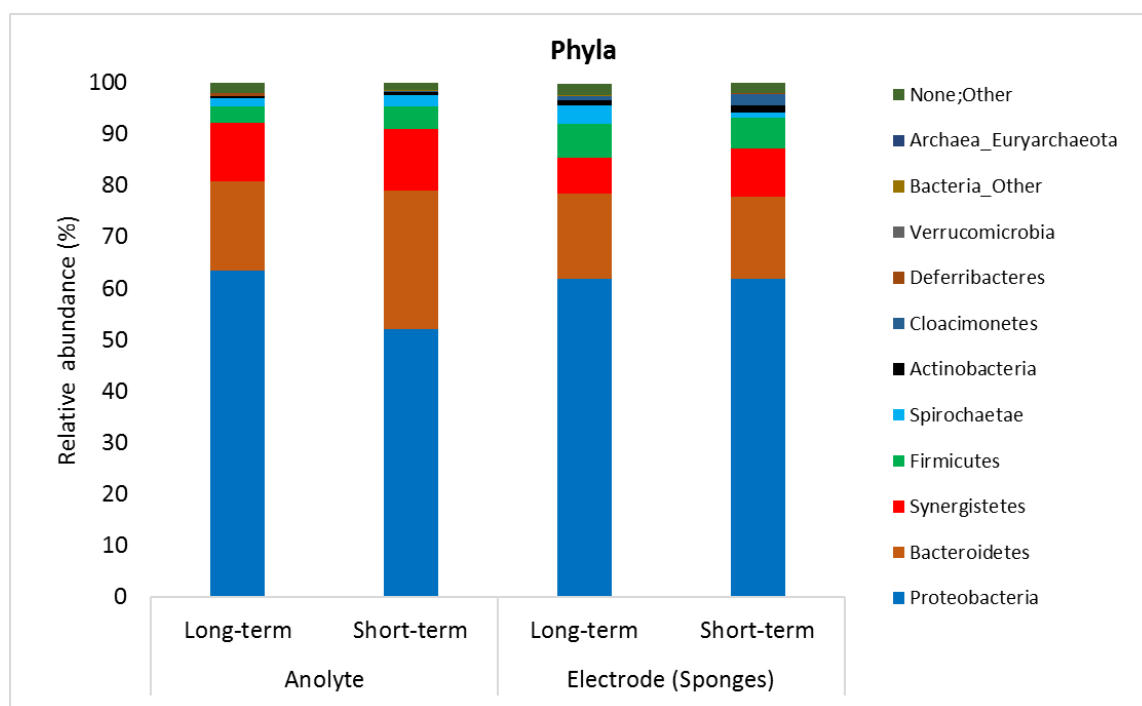
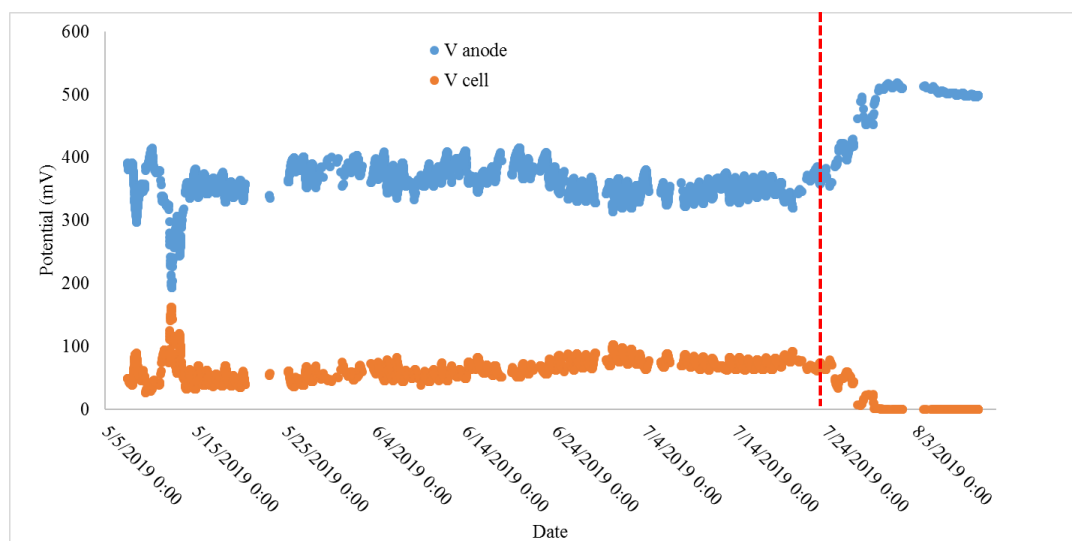


Figure 5. 10: Bacterial communities in the bioanodes of Microbial Fuel Cell in a long-term (70 days from PU/AC Inoculum) and short-term (28 days from PU/AC I) operation

5.3.3 Field test: PU/AC electrode delivers electrical current in a Plant-MFC when used as an anode

Field test result shows that the PU/AC electrode was able to deliver electric current when used as anode and coupled with graphite felt cathode (*Figure 5. 11 a*). However, the PU/AC electrode cannot act as cathode. *Figure 5. 11 b* shows that the PU/AC failed as a cathode to provide an access for oxygen reduction. The fact that the PU/AC has failed as cathode could be to various reasons (*e.g.* a too low AC load) although it was reported that oxygen reducing biocathodes have conductive[250].

A. Plant-MFC with PU/AC anode and graphite felt cathode



B. Plant-MFC with both the anode and the cathode use PU/AC electrode

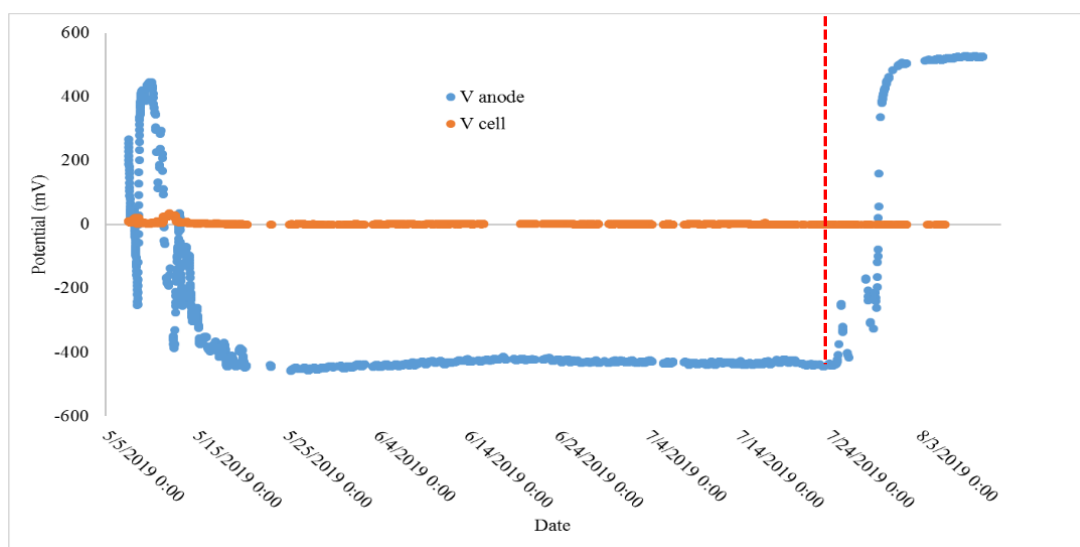


Figure 5. 11: Anode and Cell potential of Plant-MFC (a) PU/AC anode electrode and graphite felt cathode, (b) both anode and cathode were using AC/PU electrode. Both Plant-MFC were operated with 1000ohm external load. The red (dashed) line indicates that the water flow in the paddy field was stopped

On average, current density and the power density of the Plant-MFC with PU/AC anode are $2\pm 1\text{mA/m}^2$ plant growth area (PGA) and $0.2\pm 0.1\text{ mW/m}^2$ PGA, respectively. This current density is 48 times lower than power density of similar tubular Plant-MFC with graphite felt anode in the same paddy field as explained in Chapter 4 [47]. The maximum current density (5.6 mA/ m^2 PGA) and the maximum power density (0.9 mW/m^2 PGA) (11-12 May 2019 on *Figure 5. 12*) were reached just after the nearby soil was ploughed and fertilized before rice was transplanted [47].

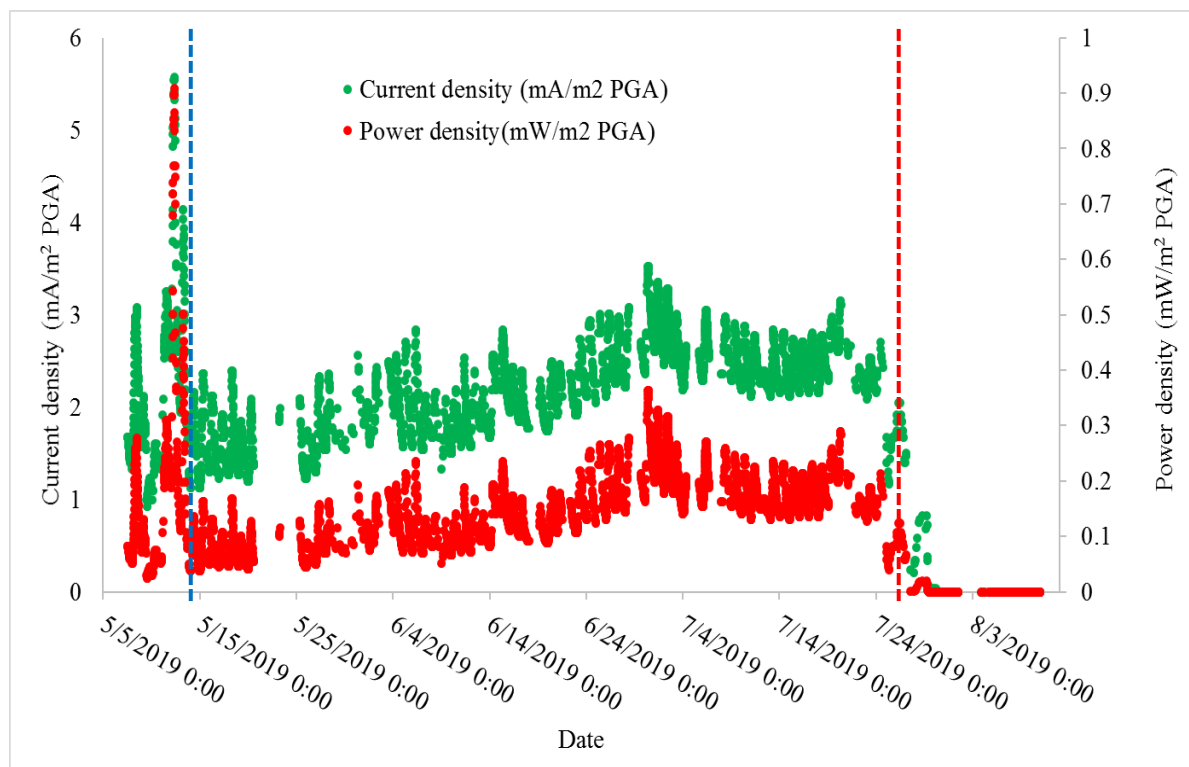


Figure 5. 12: Current density and power density of Plant-MFC with PU/AC anode. The blue (dashed) line indicates rice transplanting day. The red (dashed) line indicates that the water flow in the paddy field was stopped

5.4 Conclusion

Study shows that an alternative electrode can be developed by coating PU cube with activated carbon (AC) using a water-based dipping-drying process. This production process creates a biocompatible surface without additional energy need for PU-carbonisation or use of toxic chemicals. Biofilms were able to grow on the PU/AC electrode and enhanced conductivity. Electricity production was successfully achieved with PU/AC bioanodes in MFCs and Plant-MFC.

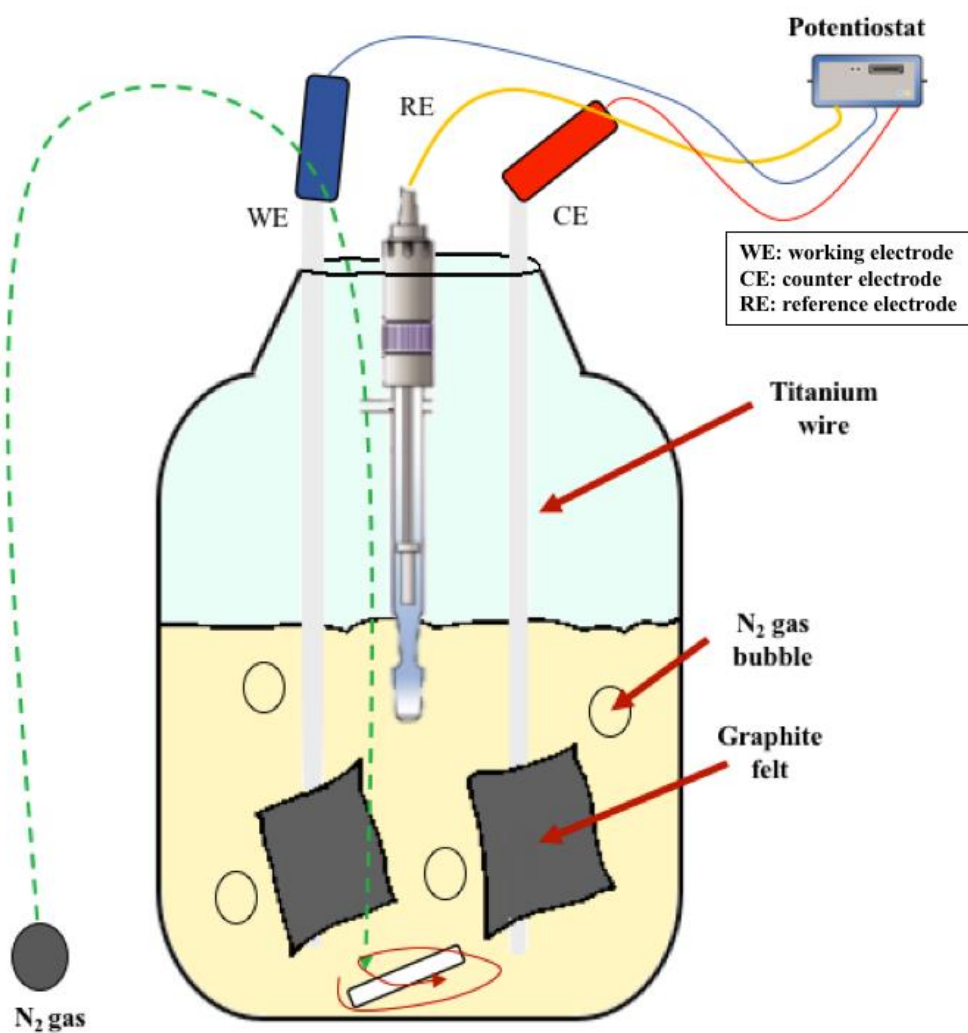
5.5 Acknowledgements

We thank to Marcel Giesbers from Wageningen Electron Microscopy Center for his assistance on the SEM analysis. This research was funded by Government of Landak Regency, West Kalimantan Province, Republic of Indonesia under an MoU with Wageningen University & Research, No 616003015. We also acknowledge Pim de Jager of Wageningen University & Plant-e B.V. for the support on the development of the data logging system.

5.5 Supplementary Materials Chapter 5

5.6.1 Supplementary Figures

Figure S5.1. Schematic for ex-situ CVs in the bioanalytes

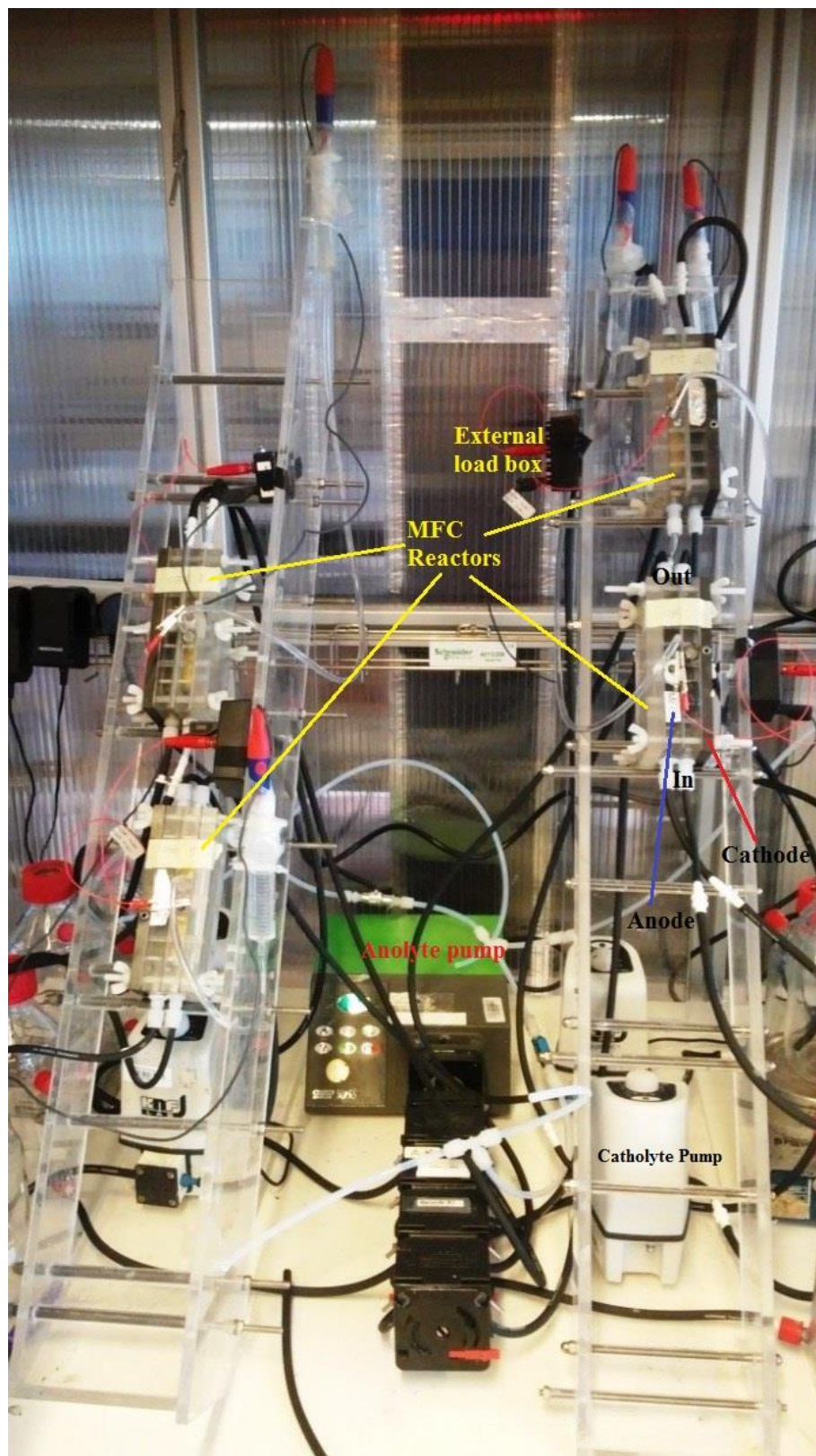


250 mL Schott Duran Bottle.

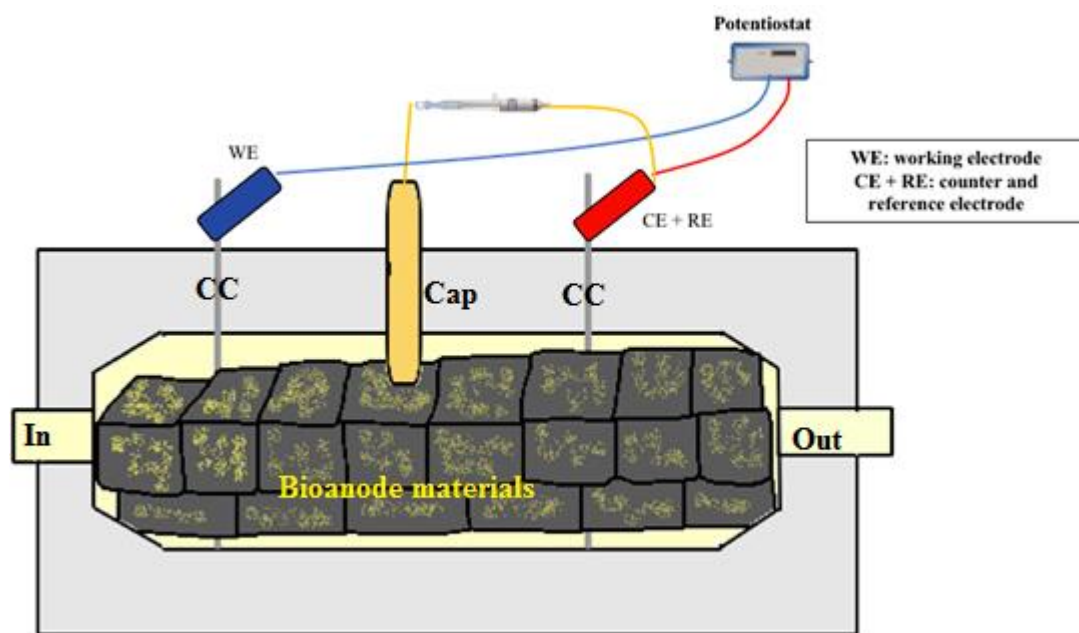
The graphite felt size is 1.5 x 2 cm. The distance between WE and CE is 3cm

Figure S5.2. (A) Real experimental set-up and (B) schematic of the setup for in-situ EIS measurements in the bioanodes

A.

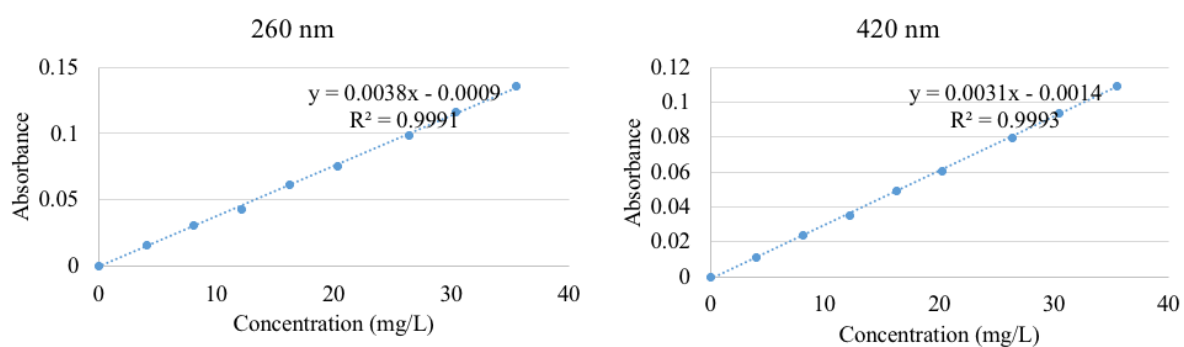


B.



CC is Titanium current collector; **Cap** is capillary filled with 3M gel KCl and connected to 3M KCl Ag/AgCl reference electrode via a tube that also filled with 3M KCl solution. **In** is inflow of analyte. **Out** is outflow of analyte.

Figure S5.3. Ferricyanide calibration curves and equations to calculate ferrocyanide



$$A_{420} = 1.058 [Fe(CN)_6^{3-}] - 0.003[Fe(CN)_6^{4-}] + 0.000925$$

$$A_{260} = 1.260 [Fe(CN)_6^{3-}] - 2.724[Fe(CN)_6^{4-}] + 0.006421$$

5.6.2 Supplementary Tables

Table S5.1. Composition of analytes and Wolfe's vitamin solution

Adapted from Ter Heijne et al., 2008 and 2007 [206,251]

Analyte: 0.020 M sodium acetate, 10 gL⁻¹ sodium 2-bromoethane sulfonate, 0.13 gL⁻¹ KCl, 0.2 gL⁻¹ NH₄Cl 0.2 gL⁻¹, 1 mL⁻¹ Wolfe's vitamin solution and 1 mL.L⁻¹ modified Wolfe's micronutrient solution, all mixed in phosphate buffer 0.05 M at pH 7

	Concentration (g/L)	CAS number
Pyridoxine	1	58-56-0
Nicotinic acid	0.5	59-67-6
Riboflavin	0.25	83-88-5
Thiamine	0.25	67-03-8
Biotin	0.2	58-85-5
Folic acid	0.2	59-30-3
Vitamin B12	0.01	68-19-9

Table S5.2. Modified Wolfe's micronutrient solution

(adapted from Helder et al., 2012 [58])

	Concentration (g/L)	CAS number
EDTA	1.5	60-00-4
MgSO ₄ -7H ₂ O	3	10034-99-8
MnSO ₄ -H ₂ O	0.5	10034-96-5
NaCl	1	7647-14-5
FeSO ₄ -7H ₂ O	0.1	7782-63-0
Co(NO ₃) ₂ -6H ₂ O	0.1	10026-22-9
ZnSO ₄ -7H ₂ O	0.1	7446-20-0
CuSO ₄ -5H ₂ O	0.01	7758-99-8
AlK(SO) ₄ -12H ₂ O	0.01	7784-24-9
H ₃ BO ₃	0.01	10043-35-3
Na ₂ MoO ₄ -2H ₂ O	0.01	10102-40-6

Table S5.3. Total Ohmic resistance of the bioelectrodes

Days	PU/AC I In-situ measurements				PU/AC II In-situ measurements			
	0	5	13	20	0	5	13	20
Ohmic resistance (Ω)	28.480	69.950	178.500	169.900	11.590	59.440	166.400	145.100
	28.460	69.310	173.400	173.100	11.670	60.080	164.600	156.000
	28.460	88.320	183.100	172.600	11.770	60.020	168.900	145.800
Average	28.467	75.860	178.333	171.867	11.677	59.847	166.633	148.967
STDEV	0.012	10.795	4.852	1.721	0.090	0.353	2.159	6.101
Conductivity (mS/cm)	9.790	10.010	10.970	11.240	9.790	10.410	10.990	11.330
Cond (ms)	56.782	58.058	63.626	65.192	51.887	55.173	58.247	60.049
Rs (m Ω)	0.018	0.017	0.016	0.015	0.019	0.018	0.017	0.017
Distance CC (cm)	5.800				5.300			
Rs (Ω)	0.000	0.000	0.000	0.000	0.000	0.000	0.000	0.000
Relectrode (Ω)	28.467				11.677			
Rbiofilm (Ω)		47.393	149.867	143.400		48.170	154.957	137.290
Rcr (Ω)	1.000	1.000	1.000	1.000	1.000	1.000	1.000	1.000
Rtotal (Ω)	29.467	76.860	179.333	172.867	12.677	60.847	167.633	149.967

Table S5.4. Biofilm conductivity calculation

The conductivity of the biofilm was calculated with the average Ohmic resistances measured ex-situ. First, the Ohmic resistivities were calculated from the Ohmic resistances by considering an area of (0.015x0.015 cm) 0.000225 m² and a length of 0.012 m (distance between electrodes during ex-situ measurements). Second, the conductivity of the biofilm was equal to the difference between the PU/AC and the PU/AC/BIO.

	Ohmic resistance (Ω)	Ohmic resistivity ($\Omega.m$)	Biofilm Ohmic resistivity ($\Omega.m$)	Biofilm conductivity (mS.cm ⁻¹)
Biofilm			6.10	1.6
PU/AC/Bio	101.584	1.905		
PU/AC	426.950	8.005		
PU	1050.367	19.694		
Graphite	0.358	0.007		

Table S5.5. Relatively abundant ($\geq 1\%$) of bacteria in the paddy field soil from phylum to genus level. The PU/AC inoculum was first developed as bioanode and consequently used to develop the PU/AC I

Table S5.5A Phyla

Phyla	Anolyte		Electrode (PU/AC cubes)	
	PU/AC Inoculum	PU/AC I	PU/AC Inoculum	PU/AC I
	70 days	28 days	70 days	28 days
Proteobacteria	63.43	52.12	61.80	61.91
Bacteroidetes	17.42	26.88	16.59	15.82
Synergistetes	11.22	11.87	7.01	9.46
Firmicutes	3.30	4.55	6.57	5.96
Spirochaetae	1.65	2.18	3.55	0.96
Actinobacteria	0.26	0.62	1.04	1.43
Cloacimonetes	0.10	0.07	0.79	2.13
Deferribacteres	0.46	0.11	0.03	0.28
Verrucomicrobia	0.02	0.02	0.02	0.00
Bacteria_Other	0.04	0.03	0.04	0.02
Archaea_Euryarchaeota	0.01	0.02	0.02	0.03
Others	2.09	1.52	2.54	2.01
TOTAL	100	100	100	100

Others are summary from phyla that less than 1%

Table S5.5B Classes

Classes	Anolyte		Electrode (PU/AC Cubes)	
	PU/AC Inoculum	PU/AC I	PU/AC Inoculum	PU/AC I
	70 days	28 days	70 days	28 days
Betaproteobacteria	48.912	40.431	56.242	46.448
Bacteroidia	10.720	18.592	10.452	9.628
Synergistia	11.221	11.870	7.015	9.456
Gammaproteobacteria	6.346	2.330	2.659	7.626
Alphaproteobacteria	0.952	0.678	1.001	5.674
Clostridia	3.154	4.465	6.470	5.486
Sphingobacteriia	6.353	7.870	5.680	5.018
LNR A2-18	0.096	0.065	0.786	2.127
Deltaproteobacteria	7.076	8.482	1.656	2.083
Actinobacteria	0.264	0.623	1.036	1.425
Flavobacteriia	0.252	0.304	0.368	1.128
Spirochaetes	1.646	2.181	3.552	0.956
Archaea	0.010	0.017	0.015	0.025
Others	2.998	2.093	3.066	2.919
TOTAL	100	100	100	100

Others are summary from classes that less than 1%

Table S5.5C Orders

Orders	Analyte		Electrode (PU/AC Cubes)	
	PU/AC Inoculum	PU/AC I	PU/AC Inoculum	PU/AC I
	70 days	28 days	70 days	28 days
Burkholderiales	35.139	19.448	45.158	26.307
Rhodocyclales	13.331	20.732	10.604	19.845
Bacteroidales	10.718	18.591	10.451	9.624
Synergistales	11.221	11.870	7.015	9.456
Pseudomonadales	5.359	1.873	2.203	5.507
Clostridiales	3.113	4.405	6.402	5.467
Sphingobacteriales	6.353	7.870	5.680	5.018
Rhizobiales	0.434	0.183	0.504	4.726
Cloacimonetes_LNRA2 -18_Uncultured bacterium	0.095	0.061	0.759	2.104
Xanthomonadales	0.889	0.327	0.354	1.949
Desulfovibrionales	6.918	8.393	1.609	1.682
Flavobacteriales	0.252	0.304	0.368	1.128
Spirochaetales	1.646	2.181	3.552	0.956
Archaea	0.011	0.023	0.019	0.035
Others	4.522	3.739	5.321	6.196
TOTAL	100	100	100	100

Others are summary from orders that less than 1%

Table S5.5D Families

Families	Analyte		Electrode (PU/AC Cubes)	
	PU/AC Inoculum	PU/AC I	PU/AC Inoculum	PU/AC I
	70 days	28 days	70 days	28 days
Rhodocyclaceae	13.331	20.732	10.604	19.845
Comamonadaceae	24.553	7.795	29.265	15.199
Alcaligenaceae	8.872	7.621	14.166	10.374
Synergistaceae	11.221	11.870	7.015	9.456
Porphyromonadaceae	8.953	14.936	7.363	6.833
Lentimicrobiaceae	6.346	7.857	5.634	4.986
Pseudomonadaceae	4.471	1.825	1.745	4.276
Brucellaceae	0.336	0.058	0.286	4.078
Rikenellaceae	1.757	3.638	3.086	2.789
Cloacimonetes_uncultur ed bacterium	0.095	0.061	0.759	2.104
Clostridiales_Family XIII	1.291	1.509	1.755	2.008
Xanthomonadaceae	0.889	0.327	0.354	1.948
Desulfovibrionaceae	6.918	8.393	1.607	1.682
Moraxellaceae	0.889	0.048	0.457	1.231
Flavobacteriaceae	0.250	0.302	0.367	1.126
Ruminococcaceae	0.529	0.622	2.263	1.098
Spirochaetaceae	1.645	2.181	3.549	0.956
Burkholderiaceae	1.652	3.910	1.686	0.677
Archaea	0.011	0.023	0.019	0.035
Others	5.991	6.293	8.019	9.299
TOTAL	100	100	100	100

Others are summary from families that less than 1%

Table S5.5E Genera

Genera	Analyte		Electrode (PU/AC Cubes)	
	PU/AC Inoculum 70 days	PU/AC I 28 days	PU/AC Inoculum 70 days	PU/AC I 28 days
Rhodocyclaceae_uncultured	12.382	19.290	5.858	18.892
Comamonas	18.071	3.659	10.623	10.249
Synergistaceae_uncultured	7.367	6.899	6.298	9.236
Kerstersia	1.563	2.860	10.769	9.017
Lentimicrobium	6.346	7.857	5.634	4.981
Pseudomonas	4.456	1.816	1.635	4.186
Ochrobactrum	0.320	0.049	0.281	4.031
Petrimonas	2.529	3.339	2.804	3.367
Hydrogenophaga	0.588	0.257	16.937	3.171
VadinBC27 wastewater-sludge group	1.757	3.635	2.978	2.788
Cloacimonetes_uncultured bacterium	0.095	0.061	0.759	2.104
Desulfovibrio	6.917	8.393	1.605	1.682
Anaerovorax	0.988	0.991	0.965	1.591
Proteiniphilum	4.652	8.769	1.250	1.370
Porphyromonadaceae_uncultured	1.269	2.037	1.475	1.266
Acinetobacter	0.889	0.048	0.457	1.231
Sphaerochaeta	1.643	2.180	3.549	0.953
Alcaligenes	6.817	4.186	2.888	0.690
Paludibacter	0.235	0.260	1.184	0.652
Pandoraea	1.399	3.587	0.755	0.646
Dechlorobacter	0.438	1.019	4.468	0.417
Aminiphilus	2.700	3.421	0.541	0.120
Cloacibacillus	1.145	1.547	0.153	0.094
Archaea	0.011	0.023	0.019	0.035
Others	15.424	13.817	16.112	17.231
TOTAL	100	100	100	100

Others are summary from genera that less than 1%

Chapter 6

General Discussion

In this thesis, research has been conducted to improve the performance of Plant-MFC while reducing its cost. The production cost of a membrane-less Plant-MFC is still dominated by the electrode cost. Therefore, we studied an alternative electrode that utilized mixture of activated carbon and sediment (Chapter 2 and 3). At the same time, we also studied long-term performance of tubular Plant-MFC in a paddy field to get insight Plant-MFC's real potential (Chapter 4). Finally, we also investigated a new electrode with a simple dipping method of activated carbon on polyurethane cubes (Chapter 5). As a starting point for discussion, a theoretical available power from a paddy field is estimated based on rice carbon rhizodeposition and paddy field methane emission. A theoretical available power gives an insight how far performance meets theoretical understanding. Based on the experimental results, we discuss the applicability of the Plant-MFC as an off-grid power source in a rural area of a theoretical Indonesian case for low power devices. For this, a technical design to power a small power usage device was made for a household in a rural area of Indonesia. The applicability was assessed on technical, social, and environmental criteria as well as economic and some scenarios were suggested which could improve the real application. Values for a plant-MFC system to fulfil basic electricity needs were calculated.

6.1 The theoretical power output of a paddy field based Plant-MFC

Paddy fields have a potential power of 58-419 mW/m². There are at least two estimations about the maximum potential power generated by plant microbial fuel cells that have been proposed. Here we discuss these two approaches and recalculate the theoretical power output for a paddy field based Plant-MFC.

6.1.1 First estimation using solar radiation conversion into photosynthetic electricity

In this estimation, the maximum potential power generation from Plant-MFC is calculated based on conversion efficiencies (CE) of solar radiation in a specific area into electricity which involves several processes (*i.e.*, photosynthetic, plant rhizodeposition, rhizodeposit availability for microorganisms, and energy recovery by the Plant-MFC). Earlier the maximum power generation of Plant-MFC was estimated to be between 1.6 and 3.2 W/m² PGA under Western European Condition (solar radiation of 150 W/m²)[231]. In this technically pursued high estimation, Strik et al based their calculation on photosynthetic efficiency of 5%, plant rhizodeposition of 70%, and 60% energy recovery by the Plant-MFC, which resulted in 2.1% conversion efficiency from solar radiation into electricity [231]. According to commonly achieved efficiencies, this estimation was overvalued because it assumed

that all plant rhizodeposits are available for electrochemically active bacteria. In addition, the plant rhizodeposition (70%) and energy recovery (60%) are also much higher than the commonly found plant rhizodeposition of 11% [252] and the achieved energy recovery of 9-10% [142,253].

An adjustment is made to calculate the maximum theoretical power generation from Plant-MFC in paddy fields (Box 6.1 as adapted from Deng, et.al [253]). The solar radiation (SR) in Indonesia is varying between 167 and 242 W/m² [254]. Rice is a C₃ type photosynthesis plant[255]. Under full-spectrum solar radiation(sunlight), theoretical maximum photosynthetic energy conversion efficiency for C₃ type plant is 4.6%[256]. However, this theoretical maximum limit is hardly achieved. A typical photosynthetic efficiency during growth phase for C₃ type plant is 3.2% [257]. The rhizodeposition of rice differs between growing seasons from early rice, late rice, and for the entire planting period which are 23.16 ± 8.87%, 28.16 ± 12.94%, and 27.00 ± 9.3%, respectively[258]. This means that the rhizodeposition of rice is ranging from 14-41%. Until now, the availability of these rhizodeposits for electrochemically active bacteria is remain unknown. However, microbial community analysis of Plant-MFC do report significant relative abundance of species (56%) *Desulfobulbaceae* and (16%) *Geobacteraceae*, which are often enriched on bioanode of microbial fuel cells[189]. This relative abundance does not directly report their activity and direct proof of being electrochemical active. However, specific *Geobacter* species are evidently electrochemically active and enrichment is taking place[102,244,259]. Therefore, a ‘fair’ estimation of the rhizodeposit availability for microorganism is 30%. Finally, the energy recovery for such Plant-MFC system is 9-10%[142,253]. Applying these more realistic values (in Equation 6.1) gives a maximum potential power generation in a tropical paddy field (Indonesia) is 21- 95 mW/m² PGA.

Box 6.1 – Conversion of solar radiation into electricity via photosynthesis and rhizodeposition in Plant-MFC system.

The theoretical power output (P) from Plant-MFC (in W/m²) is calculated using Equation (6.1)

$$P = SR \times P_{e, \text{rice}} \times R_{p, \text{rice}} \times R_a \times E_r \quad (6.1)$$

SR is solar radiation in a specific location (W/m ²)	; 167 - 242 W/m ²
P _{e, rice} is photosynthetic efficiency for rice (C ₃ type plant)	; 3.2%
R _{p, rice} is rhizodeposition of rice	; 14% - 41%
R _a is rhizodeposition availability for microorganism	; 30%
E _r is energy recovery	; 9% - 10%

6.1.2 Second estimation using available electron donors

The second estimation applies a different approach to predict the maximum potential power of Plant-MFC from a wetland. In this approach, the maximum potential power generation is estimated based on the site-specific such as plant species (e.g. primary production), climate (e.g. solar radiation and temperature) and the external carbon inflow [96]. Together all these factors provide a total amount of electron donor that will be used by the EAB to generate electricity. Using this approach, Wetser, et.al predicted that Plant-MFC is potentially able to generate a power density up to 90 and 500 mW/m² PGA in peat soil and salt marshes, respectively [96]. Moreover, based on the ability of the EAB to outcompete the methanogens for electron donors[136], it is suggested that methane emission is prevented and all available carbon donors are utilized to generate electricity. Therefore, the second approach can also be estimated using methane emission flux [46].

In the above-mentioned approach, Wetser, et.al assumed that all the carbon mass/methane are converted into electricity, so as this is not necessarily reached the predicted potential power output becomes overestimated. In fact, there is a competition between the EAB and other microorganisms (e.g., methanogens)[260,261]. At a low substrate concentration, methanogens are outcompeted by the EAB indicated by the coulombic efficiencies of 15-30% [260] only about 30% of the total carbon in the rhizosphere is proposed to be available for the electrochemically active bacteria[253]. Furthermore, using a one-dimensional process based model, methane reduction in a paddy field due to competition with Plant-MFC is predicted to be around 17-28% [262]. Using the same principle as explained by Wetser, et.al, a new calculation is made (using Equation 6.2 as presented in Box 6.2) to estimate the Plant-MFC power output in a paddy field.

The available electron donor is estimated from carbon rhizodeposition of the rice plant and from the methane production in the paddy field. The carbon rhizodeposition from the rice plant depends on the stage of rice growth [258]. The carbon rhizodeposition rate in the early rice phase (first 2 months after seedling) and in the late rice phase (last two months before harvesting) are 36-178 mg/m²/hour and 51-260 mg/m²/hour, respectively[258]. The available carbon (as electron donor) for Plant-MFC is estimated 30% of the total carbon rhizodeposition (section 6.1 first estimation), which are 11-53 mg/m²/hour and 15-78 mg/m²/hour for the early rice and the late rice phase, respectively. Using Equation 6.2, the maximum potential power generation from paddy field for early rice and late rice is 58-286 mW/m² and 83-419 mW/m², respectively. The limitation of this approach is it includes no additional external carbon flux (e.g., dead plant matters, organic fertilizer, etc) that can also be potential substrates.

Box 6.2 – Plant-MFC power output estimation using available electron donor based on available carbon (C) or Methane (CH₄).

The theoretical power output (P) from Plant-MFC (in W/m²) is calculated using Equation (6.2)

$$P = \frac{J \cdot n \cdot F \cdot U}{M \cdot t} \quad (6.2)$$

P is the power (in W/m²); J is the available electron donor for electrochemically active bacteria (in g.m⁻².hr⁻¹); n is the number of electrons (4 for carbon, 8 for methane); F is the Faraday constant (96485 A.s.mol⁻¹); U is the Plant-MFC cell voltage (0.6V based on chapter 4), M is the molar mass of electron donor (12 g.mol⁻¹ for carbon and 16 g.mol⁻¹ for methane), and t is the amount of seconds in one hour (in s.hr⁻¹).

The J values use in this thesis:

Available electron donor based on carbon rhizodeposition:

$$J = 11\text{-}53 \text{ mg.m}^{-2}\text{.hr}^{-1} \text{ for the early rice}$$

$$J = 15\text{-}78 \text{ mg.m}^{-2}\text{.hr}^{-1} \text{ for the late rice}$$

Available electron donor based on methane flux:

$$J = 11.3\text{-}40.8 \text{ mg.m}^{-2}\text{.hr}^{-1}$$

This power output bases on long term data and does not include dynamics and other environmental

Methane emission flux from a rice paddy field in Indonesia varies between 16 and 35 mg/m²/hour [263]. The methane production was estimated based on a fact that 76% of the generated methane is re-oxidized to carbon dioxide by methane oxidizing bacteria in the wetland rhizosphere [264]. Thus, the gross methane production from the paddy fields in Indonesia is 67-146 mg/m²/hour. The available methane as an electron donor is 17-28% from the total methane production (based on the model of methane reduction from rice paddy field), which is 11.3 – 40.8 mg/m²/hour [262]. Using Equation 6.2, the maximum potential power generation from paddy field is 90-330 mW/m².

It seems that both solar radiation conversion and available electron donor estimation's methods result in the same order of magnitude for total available power from the paddy field. However, for further discussion in this thesis, we decided to use the second estimation (58-419 mW/m²) as the total available power from a paddy field because it was calculated with more realistic values (*e.g., rice carbon rhizodeposition, paddy field methane emission*) for rice plants.

6.2 Plant-MFC is able to generate up to 11% of the total available power from the paddy field and still can be increased

Power generation from Plant-MFC in the paddy field can still be increased. Based on the explanation on section 6.1, the total available power from a paddy field varies from 58 mW/m^2 (3.4 mW/tube) to 419 mW/m^2 (24.5 mW/tube) dependent on the rice growth phase. On average, the Plant-MFCs in the paddy field were able to generate power of 6.6 mW/m^2 (0.4 mW/tube). This power output is only 2 - 11% of the total available power from a paddy field (see section 6.1). A 10 minutes polarization shows that the Plant-MFC can generate at least up to of 44 mW/m^2 (2.6 mW/tube) but this result is just a temporary that cannot directly be linked to the yearly average power density.

As have been shown in chapter 4, the cathode was not the limiting factor of that actual Plant-MFC since the cathode potential was stable (around 400 mV), meaning the oxygen supply was sufficient. During the wet period, the anode potential of around -200 mV until -400 mV resulted in high cell potential ($0.6\text{-}0.8 \text{ V}$). The current limitation can be explained with competing reactions (*e.g.*, methanogenesis) and limited access to electrochemically active bacteria (EAB). However, this aspect is included in the theoretical performance (section 6.1). In addition, not 100% of the soil is occupied with the Plant-MFC's anode; so not all available substrates can be used.

Several ways could possibly improve the power output of Plant-MFC in paddy field. First, it is important to understand where and when a potential donor is available; as correct placement of the Plant-MFC at hotspots of the available electron donor could increase the electricity generation. For instance, the methane emission indicates the availability of electron donor that potentially be co-utilized by the EAB. Methane is released into the atmosphere via three processes: (i) methane loss via diffusion across the water surface, (ii) methane loss as bubble (ebullition) from paddy soil, which is the major release mechanism during the land preparation and initial growth, and (iii) methane loss via the rice plant, which has been reported as the most important phenomena[265–267]. Methane is emitted via aerenchyma of leaves, nodes and panicles of the rice plants[268]. Leaves are the major release location at the early stages and node (via cracks and porous structure) are later more important [268]. The methane emission fluctuates seasonally depending on the fertilization regimes, the water management and the rice growth stages[269–272]. Soil and added organic matters (*e.g.*, rice straw) are the initial sources for methane production[266,273]. NPK fertilizer, manure and their combination increase seasonal methane fluxes by 67.4, 20.4, and 101.2%, respectively[269]. Optimization of irrigation practice from continuously flooding to intermittent irrigation will reduce the methane

emission by 50% [270]. Root and root exudates of the wetland rice plant are the major carbon sources at ripening stage [273]. There are no significant differences among the methanogens population in rice soils up to 18 cm depth [271]. The methanogenic bacteria population was low during the early growing stages of early rice, then gradually increased and reached its maximum, from the yellow maturing stage to the late rice stage [271]. The methanogens are found more in the rhizospheric soil; during the initial and peak-tillering stages, the methanogenic activities in rhizospheric soil is 1.7-2.2 times higher than those in non-rhizospheric soil [271]. By knowing when and where the potential electron donor is available, one can decide the correct place and time to install the Plant-MFC. If and to what extent the various local hotspots on current generation can be (temporarily) technically utilized is unknown.

Second, the placement of the tube could be higher, closer to an area where mixing is occurring. Earlier research in a flat plate Plant-MFC has shown that more current can be generated when anode was placed closer to the surface, but still in the anaerobic zone, which has more substrate due to local mixing (chapter 4 from [46]). In the paddy field case, mixing is predicted to happen mostly in the water and topsoil because of water management. Additional substrates from applied fertilizers will be deposited on the topsoil and spread over the paddy field by the water flow, which may supply additional alternative electron donor. In addition, root density of rice plant is decreasing over the depth. Highest root density is found in the depth between 2 and 7 cm from topsoil [274]. More carbon rhizodeposit will be found in the area with high root density because the rhizodeposition is positively correlated with the rate of root growth [275]. However, the radial oxygen loss (ROL) strongly affect the O₂ availability in the rhizosphere of rice, which will negatively affect the anode of the Plant-MFC potential [276]. The Radial oxygen loss (ROL) in the rice plant is highly dynamic and affected by the photosynthesis activity as indicated by less ROL during the night-time compared to one in the daytime [276]. Furthermore, the ROL is higher on the root of young rice than the mature one [276,277]. The oxygen concentration at which methanotrophs won the competition from heterotrophs did not depend on methane concentration, but it was highly affected by organic carbon concentrations in the paddy soil. At low organic carbon concentration rhizosphere, the ROL is mostly consumed by methane oxidizing bacteria [278]. Therefore, if temporary more oxygen and/or substrates and the placement of the electrode is fixed, the net substrate availability for EAB will likely vary with time as electron donors and competing electron acceptors are supplied at different rates at various time.

Third, a suitable mechanical treatment that does not potentially damage the Plant-MFC installation is needed to bring substrates to the Plant-MFC anode. In this research, for safety reason, the soil on top of the Plant-MFC location was not ploughed prior to the crop season after the Plant-MFCs have been

installed. Finally, a different system could be tested. For instance, granular anode materials mixed through the soil (to provide a conductive matrix) can be applied to the paddy field prior to the tubular Plant-MFC installation to potentially harvest more substrates. The granular anode material (e.g. biochar or granular activated carbon) should be able to promote electron transfer and to improve the soil quality which can increase rice yield[84,279,280]. Still, a thicker anode electrode will also increase the resistance of the Plant-MFC that will limit the possible current output.

6.3 Plant-MFC design for a small power usage device

According to chapter 4, 0.4 ± 0.1 mW/m tube of power can be generated from a one-meter tubular Plant-MFC. This power is an average performance of triplicate Plant-MFCs at a cell potential of 0.6V with 1000 ohm load; thus 0.64mA current was delivered. On such low voltage source, one needs a power harvester that can step the potential up to a certain useful potential e.g. 5V [281,282].

On designing Plant-MFC systems to power an electronic device, a 1-m length tubular Plant-MFC is used as a basis. This length is considered as an optimum length based on the Plant-MFC performance in the paddy field, in which no oxygen limitation was observed (Chapter 4). Even though, previous similar design tubular Plant-MFC in salt marsh and peat soil suggested a maximum length of 0.31m and 0.77m for passively supplied oxygen, respectively[46]. Based on the performance of this 1-m tubular Plant-MFC, a strategy to harvest power is proposed.

The tubular Plant-MFC delivers relatively low current density (0.64 mA/tube) at a high voltage (0.6V) compared to e.g. fuel cell fed with hydrogen[283]. The voltage can be increased from 0.6V to a useful potential, e.g. 5V using a power harvester [281,282]. Therefore the first strategy was to increase the current output to the current output of target devices. For this purpose, the Plant-MFC must be connected in a parallel connection (Box 6.2). The proposed design is presented in *Figure 6. 1*.

Box 6.2 – Series and parallel connection in electricity

In the electricity connection total voltage (V) and current (I) depend on how one connects the Plant-MFC as shown on the following equations:

In series connection

$$V = V_1 + V_2 + V_3 + \dots + V_n \quad (6.2)$$

$$I = I_1 = I_2 = I_3 = \dots = I_n \quad (6.3)$$

In parallel connection

$$V = V_1 = V_2 = V_3 = \dots = V_n \quad (6.4)$$

$$I = I_1 + I_2 + I_3 + \dots + I_n \quad (6.5)$$

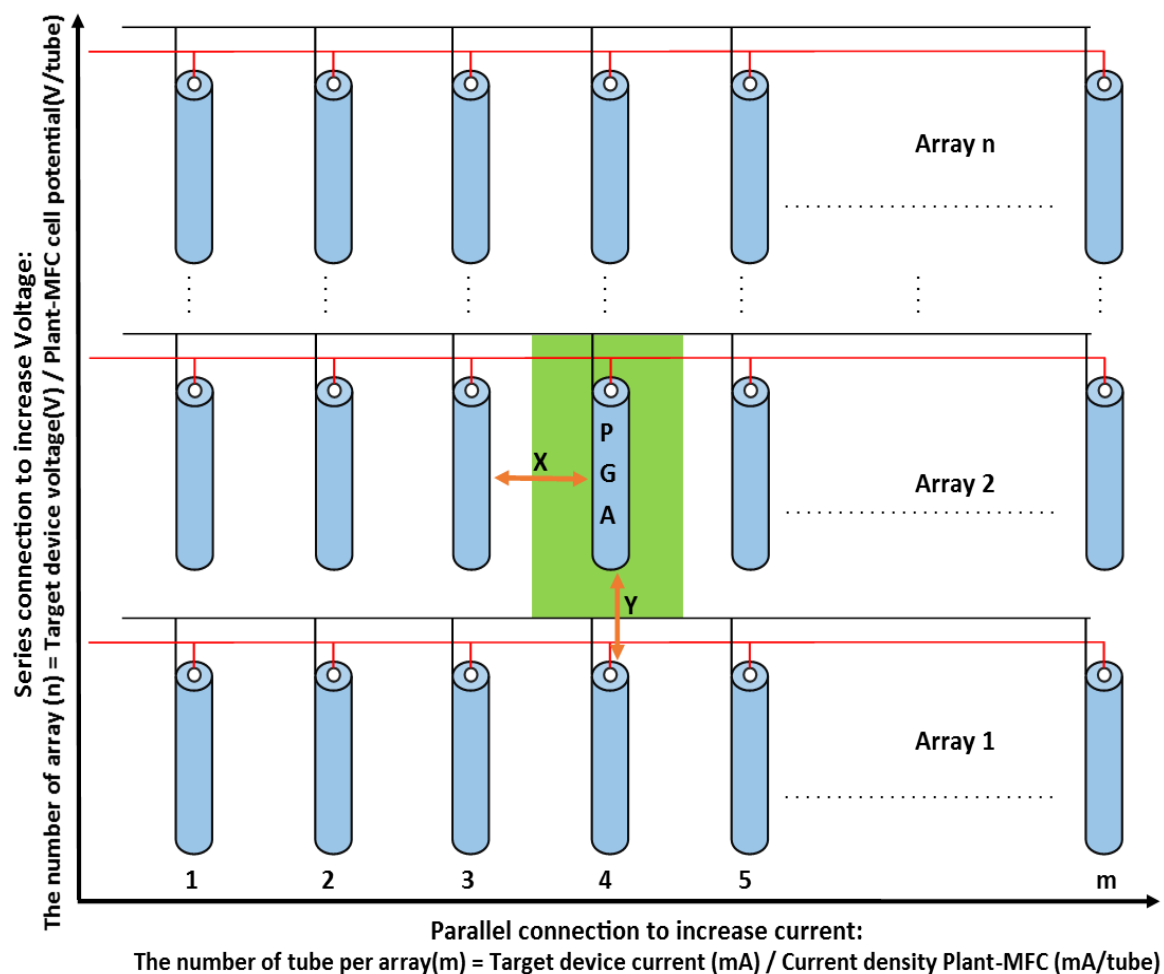


Figure 6. 1: Schematic design of tubular Plant-MFC for power harvester. Space needed (marked in green) per tubular Plant-MFC reactor is $(X + \text{reactor's diameter}) \times (Y + \text{reactor's length})$. X = space between reactors in the parallel connection and Y = space between reactors in the series connection

The number of tubes (m) in an array of parallel connection is obtained by dividing the target devices current by the current output of one Plant-MFC (0.64 mA/tube). Then, the parallel array needs to be connected in series (Box 1). The number of the parallel array in series (n) is calculated by dividing the operating voltage from target device by the cell voltage of one Plant-MFC (0.6V). Total required Plant-MFCs (tubes) to power a target device are a result of multiplication between the numbers of tubes in the parallel array (m) and the number of parallel array in the series connection (n). If the Plant-MFCs are installed in one horizontal layer with a distance of 25cm between them, space for one reactor is 0.31 m² (0.25 m² extra space (marked in green in Figure 6.1) and plant growth area/PGA (0.0585 m²). **Table 6. 1** shows total Plant-MFCs and total area for their installation to power some target devices.

Table 6. 1: Design of Plant-MFC for several target devices based on average tubular Plant-MFC performance in a rice paddy field during crop growth season

Target devices	Voltage (V)	Current (mA)	Tubes in parallel	Parallel array in series	Total tubes	Area for installation (m2)	Calculated Voltage (% overcapacity)	Calculated Current in mA (% overcapacity)	Ref
NiCd battery 1.2V; 700 mAh; 10 charging at 70mA; 1.5 V	1.5	70	109	3	327	101	1.8 (+20%)	70.1 (+0.2%)	[284]
	1.5	70	17	3	51	16	1.8 (+20%)	73.1 (+4.4%)	
5mm white LED 0.8 lumen (690mcd at 20mA, at 70° beam)	3.6	20	32	6	192	60	3.6 (+0%)	20.6 (+3%)	[29]
	3.6	20	5	6	30	9	3.6 (+0%)	21.5 (+7.5%)	
1 LED light 1 W (SMD)	5	200	311	9	2799	868	5.4 (+8%)	200.1 (+0.1%)	[31]
	5	200	47	9	423	131	5.4 (+8%)	202.1 (+1.1%)	
Cree Xlamp XM-L2 High Power LEDs; 120° view; 212 lumen	2.85	700	1088	5	5440	1687	3 (+5%)	700.1 (+0.02%)	[30]
	2.85	700	164	5	820	254	3 (+5%)	705.2 (+0.7%)	
Small solar lighting kit (7.4V; 3000mAh; 10hr charging at 300mA at 7.5 V)	7.5	300	467	13	6071	1883	7.8 (+4%)	300.5 (+0.2%)	[31]
	7.5	300	70	13	910	282	7.8 (+4%)	301 (+0.3%)	
Mobile phone Nokia 110 (3.7 V; 800mAh; 10hr charging at 80 mA and 4.5V)	4.5	80	125	8	1000	310	4.8 (+7%)	80.4 (+0.6%)	[32]
	4.5	80	19	8	152	47	4.8 (+7%)	81.7 (+2.1%)	
STS3x temperature sensor node	3.3	1.7μA	1	6	6	2	3.6(+9%)	0.64(+37821%)	[285]
	3.3	1.7μA	1	6	6	2	3.6(+9%)	4.3(+253293%)	
SHT2x (RH/T) humidity sensor node	3.6	0.9μA	1	6	6	2	3.6(+0%)	0.64(+72294%)	[286]
	3.6	0.9μA	1	6	6	2	3.6(+0%)	4.3(+483650%)	
MICA 2 sensor nodes (active mode)	3	8	13	5	65	20	3 (+0%)	8.4 (+4.6%)	[287]
	3	8	2	5	10	3	3 (+0%)	8.6 (+7.5%)	
TelosB sensor node (active mode)	3	3.3	6	5	30	9	3(+0%)	3.9(+15.8%)	[287]
	3	3.3	1	5	5	2	3(+0%)	4.3(+29%)	
Zigbee (Transfer mode)	3	12.2	20	5	100	31	3(+0%)	12.8(+4.6%)	[288]
	3	12.2	3	5	15	5	3(+0%)	12.9(+4.9%)	
LoRa (Transfer mode)	3	33.3	52	5	260	81	3(+0%)	33.5(+0.5%)	[288]
	3	33.3	8	5	40	12	3(+0%)	34.4(+3.3%)	
BLE (Transfer mode)	3	3.3	6	5	30	9	3(+0%)	3.9(+17%)	[288]
	3	3.3	1	5	5	2	3(+0%)	4.3(+30.3%)	

Note: MICA 2 sensor nodes (active mode) is a sensor node for light, temperature, humidity, barometric pressure, accelerator, GPS, RH, acoustic, Video sensor, microphone, sounder, magnetometer. At Sleep mode only needs 75μW (3V, 25μA). TelosB sensor node is a sensor node for Light, temperature, humidity. At sleep mode only needs 8μW. ZigBee is a wireless communication technology (100m range). LoRa (Long range) is a wireless communication technology (5 km range). Bluetooth low energy (BLE) is a wireless communication technology (10-50m range). **For each target device**, above: calculated from average performance (0.4 mW/tube; 0.6V, 0.64 mA/tube); below: calculated from max performance (2.6 mW/tube; 0.6V, 4.3mA/tube)

Of course, there are several factors must be considered before implementing this design into a real application. The efficiency of a DC-DC power booster, which is around 74 – 90 % [281,282], will increase the total number of tubes by 10-26%. For some target device, the power loss from the DC-DC power booster can be compensated by the overcapacity (**Table 6. 1**). It is also important to have a proper control for long term operation of Plant-MFC in series connection to avoid voltage reversal[289]. The parallel connection can be further improved using a power management system that can electronically connect the tube in parallel without directly put them in a parallel connection to minimize the voltage reversal possibility[290].

In rice cultivation, a paddy field is not always in a waterlogged condition. For instance, according to Chapter 4, the wet period is around 91day per crop season. In West Kalimantan, Indonesia, the wet period for common rice cultivation is from 1 May until 31 July (first crop season) and from 1 November until 31 January the next year (second crop season). Therefore, it is important to match the energy supply and demand between the Plant-MFC and the target devices. **Figure 6. 2** shows an example of the energy supply and demand between Plant-MFC and the 5mm LED. In this figure, 192 tubes of Plant-MFCs (**Table 6. 1**) use to power 5mm LED (3.6V, 20mA). The LED will be used for lighting 12 hours per day during the night-time. From **Figure 6. 2** one can see that during the wet period, more power is produced than is consumed. Surplus power (marked in yellow) can be stored (*i.e.* in a battery) for later use in the dry period. For this, a battery system (*e.g.* at least with 113Wh capacity) that can last long (10 years or more) and has low self-discharge (2-3% per month) is preferable[291]. The need for storage is important because the energy harvested from Plant-MFCs fluctuates during the wet period of rice growth (**Figure 6. 2**).

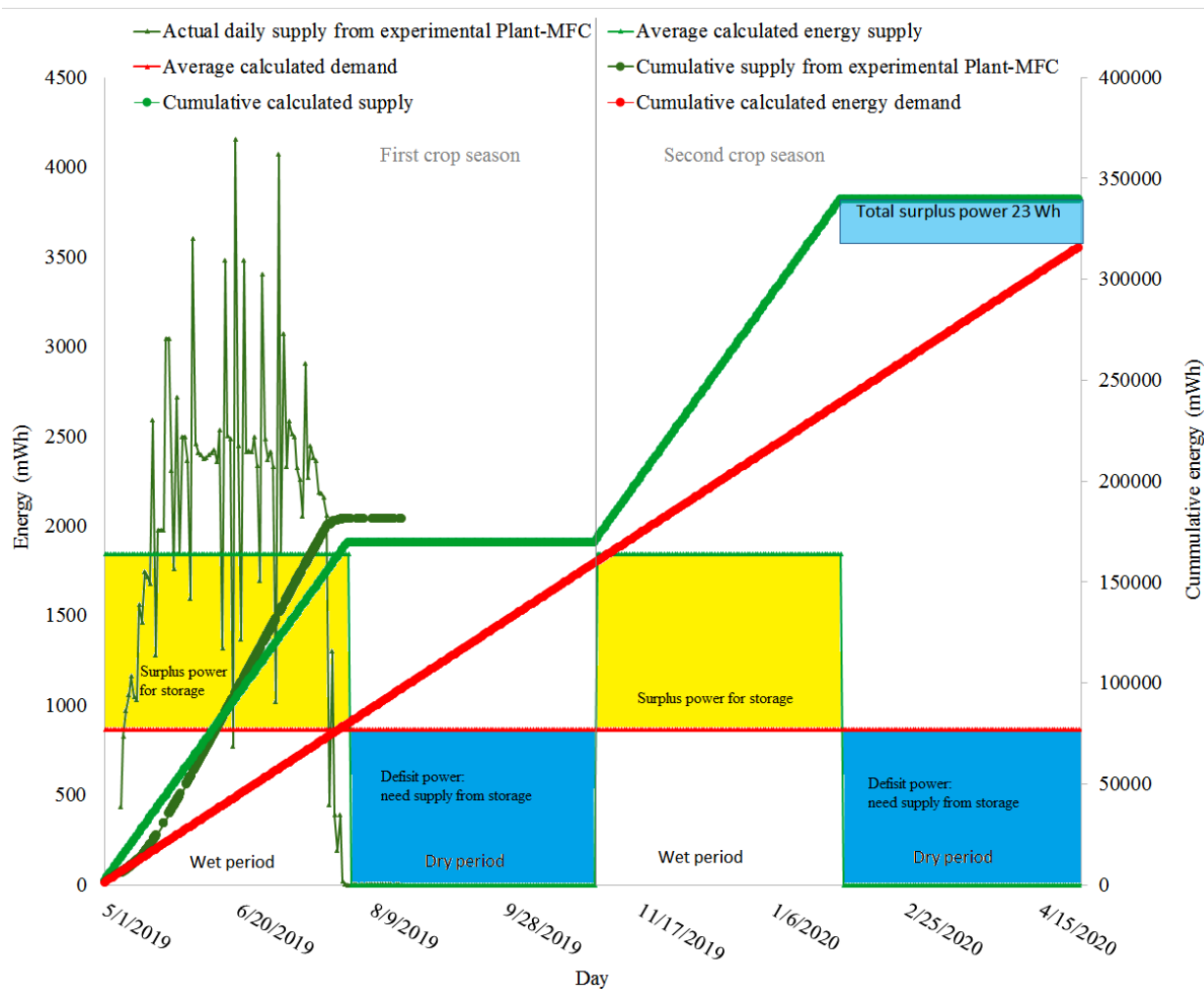


Figure 6. 2: Energy supply and demand simulation for 5mm LED (i.e. used for lighting 12 h/day) powered by 192 tubular Plant-MFC (0.4 mW/tube) in a paddy field for 1 year (2 crop seasons). **For left y-axis (for thin lines):** The dark-green line shows actual daily energy supply of tubular Plant-MFC operated in a paddy field (Chapter 4). The light-green line is average energy supply (calculated based on the average power generation of 0.4 mW/tube chapter 4). The red line is average energy demand (calculated based on constant energy demand for 5mm LED for lighting 12h/day). **For right y-axis (for thick lines):** The dark-green line is cumulative energy supply from daily energy supply of tubular Plant-MFC operated in a paddy field (Chapter 4). The light-green line is the cumulative average energy supply; The red line is the cumulative average energy demand

6.3.1 Overview of materials and cost estimation

Tubular Plant-MFC used in this study (Chapter 4) costs €23.2 per meter tube (Table 6. 2). This cost can still be reduced up to 78% by replacing the utilized material with other cheaper materials providing they will work similarly because not all electrode materials may work similarly good as shown in Chapter 3 [45]. For example, the tubular Plant-MFC cost may be reduced to €5.2/m tube when using alternative cheaper material; by replacing the silicone tube with €0.5/m RCR silicone

tube (RCR, Jiangsu, China)[292], the spacer with €0.5/m² EIMO air filter (EIMO,Guangdong, China)[293], and the graphite felt with €16.41/m² GT Graphite felt (Deqing Guotai,, Zhejiang, China)[294].

Table 6. 2: Material needed per 1-m-length Plant-MFC and its cost estimation

Plant-MFC component	Material need (per tube)	Price (Euro)	Actual price per tube (Euro)	Cost Percentage	Reference for material cost
Electrode: Graphite felt, 5 mm thickness					
Anode 1 m x 19 cm	0.19 m ²	62 m ⁻²	11.8	51%	[46]
Cathode 1 m x 10 cm	0.1 m ²	62 m ⁻²	6.2	27%	[46]
Silicone tube:					
ISS 6,Lapp Group, Stuttgart, Germany	2 m	1.82m ⁻¹	3.6	16%	[46]
Spacer 1m x 15 cm:					
Filter media VNF 290; Topswtwwfilters, Maarheeze, The Netherlands	0.15 m ²	8.5 m ⁻¹	1.3	6%	[295]
Current collector:					
Ti wire diameter 0.25mm	3 m	0.09 m ⁻¹	0.3	1%	[296]
TOTAL COST			23.2	100%	

6.3.2 Scenarios of using felt/AC/PU+AC

In chapter 3, we have shown that AC can be mixed with sediment to generate electricity with a current density of 16.1 mA/m² plant growth area and power density of 1.04 mW/m² PGA. If the graphite felt in the tubular Plant-MFC is replaced with activated carbon by retaining the same dimension (840ml for the anode and 330 ml for the cathode). Using an apparent density of 290 g/L for activated carbon [45], this amount is equal to 243.6 gr and 95.6 gr activated carbon for anode and cathode, respectively. Since AC price is much cheaper (€ 0.7/kg) in compared to the graphite felt [216], the reactor cost can be reduced up to €0.7/ reactor in combination with cheaper materials for spacer, silicone tube and current collector.

In chapter 5, we have shown proof of principle of three-dimensional robust bioanodes were successfully developed with inexpensive polyurethane foams (PU) and activated carbon (AC). Here, even less AC can be utilized for the same type of Plant-MFC reactor. We have shown that 1 kg AC per m³ PU was able to act as an electrode. If we use a PU foam sheet with a thickness of 5mm (as used in Chapter 5), the number of use activated carbon for this AC/PU electrode is only 5 g/m². This

AC/PU electrode also delivered 0.2 mW/m² PGA power output (0.01 mW/tube) when tested in the paddy field (Chapter 5). Based on this result, the capital cost for this new electrode with a thickness of 5mm is only €0.03/m² (cost AC €0.7 /kg and cost PU €5.2/m³[216,217]). Therefore, the total cost for one-meter length tubular Plant-MFC could be reduced to €0.5 in combination with cheaper materials for spacer, silicone tube and current collector. Although possible more electrode material is needed since the power output was 33 times lower than graphite felt.

6.4 Some criteria that should (likely) be met for successful use of Plant-MFC

For the successful integration of the Plant-MFC with household appliances, several criteria must be met. In this pre-assessment, Plant-MFC is envisioned to be applied as an off-grid power source (*i.e.*, in most cases are located in a remote area). The assessment criteria are listed in **Table 6. 3** below.

Table 6. 3: Techno-Economic assessment criteria of successful application of the Plant-MFC

Assessment criteria	Criteria definition
Technical	<ol style="list-style-type: none"> 1. Plant-MFC must work in a real-life condition. 2. Plant-MFC must deliver power suited for a target device. 3. Plant-MFC must be scalable via a proposed serial-parallel connection.
Economic	<ol style="list-style-type: none"> 1. Energy generation cost of Plant-MFC (€/ kWh) must not be higher than that of the energy cost from a battery source. 2. Payback period of the Plant-MFC must be lower than its expected lifetime. The payback period is calculated based on the production cost of Plant-MFC system and the energy price per kWh of primary/secondary battery price rather than the normal grid electricity price.
Environmental safety and health	The materials must be safe for the environment, not only during the production and operation but also after the lifetime.
Social	Plant-MFC technology should bring benefit for workers who produce it, consumers who use the technology and local communities at the installation location.

6.4.1 Technical criteria: Plant-MFC can power a low power consumption device

Technically, the Plant-MFC must work in a real-life condition (not only in the lab/pilot scale). For this reason, power demand and supply must be matched. **Figure 6. 3** shows that at present power density (0.4 mW/tube), Plant-MFC is suitable to power low power consumption devices (<1W) with a reasonable number of needed tubes. For instance, sensor nodes (3-6 μ W) need only 6 tubes and a 5mm white LED (72 mW) and a NiCd battery (105 mW) need 192 and 327 tubes, respectively. From **Figure 6. 3** one can see that if the average Plant-MFC power density can reach its maximum power as achieved from polarization (2.6 mW/tube), the number of tubes to power some target devices reduces significantly. At this point, Plant-MFC can be used to power a mobile phone using 152 tubes. A smaller number of tubes will reduce possible connection problem (such as voltage reversal and contact resistance) and the land use.

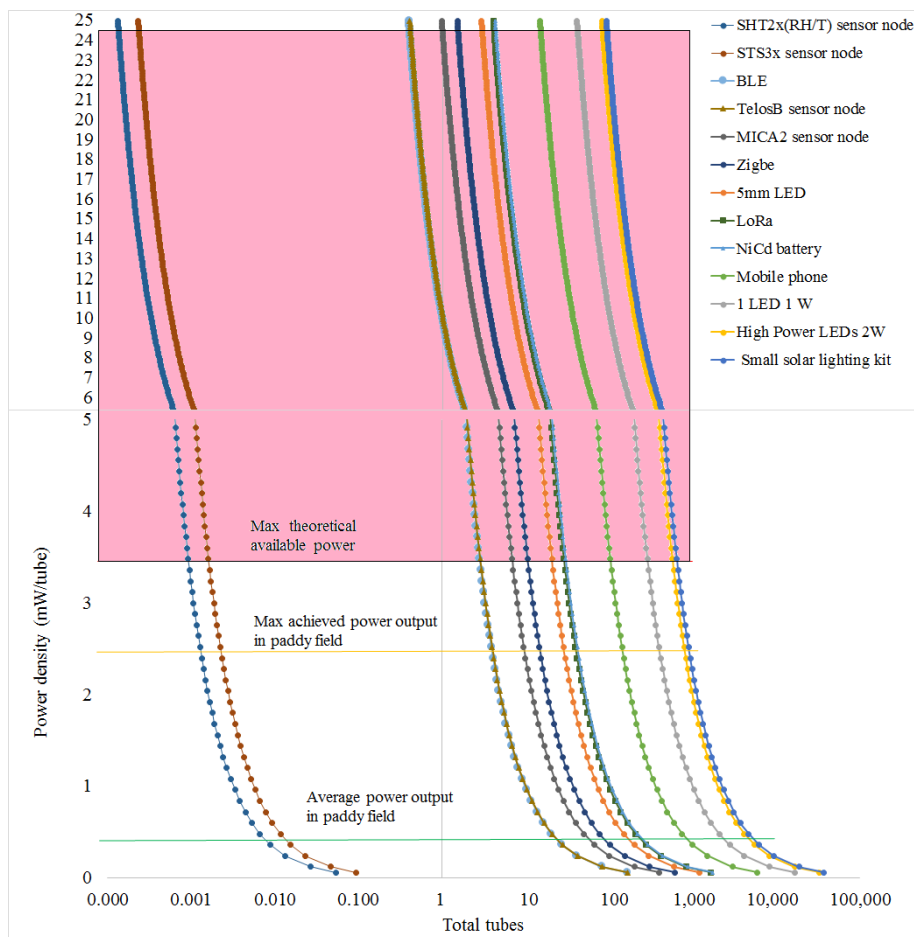


Figure 6. 3: Total needed tube to power several target devices (as presented in Table 6.1) at different Plant-MFC power densities. The area in light red indicates the maximum theoretical available power in a paddy field as calculated in section 6.1 ranges from 58 to 419 mW/m² (3.4-24.5 mW/tube). The yellow line indicates the maximum power output (44 mW/m² or 2.6 mW/tube) and the green line indicates the average power output (6.6 mW/m² or 0.4 mW/tube) of the studied Plant-MFC in the paddy field as explained in Chapter 4.

In a scalable process, high efficiency of power harvester system is needed for Plant-MFC because the power output from a single tube is low. Such a low power system is susceptible to small changes, including efficiency. Moreover, a compatible power management system that can avoid/minimize polarity reversal is in need. Finally, as has been shown in *Figure 6. 2*, power demand and supply must match. If one installs Plan-MFC in a non-permanent wetland (e.g. paddy field), energy storage is needed to store generated power for later use in the dry period.

6.4.2 Economic criteria: Plant-MFC cost is comparable to the energy cost of a battery

For implementation, Plant-MFC must meet the economic criteria. Although it is not easy to justify the economic value of such a system as potential environmental benefits are not simply returned into ‘cash’. The Plant-MFC is a power source with electricity storage capabilities (Chapter 2). Providing no substrate limitation and the anode is always in a waterlogged anaerobic condition, the Plant-MFC needs no battery because it can deliver power continuously in 24h/day (Chapter 4).

As we envisioned Plant-MFC for an off-grid power source, especially in a rural area, therefore the common electricity price (€0.2/ kWh) is cannot be used [297]. In many off-grid electrification systems, batteries are the most-used energy source [298]. Energy from batteries is much more expensive compared to grid electricity price. The cost per kWh for primary (non-rechargeable) battery such as alkaline type D cell, C cell, AA cell, AAA cell, 9 volts) is ranging from €70 to €527, with an average €286 [299]. In addition, the cost per kWh for secondary (rechargeable) battery depends on the battery type and the specific energy. On average, the cost per kWh for Lead Acid, NiCd, NiMH and Li-ion batteries are €135, €405, €405, and €585, respectively[299]. The actual cost for a battery in a remote area may be higher than the above-mentioned prices because of difficult transportation access (Chapter 4).

In this sense, the Plant-MFC could be a competitive technology as a power source. *Figure 6. 4* shows power generation cost (€/ kWh) from Plant-MFC at several production and implementation cost scenarios and two different expected lifetime. A pessimistic five-year lifetime is at least expected for the spacer, the electrode and the current collector since we have experienced no maintenance for the last 2 years from studied paddy field based tubular Plant-MFC. Furthermore, the lifetime may reach 30 years especially because no other catalysts than the electrochemically active bacteria are utilized that renews themselves all the time [300]. From *Figure 6. 4* one can see that based on present average power output of a paddy field based Plant-MFC (line A), the generation cost for the actual cost Plant-MFC with an expected lifetime of 30 years is €249/ kWh, which is already in the range of electrical power generation cost of batteries. Even so, if the cheaper available material is used for the same

expected lifetime of 30 years, the generation cost for Plant-MFC would decrease to €77/ kWh. In section 6.1, we have estimated that a paddy field has the potential to generate power up to 419 mW/m². Assuming that the Plant-MFC can utilise 50% of this available power (**Figure 6. 4** line C), the cost generation of the actual Plant-MFC within 30 year lifetime is 8.3 €/ kWh. In addition, in this calculation a moderate implementation cost of €50 per m² is added to the production cost of each Plant-MFC [300]. If the implementation cost could be reduced or neglected in case of self-installation, the actual generation cost could have been much lower than presented. The influence of this implementation cost can be clearly seen from a Plant-MFC with a production cost of €1 per tube. In this Plant-MFC, the implementation cost becomes the major cost. The implementation cost might be reduced if Plant-MFC is applied on a large scale.

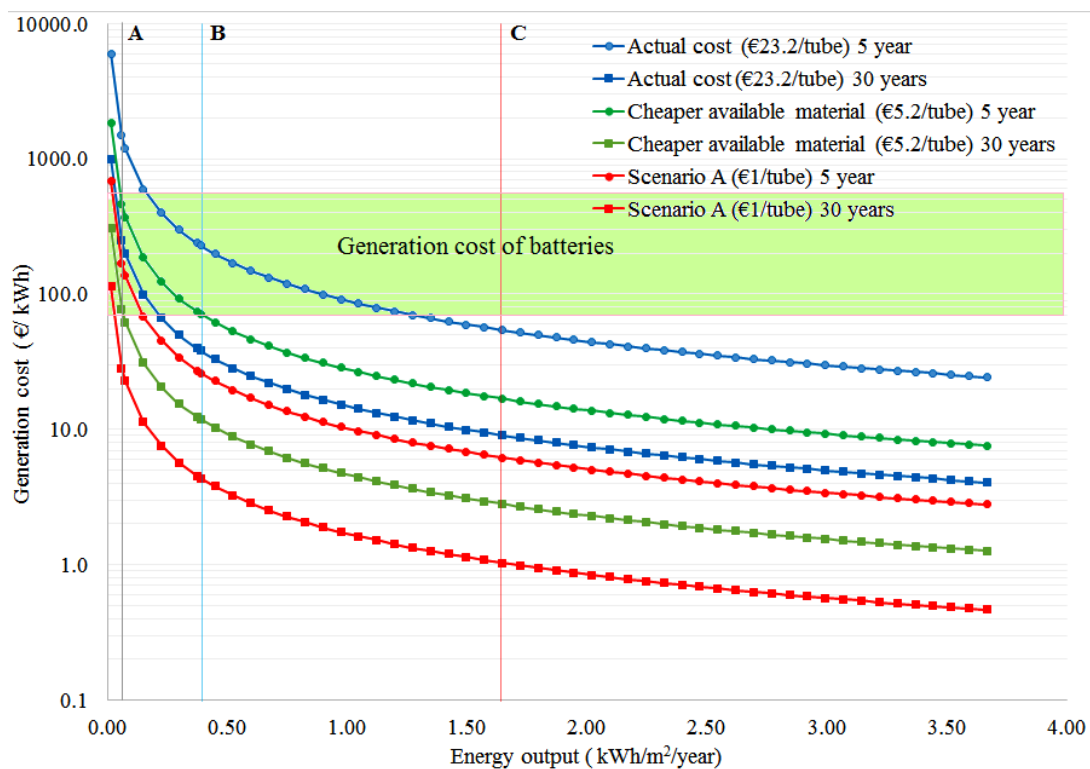


Figure 6. 4: Generation cost from Plant-MFC at several production costs assuming implementation cost €50/m². Line (A) average energy output paddy field based Plant-MFC at 6.6 mW/m² (0.4 mW/tube); (B) maximum energy output paddy field based Plant-MFC at 44 mW/m² (2.6 mW/tube); (C) 50% of the maximum theoretical energy output from paddy field based Plant-MFC ~200 mW/m² (this thesis section 6.1). The green area shows the generation cost range for batteries

Furthermore, here we also calculated the payback period of several Plant-MFCs based on the production cost relative to the energy price from a primary battery (€286/ kWh). **Figure 6. 5** shows that at present power density (0.4 mW/tube), the payback period for the actual cost (€23.2/tube) Plant-

MFC is 23.2 years. If the power density of current paddy field based Plant-MFC could reach its maximum performance as obtained from polarization (yellow line), the payback period is only 3.6 years. Reducing the Plant-MFC cost from current actual cost (€23.3/tube) to a scenario A (€1/tube) might shorten the payback period to only 1 year based on the average power output of paddy field based Plant-MFC. To sum-up, the plant MFC can be considered as economically feasible as an off-grid power source to power 5mm LED to replace kerosene lamp providing there is no serial-parallel technical connection problem.

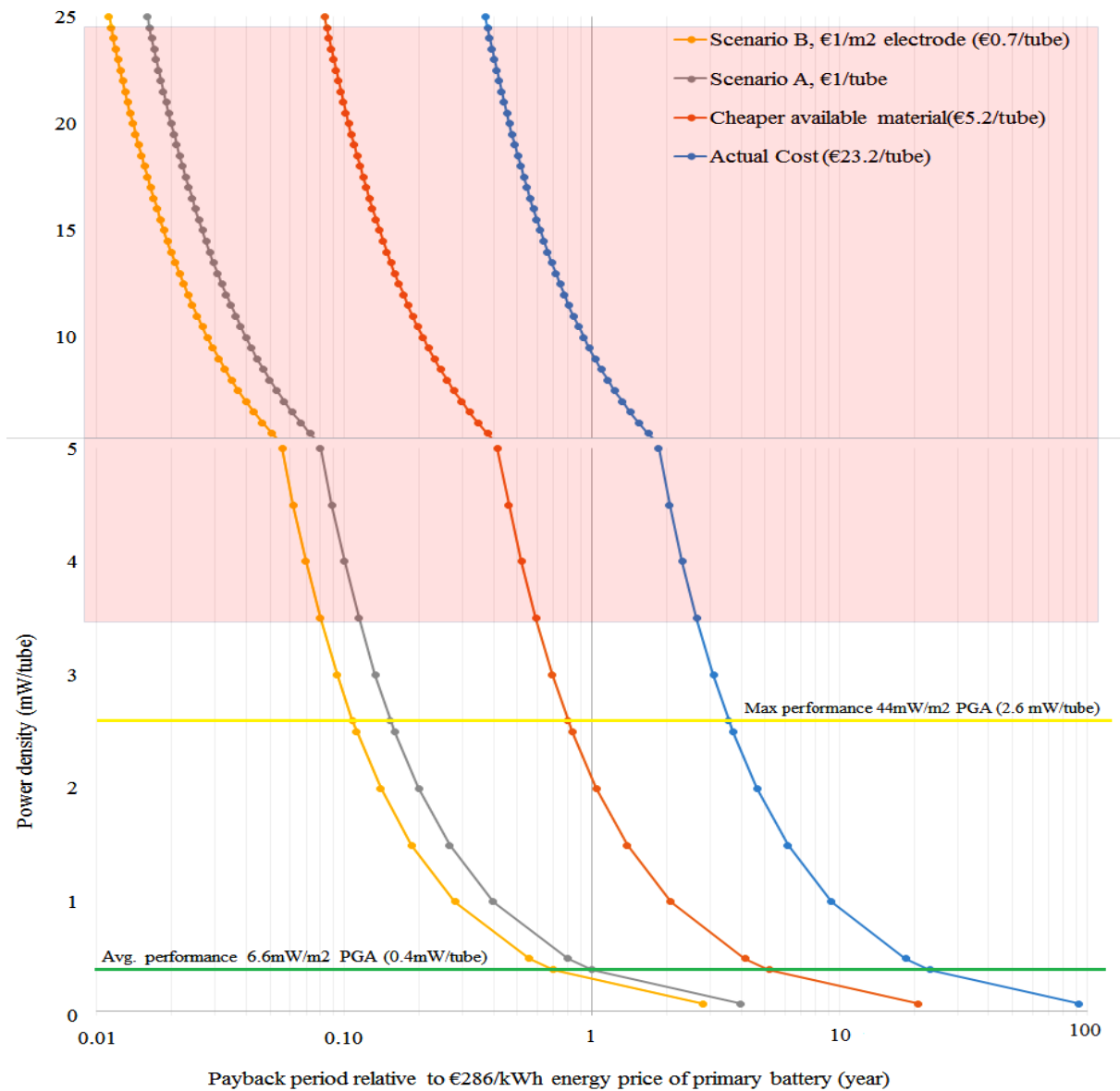


Figure 6. 5: Payback period (in year) of 1-m tubular Plant-MFC from different production cost scenarios. The area marked in light red is the maximum theoretical available power that can be extracted by 1m tubular Plant-MFC (with PGA 0.0585m²) when installed in a rice paddy field (3.4-24.5 mW/tube). The green line indicates the average power output and the yellow line indicates the maximum power output of the studied Plant-MFC in the paddy field as explained in Chapter 4

6.4.3 Environmental safety and health criteria: Plant-MFC is expected safe to implement in an environment

Ensuring that a product is safe for the environment and human health is part of product risk assessment's purpose [301,302]. Product risk assessment can be made either by suppliers/manufactures or by regulators but the ultimate responsibility for product safety sits with suppliers while the regulator has an oversight or governance role with responsibility for ensuring the suppliers comply with the law and supply products that present an acceptable safety risk to consumers [301]. In a comprehensive product risk assessment made by manufactures of a new product, it has to take into account all relevant product hazards and is the basis for the reduction of risk to acceptable level when a product is design or produced [302]. In short, a product risk assessment must consider safety in design, production and in the marketplace[301,303]. Providing that the Plant-MFC is manufactured in accordance with the ISO 10377:2013 about consumer product safety[303], the assessment in this thesis is limited only to the marketplace, which is in the product implementation in the environment. For this assessment, main components in the Plant-MFC (graphite felt for the electrode, titanium wire for the current collector, and polyester/polypropylene for the spacer and cable ties) is assessed whether it is expected to be safe for human and environment.

Graphite felt is not classified as hazardous under the Globally Harmonized System of Classification and Labelling and the US (Occupational Safety and Health Administration) OSHA Hazard Communication Standard[304]. The graphite felt may create airborne dust during its handling and therefore avoid creating and breathing airborne dust as it can irritate or harm the respiratory system. Moreover, the graphite felt dust may cause minor irritation of skin and eyes. To avoid such risk, it is important to do a precaution by wearing safety tools such as mask, gloves and google when working with graphite felt. Graphite felt is not listed as a carcinogen by the International Agency for Research on Cancer (IARC), US OSHA or the US Department of Health and Human Services National Toxicology Program (NTP) [304]. Graphite is relatively inert, stable and non-reactive material and would be expected to be of negligible consequence in the environment. This product does not contain substances that could cause it to be a hazardous waste if it is disposed. Disposal should be in accordance with applicable waste disposal regulation. Though it should be noted that various different graphite felt exists in the market, which some of them may contain pollutants. Therefore, it is important to wisely choose the one that less or not polluted.

Titanium wire is not listed as a carcinogen. It is a solid metal at room temperature with a melting point at 1675⁰C. Titanium alloys are stable at room temperature. It does not rust even in saltwater and

is safe for field application[305]. Furthermore, Titanium alloy grade 2 is commercially pure titanium that has good corrosion resistance and biocompatible, even with human body[306].

The air filter used as a spacer is made of plastic polymers such as polyester and polypropylene. According to the MSDS [307,308], these polymers are not classified as a hazardous material and are thermally stable at environmental temperature. So far, there is no negative information about ecological effect of these polymers when implemented in the waterlogged soil. However, there is a study that polyester and polyester-polyurethane can be biodegraded by *Cyanobacteria* and *Archaea* [309]. This biodegradation may shorten the expected lifetime of the product. However, to what extent is this biodegradation effect on the environment is still unknown. Therefore, providing there is no reported negative impact of the material, it considers suitable for field implementation. The installation of these polymers (as part of the Plant-MFC) in the wetland should not be seen as plastic pollution since they will be removed from the soil when the expected lifetime is reached. The waste disposal (after the Plant-MFC de-installation) should be accordance with applicable waste disposal regulation. Alternatively, an eco-friendly plastic material can be used for the replacement of current used material[310].

Alternative new developed electrode material PU/AC (Chapter 5) that using reticulated polyurethane (PU) and activated carbon (AC) is also assessed. There are two types of polyurethanes that is the ester type and the ether type[311]. Polyurethane is not regulated for carcinogenicity and no exposure limit has been established in the U.S by OSHA[312]. Reticulated PU is chemically inert and thermally stable at environmental temperature, therefore, it is not expected to react with any chemical when deployed in the environment [313]. There is also no negative information about ecological effect of PU when implemented in the waterlogged soil. Polyurethane can be biodegraded by *Pestalotiopsis* (Equadorian fungus) both in aerobic and anaerobic conditions[314]. However, it is difficult to clarify the fate of residues after degradation of the PU[311]. After the Plant-MFC de-installation, waste disposal should be accordance with applicable waste disposal regulation.

Activated carbon (AC) is flammable solid that can cause serious eye irritation and may cause respiratory irritation[315]. For human safety, this product should be handled with precautions in accordance with safety instruction[315]. Under the normal environmental condition, AC is chemically stable and non-reactive [315]. AC has also been used in water purification[221]. Moreover, AC has been widely used for in-situ sediment treatment remedy[122]. Thus, AC is considered safe for environmental implementation.

Based on the above-mentioned information, it may be that Plant-MFC is harmless to the environment providing the waste, after the lifetime of the Plant-MFC, is treated in accordance with applicable safe and clean waste disposal regulations. However, a complete life cycle assessment and real study on safety and potential direct environmental impact are still needed to give a detail justification for this technology.

6.4.4 Social criteria: community engagement is required to create a social acceptance

The social impact of a product when it is launched into a market is important to be assessed in a practical and harmonised method. For this, there is a consensus on the needs to address social issues, a workable, robust and aligned method for measuring and managing social impact at product level through the Roundtable for Product Social Metrics [316]. In this assessment, the boundary of the assessment includes those parts of the value chain that are relevant for the assessment either from cradle to grave, from cradle to gate or from gate to gate. The assessment covers the impact on at least three stakeholder group, which are worker, consumers and local communities [316]. According to the handbook for product social impact assessment, a complete product social impact assessment is design to address three main objectives: (i) make positive and negative impacts of products measurable and visible, (ii) support decision-making and communication at product level, and (iii) contribute to overall sustainability assessment [316]. However, at the current stage of development, a complete social impact assessment of Plant-MFC product is not ready yet.

Currently, the Plant-MFC product is still in an infancy stage, in which mass production of Plant-MFC product that involves many workers and consumers does not exist yet. The Plant-MFC market is still limited to research and development even though some educational and decorative products are also introduced [317]. Therefore, the social impact assessment for workers and consumers or even local communities stakeholders is hard to assess. Here we briefly self-assess some social criteria (adapted from Annex 9 of the handbook for product social impact assessment) that should be met by Plant-MFC for all three stakeholders [316]. Some relevant social topics at this stage (in our opinion) are health and safety, experienced well-being, and community engagement. The Plant-MFC must be safe for the health of workers, consumers and local communities at all its stages (production, installation, operation and end of life). The consumers should be able to experience positive feeling or emotional states (*e.g.*, feeling of green lifestyle) associated with the use of the product. Finally, community engagement with local communities at location where the Plant-MFC is implemented is required for creating social acceptance. In this way, one has reduced the risk of unnecessary vandalism, especially due to a curiosity about the product.

6.5 Outlook

6.5.1 Plant-MFC to power a sensor

In this thesis, we have shown that the Plant-MFC is theoretically possible to power a low power consumption device. Plant-MFC needs from one to few hundreds of tubes to power a device from μW to up to 0.5W (*Figure 6. 3*). As have been discussed that connecting many tubes may cause electrical problems such as voltage reversal [289], an implementation involving little or no tube connections is preferred for Plant-MFC applications to avoid serial-parallel connection problems. At current development, while increasing the power density of the Plant-MFC is needed, Plant-MFC is already suitable to power environmental sensors that only needs μW to several mW power.

At least two studies have shown that Plant-MFC can power a low energy data transmitter. First, a pot-based Plant-MFC (height= 30 cm and diameter=20 cm) was able to power a sensor node, which consists of microcontroller, sensors and Long Range (LoRa) transceiver, for ozone and carbon dioxide detection, which send the collected data to a wireless sensor network (WSN) [318]. The pot based Plant-MFC can also be considered as a bio-battery that has been discussed in Chapter 3, which in this case could be placed in a house for green decoration while powering a sensor. Second, three parallel-connected Plant-MFCs (floating Plant-MFCs in a pond) can be operated over 1-year providing power sources for low energy data transmitters [190].

Globally, the market for sensors is growing. It is predicted to continuously increase from US\$ 116.1 billion in 2019 to US\$ 190.6 billion in 2021[319]. Environmental sensors are often deployed in a hardly accessible remote area. In this case, the cost for power sources (*e.g., battery*) could be less than €10, but the labour costs associated with the battery replacement can be substantially higher than the cost of the battery itself [320]. This cost could be avoided by installing a local power harvester, for instance, the Plant-MFC based power harvester, which envisioned could be operated without any maintenance for longer periods (5-30 years).

As the principle of Plant-MFC requires waterlogged conditions to work, we suggested that this technology is suitable to power environmental sensor systems for wetlands. For instance, Plant-MFC could be integrated with peatland monitoring system, which consists of a water level sensor, soil moisture sensor, rainfall sensor, temperature sensor and GPS sensor [321]. Plant-MFC could also be integrated with agricultural sensors such as soil-related sensor and plant-related sensors which could provide relevant information about irrigation, fertilization, pest control and animal and pastures monitoring [287,322].

6.5.2 Plant-MFC function as a sensor

Apart to power a sensor, Plant-MFC can also function as a biosensor. In this thesis (Chapter 4), we have shown that Plant-MFC performance during the dry period in a paddy field has some correlations with the rain event at which the Plant-MFC was installed. Although a specific type of researches is needed to further understanding such correlation between the rain event, the state of the rain and the cell potential peak of a Plant-MFC.

Furthermore, Plant-MFC might also be utilized as a soil quality indicator. When installed in the soil, Plant-MFC anode potential represents spatial soil redox potential. This *in-situ* soil redox potential can provide essential information about soil characteristics that can function as a soil quality indicator because the redox potential regulates plant physiology and phenology, plant/pathogen interactions, nutrient availability, heavy metal toxicity, soil genesis and greenhouse gas emission [323]. However, research is still needed to understand this relationship for practical implementation.

6.5.3 Plant-MFC couple with other technologies for an additional value

Finally, as have been shown in this thesis (section 6.2) and over a decade of Plant-MFC research [324], the electricity generation is still far lower than the theoretical available value. The Plant-MFC is far away from being a potential large green electricity sources (€1493/kWh for 5 year lifetime and €249/kWh for 30 year lifetime) that could be competitive with e.g. cheap renewable electricity from solar photovoltaics (€0.053 - 0.20per kWh) or onshore wind power (€0.040 - €0.09 per kWh)[325]. In this sense, Plant-MFC application should ideally be combined with other technologies that can bring an added value for the coupled technology or combine functions using the same spatial location[46]. The latter can reduce the competition on land for e.g. energy versus food or biodiverse green infrastructure. For instance, Plant-MFC might be coupled with constructed wetland wastewater treatments [326,327], green biodiverse roofs [129], coproduction of food and electricity in paddy fields (chapter 4), methane gas mitigation and reduction[136,262], and decorative and educational devices[66]

6.6 Concluding Remark

In an off-grid area where battery still uses as power sources, Plant-MFC could be a competitive technology. Current Plant-MFC electricity cost generation (€249-€1493 per kWh) is not competitive to other renewable energy cost generation (€ 0.04-€0.2 per kWh). Novel electrode material optimisation can improve economic competitiveness. To what extent the power output can be improved towards the theoretical output is unclear. The actual energy/electron fluxes in the bioanode of the Plant-MFC are not all directly measured. Also competing processes must be quantified to reveal the limitations to understand how technical improvement could be applied. Nevertheless, Plant-MFC may be used to power various low power devices. Depending on the device, many tubes and large surface area are needed. In a conceptual design, an area of 60 m² and 192 1-meter Plant-MFC tubes are required to power 5mm LED which has comparable luminous with kerosene lamp (~1 lumen). In addition, Plant-MFC can also be used to power an environmental sensor and might function as a biosensor. The portable Plant-MFC can be considered as a bio battery, which expands the limitation at where one can install a Plant-MFC since it is moveable. Furthermore, as shown in this thesis Plant-MFC is also able to co-exist with rice production in the paddy field which can reduce the competition on land for e.g. energy versus food.

References

1. Grahn, M.; Taljehard, M.; Brynolf, S. Electricity as an Energy Carrier in Transport- Cost and Efficiency Comparison of Different Pathways. In Proceedings of the Conference Proceedings, EVS 31 & EVTeC 2018; Society of Automotive Engineers of Japan, Inc: Kobe, Japan, 2018.
2. Marchenko, O.V.; Solomin, S.V. The future energy: Hydrogen versus electricity. *International Journal of Hydrogen Energy* **2015**, *40*, 3801–3805.
3. Dincer, I. Renewable energy and sustainable development: a crucial review. *Renewable and Sustainable Energy Reviews* **2000**, *4*, 157–175.
4. IEA Available online: <https://www.iea.org/topics/electricity/> (accessed on Sep 20, 2019).
5. Kanagawa, M.; Nakata, T. Assessment of access to electricity and the socio-economic impacts in rural areas of developing countries. *Energy Policy* **2008**, *36*, 2016–2029.
6. Raugei, M.; Leccisi, E. A comprehensive assessment of the energy performance of the full range of electricity generation technologies deployed in the United Kingdom. *Energy Policy* **2016**, *90*, 46–59.
7. Ellabban, O.; Abu-Rub, H.; Blaabjerg, F. Renewable energy resources: Current status, future prospects and their enabling technology. *Renewable and Sustainable Energy Reviews* **2014**, *39*, 748–764.
8. Panwar, N.L.; Kaushik, S.C.; Kothari, S. Role of renewable energy sources in environmental protection: A review. *Renewable and Sustainable Energy Reviews* **2011**, *15*, 1513–1524.
9. Varun; Bhat, I.K.; Prakash, R. LCA of renewable energy for electricity generation systems—A review. *Renewable and Sustainable Energy Reviews* **2009**, *13*, 1067–1073.
10. Newbery, D.M. Towards a green energy economy? The EU Energy Union’s transition to a low-carbon zero subsidy electricity system – Lessons from the UK’s Electricity Market Reform. *Applied Energy* **2016**, *179*, 1321–1330.
11. IEA *Energy Access Outlook 2017*; International Energy Agency, 2017;
12. RUEN, R.U.E.N. National Energy Plan of Indonesia (Peraturan Presiden (Perpres) Nomor 22 Tahun 2017 tentang Rencana Umum Energi Nasional) 2017.
13. Kebijakan Energi Available online: <https://indonesia.go.id/narasi/indonesia-dalam-angka/ekonomi/bauran-energi-indonesia-kian-baik> (accessed on Sep 22, 2019).
14. KBRI The Hague- Country Profile Available online: <https://en.indonesia.nl/indonesia/profile/introduction> (accessed on Sep 22, 2019).
15. DJK, D.J.K. *Statistik Ketenagalistrikan Tahun 2018*; Sekretariat Jenderal Ketenagalistrikan: Jakarta, 2019;
16. Sovacool, B.; Vera, I. *Electricity and education: The benefits, barriers, and recommendations for achieving the electrification of primary and secondary schools*; United Nations Department of Economic and Social Affairs, 2014; p. 36;.
17. Diniz, A.S.A.C.; Franca, E.D.; Camara, C.F.; Morais, P.M.R.; Vilhena, L. The Important Contribution of Photovoltaics in a Rural School Electrification Program. In Proceedings of the 2006 IEEE 4th World Conference on Photovoltaic Energy Conference; 2006; Vol. 2, pp. 2528–2531.
18. DiLaura, D. A Brief History of Lighting. *Opt. Photon. News* **2008**, *19*, 22–28.
19. Lam, N.L.; Chen, Y.; Weyant, C.; Venkataraman, C.; Sadavarte, P.; Johnson, M.A.; Smith, K.R.; Brem, B.T.; Arineitwe, J.; Ellis, J.E.; et al. Household Light Makes Global Heat: High Black Carbon Emissions From Kerosene Wick Lamps. *Environ. Sci. Technol.* **2012**, *46*, 13531–13538.
20. Tedsen, E. Black Carbon Emissions from Kerosene Lamps: Potential for a new CCAC Initiative 2013.
21. Budya, H.; Yasir Arofah, M. Providing cleaner energy access in Indonesia through the megaproject of kerosene conversion to LPG. *Energy Policy* **2011**, *39*, 7575–7586.

22. Honda Genset-EP1000 Available online: <https://www.hondapowerproducts.co.id/id/products/genset/genset--ep1000> (accessed on Sep 22, 2019).
23. Honda Genset-EP2500CX Available online: <https://www.hondapowerproducts.co.id/id/products/genset/genset--ep2500cx> (accessed on Sep 22, 2019).
24. Machala, M. Kerosene Lamps vs Solar Lanterns Available online: <http://large.stanford.edu/courses/2011/ph240/machala1/> (accessed on Sep 24, 2019).
25. Mills, E. Technical and Economic Performance Analysis of Kerosene Lamps and Alternative Approaches to Illumination in Developing Countries 2003.
26. Apple, J.; Vicente, R.; Yarberr, A.; Lohse, N.; Mills, E.; Jacobson, A.; Poppendieck, D. Characterization of particulate matter size distributions and indoor concentrations from kerosene and diesel lamps. *Indoor Air* **2010**, *20*, 399–411.
27. Mills, E. *Health Impacts of Fuel-based Lighting*; University of California: California-USA, 2012; p. 25;.
28. Olsson, E.; Stenemo, E. Environmental and health impacts when replacing kerosene lamps with solar lanterns. Bachelor Thesis, Uppsala Universitet: Uppsala, 2018.
29. 5mm LED Available online: <https://www.ledsupply.com/leds/5mm-led-frosted-white-70-degree-viewing-angle> (accessed on Sep 27, 2019).
30. Cree Xlamp Available online: <https://www.ledsupply.com/leds/cree-xlamp-xm-l2-leds> (accessed on Sep 27, 2019).
31. Tokopedia Available online: <https://www.tokopedia.com/sazazaza/paket-panel-surya-4wp-4-watt-peak-komplit-battere-battery-lampu-5v-usb-1> (accessed on Sep 19, 2019).
32. Nokia Available online: https://www.nokia.com/phones/en_int/nokia-110 (accessed on Sep 19, 2019).
33. Asus Available online: https://www.asus.com/Phone/ZenFone_Selfie_ZD551KL/specifications/ (accessed on Sep 19, 2019).
34. Daewoo NS-911 Available online: <https://www.tokopedia.com/steventantra/lcd-tv-portable-95inch-daewoo-ns-911-usb-sd-mmc-fm-mp4> (accessed on Sep 22, 2019).
35. eLEDTV Available online: <https://www.eledtv.com/product/15-6-eled-tv-16e1/> (accessed on Sep 19, 2019).
36. MMP media Solutions Available online: <http://mmperkasa.com/mmp-789-hd-lombok/>.
37. Satelit Indonesia Available online: <https://www.satelitindonesia.com/2017/09/harga-dan-spesifikasi-receiver-mmp-lombok-new.html> (accessed on Sep 19, 2019).
38. Potter M. C.; Waller Augustus Desire Electrical effects accompanying the decomposition of organic compounds. *Proceedings of the Royal Society of London. Series B, Containing Papers of a Biological Character* **1911**, *84*, 260–276.
39. Davis, J.B.; Yarbrough, H.F. Preliminary Experiments on a Microbial Fuel Cell. *Science* **1962**, *137*, 615.
40. Strik, D.P.B.T.B.; Hamelers (Bert), H.V.M.; Snel, J.F.H.; Buisman, C.J.N. Green electricity production with living plants and bacteria in a fuel cell. *Int. J. Energy Res.* **2008**, *32*, 870–876.
41. Sudirjo, E.; Buisman, C.J.N.; Strik, D.P.B.T.B. Electricity generation from wetlands with activated carbon bioanode. *IOP Conference Series: Earth and Environmental Science* **2018**, *131*, 012046.
42. Logan, B.E.; Regan, J.M. Electricity-producing bacterial communities in microbial fuel cells. *Trends in Microbiology* **2006**, *14*, 512–518.
43. Rabaey, K.; Verstraete, W. Microbial fuel cells: novel biotechnology for energy generation. *Trends in Biotechnology* **2005**, *23*, 291–298.

44. Helder, M.; Strik, D.P.; Hamelers, H.V.; Buisman, C.J. The flat-plate plant-microbial fuel cell: the effect of a new design on internal resistances. *Biotechnology for Biofuels* **2012**, *5*, 70.
45. Sudirjo, E.; Buisman, C.J.N.; Strik, D.P.B.T.B. Activated Carbon Mixed with Marine Sediment is Suitable as Bioanode Material for *Spartina anglica* Sediment/Plant Microbial Fuel Cell: Plant Growth, Electricity Generation, and Spatial Microbial Community Diversity. *Water* **2019**, *11*.
46. Wetser, K. Electricity from wetlands : Technology assessment of the tubular Plant Microbial Fuel Cell with an integrated biocathode. PhD Thesis, Wageningen University & Research: Wageningen, 2016.
47. Sudirjo, E.; de Jager, P.; Buisman, C.J.N.; Strik, D.P.B.T.B. Performance and Long Distance Data Acquisition via LoRa Technology of a Tubular Plant Microbial Fuel Cell Located in a Paddy Field in West Kalimantan, Indonesia. *Sensors* **2019**, *19*.
48. Kaku, N.; Yonezawa, N.; Kodama, Y.; Watanabe, K. Plant/microbe cooperation for electricity generation in a rice paddy field. *Applied Microbiology and Biotechnology* **2008**, *79*, 43–49.
49. Kouzuma, A.; Kasai, T.; Nakagawa, G.; Yamamuro, A.; Abe, T.; Watanabe, K. Comparative Metagenomics of Anode-Associated Microbiomes Developed in Rice Paddy-Field Microbial Fuel Cells. *PLOS ONE* **2013**, *8*, e77443.
50. Ueoka, N.; Sese, N.; Sue, M.; Kouzuma, A.; Watanabe, K. Sizes of Anode and Cathode Affect Electricity Generation in Rice Paddy-Field Microbial Fuel Cells. *Journal of Sustainable Bioenergy Systems* **2016**, *Vol.06No.01*, 10–15.
51. Hamelers, H.V.M.; Ter Heijne, A.; Sleutels, T.H.J.A.; Jeremiasse, A.W.; Strik, D.P.B.T.B.; Buisman, C.J.N. New applications and performance of bioelectrochemical systems. *Applied Microbiology and Biotechnology* **2010**, *85*, 1673–1685.
52. Logan, B.E.; Hamelers, B.; Rozendal, R.; Schröder, U.; Keller, J.; Freguia, S.; Aelterman, P.; Verstraete, W.; Rabaey, K. Microbial Fuel Cells: Methodology and Technology. *Environ. Sci. Technol.* **2006**, *40*, 5181–5192.
53. Timmers, R.A.; Strik, D.P.B.T.B.; Hamelers, H.V.M.; Buisman, C.J.N. Characterization of the internal resistance of a plant microbial fuel cell. *Electrochimica Acta* **2012**, *72*, 165–171.
54. Kabutey, F.T.; Zhao, Q.; Wei, L.; Ding, J.; Antwi, P.; Quashie, F.K.; Wang, W. An overview of plant microbial fuel cells (PMFCs): Configurations and applications. *Renewable and Sustainable Energy Reviews* **2019**, *110*, 402–414.
55. Muyzer, G.; Stams, A.J.M. The ecology and biotechnology of sulphate-reducing bacteria. *Nature Reviews Microbiology* **2008**, *6*, 441.
56. Pezeshki, S.R.; DeLaune, R.D. Soil Oxidation-Reduction in Wetlands and Its Impact on Plant Functioning. *Biology* **2012**, *1*.
57. Helder, M.; Strik, D.P.B.T.B.; Hamelers, H.V.M.; Kuhn, A.J.; Blok, C.; Buisman, C.J.N. Concurrent bio-electricity and biomass production in three Plant-Microbial Fuel Cells using *Spartina anglica*, *Arundinella anomala* and *Arundo donax*. *Bioresource Technology* **2010**, *101*, 3541–3547.
58. Helder, M.; Strik, D.P.B.T.B.; Hamelers, H.V.M.; Kuijken, R.C.P.; Buisman, C.J.N. New plant-growth medium for increased power output of the Plant-Microbial Fuel Cell. *Bioresource Technology* **2012**, *104*, 417–423.
59. Timmers, R.A.; Strik, D.P.B.T.B.; Hamelers, H.V.M.; Buisman, C.J.N. Increase of power output by change of ion transport direction in a plant microbial fuel cell. *Int. J. Energy Res.* **2013**, *37*, 1103–1111.
60. Wetser, K.; Dieleman, K.; Buisman, C.; Strik, D. Electricity from wetlands: Tubular plant microbial fuels with silicone gas-diffusion biocathodes. *Applied Energy* **2017**, *185*, 642–649.
61. Heijne, A. ter Improving the cathode of a microbial fuel cell for efficient electricity production, Wageningen University: Wageningen, 2010.

62. Schampelaire, L.D.; Bossche, L.V. den; Dang, H.S.; Höfte, M.; Boon, N.; Rabaey, K.; Verstraete, W. Microbial Fuel Cells Generating Electricity from Rhizodeposits of Rice Plants. *Environ. Sci. Technol.* **2008**, *42*, 3053–3058.
63. Takanezawa, K.; Nishio, K.; Kato, S.; Hashimoto, K.; Watanabe, K. Factors Affecting Electric Output from Rice-Paddy Microbial Fuel Cells. *Bioscience, Biotechnology, and Biochemistry* **2010**, *74*, 1271–1273.
64. Timmers, R.A.; Strik, D.P.B.T.B.; Hamelers, H.V.M.; Buisman, C.J.N. Electricity generation by a novel design tubular plant microbial fuel cell. *Biomass and Bioenergy* **2013**, *51*, 60–67.
65. Wetser, K.; Sudirjo, E.; Buisman, C.J.N.; Strik, D.P.B.T.B. Electricity generation by a plant microbial fuel cell with an integrated oxygen reducing biocathode. *Applied Energy* **2015**, *137*, 151–157.
66. Plant-e Available online: <https://www.plant-e.com/en/webshop/> (accessed on Sep 20, 2019).
67. FAO, of the U.N. FAOSTAT 2019 Available online: <http://www.fao.org/faostat/en/#data/QC/visualize> (accessed on Aug 14, 2019).
68. Abbas Syed Zaghum; Rafatullah Mohd; Ismail Norli; Syakir Muhammad Izzuddin A review on sediment microbial fuel cells as a new source of sustainable energy and heavy metal remediation: mechanisms and future prospective. *International Journal of Energy Research* **2017**, *41*, 1242–1264.
69. Lowy, D.A.; Tender, L.M.; Zeikus, J.G.; Park, D.H.; Lovley, D.R. Harvesting energy from the marine sediment–water interface II: Kinetic activity of anode materials. *Biosensors and Bioelectronics* **2006**, *21*, 2058–2063.
70. Reimers, C.E.; Tender, L.M.; Fertig, S.; Wang, W. Harvesting Energy from the Marine Sediment–Water Interface. *Environ. Sci. Technol.* **2001**, *35*, 192–195.
71. Mathuriya, A.S.; Yakhmi, J.V. Microbial fuel cells – Applications for generation of electrical power and beyond. *Critical Reviews in Microbiology* **2016**, *42*, 127–143.
72. Tender, L.M.; Reimers, C.E.; Stecher III, H.A.; Holmes, D.E.; Bond, D.R.; Lowy, D.A.; Pilobello, K.; Fertig, S.J.; Lovley, D.R. Harnessing microbially generated power on the seafloor. *Nature Biotechnology* **2002**, *20*, 821.
73. Zabihallahpoor, A.; Rahimnejad, M.; Talebnia, F. Sediment microbial fuel cells as a new source of renewable and sustainable energy: present status and future prospects. *RSC Adv.* **2015**, *5*, 94171–94183.
74. de Haas, H.; Boer, W.; van Weering, T.C.E. Recent sedimentation and organic carbon burial in a shelf sea: the North Sea. *Marine Geology* **1997**, *144*, 131–146.
75. Middelburg, J.J.; Klaver, G.; Nieuwenhuize, J.; Wielemaker, A.; de Haas, W.; Vlug, T.; van der Nat, J.F.W.A. Organic matter mineralization in intertidal sediments along an estuarine gradient. *Mar Ecol Prog Ser* **1996**, *132*, 157–168.
76. Seiter, K.; Hensen, C.; Schröter, J.; Zabel, M. Organic carbon content in surface sediments—defining regional provinces. *Deep Sea Research Part I: Oceanographic Research Papers* **2004**, *51*, 2001–2026.
77. Van de Broek, M.; Temmerman, S.; Merckx, R.; Govers, G. Controls on soil organic carbon stocks in tidal marshes along an estuarine salinity gradient. *Biogeosciences* **2016**, *13*, 6611–6624.
78. Kim, Y.; Hatzell, M.C.; Hutchinson, A.J.; Logan, B.E. Capturing power at higher voltages from arrays of microbial fuel cells without voltage reversal. *Energy Environ. Sci.* **2011**, *4*, 4662–4667.
79. Dewan, A.; Beyenal, H.; Lewandowski, Z. Intermittent Energy Harvesting Improves the Performance of Microbial Fuel Cells. *Environ. Sci. Technol.* **2009**, *43*, 4600–4605.
80. Thomas, Y.R.J.; Picot, M.; Carer, A.; Berder, O.; Sentieys, O.; Barrière, F. A single sediment-microbial fuel cell powering a wireless telecommunication system. *Journal of Power Sources* **2013**, *241*, 703–708.

81. Kumar, G.G.; Sarathi, V.G.S.; Nahm, K.S. Recent advances and challenges in the anode architecture and their modifications for the applications of microbial fuel cells. *Biosensors and Bioelectronics* **2013**, *43*, 461–475.
82. Xie, X.; Criddle, C.; Cui, Y. Design and fabrication of bioelectrodes for microbial bioelectrochemical systems. *Energy Environ. Sci.* **2015**, *8*, 3418–3441.
83. Arends, J.B.A.; Blondeel, E.; Tennison, S.R.; Boon, N.; Verstraete, W. Suitability of granular carbon as an anode material for sediment microbial fuel cells. *Journal of Soils and Sediments* **2012**, *12*, 1197–1206.
84. Huggins, T.; Wang, H.; Kearns, J.; Jenkins, P.; Ren, Z.J. Biochar as a sustainable electrode material for electricity production in microbial fuel cells. *Bioresource Technology* **2014**, *157*, 114–119.
85. Zhang, L.L.; Zhao, X.S. Carbon-based materials as supercapacitor electrodes. *Chem. Soc. Rev.* **2009**, *38*, 2520–2531.
86. Kalathil, S.; Lee, J.; Cho, M.H. Granular activated carbon based microbial fuel cell for simultaneous decolorization of real dye wastewater and electricity generation. *New Biotechnology* **2011**, *29*, 32–37.
87. Manickam, S.S.; Karra, U.; Huang, L.; Bui, N.-N.; Li, B.; McCutcheon, J.R. Activated carbon nanofiber anodes for microbial fuel cells. *Carbon* **2013**, *53*, 19–28.
88. Borsje, C.; Liu, D.; Sleutels, T.H.J.A.; Buisman, C.J.N.; ter Heijne, A. Performance of single carbon granules as perspective for larger scale capacitive bioanodes. *Journal of Power Sources* **2016**, *325*, 690–696.
89. Malvankar, N.S.; Mester, T.; Tuominen, M.T.; Lovley, D.R. Supercapacitors Based on c-Type Cytochromes Using Conductive Nanostructured Networks of Living Bacteria. *ChemPhysChem* **2012**, *13*, 463–468.
90. Liu, Y.; Bond, D.R. Long-Distance Electron Transfer by *G. sulfurreducens* Biofilms Results in Accumulation of Reduced c-Type Cytochromes. *ChemSusChem* **2012**, *5*, 1047–1053.
91. Deeke, A.; Sleutels, T.H.J.A.; Hamelers, H.V.M.; Buisman, C.J.N. Capacitive Bioanodes Enable Renewable Energy Storage in Microbial Fuel Cells. *Environ. Sci. Technol.* **2012**, *46*, 3554–3560.
92. Kannan, A.M.; Renugopalakrishnan, V.; Filipek, S.; Li, P.; Audette, G.F.; Munukutla, L. Bio-batteries and bio-fuel cells: leveraging on electronic charge transfer proteins. *J Nanosci Nanotechnol* **2009**, *9*, 1665–1678.
93. Jourdin, L.; Raes, S.M.T.; Buisman, C.J.N.; Strik, D.P.B.T.B. Critical Biofilm Growth throughout Unmodified Carbon Felts Allows Continuous Bioelectrochemical Chain Elongation from CO₂ up to Caproate at High Current Density. *Frontiers in Energy Research* **2018**, *6*, 7.
94. Sacco, N.J.; Figuerola, E.L.M.; Pataccini, G.; Bonetto, M.C.; Erijman, L.; Cortón, E. Performance of planar and cylindrical carbon electrodes at sedimentary microbial fuel cells. *Bioresource Technology* **2012**, *126*, 328–335.
95. Scott, K.; Cotlarciuc, I.; Hall, D.; Lakeman, J.B.; Browning, D. Power from marine sediment fuel cells: the influence of anode material. *Journal of Applied Electrochemistry* **2008**, *38*, 1313.
96. Wetser, K.; Liu, J.; Buisman, C.; Strik, D. Plant microbial fuel cell applied in wetlands: Spatial, temporal and potential electricity generation of *Spartina anglica* salt marshes and *Phragmites australis* peat soils. *Biomass and Bioenergy* **2015**, *83*, 543–550.
97. Malvankar, N.S.; King, G.M.; Lovley, D.R. Centimeter-long electron transport in marine sediments via conductive minerals. *The ISME Journal* **2014**, *9*, 527.
98. Roden, E.E.; Kappler, A.; Bauer, I.; Jiang, J.; Paul, A.; Stoesser, R.; Konishi, H.; Xu, H. Extracellular electron transfer through microbial reduction of solid-phase humic substances. *Nature Geosci* **2010**, *3*, 417–421.

99. Liu, J.; Zhang, F.; He, W.; Zhang, X.; Feng, Y.; Logan, B.E. Intermittent contact of fluidized anode particles containing exoelectrogenic biofilms for continuous power generation in microbial fuel cells. *Journal of Power Sources* **2014**, *261*, 278–284.
100. Wei, J.; Liang, P.; Cao, X.; Huang, X. Use of inexpensive semicoke and activated carbon as biocathode in microbial fuel cells. *Bioresource Technology* **2011**, *102*, 10431–10435.
101. Sevilla, M.; Mokaya, R. Energy storage applications of activated carbons: supercapacitors and hydrogen storage. *Energy Environ. Sci.* **2014**, *7*, 1250–1280.
102. Schrott, G.D.; Bonanni, P.S.; Robuschi, L.; Esteve-Nuñez, A.; Busalmen, J.P. Electrochemical insight into the mechanism of electron transport in biofilms of *Geobacter sulfurreducens*. *Electrochimica Acta* **2011**, *56*, 10791–10795.
103. Molenaar, S.D.; Mol, A.R.; Sleutels, T.H.J.A.; ter Heijne, A.; Buisman, C.J.N. Microbial Rechargeable Battery: Energy Storage and Recovery through Acetate. *Environ. Sci. Technol. Lett.* **2016**, *3*, 144–149.
104. Yates, M.D.; Ma, L.; Sack, J.; Golden, J.P.; Strycharz-Glaven, S.M.; Yates, S.R.; Tender, L.M. Microbial Electrochemical Energy Storage and Recovery in a Combined Electrotrophic and Electrogenic Biofilm. *Environ. Sci. Technol. Lett.* **2017**, *4*, 374–379.
105. Wagner, R.C.; Call, D.F.; Logan, B.E. Optimal Set Anode Potentials Vary in Bioelectrochemical Systems. *Environ. Sci. Technol.* **2010**, *44*, 6036–6041.
106. Schroder, U. Anodic electron transfer mechanisms in microbial fuel cells and their energy efficiency. *Phys. Chem. Chem. Phys.* **2007**, *9*, 2619–2629.
107. Logan, B.E. Exoelectrogenic bacteria that power microbial fuel cells. *Nature Reviews Microbiology* **2009**, *7*, 375.
108. Lee, D.-J.; Liu, X.; Weng, H.-L. Sulfate and organic carbon removal by microbial fuel cell with sulfate-reducing bacteria and sulfide-oxidising bacteria anodic biofilm. *Bioresource Technology* **2014**, *156*, 14–19.
109. Rao, A.M.F.; Malkin, S.Y.; Hidalgo-Martinez, S.; Meysman, F.J.R. The impact of electrogenic sulfide oxidation on elemental cycling and solute fluxes in coastal sediment. *Geochimica et Cosmochimica Acta* **2016**, *172*, 265–286.
110. van den Ende, F.P.; Meier, J.; van Gemerden, H. Syntrophic growth of sulfate-reducing bacteria and colorless sulfur bacteria during oxygen limitation. *FEMS Microbiology Ecology* **1997**, *23*, 65–80.
111. Rabaey, K.; Van de Sompel, K.; Maignien, L.; Boon, N.; Aelterman, P.; Clauwaert, P.; De Schampelaere, L.; Pham, H.T.; Vermeulen, J.; Verhaege, M.; et al. Microbial Fuel Cells for Sulfide Removal. *Environ. Sci. Technol.* **2006**, *40*, 5218–5224.
112. Zhang, T.; Bain, T.S.; Barlett, M.A.; Dar, S.A.; Snoeyenbos-West, O.L.; Nevin, K.P.; Lovley, D.R. Sulfur oxidation to sulfate coupled with electron transfer to electrodes by *Desulfuromonas* strain TZ1. *Microbiology* **2014**, *160*, 123–129.
113. Tan, W.-F.; Norde, W.; Koopal, L.K. Humic substance charge determination by titration with a flexible cationic polyelectrolyte. *Geochimica et Cosmochimica Acta* **2011**, *75*, 5749–5761.
114. ter Heijne, A.; de Rink, R.; Liu, D.; Klok, J.B.M.; Buisman, C.J.N. Bacteria as an Electron Shuttle for Sulfide Oxidation. *Environ. Sci. Technol. Lett.* **2018**, *5*, 495–499.
115. Roldán, S.; Granda, M.; Menéndez, R.; Santamaría, R.; Blanco, C. Mechanisms of Energy Storage in Carbon-Based Supercapacitors Modified with a Quinoid Redox-Active Electrolyte. *J. Phys. Chem. C* **2011**, *115*, 17606–17611.
116. Hu, S.; Niu, Z.; Chen, Y.; Li, L.; Zhang, H. Global wetlands: Potential distribution, wetland loss, and status. *Science of The Total Environment* **2017**, *586*, 319–327.
117. Kingsford, R.T.; Basset, A.; Jackson, L. Wetlands: conservation's poor cousins. *Aquatic Conservation: Marine and Freshwater Ecosystems* **2016**, *26*, 892–916.
118. Davidson, N.C.; Finlayson, C.M. Updating global coastal wetland areas presented in Davidson and Finlayson (2018). *Mar. Freshwater Res.* **2019**.

119. Dixon, M.J.R.; Loh, J.; Davidson, N.C.; Beltrame, C.; Freeman, R.; Walpole, M. Tracking global change in ecosystem area: The Wetland Extent Trends index. *Biological Conservation* **2016**, *193*, 27–35.
120. Bai, J.; Jia, J.; Zhang, G.; Zhao, Q.; Lu, Q.; Cui, B.; Liu, X. Spatial and temporal dynamics of heavy metal pollution and source identification in sediment cores from the short-term flooding riparian wetlands in a Chinese delta. *Environmental Pollution* **2016**, *219*, 379–388.
121. Varjani, S.J.; Upasani, V.N. A new look on factors affecting microbial degradation of petroleum hydrocarbon pollutants. *International Biodeterioration & Biodegradation* **2017**, *120*, 71–83.
122. Patmont, C.R.; Ghosh, U.; LaRosa, P.; Menzie, C.A.; Luthy, R.G.; Greenberg, M.S.; Cornelissen, G.; Eek, E.; Collins, J.; Hull, J.; et al. In situ sediment treatment using activated carbon: A demonstrated sediment cleanup technology. *Integrated Environmental Assessment and Management* **2015**, *11*, 195–207.
123. Karanfil, T.; Kilduff, J.E. Role of Granular Activated Carbon Surface Chemistry on the Adsorption of Organic Compounds. 1. Priority Pollutants. *Environ. Sci. Technol.* **1999**, *33*, 3217–3224.
124. Li, L.; Quinlivan, P.A.; Knappe, D.R.U. Effects of activated carbon surface chemistry and pore structure on the adsorption of organic contaminants from aqueous solution. *Carbon* **2002**, *40*, 2085–2100.
125. Lee, J.; Kim, J.; Hyeon, T. Recent Progress in the Synthesis of Porous Carbon Materials. *Advanced Materials* **2006**, *18*, 2073–2094.
126. Xu, P.; Xiao, E.-R.; Xu, D.; Zhou, Y.; He, F.; Liu, B.-Y.; Zeng, L.; Wu, Z.-B. Internal nitrogen removal from sediments by the hybrid system of microbial fuel cells and submerged aquatic plants. *PLOS ONE* **2017**, *12*, e0172757.
127. Zhou, Y.-L.; Wu, H.-F.; Yan, Z.-S.; Cai, H.-Y.; Jiang, H.-L. The enhanced survival of submerged macrophyte *Potamogeton malaiianus* by sediment microbial fuel cells. *Ecological Engineering* **2016**, *87*, 254–262.
128. Kouzuma, A.; Kaku, N.; Watanabe, K. Microbial electricity generation in rice paddy fields: recent advances and perspectives in rhizosphere microbial fuel cells. *Applied Microbiology and Biotechnology* **2014**, *98*, 9521–9526.
129. Helder, M.; Chen, W.-S.; van der Harst, E.J.M.; Strik, D.P.B.T.B.; Hamelers, H. (Bert) V.M.; Buisman, C.J.N.; Potting, J. Electricity production with living plants on a green roof: environmental performance of the plant-microbial fuel cell. *Biofuels, Bioprod. Bioref.* **2013**, *7*, 52–64.
130. Timmers, R.A.; Strik, D.P.B.T.B.; Hamelers, H.V.M.; Buisman, C.J.N. Long-term performance of a plant microbial fuel cell with *Spartina anglica*. *Applied Microbiology and Biotechnology* **2010**, *86*, 973–981.
131. Gray, A.J.; Marshall, D.F.; Raybould, A.F. A Century of Evolution in *Spartina anglica*. In *Advances in Ecological Research*; Begon, M., Fitter, A.H., Macfadyen, A., Eds.; Academic Press, 1991; Vol. 21, pp. 1–62 ISBN 0065-2504.
132. Raybould, A.F.; Gray, A.J.; Lawrence, M.J.; Marshall, D.F. The evolution of *Spartina anglica* C. E. Hubbard (Gramineae): genetic variation and status of the parental species in Britain. *Biological Journal of the Linnean Society* **1991**, *44*, 369–380.
133. Nehring, S.; Adersen, H. NOBANIS – Invasive Alien Species Fact Sheet – *Spartina anglica* 2006.
134. Nitorisavut, R.; Regmi, R. Plant microbial fuel cells: A promising biosystems engineering. *Renewable and Sustainable Energy Reviews* **2017**, *76*, 81–89.
135. Salinas-Juárez, M.G.; Roquero, P.; Durán-Domínguez-de-Bazúa, M. del C. Plant and microorganisms support media for electricity generation in biological fuel cells with living hydrophytes. *Bioelectrochemistry* **2016**, *112*, 145–152.

136. Arends, J.B.A.; Speeckaert, J.; Blondeel, E.; De Vrieze, J.; Boeckx, P.; Verstraete, W.; Rabaey, K.; Boon, N. Greenhouse gas emissions from rice microcosms amended with a plant microbial fuel cell. *Applied Microbiology and Biotechnology* **2014**, *98*, 3205–3217.
137. Timmers, R.A.; Rothballer, M.; Strik, D.P.B.T.B.; Engel, M.; Schulz, S.; Schloter, M.; Hartmann, A.; Hamelers, B.; Buisman, C. Microbial community structure elucidates performance of *Glyceria maxima* plant microbial fuel cell. *Applied Microbiology and Biotechnology* **2012**, *94*, 537–548.
138. Bombelli, P.; Iyer, D.M.R.; Covshoff, S.; McCormick, A.J.; Yunus, K.; Hibberd, J.M.; Fisher, A.C.; Howe, C.J. Comparison of power output by rice (*Oryza sativa*) and an associated weed (*Echinochloa glabrescens*) in vascular plant bio-photovoltaic (VP-BPV) systems. *Applied Microbiology and Biotechnology* **2013**, *97*, 429–438.
139. Regmi, R.; Nitorisavut, R.; Charoenroongtavee, S.; Yimkhaophon, W.; Phanthurat, O. Earthen Pot–Plant Microbial Fuel Cell Powered by Vetiver for Bioelectricity Production and Wastewater Treatment. *CLEAN – Soil, Air, Water* **2018**, *46*, 1700193.
140. Md Khudzari, J.; Gariépy, Y.; Kurian, J.; Tartakovsky, B.; Raghavan, G.S.V. Effects of biochar anodes in rice plant microbial fuel cells on the production of bioelectricity, biomass, and methane. *Biochemical Engineering Journal* **2019**, *141*, 190–199.
141. Borsje, C.; Sleutels, T.; Saakes, M.; Buisman, C.J.N.; ter Heijne, A. The Granular Capacitive Moving Bed Reactor for the scale up of bioanodes. *Journal of Chemical Technology & Biotechnology* **2019**, *0*.
142. Sudirjo, E.; Buisman, C.J.N.; Strik, D.P.B.T.B. Marine Sediment Mixed With Activated Carbon Allows Electricity Production and Storage From Internal and External Energy Sources: A New Rechargeable Bio-Battery With Bi-Directional Electron Transfer Properties. *Frontiers in Microbiology* **2019**, *10*, 934.
143. Alslaibi, T.M.; Abustan, I.; Ahmad, M.A.; Foul, A.A. A review: production of activated carbon from agricultural byproducts via conventional and microwave heating. *Journal of Chemical Technology & Biotechnology* **2013**, *88*, 1183–1190.
144. Menya, E.; Olupot, P.W.; Storz, H.; Lubwama, M.; Kiros, Y. Production and performance of activated carbon from rice husks for removal of natural organic matter from water: A review. *Chemical Engineering Research and Design* **2018**, *129*, 271–296.
145. Hale, S.E.; Jensen, J.; Jakob, L.; Oleszczuk, P.; Hartnik, T.; Henriksen, T.; Okkenhaug, G.; Martinsen, V.; Cornelissen, G. Short-Term Effect of the Soil Amendments Activated Carbon, Biochar, and Ferric Oxyhydroxide on Bacteria and Invertebrates. *Environ. Sci. Technol.* **2013**, *47*, 8674–8683.
146. Igalavithana, A.D.; Ok, Y.S.; Usman, A.R.A.; Al-Wabel, M.I.; Oleszczuk, P.; Lee, S.S. The Effects of Biochar Amendment on Soil Fertility. In *Agricultural and Environmental Applications of Biochar: Advances and Barriers*; SSSA Special Publication; Soil Science Society of America, Inc.: Madison, WI, 2016; pp. 123–144 ISBN 978-0-89118-967-1.
147. Bakker, J.P. Restoration of Salt Marshes. In J.V. Andel, & J. Aronson (Eds.). In *Restoration Ecology: The New Frontier*; s.n., 2012; pp. 248--262 ISBN 978-1-4443-3636-8.
148. Deltares Pioneer salt marsh restoration for coastal protection - Eastern Scheldt, NL Available online: <https://publicwiki.deltares.nl/display/BTG/Pioneer+salt+marsh+restoration+for+coastal+protection+-+Eastern+Scheldt%2C+NL> (accessed on Jul 1, 2019).
149. Wetland International Building with Nature Indonesia - reaching scale for coastal resilience Available online: <https://www.wetlands.org/publications/building-with-nature-in-indonesia/> (accessed on Jul 1, 2019).
150. de Smit, S.M.; de Leeuw, K.D.; Buisman, C.J.N.; Strik, D.P.B.T.B. Continuous n-valerate formation from propionate and methanol in an anaerobic chain elongation open-culture bioreactor. *Biotechnology for Biofuels* **2019**, *12*, 132.

151. Takahashi, S.; Tomita, J.; Nishioka, K.; Hisada, T.; Nishijima, M. Development of a Prokaryotic Universal Primer for Simultaneous Analysis of Bacteria and Archaea Using Next-Generation Sequencing. *PLOS ONE* **2014**, *9*, e105592.
152. Edgar, R.C. Search and clustering orders of magnitude faster than BLAST. *Bioinformatics* **2010**, *26*, 2460–2461.
153. Quast, C.; Pruesse, E.; Yilmaz, P.; Gerken, J.; Schweer, T.; Yarza, P.; Peplies, J.; Glöckner, F.O. The SILVA ribosomal RNA gene database project: improved data processing and web-based tools. *Nucleic Acids Research* **2012**, *41*, D590–D596.
154. Wang, Q.; Garrity, G.M.; Tiedje, J.M.; Cole, J.R. Naive Bayesian classifier for rapid assignment of rRNA sequences into the new bacterial taxonomy. *Appl Environ Microbiol* **2007**, *73*, 5261–5267.
155. Caporaso, J.G.; Kuczynski, J.; Stombaugh, J.; Bittinger, K.; Bushman, F.D.; Costello, E.K.; Fierer, N.; Peña, A.G.; Goodrich, J.K.; Gordon, J.I.; et al. QIIME allows analysis of high-throughput community sequencing data. *Nature Methods* **2010**, *7*, 335.
156. Koo, H.; Hakim, J.A.; Morrow, C.D.; Andersen, D.T.; Bej, A.K. Chapter 9 - Microbial Community Composition and Predicted Functional Attributes of Antarctic Lithobionts Using Targeted Next-Generation Sequencing and Bioinformatics Tools. In *Methods in Microbiology*; Gurtler, V., Trevors, J.T., Eds.; Academic Press, 2018; Vol. 45, pp. 243–290 ISBN 0580-9517.
157. Giusti, D.M.; Conway, R.A.; Lawson, C.T. Activated Carbon Adsorption of Petrochemicals. *Journal (Water Pollution Control Federation)* **1974**, *46*, 947–965.
158. Mugisidi, D.; Ranaldo, A.; Soedarsono, J.W.; Hikam, M. Modification of activated carbon using sodium acetate and its regeneration using sodium hydroxide for the adsorption of copper from aqueous solution. *Carbon* **2007**, *45*, 1081–1084.
159. Wilson, K.; Yang, H.; Seo, C.W.; Marshall, W.E. Select metal adsorption by activated carbon made from peanut shells. *Bioresource Technology* **2006**, *97*, 2266–2270.
160. Wang, C.-M.; Chung, T.-W.; Huang, C.-M.; Wu, H. Adsorption Equilibria of Acetate Compounds on Activated Carbon, Silica Gel, and 13X Zeolite. *J. Chem. Eng. Data* **2005**, *50*, 811–816.
161. Wang, Z.; Nie, E.; Li, J.; Yang, M.; Zhao, Y.; Luo, X.; Zheng, Z. Equilibrium and kinetics of adsorption of phosphate onto iron-doped activated carbon. *Environmental Science and Pollution Research* **2012**, *19*, 2908–2917.
162. Boopathy, R.; Karthikeyan, S.; Mandal, A.B.; Sekaran, G. Adsorption of ammonium ion by coconut shell-activated carbon from aqueous solution: kinetic, isotherm, and thermodynamic studies. *Environmental Science and Pollution Research* **2013**, *20*, 533–542.
163. Demiral, H.; Gündüzoğlu, G. Removal of nitrate from aqueous solutions by activated carbon prepared from sugar beet bagasse. *Bioresource Technology* **2010**, *101*, 1675–1680.
164. Hong, S.; Cannon, F.S.; Hou, P.; Byrne, T.; Nieto-Delgado, C. Sulfate removal from acid mine drainage using polypyrrole-grafted granular activated carbon. *Carbon* **2014**, *73*, 51–60.
165. Bolan, N.S.; Elliott, J.; Gregg, P.E.H.; Weil, S. Enhanced dissolution of phosphate rocks in the rhizosphere. *Biology and Fertility of Soils* **1997**, *24*, 169–174.
166. Lambers, H.; Clements, J.C.; Nelson, M.N. How a phosphorus-acquisition strategy based on carboxylate exudation powers the success and agronomic potential of lupines (*Lupinus*, Fabaceae). *American Journal of Botany* **2013**, *100*, 263–288.
167. Reish, D.J. Annelid Available online: <https://www.britannica.com/animal/annelid> (accessed on Jul 1, 2019).
168. Cunha, L.; Brown, G.G.; Stanton, D.W.G.; Da Silva, E.; Hansel, F.A.; Jorge, G.; McKey, D.; Vidal-Torrado, P.; Macedo, R.S.; Velasquez, E.; et al. Soil Animals and Pedogenesis: The Role of Earthworms in Anthropogenic Soils. *Soil Science* **2016**, *181*.

169. Liu, B.; Ji, M.; Zhai, H. Anodic potentials, electricity generation and bacterial community as affected by plant roots in sediment microbial fuel cell: Effects of anode locations. *Chemosphere* **2018**, *209*, 739–747.
170. Osorio de la Rosa, E.; Vázquez Castillo, J.; Carmona Campos, M.; Barbosa Pool, R.G.; Becerra Nuñez, G.; Castillo Atoche, A.; Ortegón Aguilar, J. Plant Microbial Fuel Cells–Based Energy Harvester System for Self-powered IoT Applications. *Sensors* **2019**, *19*.
171. Fang, Z.; Cheng, S.; Wang, H.; Cao, X.; Li, X. Feasibility study of simultaneous azo dye decolorization and bioelectricity generation by microbial fuel cell-coupled constructed wetland: substrate effects. *RSC Adv.* **2017**, *7*, 16542–16552.
172. Song, H.; Zhang, S.; Long, X.; Yang, X.; Li, H.; Xiang, W. Optimization of Bioelectricity Generation in Constructed Wetland-Coupled Microbial Fuel Cell Systems. *Water* **2017**, *9*.
173. Liu, S.; Song, H.; Li, X.; Yang, F. Power Generation Enhancement by Utilizing Plant Photosynthate in Microbial Fuel Cell Coupled Constructed Wetland System. *International Journal of Photoenergy* **2013**, *2013*, 10.
174. Tapia, N.F.; Rojas, C.; Bonilla, C.A.; Vargas, I.T. A New Method for Sensing Soil Water Content in Green Roofs Using Plant Microbial Fuel Cells. *Sensors (Basel)* **2017**, *18*, 71.
175. Koop-Jakobsen, K.; Wenzhöfer, F. The Dynamics of Plant-Mediated Sediment Oxygenation in *Spartina anglica* Rhizospheres—a Planar Optode Study. *Estuaries and Coasts* **2015**, *38*, 951–963.
176. Timmers, R.A.; Strik, D.P.B.T.B.; Arampatzoglou, C.; Buisman, C.J.N.; Hamelers, H.V.M. Rhizosphere anode model explains high oxygen levels during operation of a *Glyceria maxima* PMFC. *Bioresource Technology* **2012**, *108*, 60–67.
177. Caizán-Juanarena, L.; Servin-Balderas, I.; Chen, X.; Buisman, C.J.N.; ter Heijne, A. Electrochemical and microbiological characterization of single carbon granules in a multi-anode microbial fuel cell. *Journal of Power Sources* **2019**.
178. Lasher, C.; Dyszynski, G.; Everett, K.; Edmonds, J.; Ye, W.; Sheldon, W.; Wang, S.; Joye, S.B.; Moran, M.A.; Whitman, W.B. The Diverse Bacterial Community in Intertidal, Anaerobic Sediments at Sapelo Island, Georgia. *Microbial Ecology* **2009**, *58*, 244–261.
179. Wang, M.; Chen, J.-K.; Li, B. Characterization of Bacterial Community Structure and Diversity in Rhizosphere Soils of Three Plants in Rapidly Changing Salt Marshes Using 16S rDNA. *Pedosphere* **2007**, *17*, 545–556.
180. Wang, M.; Yang, P.; Falcão Salles, J. Distribution of Root-Associated Bacterial Communities Along a Salt-Marsh Primary Succession. *Frontiers in Plant Science* **2016**, *6*, 1188.
181. Leloup, J.; Fossing, H.; Kohls, K.; Holmkvist, L.; Borowski, C.; Jørgensen, B.B. Sulfate-reducing bacteria in marine sediment (Aarhus Bay, Denmark): abundance and diversity related to geochemical zonation. *Environmental Microbiology* **2009**, *11*, 1278–1291.
182. Burdorf, L.D.W.; Tramper, A.; Seitaj, D.; Meire, L.; Hidalgo-Martinez, S.; Zetsche, E.-M.; Boschker, H.T.S.; Meysman, F.J.R. Long-distance electron transport occurs globally in marine sediments. *Biogeosciences* **2017**, *14*, 683–701.
183. Larsen, S.; Nielsen, L.P.; Schramm, A. Cable bacteria associated with long-distance electron transport in New England salt marsh sediment. *Environmental Microbiology Reports* **2015**, *7*, 175–179.
184. Barton, L.L.; Fauque, G.D. Chapter 2 Biochemistry, Physiology and Biotechnology of Sulfate-Reducing Bacteria. In *Advances in Applied Microbiology*; Academic Press, 2009; Vol. 68, pp. 41–98 ISBN 0065-2164.
185. Thomas, F.; Giblin, A.E.; Cardon, Z.G.; Sievert, S.M. Rhizosphere heterogeneity shapes abundance and activity of sulfur-oxidizing bacteria in vegetated salt marsh sediments. *Frontiers in Microbiology* **2014**, *5*, 309.

186. Ahn, J.-H.; Jeong, W.-S.; Choi, M.-Y.; Kim, B.-Y.; Song, J.; Weon, H.-Y. Phylogenetic Diversity of Dominant Bacterial and Archaeal Communities in Plant-Microbial Fuel Cells Using Rice Plants. *J. Microbiol. Biotechnol* **2014**, *24*, 1707–1718.
187. Chen, Z.; Huang, Y.; Liang, J.; Zhao, F.; Zhu, Y. A novel sediment microbial fuel cell with a biocathode in the rice rhizosphere. *Bioresource Technology* **2012**, *108*, 55–59.
188. Costanzo, E. The influence of an electric field on the growth of soy seedlings. *Journal of Electrostatics* **2008**, *66*, 417–420.
189. De Schampelaire, L.; Cabezas, A.; Marzorati, M.; Friedrich, M.W.; Boon, N.; Verstraete, W. Microbial Community Analysis of Anodes from Sediment Microbial Fuel Cells Powered by Rhizodeposits of Living Rice Plants. *Applied and Environmental Microbiology* **2010**, *76*, 2002–2008.
190. Schievano, A.; Colombo, A.; Grattieri, M.; Trasatti, S.P.; Liberale, A.; Tremolada, P.; Pino, C.; Cristiani, P. Floating microbial fuel cells as energy harvesters for signal transmission from natural water bodies. *Journal of Power Sources* **2017**, *340*, 80–88.
191. Augustin, A.; Yi, J.; Clausen, T.; Townsley, M.W. A Study of LoRa: Long Range & Low Power Networks for the Internet of Things. *Sensors* **2016**, *16*.
192. Petäjäjärvi, J.; Mikhaylov, K.; Pettissalo, M.; Janhunen, J.; Iinatti, J. Performance of a low-power wide-area network based on LoRa technology: Doppler robustness, scalability, and coverage. *International Journal of Distributed Sensor Networks* **2017**, *13*, 1550147717699412.
193. Sanchez-Iborra, R.; Sanchez-Gomez, J.; Ballesta-Viñas, J.; Cano, M.-D.; Skarmeta, F.A. Performance Evaluation of LoRa Considering Scenario Conditions. *Sensors* **2018**, *18*.
194. IRRI *Growing rice, cultivating partnerships: 40 years of Indonesia-IRRI collaboration*; International Rice Research Institute: Los Baños (Philippines), 2015;
195. BBPADI Inpari 30 Ciharang Sub 1 Available online: <http://bbpadi.litbang.pertanian.go.id/index.php/varietas-padi/inbrida-padi-sawah-inpari/inpari-30-ciherang-sub-1> (accessed on Aug 19, 2019).
196. 1st BASE *Next Generation Sequencing (NGS) Project Report for NGS Order ID 10419*; Axil Scientific Pte Ltd: Singapore, 2018; p. 7;.
197. Mano, M. Precise and continuous measurement of plant heights in an agricultural field using a time-lapse camera. *Journal of Agricultural Meteorology* **2017**, *73*, 100–108.
198. Roger, P. The impact of pesticides on wetland rice field microflora: A review. In; 1995; pp. 271–308 ISBN 0-7923-9522-0.
199. Cao, X.; Song, H.; Yu, C.; Li, X. Simultaneous degradation of toxic refractory organic pesticide and bioelectricity generation using a soil microbial fuel cell. *Bioresource Technology* **2015**, *189*, 87–93.
200. Moqsud, M.A.; Yoshitake, J.; Bushra, Q.S.; Hyodo, M.; Omine, K.; Strik, D. Compost in plant microbial fuel cell for bioelectricity generation. *Waste Management* **2015**, *36*, 63–69.
201. Wang, L.; Xie, B.; Gao, N.; Min, B.; Liu, H. Urea removal coupled with enhanced electricity generation in single-chambered microbial fuel cells. *Environmental Science and Pollution Research* **2017**, *24*, 20401–20408.
202. Kuntke, P.; Śmiech, K.M.; Bruning, H.; Zeeman, G.; Saakes, M.; Sleutels, T.H.J.A.; Hamelers, H.V.M.; Buisman, C.J.N. Ammonium recovery and energy production from urine by a microbial fuel cell. *Water Research* **2012**, *46*, 2627–2636.
203. Lin, B.; Lu, Y. Bacterial and archaeal guilds associated with electrogenesis and methanogenesis in paddy field soil. *Geoderma* **2015**, *259–260*, 362–369.
204. Roe, G.H. OROGRAPHIC PRECIPITATION. *Annu. Rev. Earth Planet. Sci.* **2004**, *33*, 645–671.
205. Strik, D.P.B.T.B.; Picot, M.; Buisman, C.J.N.; Barriere, F. pH and Temperature Determine Performance of Oxygen Reducing Biocathodes. *Electroanalysis* **2013**, *25*, 652–655.

206. Ter Heijne, A.; Hamelers, H.V.M.; Saakes, M.; Buisman, C.J.N. Performance of non-porous graphite and titanium-based anodes in microbial fuel cells. *Electrochimica Acta* **2008**, *53*, 5697–5703.
207. Malvankar, N.S.; Lau, J.; Nevin, K.P.; Franks, A.E.; Tuominen, M.T.; Lovley, D.R. Electrical Conductivity in a Mixed-Species Biofilm. *Applied and Environmental Microbiology* **2012**, *78*, 5967–5971.
208. Perez-Rodriguez, P.; Ovando-Medina, V.M.; Martinez-Amador, S.Y.; Rodriguez-de la Garza, J.A. Bioanode of polyurethane/graphite/polypyrrole composite in microbial fuel cells. *Biotechnology and Bioprocess Engineering* **2016**, *21*, 305–313.
209. Stoll, Z.A.; Ma, Z.K.; Trivedi, C.B.; Spear, J.R.; Xu, P. Sacrificing power for more cost-effective treatment: A techno-economic approach for engineering microbial fuel cells. *Chemosphere* **2016**, *161*, 10–18.
210. Yuan, Y.; Kim, S. Improved performance of a microbial fuel cell with polypyrrole/carbon black composite coated carbon paper anodes. *Bulletin of the Korean Chemical Society* **2008**, *29*, 1344–1348.
211. Yuan, Y.; Zhou, S.G.; Liu, Y.; Tang, J.H. Nanostructured Macroporous Bioanode Based on Polyaniline-Modified Natural Loofah Sponge for High-Performance Microbial Fuel Cells. *Environmental Science & Technology* **2013**, *47*, 14525–14532.
212. Liu, M.M.; Zhou, M.H.; Yang, H.J.; Zhao, Y.Y.; Hu, Y.S. A cost-effective polyurethane based activated carbon sponge anode for high-performance microbial fuel cells. *Rsc Advances* **2015**, *5*, 84269–84275.
213. Xie, X.; Ye, M.; Hu, L.; Liu, N.; McDonough, J.R.; Chen, W.S.; Alshareef, H.N.; Criddle, C.S.; Cui, Y. Carbon nanotube-coated macroporous sponge for microbial fuel cell electrodes. *Energy Environ. Sci.* **2012**, *5*, 5265–5270.
214. Jin, Z.; Yan, X.D.; Yu, Y.H.; Zhao, G.J. Sustainable activated carbon fibers from liquefied wood with controllable porosity for high-performance supercapacitors. *Journal of Materials Chemistry A* **2014**, *2*, 11706–11715.
215. Zhao, F.; Rahunen, N.; Varcoe, J.R.; Chandra, A.; Avignone-Rossa, C.; Thumser, A.E.; Slade, R.C. Activated carbon cloth as anode for sulfate removal in a microbial fuel cell. *Environ Sci Technol* **2008**, *42*, 4971–6.
216. AC price Available online: https://www.alibaba.com/product-detail/Coal-granular-Activated-Carbon-In-Water_62059260531.html? (accessed on Sep 30, 2019).
217. King Sponge PU Available online: https://www.alibaba.com/product-detail/Factory-Directly-Sell-Custom-10-15_60507687115.html? (accessed on Sep 30, 2019).
218. Xie, X.; Yu, G.; Liu, N.; Bao, Z.; Criddle, C.S.; Cui, Y. Graphene-sponges as high-performance low-cost anodes for microbial fuel cells. *Energy & Environmental Science* **2012**, *5*.
219. Xie, X.; Hu, L.; Pasta, M.; Wells, G.F.; Kong, D.; Criddle, C.S.; Cui, Y. Three-Dimensional Carbon Nanotube-Textile Anode for High-Performance Microbial Fuel Cells. *Nano Lett.* **2011**, *11*, 291–296.
220. Pérez-Rodríguez, P.; Ovando-Medina, V.M.; Martínez-Amador, S.Y.; Rodríguez-de la Garza, J.A. Bioanode of polyurethane/graphite/polypyrrole composite in microbial fuel cells. *Biotechnology and Bioprocess Engineering* **2016**, *21*, 305–313.
221. Cabot, N.A.C. SDS Norit PK1-3 Available online: <http://www.cabotcorp.nl/solutions/products-plus/activated-carbon/granulated> (accessed on Oct 21, 2019).
222. ter Heijne, A.; Schaezle, O.; Gimenez, S.; Navarro, L.; Hamelers, B.; Fabregat-Santiago, F. Analysis of bio-anode performance through electrochemical impedance spectroscopy. *Bioelectrochemistry* **2015**, *106*, 64–72.
223. Fricke, K.; Harnisch, F.; Schroder, U. On the use of cyclic voltammetry for the study of anodic electron transfer in microbial fuel cells. *Energy Environ. Sci.* **2008**, *1*, 144–147.

224. Marsili, E.; Sun, J.; Bond, D.R. Voltammetry and Growth Physiology of *Geobacter sulfurreducens* Biofilms as a Function of Growth Stage and Imposed Electrode Potential. *Electroanalysis* **2010**, *22*, 865–874.
225. Harnisch, F.; Freguia, S. A Basic Tutorial on Cyclic Voltammetry for the Investigation of Electroactive Microbial Biofilms. *Chemistry-an Asian Journal* **2012**, *7*, 466–475.
226. Babauta, J.; Renslow, R.; Lewandowski, Z.; Beyenal, H. Electrochemically active biofilms: facts and fiction. A review. *Biofouling* **2012**, *28*, 789–812.
227. Bard, A.J.; Faulkner, L.R.; Leddy, J.; Zoski, C.G. *Electrochemical methods: fundamentals and applications*; Wiley New York, 1980; Vol. 2;.
228. Sleutels, T.H.J.A.; Hamelers, H.V.M.; Rozendal, R.A.; Buisman, C.J.N. Ion transport resistance in Microbial Electrolysis Cells with anion and cation exchange membranes. *International Journal of Hydrogen Energy* **2009**, *34*, 3612–3620.
229. Skyllas-Kazacos, M.; Chakrabarti, M.H.; Hajimolana, S.A.; Mjalli, F.S.; Saleem, M. Progress in Flow Battery Research and Development. *Journal of the Electrochemical Society* **2011**, *158*, R55–R79.
230. Zhang, Y.Z.; Mo, G.Q.; Li, X.W.; Zhang, W.D.; Zhang, J.Q.; Ye, J.S.; Huang, X.D.; Yu, C.Z. A graphene modified anode to improve the performance of microbial fuel cells. *Journal of Power Sources* **2011**, *196*, 5402–5407.
231. Strik, D.P.B.T.B.; Timmers, R.A.; Helder, M.; Steinbusch, K.J.J.; Hamelers, H.V.M.; Buisman, C.J.N. Microbial solar cells: applying photosynthetic and electrochemically active organisms. *Trends in Biotechnology* **2011**, *29*, 41–49.
232. Ter Heijne, A.; Schaetzle, O.; Gimenez, S.; Fabregat-Santiago, F.; Bisquert, J.; Strik, D.P.B.T.B.; Barriere, F.; Buisman, C.J.N.; Hamelers, H.V.M. Identifying charge and mass transfer resistances of an oxygen reducing biocathode. *Energy & Environmental Science* **2011**, *4*, 5035–5043.
233. Gago, A.S.; Ansar, A.S.; Gazdzicki, P.; Wagner, N.; Arnold, J.; Friedrich, K.A. Low Cost Bipolar Plates for Large Scale PEM Electrolyzers. *ECS Transactions* **2014**, *64*, 1039–1048.
234. Bowen, H.J.M. Absorption by Polyurethane Foams - New Method of Separation. *Journal of the Chemical Society a -Inorganic Physical Theoretical* **1970**, 1082-.
235. Thirumal, M.; Khastgir, D.; Singha, N.K.; Manjunath, B.S.; Naik, Y.P. Effect of foam density on the properties of water blown rigid polyurethane foam. *Journal of Applied Polymer Science* **2008**, *108*, 1810–1817.
236. Pinto, M.L.; Pires, J.; Carvalho, A.P.; de Carvalho, M.B.; Bordado, J.C. Characterization of adsorbent materials supported on polyurethane foams by nitrogen and toluene adsorption. *Microporous and Mesoporous Materials* **2005**, *80*, 253–262.
237. FXI Technical Products Function Sheet Polyurethane foams Available online: http://fxi.com/assets/pdf/FS_MEC4.pdf (accessed on Oct 28, 2019).
238. Huysman, P.; Vanmeenen, P.; Vanassche, P.; Verstraete, W. Factors Affecting The Colonization of Non Porous and Porous Packing Materials in Model Upflow Methane Reactors. *Biotechnology Letters* **1983**, *5*, 643–648.
239. Qiao, Y.; Bao, S.J.; Li, C.M.; Cui, X.Q.; Lu, Z.S.; Guo, J. Nanostructured polyaniline/titanium dioxide composite anode for microbial fuel cells. *Acs Nano* **2008**, *2*, 113–119.
240. Chen, S.; Hou, H. Three-dimensional laminar wavelike carbon anode material of microbiological fuel cell and preparation method thereof 2014, 8.
241. Marsili, E.; Rollefson, J.B.; Baron, D.B.; Hozalski, R.M.; Bond, D.R. Microbial Biofilm Voltammetry: Direct Electrochemical Characterization of Catalytic Electrode-Attached Biofilms. *Applied and Environmental Microbiology* **2008**, *74*, 7329–7337.
242. Santoro, C.; Arbizzani, C.; Erable, B.; Ieropoulos, I. Microbial fuel cells: From fundamentals to applications. A review. *Journal of Power Sources* **2017**, *356*, 225–244.

243. Li, C.; Lesnik, K.L.; Liu, H. Conductive properties of methanogenic biofilms. *Bioelectrochemistry* **2018**, *119*, 220–226.
244. Malvankar, N.S.; Tuominen, M.T.; Lovley, D.R. Biofilm conductivity is a decisive variable for high-current-density *Geobacter sulfurreducens* microbial fuel cells. *Energy & Environmental Science* **2012**, *5*, 5790–5797.
245. Liang, P.; Wang, H.; Xia, X.; Huang, X.; Mo, Y.; Cao, X.; Fan, M. Carbon nanotube powders as electrode modifier to enhance the activity of anodic biofilm in microbial fuel cells. *Biosensors and Bioelectronics* **2011**, *26*, 3000–3004.
246. Lee, H.S.; Dhar, B.R.; An, J.; Rittmann, B.E.; Ryu, H.; Domingo, J.W.S.; Ren, H.; Chae, J. The Roles of Biofilm Conductivity and Donor Substrate Kinetics in a Mixed-Culture Biofilm Anode. *Environmental Science & Technology* **2016**, *50*, 12799–12807.
247. Morita, M.; Malvankar, N.S.; Franks, A.E.; Summers, Z.M.; Giloteaux, L.; Rotaru, A.E.; Rotaru, C.; Lovley, D.R. Potential for Direct Interspecies Electron Transfer in Methanogenic Wastewater Digester Aggregates. *Mbio* **2011**, *2*.
248. Li, C.; Lesnik, K.L.; Fan, Y.; Liu, H. Redox Conductivity of Current-Producing Mixed Species Biofilms. *PLOS ONE* **2016**, *11*, e0155247.
249. Borole, A.P.; Reguera, G.; Ringeisen, B.; Wang, Z.W.; Feng, Y.J.; Kim, B.H. Electroactive biofilms: Current status and future research needs. *Energy & Environmental Science* **2011**, *4*, 4813–4834.
250. Huang, L.; Regan, J.M.; Quan, X. Electron transfer mechanisms, new applications, and performance of biocathode microbial fuel cells. *Bioresource Technology* **2011**, *102*, 316–323.
251. Ter Heijne, A.; Hamelers, H.V.M.; Buisman, C.J.N. Microbial fuel cell operation with continuous biological ferrous iron oxidation of the catholyte. *Environmental Science & Technology* **2007**, *41*, 4130–4134.
252. Pausch, J.; Kuzyakov, Y. Carbon input by roots into the soil: Quantification of rhizodeposition from root to ecosystem scale. *Global Change Biology* **2018**, *24*, 1–12.
253. Deng, H.; Chen, Z.; Zhao, F. Energy from Plants and Microorganisms: Progress in Plant–Microbial Fuel Cells. *ChemSusChem* **2012**, *5*, 1006–1011.
254. Indonesia Solar GIS Available online: <https://solargis.com/maps-and-gis-data/download/indonesia> (accessed on Sep 27, 2019).
255. Sage, R.F. C3 versus C4 photosynthesis in rice: ecophysiological perspectives**Sheehy JE, Mitchell PL, Hardy B. editors. 2000. Redesigning rice photosynthesis to increase yield. Proceedings of the Workshop on The Quest to Reduce Hunger: Redesigning Rice Photosynthesis, 30 Nov.-3 Dec. 1999. Los Baños, Philippines. Makati City (Philippines): International Rice Research Institute and Amsterdam (The Netherlands): Elsevier Science B.V. 293 p. In *Studies in Plant Science*; Sheehy, J.E., Mitchell, P.L., Hardy, B., Eds.; Elsevier, 2000; Vol. 7, pp. 13–35 ISBN 0928-3420.
256. Zhu, X.-G.; Long, S.P.; Ort, D.R. Improving Photosynthetic Efficiency for Greater Yield. *Annu. Rev. Plant Biol.* **2010**, *61*, 235–261.
257. Blankenship, R.E.; Tiede, D.M.; Barber, J.; Brudvig, G.W.; Fleming, G.; Ghirardi, M.; Gunner, M.R.; Junge, W.; Kramer, D.M.; Melis, A.; et al. Comparing Photosynthetic and Photovoltaic Efficiencies and Recognizing the Potential for Improvement. *Science* **2011**, *332*, 805.
258. Wang, H.; Zhang, J.; Wu, K.; Ni, F. Measuring the rhizodeposition of carbon by rice: an approach based on carbon flux observations. *Soil Science and Plant Nutrition* **2017**, *63*, 499–506.
259. Sun, D.; Chen, J.; Huang, H.B.; Liu, W.F.; Ye, Y.L.; Cheng, S.A. The effect of biofilm thickness on electrochemical activity of *Geobacter sulfurreducens*. *International Journal of Hydrogen Energy* **2016**, *41*, 16523–16528.

260. Sleutels, T.H.J.A.; Hamelers, H.V.M.; Buisman, C.J.N. Effect of mass and charge transport speed and direction in porous anodes on microbial electrolysis cell performance. *Bioresource Technology* **2011**, *102*, 399–403.
261. Sleutels, T.H.J.A.; Lodder, R.; Hamelers, H.V.M.; Buisman, C.J.N. Improved performance of porous bio-anodes in microbial electrolysis cells by enhancing mass and charge transport. *International Journal of Hydrogen Energy* **2009**, *34*, 9655–9661.
262. Rizzo, A.; Boano, F.; Revelli, R.; Ridolfi, L. Can microbial fuel cells be an effective mitigation strategy for methane emissions from paddy fields? *Ecological Engineering* **2013**, *60*, 167–171.
263. Nugroho, S.G.; Lumbanraja, J.; Suprpto, H.; Sunyoto; Ardjasa, W.S.; Haraguchi, H.; Kimura, M. Three-year measurement of methane emission from an Indonesian paddy field. *Plant and Soil* **1996**, *181*, 287–293.
264. Brix, H.; Sorrell, B.K.; Lorenzen, B. Are Phragmites-dominated wetlands a net source or net sink of greenhouse gases? *Aquatic Botany* **2001**, *69*, 313–324.
265. Seiler, W.; Conrad, R.; Scharffe, D. Field studies of methane emission from termite nests into the atmosphere and measurements of methane uptake by tropical soils. *Journal of Atmospheric Chemistry* **1984**, *1*, 171–186.
266. Schütz, H.; Holzapfel-Pschorn, A.; Conrad, R.; Rennenberg, H.; Seiler, W. A 3-year continuous record on the influence of daytime, season, and fertilizer treatment on methane emission rates from an Italian rice paddy. *Journal of Geophysical Research: Atmospheres* **1989**, *94*, 16405–16416.
267. IPCC Methane Emissions from Rice Cultivation:Flooded Rice Fields. Revised 1996 IPCC Guidelines for National Greenhouse Gas Inventories: Reference Manual 1996.
268. Wang, B.; Neue, H.U.; Samonte, H.P. Role of rice in mediating methane emission. *Plant and Soil* **1997**, *189*, 107–115.
269. Kong, D.; Li, S.; Jin, Y.; Wu, S.; Chen, J.; Hu, T.; Wang, H.; Liu, S.; Zou, J. Linking methane emissions to methanogenic and methanotrophic communities under different fertilization strategies in rice paddies. *Geoderma* **2019**, *347*, 233–243.
270. Zhang, B.; Tian, H.; Ren, W.; Tao, B.; Lu, C.; Yang, J.; Banger, K.; Pan, S. Methane emissions from global rice fields: Magnitude, spatiotemporal patterns, and environmental controls. *Global Biogeochemical Cycles* **2016**, *30*, 1246–1263.
271. Min, H.; Zhao, Y.H.; Chen, M.C.; Zhao, Y. Methanogens in paddy rice soil. *Nutrient Cycling in Agroecosystems* **1997**, *49*, 163–169.
272. Watanabe, A.; Kajiwara, M.; Tashiro, T.; Kimura, M. Influence of rice cultivar on methane emission from paddy fields. *Plant and Soil* **1995**, *176*, 51–56.
273. Neue, H.U.; Wassmann, R.; Lantin, R.S.; Alberto, M.C.R.; Aduna, J.B.; Javellana, A.M. Factors affecting methane emission from rice fields. *Atmospheric Environment* **1996**, *30*, 1751–1754.
274. Li, S.; Zuo, Q.; Wang, X.; Ma, W.; Jin, X.; Shi, J.; Ben-Gal, A. Characterizing roots and water uptake in a ground cover rice production system. *PLOS ONE* **2017**, *12*, e0180713.
275. Lu, Y.; Watanabe, A.; Kimura, M. Input and distribution of photosynthesized carbon in a flooded rice soil. *Global Biogeochemical Cycles* **2002**, *16*, 32–1.
276. Larsen, M.; Santner, J.; Oburger, E.; Wenzel, W.W.; Glud, R.N. O₂ dynamics in the rhizosphere of young rice plants (*Oryza sativa* L.) as studied by planar optodes. *Plant Soil* **2015**, *390*, 279–292.
277. Colmer, T.D. Aerenchyma and an inducible barrier to radial oxygen loss facilitate root aeration in upland, paddy and deep-water rice (*Oryza sativa* L.). *Ann Bot* **2003**, *91 Spec No*, 301–309.
278. van Bodegom, P.; Stams, F.; Mollema, L.; Boeke, S.; Leffelaar, P. Methane oxidation and the competition for oxygen in the rice rhizosphere. *Appl Environ Microbiol* **2001**, *67*, 3586–3597.
279. Chen, S.; Rotaru, A.-E.; Shrestha, P.M.; Malvankar, N.S.; Liu, F.; Fan, W.; Nevin, K.P.; Lovley, D.R. Promoting Interspecies Electron Transfer with Biochar. **2014**, *4*, 5019.

280. Thammason, N.; Vityakon, P.; Lawongsa, P.; Saenjan, P. Biochar and rice straw have different effects on soil productivity, greenhouse gas emission and carbon sequestration in Northeast Thailand paddy soil. *Agriculture and Natural Resources* **2016**, *50*, 192–198.
281. N. Degrenne; F. Buret; F. Morel; S. Adami; D. Labrousse; B. Allard; A. Zaoui Self-starting DC:DC boost converter for low-power and low-voltage microbial electric generators. In Proceedings of the 2011 IEEE Energy Conversion Congress and Exposition; 2011; pp. 889–896.
282. TI DC Booster Available online: <http://www.ti.com/product/TPS61202> (accessed on Sep 26, 2019).
283. Dekel, D.R. Review of cell performance in anion exchange membrane fuel cells. *Journal of Power Sources* **2018**, *375*, 158–169.
284. NiCd battery Available online: <https://nl.rs-online.com/web/p/aa-rechargeable-batteries/3783326/> (accessed on Sep 27, 2019).
285. Temperature sensor Available online: <https://www.sensirion.com/en/environmental-sensors/temperature-sensors/> (accessed on Oct 2, 2019).
286. Humidity sensor Available online: <https://www.sensirion.com/en/environmental-sensors/humidity-sensors/humidity-temperature-sensor-sht2x-digital-i2c-accurate/> (accessed on Oct 2, 2019).
287. Aqeel-ur-Rehman; Abbasi, A.Z.; Islam, N.; Shaikh, Z.A. A review of wireless sensors and networks' applications in agriculture. *Computer Standards & Interfaces* **2014**, *36*, 263–270.
288. Jawad, M.H.; Nordin, R.; Gharghan, K.S.; Jawad, M.A.; Ismail, M. Energy-Efficient Wireless Sensor Networks for Precision Agriculture: A Review. *Sensors* **2017**, *17*.
289. Oh, S.-E.; Logan, B.E. Voltage reversal during microbial fuel cell stack operation. *Journal of Power Sources* **2007**, *167*, 11–17.
290. Ewing, T.; Ha, P.T.; Babauta, J.T.; Tang, N.T.; Heo, D.; Beyenal, H. Scale-up of sediment microbial fuel cells. *Journal of Power Sources* **2014**, *272*, 311–319.
291. Battery performance Available online: <https://www.mpoweruk.com/performance.htm> (accessed on Oct 4, 2019).
292. RCR Silicone Available online: https://www.alibaba.com/product-detail/Customized-color-silicone-rubber-tube-for_60769031264.html (accessed on Sep 26, 2019).
293. EIMO air filter Available online: https://www.alibaba.com/product-detail/Auto-car-air-filter-nonwoven-filter_60838771795.html? (accessed on Sep 26, 2016).
294. GT Graphite Felt Available online: https://www.alibaba.com/product-detail/activated-carbon-fiber-Fireproof-Carbon-fiber_60762857546.html? (accessed on Sep 26, 2019).
295. MVHR Filters Available online: <https://www.topswtwwfilters.nl/en/accessories/filter-media/filter-media-vnf-290-5-m2-filter-g3-t97002> (accessed on Sep 26, 2019).
296. Titanium shop Available online: http://titaniumshop.nl/index.php?action=page&group_id=10000107&lang=nl (accessed on Sep 26, 2019).
297. Statista Electricity prices Available online: <https://www.statista.com/statistics/418106/electricity-prices-for-households-in-netherlands/> (accessed on Oct 12, 2019).
298. Eurobat Battery Energy Storage for Rural Electrification Systems Guidance Document 2013.
299. Battery University Cost of Mobile and Renewable Power Available online: https://batteryuniversity.com/index.php/learn/article/bu_1006_cost_of_mobile_power (accessed on Oct 11, 2019).
300. Timmers, R. Electricity generation by living plants in a plant microbial fuel cell, Wageningen University & Research: Wageningen, The Netherlands, 2012.

301. DSTI-OECD *Product Risk Assessment Practices of Regulatory Agencies*; Summary of discussions at Workshops and Meetings of the OECD Working Party on Consumer Product Safety; Secretary-General of the OECD: Australia, 2006; p. 19;.
302. GROW.B1 EU general risk assessment methodology (Action 5 of Multi-Annual Action Plan for the surveillance of product in the EU (COM(2013) 76) 2015.
303. ISO 10377:2013 ISO 10377:2013 Consumer product safety — Guidelines for suppliers Available online: <https://www.iso.org/standard/45967.html> (accessed on Oct 18, 2019).
304. Morgan Advande Materials MSDS Graphite felt Available online: http://www.morganspecialtygraphite.com/media/3314/sds_na_sc102_specialty_carbon_fiber.pdf (accessed on Oct 13, 2019).
305. Wyman-Gordon, C. MSDS Ti Alloy Available online: http://precastcorp.com/web/user_content/files/titanium_alloys_1.pdf (accessed on Oct 13, 2019).
306. Kleinmetals MSDS Ti grade 2 Available online: <http://www.kleinmetals.ch/shop/datenblatt/E/702.pdf> (accessed on Oct 13, 2019).
307. 3M, C. MSDS Air filter Available online: <http://www1.msdirect.com/MSDS/MSDS00023/53337903-20111224.PDF> (accessed on Oct 13, 2019).
308. Actrol Parts Pty, L. MSDS Polyester filter Available online: https://www.velocityair.com.au/forms/Air%20Diffusion%20and%20Filters/Air_Filter_Media_A3300S__Cat_No_628850_-MSDS.pdf (accessed on Oct 13, 2019).
309. Cappitelli, F.; Principi, P.; Sorlini, C. Biodeterioration of modern materials in contemporary collections: can biotechnology help? *Trends in Biotechnology* **2006**, *24*, 350–354.
310. Whittaker Report Eco-Friendly Plastics Available online: <https://whittakerassociates.com/eco-friendly-plastics/> (accessed on Oct 18, 2019).
311. Tokiwa, Y.; Calabia, P.B.; Ugwu, U.C.; Aiba, S. Biodegradability of Plastics. *International Journal of Molecular Sciences* **2009**, *10*.
312. FXI Polyurethane foam 2014.
313. Dernehl, C.U. Health Hazards Associated with Polyurethane Foams. *Journal of Occupational and Environmental Medicine* **1966**, *8*.
314. Russell, J.R.; Huang, J.; Anand, P.; Kucera, K.; Sandoval, A.G.; Dantzler, K.W.; Hickman, D.; Jee, J.; Kimovec, F.M.; Koppstein, D.; et al. Biodegradation of Polyester Polyurethane by Endophytic Fungi. *Appl. Environ. Microbiol.* **2011**, *77*, 6076.
315. Activated Carbon MSDS Available online: https://beta-static.fishersci.com/content/dam/fishersci/en_US/documents/programs/education/regulatory-documents/sds/chemicals/chemicals-c/S25246.pdf (accessed on Oct 18, 2019).
316. Frontes, J. *Handbook for Social Impact Assessment*; Version 3.0.; PRé Consultants BV, 2016;
317. PLANT-E, B. Plant-e Available online: <https://www.plant-e.com/en/over-ons/> (accessed on Oct 13, 2019).
318. Ayala-Ruiz, D.; Castillo Atoche, A.; Ruiz-Ibarra, E.; Osorio de la Rosa, E.; Vázquez Castillo, J. A Self-Powered PMFC-Based Wireless Sensor Node for Smart City Applications. *Wireless Communications and Mobile Computing* **2019**, *2019*, 10.
319. Hayat, H.; Griffiths, T.; Brennan, D.; Lewis, P.R.; Barclay, M.; Weirman, C.; Philip, B.; Searle, R.J. The State-of-the-Art of Sensors and Environmental Monitoring Technologies in Buildings. *Sensors* **2019**, *19*.
320. Navarro, M.; Davis, W.T.; Villalba, G.; Li, Y.; Zhong, X.; Erratt, N.; Liang, X.; Liang, Y. Towards Long-Term Multi-Hop WSN Deployments for Environmental Monitoring: An Experimental Network Evaluation. *Journal of Sensor and Actuator Networks* **2014**, *3*.
321. BRG, B.R.G. *Three Years of Peatland Restoration in Indonesia Report*; The Peatland Restoration Agency of The Republic of Indonesia: Jakarta, 2019; p. 46;.

322. Ojha, T.; Misra, S.; Raghuwanshi, N.S. Wireless sensor networks for agriculture: The state-of-the-art in practice and future challenges. *Computers and Electronics in Agriculture* **2015**, *118*, 66–84.
323. Husson, O.; Husson, B.; Brunet, A.; Babre, D.; Alary, K.; Sarthou, J.-P.; Charpentier, H.; Durand, M.; Benada, J.; Henry, M. Practical improvements in soil redox potential (Eh) measurement for characterisation of soil properties. Application for comparison of conventional and conservation agriculture cropping systems. *Analytica Chimica Acta* **2016**, *906*, 98–109.
324. Regmi, R.; Nitorisavut, R.; Ketchaimongkol, J. A decade of plant-assisted microbial fuel cells: looking back and moving forward. *Biofuels* **2018**, *9*, 605–612.
325. IRENA *Renewable Power Generation Costs in 2018*; International Renewable Energy Agency: Abu Dhabi, 2019; p. 88;.
326. Venkata Mohan, S.; Mohanakrishna, G.; Chiranjeevi, P. Sustainable power generation from floating macrophytes based ecological microenvironment through embedded fuel cells along with simultaneous wastewater treatment. *Bioresource Technology* **2011**, *102*, 7036–7042.
327. Guadarrama-Pérez, O.; Gutiérrez-Macías, T.; García-Sánchez, L.; Guadarrama-Pérez, V.H.; Estrada-Arriaga, E.B. Recent advances in constructed wetland-microbial fuel cells for simultaneous bioelectricity production and wastewater treatment: A review. *International Journal of Energy Research* **2019**, *43*, 5106–5127.

Summary

As an energy carrier, electricity access is one of important aspect for human development. There is a positive correlation between electricity consumption per capita and human development index (HDI) and also gross domestic product (GDP). However, the world electrification is not equally distributed. Most of those who do not have electricity access live in rural areas and located in developing countries. In these area, some people use polluted kerosene lamps as their light source or expensive gasoline generator as their electricity source. Other than that, battery is also widely used as a power source. In addition to the unequal electrification, the world electricity generation is still dominated by fossil fuel sources that has a negative impact on the environment, increased health risk and global climate change. Therefore, it is important to shift from conventional energy source to low-carbon renewable electricity sources.

This thesis “**Plant Microbial Fuel Cell in Paddy Field: a power source for rural area**“ aims to assess the applicability of the plant microbial fuel cell (Plant-MFC) as a low power off-grid power source in a rural area for a theoretical Indonesian case. To achieve this, a technical design was made for a household in rural area of Indonesia based on the latest research developments. Then, the applicability was assessed on technical, social, and environmental safety and health criteria as well as economics and some scenarios were suggested which could improve the real application. Values for a plant-MFC system to fulfil basic electricity needs were calculated.

The main highlights and findings on this work are summarized in accordance with the chapters outlined in this thesis as following.

Chapter 2 “**Marine Sediment Mixed with Activated Carbon Allows Electricity Production and Storage from Internal and External Energy Sources: A New Rechargeable Bio-Battery with Bi-Directional Electron Transfer Properties**” investigates the abilities of marine sediment and activated carbon to store and generate electricity in a bio-battery. In this work, several mixture of marine sediment and activated carbon were studied in a bio electrochemical system (BES). When operated in the MFC mode, the system generated electricity with solely marine sediment as the anode electron donor, resulted in the creation of a bio-battery. The results show that by usage of marine sediment and activated carbon (AC) electricity was generated and stored. The internal electrical storage density is 0.3 mWh/kg AC marine anode. These insights give opportunities to apply such BES systems as e.g. *ex-situ* bio-battery to store and use electricity for off-grid purpose in remote areas.

Chapter 3 “**Activated Carbon Mixed with Marine Sediment is Suitable as Bioanode Material for *Spartina anglica* Sediment/Plant Microbial Fuel Cell: Plant Growth, Electricity Generation, and Spatial Microbial Community Diversity**” aims to investigate the suitability of a mixture of activated carbon and marine sediment as a bioanode in a plant-MFC system with *Spartina anglica*. This work focused on study how different mixtures of the activated carbon (AC) and the marine sediment (MS) as an anode material affected the plant vitality, electricity generation and spatial microbial community. Results show that *Spartina anglica* grew in all of the plant-MFCs, although the growth was less fertile in the 100% activated carbon Plant-MFC. On long-term (2 weeks) performance, mixture of 33% and 67% marine sediment outperformed other Plant-MFCs in terms of

current density (16.1 mA/m^2 plant growth area) and power density (1.04 mW/m^2 plant growth area). Results also show a high diversity of microbial communities dominated by *Proteobacteria* and indicates that the bacterial communities were affected by the anode composition. These findings show that the mixture of activated carbon and marine sediment are suitable material for bioanodes and could be useful for the application of Plant-MFC in a real wetland.

Chapter 4 “**Performance and Long Distance Data Acquisition via LoRa Technology of a Tubular Plant Microbial Fuel Cell Located in a Paddy Field in West Kalimantan, Indonesia**” provide an insight about the field performance of tubular Plant-MFC. In this study, one-meter tubular Plant-MFC with graphite felt anode and cathode were installed in triplicates in a paddy field for four rice growth seasons. An online data acquisition using LoRa technology was developed to investigate the performance of the tubular Plant-MFC over the final whole rice paddy growing season. The result revealed that the Plant-MFC do not negatively affect the rice growth. A continuous electricity generation was achieved during a wet period in the crop season. On average the Plant-MFC generated power of 6.6 mW/m^2 plant growth area (0.4 mW per meter tube). The Plant-MFC also shows a potential to be used as a bio sensor, e.g. rain event indicator, during a dry period between the crop seasons.

Chapter 5 “**A Thin Layer of Activated Carbon Deposited on Polyurethane Cube Leads to New Conductive Bioanode for (Plant) Microbial Fuel Cell**” exploits the potential of electrochemically active self-assembled biofilms to fabricate three-dimensional bio electrodes for of (plant) microbial fuel cells with minimum use of electrode materials. For this purpose, polyurethane foams coated with activated carbon was prepared and studied as platform bio anodes for harvesting electric current in lab microbial fuel cells (MFCs) and field Plant-MFCs. Results show that electric conductivity of the PU/AC electrode enhance over time during bioanode development. The maximum current and power density of an acetate fed MFC reached 3 mA/m^2 projected surface area of anode compartment and 22 mW/m^3 anode compartment. The field test of the Plant-MFC reached a maximum performance of 0.9 mW/m^2 plant growth area at a current density of 5.6 mA/m^2 PGA. A rice paddy field test showed that the PU/AC electrode was suitable as anode material in combination with a graphite felt cathode.

Finally, the main findings of this thesis are summarized and discussed in Chapter 6, “**General Discussion**”. In this chapter, a theoretical available power for Plant-MFC system from a paddy field is presented to give an insight how far performance of current Plant-MFC meets theoretical understanding. Based on the experimental results, this chapter answers the thesis goal to discuss the applicability of the Plant-MFC as an off-grid power source in a rural area by assessing its technical, economic, social, and environmental safety and health criteria. Finally, an outlook for future Plant-MFC application is provided.

Ikhtisar

Sebagai pembawa energi, akses terhadap listrik menjadi salah satu aspek penting dalam pembangunan manusia. Ada sebuah hubungan yang positif antara pemakaian listrik per kapita dengan indeks pembangunan manusia (IPM) and juga pendapatan domestik bruto (PDB). Akan tetapi, tingkat elektrifikasi di dunia saat ini tidak tersebar dengan merata. Kebanyakan mereka yang tidak memiliki akses terhadap listrik bermukim di daerah-daerah pedalaman dan berada di negara-negara berkembang. Di daerah-daerah tersebut, sebagian masyarakat masih menggunakan lampu minyak tanah sebagai sumber penerangan mereka atau genset berbahan bakar bensin sebagai sumber tenaga listrik mereka. Selain itu, baterai juga masih digunakan secara luas sebagai sumber daya listrik. Selain elektrifikasi yang tidak merata, saat ini pembangkit-pembangkit listrik di dunia masih didominasi oleh sumber bahan bakar fosil yang berdampak negatif terhadap lingkungan, kesehatan, dan perubahan iklim global. Oleh karena itu, penting untuk beralih dari sumber energi konvensional ke sumber listrik terbarukan rendah karbon.

Disertasi ini "**Plant Microbial Fuel Cell in Paddy Field: a power source for rural area** (Sel Bahan Bakar Mikroba Tanaman di Sawah: sumber tenaga untuk daerah pedalaman)" bertujuan untuk menilai penerapan sel bahan bakar mikroba tanaman (SBBMT) sebagai sumber daya listrik yang berdaya rendah di daerah pedalaman untuk sebuah kasus teoritis Indonesia. Untuk mencapai tujuan ini, sebuah desain teknis dibuat untuk rumah tangga di daerah pedalaman Indonesia berdasarkan perkembangan penelitian terbaru. Kemudian, kemungkinan penerapan SBBMT dinilai berdasarkan kriteria teknis, ekonomi, sosial, dan keselamatan lingkungan dan kesehatan. Beberapa skenario yang dapat meningkatkan aplikasi nyata juga disarankan. Akhirnya, harga/nilai untuk sistem SBBMT untuk memenuhi kebutuhan listrik dasar dihitung.

Sorotan utama dan temuan-temuan pada pekerjaan ini dirangkum sesuai dengan bab-bab yang diuraikan dalam disertasi ini sebagai berikut.

Bab 2 "**Marine Sediment Mixed with Activated Carbon Allows Electricity Production and Storage from Internal and External Energy Sources: A New Rechargeable Bio-Battery with Bi-Directional Electron Transfer Properties** (Sedimen Laut yang Dicampur Dengan Karbon Aktif Memungkinkan Produksi dan Penyimpanan Listrik dari Sumber Energi Internal dan Eksternal: Baterai Biologis Isi Ulang Baru dengan Properti Transfer Elektron Dua Arah)" menyelidiki kemampuan sedimen laut dan karbon aktif (KA) untuk menyimpan dan menghasilkan listrik di dalam sebuah baterai biologis. Dalam karya ini, beberapa campuran sedimen laut dan karbon aktif dipelajari dalam sistem elektrokimia biologis. Ketika dioperasikan dalam mode MFC (sel bahan bakar mikroba), sistem dapat menghasilkan listrik dengan hanya menggunakan sedimen laut sebagai donor elektron di dalam anoda, menghasilkan penciptaan baterai biologis. Hasil menunjukkan bahwa dengan penggunaan sedimen laut dan karbon aktif, listrik dihasilkan dan disimpan. Kepadatan penyimpanan listrik internal adalah 0,3 mWh/kg anoda KA-sedimen laut. Wawasan ini memberikan peluang untuk menerapkan sistem elektrokimia biologis, seperti misalnya baterai biologis *ex-situ*, untuk menyimpan dan menggunakan listrik untuk keperluan di daerah terpencil secara luring.

Bab 3 "**Activated Carbon Mixed with Marine Sediment is Suitable as Bioanode Material for *Spartina anglica* Sediment/Plant Microbial Fuel Cell: Plant Growth, Electricity Generation, and Spatial Microbial Community Diversity** (Karbon Aktif yang Dicampur dengan Sedimen Laut Cocok sebagai Bahan Bioanoda Sel Bahan Bakar Mikroba Tanaman/Sedimen dengan *Spartina anglica*: Pertumbuhan Tanaman, Pembangkitan Listrik, dan Keragaman Komunitas Mikroba Spasial)" bertujuan untuk menyelidiki kesesuaian campuran karbon aktif dan sedimen laut sebagai bioanoda dalam sistem SBBMT dengan *Spartina anglica*. Karya ini difokuskan pada studi bagaimana berbagai campuran karbon aktif (KA) dan sedimen laut (SL) sebagai bahan anoda mempengaruhi

daya hidup tanaman, pembangkit listrik dan komunitas mikroba spasial. Hasil menunjukkan bahwa *Spartina anglica* tumbuh disemua SBBMT, meskipun pertumbuhannya kurang subur di SBBMT dengan 100% karbon aktif sebagai anoda. Pada kinerja jangka panjang (2 minggu), campuran 33% KA dan 67% SL mengungguli SBBMT lainnya dalam hal kerapatan arus listrik ($16,1 \text{ mA/m}^2$ area pertumbuhan tanaman (APT)) dan kerapatan daya ($1,04 \text{ mW/m}^2$ APT). Hasil penelitian juga menunjukkan keberagaman yang tinggi dari komunitas mikroba yang didominasi oleh *Proteobacteria* dan menunjukkan bahwa komunitas bakteri dipengaruhi oleh komposisi anoda. Temuan ini menunjukkan bahwa campuran karbon aktif dan sedimen laut adalah bahan yang cocok untuk bioanoda dan dapat berguna untuk aplikasi lapangan SBBMT di lahan basah.

Bab 4 " Performance and Long Distance Data Acquisition via LoRa Technology of a Tubular Plant Microbial Fuel Cell Located in a Paddy Field in West Kalimantan, Indonesia (Kinerja dan Akuisisi Data Jarak Jauh melalui Teknologi LoRa dari Sel Bahan Bakar Mikroba Tanaman berbentuk Tubular yang Berlokasi di Sawah di Kalimantan Barat, Indonesia)" memberikan wawasan tentang kinerja lapangan SBBMT tubular. Dalam studi ini, satu meter SBBMT tubular dengan anoda dan katoda terbuat dari laken grafit dipasang sebanyak rangkap tiga di sawah selama empat musim tanam padi. Perolehan data daring menggunakan teknologi LoRa dikembangkan untuk menyelidiki kinerja SBBMT tubular selama musim tanam padi terakhir. Hasil penelitian menunjukkan bahwa SBBMT tidak berpengaruh buruk terhadap pertumbuhan padi. Pembangkitan listrik secara berkelanjutan dicapai selama periode basah dimusim tanam. Rata-rata SBBMT menghasilkan kerapatan daya sebesar $6,6 \text{ mW/m}^2$ APT ($0,4 \text{ mW}$ per meter SBBMT). SBBMT juga menunjukkan potensi untuk dapat digunakan sebagai sensor biologis, misalnya sebagai indikator terjadinya hujan, selama periode kering sawah.

Bab 5 " A Thin Layer of Activated Carbon Deposited on Polyurethane Cube Leads to New Conductive Bioanode for (Plant) Microbial Fuel Cell (Lapisan Tipis Karbon Aktif yang Diendapkan pada Kubus Poliuretana mengasikkan Bioanoda Konduktif Baru untuk Sel Bahan Bakar Mikroba (Tanaman))" memanfaatkan potensi pembentukan biofilm secara elektrokimia untuk membuat elektroda biologis tiga dimensi bagi SBBMT dengan penggunaan minimum bahan elektroda. Untuk tujuan ini, busa poliuretana (PU) yang dilapisi dengan karbon aktif (KA) disiapkan dan dipelajari sebagai dasar anoda biologis untuk memanen arus listrik dalam sel bahan bakar mikroba di laboratorium dan di lapangan. Hasil menunjukkan bahwa daya penerus listrik pada elektroda PU/KA meningkat dari waktu ke waktu selama proses perkembangan anoda biologis. Kerapatan arus maksimum dan daya dari sel bahan bakar mikroba umpan asetat mencapai 3 mA/m^2 luas permukaan anoda dan 22 mW/m^3 volum anoda. Uji lapangan SBBMT mencapai kinerja maksimum $0,9 \text{ mW/m}^2$ APT dengan kerapatan arus sebesar $5,6 \text{ mA/m}^2$ APT. Hasil pengujian di sawah menunjukkan bahwa elektroda PU/AC cocok sebagai bahan anoda dalam kombinasi dengan katoda berbahan laken grafit.

Akhirnya, temuan utama dari disertasi ini dirangkum dan dibahas dalam Bab 6, "**General Discussion** (Diskusi Umum)". Dalam bab ini, daya teoretis yang tersedia di sawah untuk sistem SBBMT disajikan untuk memberikan wawasan seberapa jauh kinerja SBBMT saat ini memenuhi pemahaman teoritis. Berdasarkan hasil percobaan, bab ini menjawab tujuan disertasi untuk membahas penerapan SBBMT sebagai sumber listrik luring (*off-grid*) di daerah pedalaman dengan menilai kriteria teknis, ekonomi, sosial, dan keselamatan lingkungan dan kesehatan. Akhirnya, prospek untuk aplikasi SBBMT di masa depan beberkan.

Isi ringkas

Njaji pemaba tanaga, ada angin ia listrik njaji salah sote banda nang panting dalap m'maju idup keleno. Ada obongan nang baik antara listrik nang dingguna satiap keleno duan indek pembangunan keleno, uga duan pangaselan domestik kotor. Tapi, sambongan listrik nang ada ka dunia kini ari ntu angin merate. Kobo umpu iya nang angin balistrik na biase ia badiapm ka binua-binua nang monggo duan ka nagara-nagara nang gi angin maju. Ka binua-binua nang di madah na tadi, urakng kampung ia ada nang nompok pelita ontok panarakng malam ari duan ada uga nang ngidup masen genset ontok listrik. Selain na, banyak uga nang ngguna batu baterai ontok sumber listrik ia. Salait masalah sambongan listrik nang angin merate, sampe mpitu ari sabagian aya masen-masen pengasel listrik masih makai minyak bumi nang diri nao angin baik ontok utat diri, ontok idup keleno duan ontok iklim dunia. Karna na, panting ontok diri beraleh dari sumber tanaga lama nang ngasel banyak karbon pangotor ka sumber listrik nang bisa dimbaru nang inik karbon.

Disertasi ntu “**Plant Microbial Fuel Cell in Paddy Field: a power source for rural area** (Sel Bahan Tunu Mikroba Tanaman ka Uma Paya: sumber tanaga ontok binua nang monggo)” batujuan ontok nele apekah Sel Bahan Tunu Mikroba Tanaman (SBTMT) bisa njaji sumber tanaga ka luar jaringan listrik nang batanaga amuk ka binua nang monggo ontok contoh kasus teoritis Indonesia. Ontok nyacah tujuan na, sote rancangan teknis dinggawe ontok rumah ka binua monggo di Indonesia duan dasar asel-asel panalitian nang baru. Lalu, kamungkinan ontok makai SBTMT dingaji uga dari sisi teknis, ekonomi, sosial duan kasalamatan utat sakitar wan kasehatan keleno. Beberape ncana uga dimere ontok bisa m'maik aplikasi nyata ia. Akher ia, itongan uga dimuat ontok nele apekah sestem SBTMT bisa ontok nyukup listrik nang dimaralu.

Togoan utama duan panamu-panamu dalap pegawe ntu dingerangkum sasuai duan bab-bab nang dinjalas dalap disertasi ntu bage pitu.

Bab 2 “**Marine Sediment Mixed with Activated Carbon Allows Electricity Production and Storage from Internal and External Energy Sources: A New Rechargeable Bio-Battery with Bi-Directional Electron Transfer Properties** (Lolok laut nang dingucal duan karbon aktif bisa ngasel duan ngombes listrik dari sumber tanaga dari dalap duan luar: Bateri biologis isi ulang baru duan sipat-sipat pinah elektron dua arah)” neliti tantang kamampuan lolok laut duan karbon aktif ontok ngasel duan ngombes listrik ka dalap sabuah bateri biologis. Dalap pegawe ntu, beberape campuran lolok laut duan karbon aktif dimalajar dalap sestem elektrokimia biologis. Waktu di njalat dalap pungsi MFC (sel bahan tunu mikroba), sestem ngesel listrik. Lolok laut nang njaji sote-sote ia sumber elektron ka dalap anoda, ngasel bateri biologis. Asel panalitian mere tahu diri kalo lolok laut duan karbon aktif bisa ngasel duan ngombes listrik. Karapatan pengombesan listrik dari dalap ia na sakitar 0,3 mWh/kg anoda KA-lolok laut. Panamuan ntu mere paluang ontok ngguna sestem elektrokimia biologis ntu, misal ia njaji bateri biologis nang bisa dimakai ontok binu-binua nang monggo.

Bab 3 “**Activated Carbon Mixed with Marine Sediment is Suitable as Bioanode Material for *Spartina anglica* Sediment/Plant Microbial Fuel Cell: Plant Growth, Electricity Generation, and Spatial Microbial Community Diversity** (Karbon Aktif nang dingucal duan Lolok Laut Bisa Njaji Bioanoda Sel Bahan Tunu Mikroba Tanaman/Lolok duan *Spartina anglica*: Patumuhan Tanaman, Pambangkitan Listrik, duan Janis-janis Mikroba ia)” batujuan ontok ngago kacocokan campuran karbon aktif duan lolok laut ontok njaji bioanoda ka dalap sestem SBTMT duan *Spartina anglica*. Pegawe ntu dimusat ontok nele bagemane pengaruh macam-macam janis campuran karbon aktif duan lolok laut nang dingguna njaji bahan anoda ka kamampuan idup tanaman, pambangkitan listrik, duan kalompok mikroba ka dalap ia. Asel ia nonjokkan kalo *Spartina anglica* tumuh ka samua SBTMT, cuma angin gila ombok ka SBTMT nang cuma dingisi duan karbon aktif. Dalap jangka panyakng (2 minggu), 33% karbon aktif duan 67% lolok laut ngalabihi SBTMT nang lait ia dalap hal

karapatan arus listrik ($16,1 \text{ mA/m}^2$ tempat tumbuh tanaman(TTT)) duan karapatan tanaga $1,04 \text{ mW/m}^2$ TTT. Asel pegawe uga nonjokkan kalo kalompok mikroba nang ada ka dalapm anoda na mbada banyak macam janis ia. Janis nang paling banyak adalah *Proteobacteria*. Janis-janis kalompok mikroba ntu kana pangaruh dari janis campuran anoda ia. Tamuan ntu mere tau kalo campuran karbon aktif duan lolok laut na cocok ontok njaji bahan bioanoda duan bisa baguna ontok dimakai dalap sestem SBTMT ka taya paya.

Bab 4 " Performance and Long Distance Data Acquisition via LoRa Technology of a Tubular Plant Microbial Fuel Cell Located in a Paddy Field in West Kalimantan, Indonesia (Onjok Gawe duan Ngompol Data Dari Jauh Ngguna Teknologi LoRa dari Sel Bahan Tunu Mikroba Tanaman Tubular ka Uma Paya ka Kalimantan Barat, Indonesia)" mere tau tantang onjok gawe lapangan dari SBTMT tubular. Dalap panalitian ntu, sameter SBTMT tubular nang anoda duan katoda ia tabuat dari laken grafit dimasang rangkap tege salama ampat mosem nanam padi. Pangompolan data dari jauh ngguna teknologi LoRa dingarancang ontok nele onjok pegawe SBTMT tubular salama mosem tanam padi nang kaampat. Asel panalitian mere tau kalo SBTMT tubular angin maba pangaruh nang jaek ka kaombok'an padi. Listrik di ngasel tarus manarus salama paya dingae'. Rate-rate SBTMT tubular ngasel karapatan tanaga $6,6 \text{ mW/m}^2$ TTT ($0,4 \text{ mW}$ satiap SBTMT). SBTMT bisa uga njaji sensor biologis, misal ia njaji penanda ujat salama paya dingarikng.

Bab 5 " A Thin Layer of Activated Carbon Deposited on Polyurethane Cube Leads to New Conductive Bioanode for (Plant) Microbial Fuel Cell (Lapisan Tipis Karbon Aktif nang dingandap ka Busa Poliuretana Njaji Bioanoda Konduktif nang Baru ontok Sel Bahan Tunu Mikroba Tanaman)" ngguna potensi biofilm sacara elektrokimia ontok nggawe elektroda biologis tege dimensi ontok SBTMT duan bahan elektroda nang inik. Ontok ntu, busa pilouretana (PU) nang dingalapis duan karbon aktif(KA) dinyiap duan dimalajar njaji tempat pamole anoda biologis ontok nganyi arus listrik dalap sel bahan tunu mikroba (SBTM) ka laboratorium duan ka lapangan. Asel nonjokkan kalo konduktivitas listrik elektroda PU/KA batamah dari waktu ka waktu salama pangambangan elektroda biologis. Karapatan arus nang paling tinggi duan tanaga dari SBTM nang dinyolo umpat asetat nyacah 3 mA/m^2 luas anoda duan 22 mW/m^3 isi anoda. Pangujian ka lapangan SBTMT tubular ncapai onjok gawe paling tingi $0,9 \text{ mW/m}^2$ TTT duan karapatan arus ia $5,6 \text{ mW/m}^2$ TTT. Asel pangujian ka uma paya nonjokkan kalo elektroda PU/AC cocok ontok njaji bahan anoda nang dingawan duan katoda dari laken grafit.

Penyantak ia, tamuan utama dari disertasi ntu dingerangkum duan dibahas dalap bab 6, "**General Discussion** (Diskusi Omom)". Dalap bab ntu, tanaga teoritis nang tasadia ka uma paya ontok sestem SBTMT dinjalas ontok mere tahu sabarape jauh dah onjok pegawe dari SBTMT kini ari ntu mampu nyacah pamahaman teoritis ia. Ngguna asel panalitian, bab ntu mere jawaban ka tujuan disertasi ontok mbahas kamungkinan pamakaian SBTMT njaji sumber listrik ontok binua-binua nang monggo. Ontok ntu, kriteria teknik, ekonomi, sosial, duan kasalamatan lengkongan duan kasehatan keleno di mbahas sote-sote. Pangabis ia, pandangan-pandangan tantang kamungkinan pemakaian SBTMT ontok masa depan di mbahas uga.

Acknowledgement

I felt that pursuing a PhD process is like a journey finding a route to hike a mountaintop. You will face many challenges during the journey; sometime you need to change your compass or step back to avoid steep cliffs or valleys. However, as long as you have a best guidance and support, courage, fight mentality, and keep hiking, you will reach the top. Now, I am almost reaching that PhD mountaintop. When you read this, it means, hopefully, I am a PhD, 😊.

I extend my sincerest thank to everyone who has involved and contributed to the journey of my PhD until its completion. My first thank to my co-promotor and supervisor, David, who trusted and gave me an opportunity to be part of his team. I really appreciate your kindness and constructive feedback and continuous support toward me. Thank you for your insightful discussions, critical feedback on all manuscripts, and your guidance, encouragement and help to develop an ability to conduct research and published it. My thanks also to my promotor, Cees, for his support through the PhD process. Thank you for the opportunity to join your research group, the bio recovery group and for the challenge and guidance to develop my ability to be an independent researcher. I will miss the journey to your hometown in Harich, at which the meeting and togetherness are combined. I also thank the Government of Landak Regency who provided a scholarship that make me possible to pursue this degree. My special thanks to Bapak Adrianus Asia Sidot who encouraged me to pursue my PhD back to Wageningen.

I am grateful to colleagues at ETE. I really enjoy the spirit of togetherness in this department. I will miss the department trip, the monthly drink (with speech), the cakes/cookies at coffee break, the publication's champagne in the morning, the Christmas dinner, the ETE sport team, and the entire togetherness events. I thank to the ETE secretary team, especially Liesbeth who helped me from the beginning until end of my PhD with all paper works related businesses. I also thank the ETE-Lab team (Katja, Livio, Hans, Jean, Pieter, Vinnie, Bert) who helped me during the research. I thank to all of my officemates; to the first edition officemates mates Azie, Dandan, Laura, Leire, and Rosanne, we are the best officemates ever; and to the latest joined officemate, Vincent and Minh, who keep the "gender balance" in the office. I also thank to all colleagues who often spent their Thursday evening in our coffee corner for a good "proost" and a lively chat; Livio, Dainis, Vinnie, Jean, Laura, Dandan, Kamonashi, Pradip, Leire, Koen & Koen, Ludo, Thomas, Carlos, Adrian, Andrea, Shiyang, Bingnan, Momo, Tim, Hardy, Miriam, Harry, Nora, Pim, Joeri, Dilan, Selin, Rieks, Roxanni, Kasper, Merijn, Annemerel, Margo, Sanne, Ivonne, Elackiya, Silvia, Ilse, and many more that I cannot list here. I really enjoyed our Thursday evening moment. Also, I thank to all of my students (Matteo, Rens, Paola, Dwi, and Christian) who did their thesis with me and contributed to this thesis.

Saya juga berterimakasih kepada teman-teman sesama PhD dan Postdoc Indonesia yang ada di Wageningen yang telah menjadi keluarga besar untuk saling menguatkan dan berbagi cerita. Teman-teman semasa master yang kembali ke dan masih di Wageningen, Eka dan Mas Yusuf dan Kirana, Nila dan Anto beserta Amar, Tsara dan Farah, Indraningrat, Silvia, Dasep, Titis, Linda, Nuning, Taupik dan Pini, Akhirta, Belinda, William dan Sisi, Hachi, Indra dan Novi, dan Mbak Sarita Uda. Kawan-kawan ngopi Axis Eksis, Ayusta, Belinda, Alim, Hachi, Erick, Fiametta, Silvia dan Mbak Ita. Tetangga-tetangga di Herenstrat dan seputaran pusat kota, Dian dan suaminya Mugni beserta anak-

anaknya, Windi dan suaminya Mustaghfirin, Vina dan suaminya Fariduddin, Alim dan istrinya Ayu, Yohanes dan istrinya Asmihara dan Kang Samuel. Terimakasih sudah menjadi tetangga yang baik dan menyenangkan. Juga ucapan terima kasih atas kebersamaan di Wageningen kepada teman-teman PhD yang sudah duluan kembali ke Indonesia, Pak Sakti, Pak Panca, Pak Taufik, Mas Reo, Mbak Dian, Pak Erry, Bang Audrey dan Ci Meli. Terima kasih juga kepada Mas Fahrizah dan Mbak Zulfia, Mas Sahri dan Mbak Suparmi, Mas Eko dan Mbak Andra dan teman-teman NU yang sering mengundang makan dan silaturahmi setelah pengajian selesai. Serta seluruh teman-teman PhD lainnya yang saya tidak bisa saya sebutkan satu persatu di sini. Sekali lagi terimakasih atas kebersamaannya semoga komunikasi dan silaturahmi kita tetap terjalin saat kembali ke tanah air.

Akhirnya, saya sangat berterimakasih atas dukungan dari seluruh keluarga, Bapak dan Ibu beserta adik-adik saya. Terimakasih khusus kepada istri saya tercinta, Natalina, yang rela berkorban menemani saya selama pendidikan doktoral ini. Terimakasih atas segala cinta dan pengorbanannya. Terimakasih juga untuk anak kami, Jonathans, yang selalu membawa keceriaan dalam keluarga, semoga kelak kamu bisa mengenyam pendidikan yang tinggi juga nak.

Adil ka' Talino, Bacuramin Ka' Saruga, Basengat ka' Jubata.

Wageningen, 12 February 2020

Emilius Sudirjo

Emilius Sudirjo



Personal Info

Date of Birth	28 May 1984
Place of Birth	Kuala Behe, Landak Regency, West Kalimantan, Indonesia
Nationality	Indonesian
Marital status	Marriage
Children	1 son

Education

Feb 2016 – Feb 2020	PhD in Environmental Technology, Wageningen University & Research, Wageningen
Sept 2011 – Sept 2013	MSc in Environmental Sciences, Wageningen University & Research, Wageningen
Aug 2001 – Jan 2006	BSc in Engineering (<i>Sarjana Teknik</i>), Universitas Indonesia, Depok, Indonesia Major in Gas and Petrochemical/Chemical Engineering
July 1998 – June 2001	State Senior High School (Sekolah Menengah Umum Negeri) No.1 Singkawang, West Kalimantan, Indonesia
July 1995 – June 1998	State Junior High School (Sekolah Menengah Pertama Negeri) No.1, Ngabang, West Kalimantan
July 1989 – June 1995	State Basic School (Sekolah Dasar Negeri) No.11 Permiit, Landak Regency, West Kalimantan, Indonesia

Experience

- 2009 – Present **Civil Servant**, Government of Landak Regency, West Kalimantan Province, Indonesia
- 2016 – 2020 **PhD Candidate**, Wageningen University & Research, Wageningen
Plant Microbial Fuel Cell in Paddy Field: a power source for rural area
- 2013 **Intern researcher**, Center of Biomass and Renewable Energy, Department of Chemical Engineering, Diponegoro University, Semarang, Indonesia
Laboratory research on utilizing palm oil mill effluent (POME) to generate biogas in an UASB reactor system.
- 2012 – 2013 **MSc Thesis**, Wageningen University & Research, Wageningen
Maximizing Power Output of Plant Microbial Fuel Cell (PMFC) using a Bio Cathode
- 2006 – 2009 **Teacher and Head of Chemical Laboratory**, St. Paul Private Senior High School, Pontianak, Indonesia
- 2005 – 2006 **BSc Thesis**, Chemical Engineering Department, Universitas Indonesia, Depok, Indonesia
Determination of benzene-toluene distribution in the activated carbon fixed-bed adsorption column

List of Publications

Sudirjo, E.; de Jager, P.; Buisman, C.J.; Strik, D.P. Performance and Long Distance Data Acquisition via LoRa Technology of a Tubular Plant Microbial Fuel Cell Located in a Paddy Field in West Kalimantan, Indonesia. *Sensors* **2019**, *19*, 4647. <https://doi.org/10.3390/s19214647>

Sudirjo, E.; Buisman, C.J.; Strik, D.P. Activated Carbon Mixed with Marine Sediment is Suitable as Bioanode Material for *Spartina anglica* Sediment/Plant Microbial Fuel Cell: Plant Growth, Electricity Generation, and Spatial Microbial Community Diversity. *Water* **2019**, *11*, 1810. <https://doi.org/10.3390/w11091810>

Sudirjo E, Buisman CJN and Strik DPBTB (2019) Marine Sediment Mixed With Activated Carbon Allows Electricity Production and Storage From Internal and External Energy Sources: A New Rechargeable Bio-Battery With Bi-Directional Electron Transfer Properties. *Front. Microbiol.* 10:934. <https://doi.org/10.3389/fmicb.2019.00934>

Sudirjo, E.; Buisman, C.J.N.; Strik, D.P.B.T.B. Electricity generation from wetlands with activated carbon bioanode. *IOP Conf. Ser. Earth Environ. Sci.* **2018**, *131*, 012046. <https://doi.org/10.1088/1755-1315/131/1/012046>

Sudirjo, E.; Wetser, K.; Strik, D.; Buisman, C. Maximizing power output of Plant Microbial Fuel Cell with sustainable bio cathodes; *Proceedings 2nd International Plant Power Symposium.* **2012**; DOI: 10.13140/2.1.2061.3447

Sudirjo, E. Penentuan Distribusi Benzena-Toluena Pada Kolom Adsorpsi Fixed Bed Karbon Aktif. Bachelor Thesis, Fakultas Teknik Universitas Indonesia: Depok, 2005. <http://152.118.24.168/detail?id=20247410>

Wetser, K.; **Sudirjo, E.**; Buisman, C.J.N.; Strik, D.P.B.T.B. Electricity generation by a plant microbial fuel cell with an integrated oxygen reducing biocathode. *Appl. Energy* **2015**, *137*, 151–157. <https://doi.org/10.1016/j.apenergy.2014.10.006>

Hadiyanto, H.; Muslihuddin, M.; **Sudirjo, E.**; Padetya, N. Utilizing Palm Oil Mill Waste for Co-Production of Biogas and Microalgae Biomass. *IOP Conf. Ser. Earth Environ. Sci.* **2019**, *248*, 012073. <https://doi.org/10.1088/1755-1315/248/1/012073>



*Netherlands Research School for the
Socio-Economic and Natural Sciences of the Environment*

D I P L O M A

for specialised PhD training

The Netherlands research school for the
Socio-Economic and Natural Sciences of the Environment
(SENSE) declares that

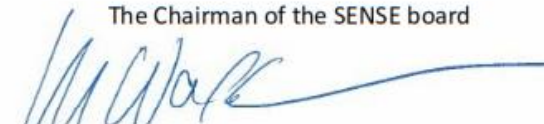
Emilius Sudirjo

born on 28 May 1984 in Kuala Behe, Indonesia

has successfully fulfilled all requirements of the
educational PhD programme of SENSE.

Wageningen, 12 February 2020

The Chairman of the SENSE board



Prof. dr. Martin Wassen

the SENSE Director of Education



Dr. Ad van Dommelen

The SENSE Research School has been accredited by the Royal Netherlands Academy of Arts and Sciences (KNAW)



K O N I N K L I J K E N E D E R L A N D S E
A K A D E M I E V A N W E T E N S C H A P P E N



The SENSE Research School declares that **Emilius Sudirjo** has successfully fulfilled all requirements of the educational PhD programme of SENSE with a work load of 38.0 EC, including the following activities:

SENSE PhD Courses

- o Environmental research in context (2016)
- o Research in context activity: 'Co-organizing Wageningen Indonesia Scientific Exposure (WISE) 2017 meeting (8-9 March 2017, Wageningen)'
- o Making an Impact! How to increase the societal relevance of your PhD research (2016)
- o Data Management Planning (2016)
- o Scientific Publishing (2016) & Efficient Writing Strategy (2016) & Scientific Writing (2019)
- o Reviewing a Scientific Paper(2017)
- o Brain-friendly working & writing, Wageningen Graduate Schools (2018)

External training at a foreign research institute

- o PhD study trip to Tsinghua University, China Agricultural University, Chinese Academy of Sciences, Xi'an University of Architecture and Technology, Xi'an Siyuan University, Xi'an Jiaotong University, Jiangnan University, Tongji University and technical visit to several companies (MAPUNI, BCEER, Amway), China (2016)

Management and Didactic Skills Training

- o Supervising four MSc students and one BSc student with thesis (2016-2019)
- o Teaching in the BSc course 'Renewable energy' (2016-2019)
- o Teaching in the BSc course 'Introduction Environmental Technology' (2018)
- o Guest lecturer on "Kapita Selekta" course on 'Chemical Engineering,' University of Indonesia (2019)
- o Organizing Committee of Wageningen Indonesia Scientific Exposure (WISE) 2016
- o Steering Committee Wageningen Indonesia Scientific Exposure (WISE) 2019

Oral Presentations

- o *Electricity from living plants*. Academic Workshop on Environmental Biotechnology between Xi'an Jiaotong University (XJTU, China) and Wageningen University, 14 June 2016, Xián, China
- o **Best presentation award:** *Electricity generation from wetlands with activated carbon bio-anode*, International Conference on Green Agro-industry and Bio economy, 24 – 25 October 2017, Batu, Malang, Indonesia
- o *Co-production of energy and food: Generating electricity in a rice paddy field with plant microbial fuel cell*. Wageningen UR- Indonesian Network Scientific Exposure, 5 – 6 July 2018, Cibinong, Bogor, Indonesia

SENSE coordinator PhD education

Dr. ir. Peter Vermeulen

The research described in this thesis was financed by Government of Landak Regency, West Kalimantan Province, Republic of Indonesia under MoU with Wageningen University & Research No 6160030150

Financial support from Wageningen University for printing this thesis is gratefully acknowledge.

Cover design by Emilius Sudirjo. Front cover foto is the Plant-MFC set-up (from Chapter 4) in a Paddy field in Sebol, Bengkayang, West Kalimantan, Indonesia. Back cover foto shows my mother and my son collecting snails in the same paddy field.

Printed by: ProefschriftMaken || DigiForce (www.proefschriftmaken.nl)

This thesis is printed on FSC certified paper.